

University of Windsor

Scholarship at UWindor

Electronic Theses and Dissertations

Theses, Dissertations, and Major Papers

10-17-2019

The role of approach flow and blockage on local scour around circular cylinders with and without countermeasures

Priscilla D. Williams
University of Windsor

Follow this and additional works at: <https://scholar.uwindsor.ca/etd>

Recommended Citation

Williams, Priscilla D., "The role of approach flow and blockage on local scour around circular cylinders with and without countermeasures" (2019). *Electronic Theses and Dissertations*. 8154.
<https://scholar.uwindsor.ca/etd/8154>

This online database contains the full-text of PhD dissertations and Masters' theses of University of Windsor students from 1954 forward. These documents are made available for personal study and research purposes only, in accordance with the Canadian Copyright Act and the Creative Commons license—CC BY-NC-ND (Attribution, Non-Commercial, No Derivative Works). Under this license, works must always be attributed to the copyright holder (original author), cannot be used for any commercial purposes, and may not be altered. Any other use would require the permission of the copyright holder. Students may inquire about withdrawing their dissertation and/or thesis from this database. For additional inquiries, please contact the repository administrator via email (scholarship@uwindsor.ca) or by telephone at 519-253-3000ext. 3208.

**The role of approach flow and blockage on local scour around circular cylinders
with and without countermeasures**

by

Priscilla D. Williams

A Dissertation

Submitted to the Faculty of Graduate Studies
through the Department of Civil and Environmental Engineering
in Partial Fulfillment of the Requirements for
the Degree of Doctor of Philosophy
at the University of Windsor

Windsor, Ontario, Canada

2019

© 2019 Priscilla D. Williams

**The role of approach flow and blockage on local scour around circular cylinders
with and without countermeasures**

by

Priscilla D. Williams

APPROVED BY:

R. Ettema, External Examiner
Colorado State University

R. Barron
Department of Mathematics and Statistics

N. Biswas
Department of Civil and Environmental Engineering

T. Bolisetti
Department of Civil and Environmental Engineering

V. Roussinova, Co-Advisor
Department of Mechanical, Automotive and Materials Engineering

R. Balachandar, Advisor
Department of Civil and Environmental Engineering

October 11, 2019

DECLARATION OF CO-AUTHORSHIP/PREVIOUS PUBLICATION

I. Co-Authorship

I hereby declare that this thesis incorporates material that is the result of joint research, as follows:

This thesis incorporates the outcome of joint research under the supervision of Dr. Ram Balachandar and Dr. Vesselina Roussinova. The collaboration is covered in Chapters 2, 3, 4 and 5 of the thesis. In all cases, the key ideas, primary contributions, experimental designs, data analysis, interpretation, and writing were performed by the author, and the contribution of co-authors was primarily through the provision of supervision.

I am aware of the University of Windsor Senate Policy on Authorship and I certify that I have properly acknowledged the contribution of other researchers to my thesis, and have obtained written permission from each of the co-author(s) to include the above material(s) in my thesis.

I certify that, with the above qualification, this thesis, and the research to which it refers, is the product of my own work.

II. Previous Publication

This thesis includes 3 original papers that have been previously or will be submitted for publication in peer reviewed journals, as follows:

Thesis chapter	Publication title/full citation	Publication status
<i>Chapter 3</i>	Role of channel aspect ratio on flow over a porous bed	<i>to be submitted</i>
<i>Chapter 4</i>	Role of channel blockage ratio on local scour flow field mechanisms	<i>to be submitted</i>
<i>Chapter 5</i>	Particle Image Velocimetry evaluation of flow-altering countermeasures for local scour around a submerged circular cylinder	<i>submitted for publication</i>

I certify that I have obtained a written permission from the copyright owner(s) to include the above published material(s) in my thesis. I certify that the above material describes work completed during my registration as a graduate student at the University of Windsor.

III. General

I declare that, to the best of my knowledge, my thesis does not infringe upon anyone's copyright nor violate any proprietary rights and that any ideas, techniques, quotations, or any other material from the work of other people included in my thesis, published or otherwise, are fully acknowledged in accordance with the standard referencing practices. Furthermore, to the extent that I have included copyrighted material that surpasses the bounds of fair dealing within the meaning of the Canada Copyright Act, I certify that I have obtained a written permission from the copyright owner(s) to include such material(s) in my thesis.

I declare that this is a true copy of my thesis, including any final revisions, as approved by my thesis committee and the Graduate Studies office, and that this thesis has not been submitted for a higher degree to any other University or Institution.

ABSTRACT

Local scour modelling has been established as an imperative tool in the understanding of local scour mechanisms and development of effective design methodologies for use in practice. However, there are limitations in physical scale modelling which must be fully understood in order to acquire useful experimental results to this end. In hydraulic modelling, facility constraints often result in dimensionless geometric parameters which are considerably altered from prototype conditions. Channel width b in a typical laboratory flume is limited, resulting in small values of channel aspect ratio AR (b/h , where h is flow depth). To further complicate matters, cylinder diameter D in local scour studies must be maximized to obtain a measurable scour pattern and maintain acceptably high relative coarseness D/d_{50} (where d_{50} is the median diameter of bed material). This results in cylinder sizes which pose a significant blockage to flow.

While blockage effects have been explored for a cylinder mounted on a fixed bed, the effect of blockage ratio (D/b) for a cylinder in an erodible bed has only been explored through comparison of bed formations. In order to fully understand the effect of sidewall proximity on the flow field surrounding a cylinder under equilibrium of local scour, detailed velocity measurements are required. Furthermore, the effect of D/b on local scour must be isolated by holding all other scour-governing parameters constant. In order to achieve this, channel width b has been altered in the present investigation by movable flume sidewalls. In altering b , the channel aspect ratio AR is also affected. Particle Image Velocimetry (PIV) measurements have been undertaken in order to explore the effects of channel aspect ratio on open-channel flow over a porous bed. The effects of increasing vertical confinement (decreasing h) and horizontal confinement (decreasing b) are explored by comparison of

mean and turbulence properties as well as third-order turbulent moments and quadrant analysis.

The findings are then applied to an investigation of the role of D/b on the flow field mechanisms surrounding an emergent circular cylinder under equilibrium of clear-water scour. Changes in the distribution of time-averaged flow velocity, Reynolds shear stress and spanwise vorticity are presented and related to the bed formation. Increasing sidewall proximity is observed to confine the wake region and therefore influence the geometry of the dune downstream of the cylinder. The dune geometry subsequently affects the features in the surrounding flow field, and the streamwise velocity upstream of the cylinder is reduced as D/b increases.

A primary objective of scour modelling is development of countermeasures for mitigation of the mechanisms which drive local scour. Lastly, an investigation of two types of scour countermeasures was carried out for flow around a submerged circular cylinder at equilibrium of clear-water scour. Based on fluid dynamic considerations, a vertical splitter plate and a horizontal base plate were chosen as potential flow-altering devices and the efficacy of these devices for scour mitigation are explored. PIV measurements also facilitate understanding of the methods by which each countermeasure affects the flow field mechanisms surrounding the cylinder, and the distribution of flow velocity and Reynolds shear stress are presented. The vertical splitter plate is found to affect the interaction between shear layers in the wake region, reducing the depth of scour downstream of the cylinder. The horizontal base plate is found to eliminate scour upstream of the cylinder altogether by protecting the bed around the sides of the cylinder where shear stress is maximized.

DEDICATION

“For by thee I have run through a troop; and by my God have I leaped over a wall.”

Psalms 18:29 KJV

ACKNOWLEDGEMENTS

I would like to extend my thanks to the following individuals for their contribution to this dissertation.

To my supervisor, Dr. Ram Balachandar, and my co-supervisor, Dr. Vesselina Roussinova; thank you for your daily instruction and guidance during this process.

To the members of my doctoral committee, thank you for your insight and comments. To Dr. Ronald Barron, thank you for your weekly input and perspectives. To Dr. Tirupati Bolisetti, thank you for your mentorship over the past 12 years. To Dr. Nihar Biswas, thank you for your counsel and advice.

To Matthew St. Louis, thank you for your help and patience in the lab. To Ahmad Al-Hayale and Mia Marrocco; thank you for helping with the heavy lifting.

To my colleagues Dr. Vimaldoss Jesudhas, Dr. Kohei Fukuda, Junting Chen and Subhadip Das; thank you for your contributions, technical and otherwise.

To Kiri McDermott-Berryman, Amy Hucal, Emily Southcott and Georgiana Madar; thank for your friendship (and for always picking up the phone). To my goddaughter, Claire Stefania, thank you for making me smile during the home stretch. To my nephews, Alexander Anthony and Anthony John; thank you for keeping me entertained.

To my parents, Lawrence and Josephine Williams, and my sister, Rebecca Williams; thank you for your love and support.

TABLE OF CONTENTS

DECLARATION OF CO-AUTHORSHIP/PREVIOUS PUBLICATION	iii
ABSTRACT.....	v
DEDICATION.....	vii
ACKNOWLEDGEMENTS.....	viii
LIST OF TABLES.....	xii
LIST OF FIGURES	xiii
LIST OF ABBREVIATIONS/SYMBOLS.....	xx
1 INTRODUCTION.....	1
1.1 The cost of scour	1
1.2 The mechanism of local scour.....	2
1.3 Scale effects in hydraulic modelling	4
1.4 The influence of blockage ratio D/b on local scour	6
1.5 Use of Particle Image Velocimetry (PIV) in scour experiments in literature	7
1.6 Description of thesis objectives.....	9
1.7 Structure of thesis and scope of experimental work	10
1.8 References	14
2 METHODOLOGY	17
2.1 Description of experimental facility.....	17
2.2 Experimental program.....	18
2.3 Test methodology	20
2.4 Particle Image Velocimetry (PIV) system	21
2.5 PIV processing details.....	23
2.6 References	30
3 ROLE OF CHANNEL ASPECT RATIO ON FLOW OVER A POROUS BED.....	31
3.1 Introduction	31
3.2 Background	39
3.3 Results and discussion.....	44

3.3.1	Distribution of streamwise velocity, velocity deficit and turbulence intensities	45
3.3.2	Distribution of third-order turbulent moments	53
3.3.3	Distribution of normalised Reynolds shear stress $-\overline{uv}/u_\tau^2$	56
3.3.4	Effect of sidewall proximity on mean and turbulence properties	65
3.4	Conclusions and recommendations	66
3.5	References	91
4	ROLE OF CHANNEL BLOCKAGE RATIO ON LOCAL SCOUR FLOW FIELD MECHANISMS	97
4.1	Introduction	97
4.2	Background	99
4.2.1	The effect of blockage ratio D/b on flow around cylinders	99
4.2.2	Blockage effects in scour literature	102
4.2.3	Previous investigations on the influence of blockage ratio D/b on relative scour depth d_{se}/D	103
4.3	Methodology	105
4.4	Results and discussion	107
4.4.1	Approach flow conditions	107
4.4.2	Comparison of bed profiles	108
4.4.3	Distribution of normalised mean streamwise velocity U/U_e	118
4.4.4	Distribution of normalised Reynolds shear stress $-\overline{uv}/U_e^2$	120
4.4.5	Distribution of spanwise vorticity Ω	122
4.5	Conclusions and recommendations	122
4.6	References	142
5	EVALUATION OF FLOW-ALTERING COUNTERMEASURES FOR LOCAL SCOUR AROUND A CIRCULAR CYLINDER	146
5.1	Introduction	146
5.1.1	A review of scour countermeasures	146
5.1.2	Circular and rectangular collars	148
5.1.3	Splitter plates	150
5.1.4	Scour at submerged cylinders	152

5.1.5	Motivation and problem background.....	152
5.2	Methodology	154
5.3	Results and discussion.....	157
5.3.1	Comparison of bed profiles.....	157
5.3.2	Distribution of normalised mean streamwise velocity U/U_e	168
5.3.3	Distribution of normalised Reynolds shear stress $-\overline{uv}/U_e^2$	174
5.4	Conclusions and recommendations.....	177
5.5	References	194
6	CONCLUSIONS AND RECOMMENDATIONS.....	199
	APPENDICES	205
	Appendix A: Figure permissions.....	205
	Appendix B: Bed profile measurements	213
	Appendix C: Summary of PIV measurement details	247
	Appendix D: Uncertainty analysis of PIV measurements.....	250
	VITA AUCTORIS	253

LIST OF TABLES

Table 1.1: Description of thesis structure	11
Table 2.1: Test parameters for experimental program in Chapters 3, 4 and 5.....	19
Table 3.1: Parameters for flume experiments of the current investigation and in literature	48
Table 3.2: Summary of the effect of horizontal and vertical confinement on flow characteristics.....	64
Table 4.1: Description of literature experiments with large blockage ratio D/b	103
Table 4.2: Test parameters for local scour experiments	106
Table 5.1: Experimental conditions for tests E1, E2 and E3	155
Table 5.2: Comparison of experimental conditions with tests from literature	161

LIST OF FIGURES

Figure 1.1: Schoharie Creek Bridge collapse in NY, 1987 (Croyle 2017).....	12
Figure 1.2: Arroyo Pasajero bridge collapse in CA, 1995 (Richardson 1995).....	12
Figure 1.3: Bonnybrook Bridge collapse in AB, 2013 (Government of Canada 2014) ...	13
Figure 1.4: Large-scale clear-water scour test with $D = 0.91$ m, $b = 6$ m ($D/b = 0.15$) (Sheppard et al. 2004); figure used with permission from ASCE	13
Figure 2.1: Schematic of horizontal laboratory flume used for experimentation	27
Figure 2.2: Location of planes of interest in local scour experimentation.....	27
Figure 2.3: Schematic of experimental set-up for local scour experiments around an emergent cylinder (top) and a submerged cylinder (bottom).....	28
Figure 2.4: Schematic of planar Particle Image Velocimetry (PIV) setup for local scour experiments	29
Figure 3.1: Distribution of (a) U^+ vs. y^+ (b) $U_e^+ - U^+$ vs. y/δ (inset with logarithmic scaling included), (c) streamwise turbulence intensity u_{rms}/u_τ vs. y/δ and (d) vertical turbulence intensity v_{rms}/u_τ vs. y/δ for tests R1, R3 and R5 (present investigation), S1, S2 and S3 (Roussinova et al. 2008) and FS1, FR1 and FR2 (Flack et al. 2005)	68
Figure 3.2: Distribution of (a) streamwise turbulence intensity u_{rms}/u_τ for tests R1 and R4 (AR = 3.3), (b) vertical turbulence intensity v_{rms}/u_τ for tests R1 and R4 (AR = 3.3), (c) streamwise turbulence intensity u_{rms}/u_τ for tests R3 and R6 (AR = 6.6) and (d) vertical turbulence intensity v_{rms}/u_τ for tests R3 and R6 (AR = 6.6) over flow depth y normalised by boundary layer thickness δ	69
Figure 3.3: Distribution of (a) streamwise turbulence intensity u_{rms}/u_τ and (b) vertical turbulence intensity v_{rms}/u_τ for tests R1 and R2 ($b = 0.4$ m), (c) streamwise turbulence intensity u_{rms}/u_τ and (d) vertical turbulence intensity v_{rms}/u_τ for tests R3 and R4 ($b = 0.8$ m), (e) streamwise turbulence intensity u_{rms}/u_τ and (f) vertical turbulence intensity v_{rms}/u_τ for tests R5 and R6 ($b = 1.22$ m) over flow depth normalised by boundary layer thickness y/δ	70
Figure 3.4: Distribution of (a) streamwise turbulence intensity $u_{rms}/(u_{rms})_e$ and (b) vertical turbulence intensity $v_{rms}/(u_{rms})_e$ for tests R1 and R2 ($b = 0.4$ m), (c) streamwise turbulence intensity $u_{rms}/(u_{rms})_e$ and (d) vertical turbulence intensity $v_{rms}/(u_{rms})_e$ for tests R3 and R4 ($b = 0.8$ m), (e) streamwise turbulence intensity $u_{rms}/(u_{rms})_e$ and (f) vertical turbulence intensity $v_{rms}/(u_{rms})_e$ for tests R5 and R6 ($b = 1.22$ m) over y/δ_I , where y is flow depth and δ_I is the	

location at which u_{rms} reaches the free-stream streamwise turbulence intensity $(u_{rms})_e$ 71

Figure 3.5: Distribution of the ratio of streamwise turbulence intensity to vertical turbulence intensity v_{rms}/u_{rms} for (a) tests R1 and R2 ($b = 0.4$ m), (b) tests R3 and R4 ($b = 0.8$ m) and (c) tests R5 and R6 ($b = 1.22$ m) over flow depth normalised by boundary layer thickness y/δ 72

Figure 3.6: Distribution of (a) streamwise transport of the streamwise component of normal stress $\overline{u^3}$, (b) vertical transport of the vertical component of normal stress $\overline{v^3}$ (c) vertical transport of the streamwise component of normal stress $\overline{u^2v}$ and (d) the streamwise transport of the vertical component of normal stress $\overline{uv^2}$ for tests R1, R3 and R5 ($h = 0.12$ m) over flow depth normalised by boundary layer thickness y/δ 73

Figure 3.7: Distribution of (a) streamwise transport of the streamwise component of normal stress $\overline{u^3}$, (b) vertical transport of the vertical component of normal stress $\overline{v^3}$ (c) vertical transport of the streamwise component of normal stress $\overline{u^2v}$ and (d) the streamwise transport of the vertical component of normal stress $\overline{uv^2}$ for tests R1 and R2 ($b = 0.4$ m) over flow depth normalised by boundary layer thickness y/δ 74

Figure 3.8: Distribution of (a) streamwise transport of the streamwise component of normal stress $\overline{u^3}$, (b) vertical transport of the vertical component of normal stress $\overline{v^3}$ (c) vertical transport of the streamwise component of normal stress $\overline{u^2v}$ and (d) the streamwise transport of the vertical component of normal stress $\overline{uv^2}$ for tests R3 and R4 ($b = 0.8$ m) over flow depth normalised by boundary layer thickness y/δ 75

Figure 3.9: Distribution of (a) streamwise transport of the streamwise component of normal stress $\overline{u^3}$, (b) vertical transport of the vertical component of normal stress $\overline{v^3}$ (c) vertical transport of the streamwise component of normal stress $\overline{u^2v}$ and (d) the streamwise transport of the vertical component of normal stress $\overline{uv^2}$ for tests R5 and R6 ($b = 1.22$ m) over flow depth normalised by boundary layer thickness y/δ 76

Figure 3.10: Distribution of the Reynolds shear stress normalised with friction velocity $-\overline{uv}/u_\tau^2$ for tests R1 – R6 (present investigation) and FS1 (Flack et al. 2005) over flow depth normalised by boundary layer thickness y/δ 77

Figure 3.11: Distribution of the contributions of (a) Q1 outward interactions ($u > 0, v > 0$), (b) Q2 ejection events ($u < 0, v > 0$), (c) Q3 inward interactions ($u < 0, v < 0$) and (d) Q4 sweep events ($u > 0, v < 0$) for which $H = 0$ to the total Reynolds shear stress $-\overline{uv}$ for tests R1, R3 and R5 ($h = 0.12$ m) over flow depth normalised by boundary layer thickness y/δ 78

- Figure 3.12: Distribution of the contributions of (a) Q1 outward interactions ($u > 0, v > 0$), (b) Q2 ejection events ($u < 0, v > 0$), (c) Q3 inward interactions ($u < 0, v < 0$) and (d) Q4 sweep events ($u > 0, v < 0$) for which $H = 0$ to the total Reynolds shear stress $-\overline{uv}$ for tests R1 and R4 ($AR = 3.3$) over flow depth normalised by boundary layer thickness y/δ 79
- Figure 3.13: Distribution of the contributions of (a) Q1 outward interactions ($u > 0, v > 0$), (b) Q2 ejection events ($u < 0, v > 0$), (c) Q3 inward interactions ($u < 0, v < 0$) and (d) Q4 sweep events ($u > 0, v < 0$) for which $H = 0$ to the total Reynolds shear stress $-\overline{uv}$ for tests R3 and R6 ($AR = 6.6$) over flow depth normalised by boundary layer thickness y/δ 80
- Figure 3.14: Distribution of the contributions of (a) Q1 outward interactions ($u > 0, v > 0$), (b) Q2 ejection events ($u < 0, v > 0$), (c) Q3 inward interactions ($u < 0, v < 0$) and (d) Q4 sweep events ($u > 0, v < 0$) for which $H = 0$ to the total Reynolds shear stress $-\overline{uv}$ for tests R1 and R2 ($b = 0.4$ m) over flow depth normalised by boundary layer thickness y/δ 81
- Figure 3.15: Distribution of the contributions of (a) Q1 outward interactions ($u > 0, v > 0$), (b) Q2 ejection events ($u < 0, v > 0$), (c) Q3 inward interactions ($u < 0, v < 0$) and (d) Q4 sweep events ($u > 0, v < 0$) for which $H = 0$ to the total Reynolds shear stress $-\overline{uv}$ for tests R3 and R4 ($b = 0.8$ m) over flow depth normalised by boundary layer thickness y/δ 82
- Figure 3.16: Distribution of the contributions of (a) Q1 outward interactions ($u > 0, v > 0$), (b) Q2 ejection events ($u < 0, v > 0$), (c) Q3 inward interactions ($u < 0, v < 0$) and (d) Q4 sweep events ($u > 0, v < 0$) for which $H = 0$ to the total Reynolds shear stress $-\overline{uv}$ for tests R5 and R6 ($b = 1.22$ m) over flow depth normalised by boundary layer thickness y/δ 83
- Figure 3.17: Distribution of the contributions of (a) Q1 outward interactions ($u > 0, v > 0$), (b) Q2 ejection events ($u < 0, v > 0$), (c) Q3 inward interactions ($u < 0, v < 0$) and (d) Q4 sweep events ($u > 0, v < 0$) for which $H = 1$ to the total Reynolds shear stress $-\overline{uv}$ for tests R1, R3 and R5 ($h = 0.12$ m) over flow depth normalised by boundary layer thickness y/δ 84
- Figure 3.18: Distribution of the contributions of (a) Q1 outward interactions ($u > 0, v > 0$), (b) Q2 ejection events ($u < 0, v > 0$), (c) Q3 inward interactions ($u < 0, v < 0$) and (d) Q4 sweep events ($u > 0, v < 0$) for which $H = 1$ to the total Reynolds shear stress $-\overline{uv}$ for tests R1 and R2 ($b = 0.4$ m) over flow depth normalised by boundary layer thickness y/δ 85
- Figure 3.19: Distribution of the contributions of (a) Q1 outward interactions ($u > 0, v > 0$), (b) Q2 ejection events ($u < 0, v > 0$), (c) Q3 inward interactions ($u < 0, v < 0$) and (d) Q4 sweep events ($u > 0, v < 0$) for which $H = 1$ to the total Reynolds shear stress $-\overline{uv}$ for tests R3 and R4 ($b = 0.8$ m) over flow depth normalised by boundary layer thickness y/δ 86

- Figure 3.20: Distribution of the contributions of (a) Q1 outward interactions ($u > 0, v > 0$), (b) Q2 ejection events ($u < 0, v > 0$), (c) Q3 inward interactions ($u < 0, v < 0$) and (d) Q4 sweep events ($u > 0, v < 0$) for which $H = 1$ to the total Reynolds shear stress $-\overline{uv}$ for tests R5 and R6 ($b = 1.22$ m) over flow depth normalised by boundary layer thickness y/δ 87
- Figure 3.21: Distribution of the number of (a) Q1 inward interactions ($u > 0, v > 0$), (b) Q2 ejection events ($u < 0, v > 0$), (c) Q3 outward interactions ($u < 0, v < 0$) and (d) Q4 sweep events ($u > 0, v < 0$) normalised with the total number of events with $H = 1$ for tests R1, R3 and R5 ($h = 0.12$ m) over the flow depth y normalised with boundary layer thickness δ 88
- Figure 3.22: Distribution of the number of (a) Q1 inward interactions ($u > 0, v > 0$), (b) Q2 ejection events ($u < 0, v > 0$), (c) Q3 outward interactions ($u < 0, v < 0$) and (d) Q4 sweep events ($u > 0, v < 0$) normalised with the total number of events with $H = 1$ for tests R2, R4 and R6 ($h > 0.12$ m) over the flow depth y normalised with boundary layer thickness δ 89
- Figure 3.23: Distribution of (a) U/U_e (inset with U^+ vs. y^+ included), (b) Reynolds shear stress normalised with shear velocity $-\overline{uv}/u_\tau^2$ (c) streamwise turbulence intensity u_{rms}/u_τ and (d) vertical turbulence intensity v_{rms}/u_τ for tests R5 ($Z = 0$) and R5-C ($Z = 0.32$ m) over the flow depth y normalised with boundary layer thickness δ 90
- Figure 4.1: Description of channel flow around a circular cylinder with blockage ratio D/b 124
- Figure 4.2: Photographs of equilibrium scour profiles with $D/b = 0.05$ (left) and $D/b = 0.10$ (right) (Williams et al. 2018) 124
- Figure 4.3: Distribution of streamwise velocity U (m/s) for two streamwise locations in the central plane ($Z/D = 0$) in the absence of the cylinder for (a) test B1 ($b = 0.4$ m), (b) B2 ($b = 0.8$ m) and (c) B3 ($b = 1.22$ m) 125
- Figure 4.4: Distribution of (a) streamwise velocity U , (b) Reynolds shear stress $-\overline{uv}/U_e^2$, (c) streamwise turbulence strength u_{rms} and (d) vertical turbulence strength v_{rms} for approach flow of tests B1, B2 and B3 in the absence of the cylinder 125
- Figure 4.5: Photographs of equilibrium scour formation for test B1 ($D/b = 0.14$, left), test B2 ($D/b = 0.07$, middle) and test B3 ($D/b = 0.05$, right) 126
- Figure 4.6: Plan-view profile measurements of equilibrium scour formation for tests B1, B2 and B3 in XZ plane 127
- Figure 4.7: Bed profile measurements of equilibrium scour formation for tests B1, B2 and B3 in XY plane along (a) the central plane with $Z/D = 0$, (b) the near-cylinder

plane with $Z/D \approx 0.5$ and (c) the mid-cylinder-wall plane with variable Z/D	128
Figure 4.8: Bed profile measurements in (a) the XZ plane at $Y/D = 0$ and (b) the XY plane at $Z/D = 0$ for tests S1 ($D/b = 0.14$), S2 ($D/b = 0.07$) and S3 ($D/b = 0.05$) .	129
Figure 4.9: Distribution of mean streamwise velocity U/U_e , mean vertical velocity V/U_e and Reynolds shear stress $-\overline{uv}/U_e^2$ over the depth of flow in plane A ($Z/D = 0$) for $X/D = \{-2.0, -1.0, 1.0, 2.0, 7.0\}$	130
Figure 4.10: Distribution of mean streamwise velocity U/U_e , mean vertical velocity V/U_e and Reynolds shear stress $-\overline{uv}/U_e^2$ over the depth of flow in plane B ($Z/D \approx 0.5$) for $X/D = \{-2.0, -0.5, 0, 0.5, 2.0, 7.0\}$	131
Figure 4.11: Distribution of the contribution of Q2 ejection events ($u < 0, v > 0$) at (a) $X/D = -0.5$ for $H = 0$, (b) $X/D = 0.5$ for $H = 0$, (c) $X/D = -0.5$ for $H = 1.75$ and (d) $X/D = 0.5$ for $H = 1.75$	132
Figure 4.12: Distribution of the contribution of Q4 sweep events ($u > 0, v < 0$) at (a) X/D $= -0.5$ for $H = 0$, (b) $X/D = 0.5$ for $H = 0$, (c) $X/D = -0.5$ for $H = 1.75$ and (d) $X/D = 0.5$ for $H = 1.75$	133
Figure 4.13: Bed profile measurements of equilibrium scour formation for tests B1, B2 and B3 in YZ plane along (a) the upstream spanwise plane ($X/D = -1.3$), (b) the spanwise central plane ($X/D = 0$) and (c) the downstream spanwise plane ($X/D = 1.75$)	134
Figure 4.14: Distribution of normalised streamwise velocity U/U_e in the central plane (plane A, $Z/D = 0$) for (a) test B1 ($D/b = 0.14$), (b) test B2 ($D/b = 0.07$) and (c) test B3 ($D/b = 0.05$)	135
Figure 4.15: Distribution of normalised streamwise velocity U/U_e in the near-cylinder plane (plane B, $Z/D \approx 0.5$) for (a) test B1 ($D/b = 0.14$), (b) test B2 ($D/b = 0.07$) and (c) test B3 ($D/b = 0.05$)	136
Figure 4.16: Distribution of normalised streamwise velocity U/U_e in the mid-cylinder- wall plane (plane C, $Z/D = \text{variable}$) for (a) test B1 ($D/b = 0.14$), (b) test B2 ($D/b = 0.07$) and (c) test B3 ($D/b = 0.05$)	137
Figure 4.17: Distribution of the normalised Reynolds shear stress $-\overline{uv}/U_e^2$ in the central plane (plane A, $Z/D = 0$) for (a) test B1 ($D/b = 0.14$), (b) test B2 ($D/b = 0.07$) and (c) test B3 ($D/b = 0.05$)	138
Figure 4.18: Distribution of the normalised Reynolds shear stress $-\overline{uv}/U_e^2$ in the near- cylinder plane (plane B, $Z/D \approx 0.5$) for (a) test B1 ($D/b = 0.14$), (b) test B2 ($D/b = 0.07$) and (c) test B3 ($D/b = 0.05$)	139

Figure 4.19: Distribution of the normalised Reynolds shear stress $-\overline{uv}/U_e^2$ in the mid-cylinder-wall plane (plane C, variable Z/D) for (a) test B1 ($D/b = 0.14$) and (b) test B2 ($D/b = 0.07$).....	140
Figure 4.20: Distribution of the spanwise vorticity Ω in the central plane (plane A, $Z/D = 0$) for (a) test B1 ($D/b = 0.14$), (b) test B2 ($D/b = 0.07$) and (c) test B3 ($D/b = 0.05$)	141
Figure 5.1: Scour formation for flow around a circular cylinder ($D = 0.062$ m) with a back splitter plate of length $2D$ and height $1.2D$, from Wu et al. (2018); figure used with permission from Wiley	179
Figure 5.2: Bed profile images from Lachaussee et al. (2018) for a submerged cylinder with (a) no scour ($Re_D \approx 1000$), (b) low U/U_c , ($Re_D \approx 2100$) (c) high U/U_c ($Re_D \approx 3200$) with horizontal base plate and (d) high U/U_c ($Re_D \approx 3200$) with no base plate (WS = wake scour, HSS = horseshoe scour); figure used with permission from APS	179
Figure 5.3: Schematic of submerged cylinder and countermeasure configuration for tests E1 (no countermeasure), E2 (cylinder with vertical plate) and E3 (cylinder with horizontal plate)	180
Figure 5.4: Approach flow velocity characteristics used for tests E1, E2 and E3, including (a) mean streamwise velocity and (b) Reynolds shear stress $-\overline{uv}/U_e^2$	181
Figure 5.5: Plan-view photographs of tests E1 (submerged cylinder), E2 (submerged cylinder with vertical plate) and E3 (submerged cylinder with horizontal plate).....	182
Figure 5.6: Plan view profile measurements of equilibrium scour formation for tests B1, E1, E2 and E3 in XZ plane ($Y/D = 0$)	183
Figure 5.7: Illustration of shear layer interaction in the wake of a circular cylinder without a splitter plate (above) and with a splitter plate of length greater than $1.5D$ (below) (from Anderson and Szewczyk 1997); figure used with permission from Copyright Clearance Center	184
Figure 5.8: Bed profile measurements of equilibrium scour formation for tests B1, E1, E2 and E3 in XY plane along (a) central plane (plane A, $Z/D = 0$), (b) near-cylinder plane (plane B, $Z/D \approx 0.5$) and (c) mid-cylinder-wall plane (plane C, $Z/D = 2.0$).....	185
Figure 5.9: Distribution of mean streamwise velocity U/U_e , mean vertical velocity V/U_e and Reynolds shear stress $-\overline{uv}/U_e^2$ over the depth of flow in plane B for $X/D = \{-2.0, -0.5, 0, 0.5, 2.0, 7.0\}$	186

Figure 5.10: Distribution of mean streamwise velocity U/U_e , mean vertical velocity V/U_e and Reynolds shear stress $-\overline{uv}/U_e^2$ over the depth of flow in plane A for $X/D = \{-2.0, -1, 1.0, 2.0, 7.0\}$	187
Figure 5.11: Transverse bed profile measurements of equilibrium scour formation for tests B1, E1, E2 and E3 in YZ plane along (a) spanwise upstream plane ($X/D = -1.3$), (b) spanwise central plane ($X/D = 0$ for tests B1, E1 and E2, $X/D = 0.5$ for test E3) and (c) spanwise downstream plane ($X/D = 1.75$)	188
Figure 5.12: Distribution of normalised streamwise velocity U/U_e in the central plane (plane A, $Z/D = 0$) for (a) test E1 (submerged cylinder), (b) test E2 (submerged cylinder with vertical plate) and (c) test E3 (submerged cylinder with horizontal plate)	189
Figure 5.13: Distribution of normalised streamwise velocity U/U_e in the near-cylinder plane (plane B, $Z/D \approx 0.5$) for (a) test E1 (submerged cylinder), (b) test E2 (submerged cylinder with vertical plate) and (c) test E3 (submerged cylinder with horizontal plate)	190
Figure 5.14: Distribution of normalised streamwise velocity U/U_e in the mid-cylinder-wall plane (plane C, $Z/D = 2.0$) for (a) test E1 (submerged cylinder), (b) test E2 (submerged cylinder with vertical plate) and (c) test E3 (submerged cylinder with horizontal plate)	191
Figure 5.15: Distribution of Reynolds shear stress $-\overline{uv}/U_e^2$ in the central plane (plane A, $Z/D = 0$) for (a) test E1 (submerged cylinder), (b) test E2 (submerged cylinder with vertical plate) and (c) test E3 (submerged cylinder with horizontal plate)	192
Figure 5.16: Distribution of Reynolds shear stress $-\overline{uv}/U_e^2$ in the near-cylinder plane (plane B, $Z/D \approx 0.5$) for (a) test E1 (submerged cylinder), (b) test E2 (submerged cylinder with vertical plate) and (c) test E3 (submerged cylinder with horizontal plate)	193

LIST OF ABBREVIATIONS/SYMBOLS

AR	b/h , channel aspect ratio
ASTM	American Society for Testing and Materials
b	channel width
B	constant in logarithmic law equation
C	discrete cross-correlation function for PIV processing
C_c	coefficient of sediment gradation
C_D	drag coefficient of cylinder
C_u	coefficient of sediment uniformity
D	cylinder diameter
D/b	blockage ratio
$(D/b)_{max}$	maximum value of blockage ratio
D/d_{50}	relative coarseness
d_{16}	sediment particle size of which 16 percent is finer
d_{50}	median sediment diameter
d_{84}	sediment particle size of which 84 percent is finer
d_{se}	maximum equilibrium scour depth
d_{se}/D	relative scour depth
Δt	time step between concurrent laser pulses in PIV system
ΔU^+	roughness function
h	flow depth
H	height of submerged cylinder
H	Reynolds shear stress magnitude parameter
h/D	flow shallowness

H_l	height of vertical splitter plate
i	vertical coordinate direction for PIV images
j	streamwise coordinate direction for PIV images
k	height of roughness elements
k	U_s/U
k_c	U_s/U_c
k_s	equivalent sand roughness height
k_s^+	$k_s u_\tau / \nu$, length scale for inner region of flow over rough wall
l	length of vertical splitter plate
l_l	length of horizontal plate
Q	flowrate
Re or Re_h	Reynolds number based on flow depth
Re_D	Reynolds number based on cylinder diameter
S	energy slope
U	mean streamwise velocity
u	fluctuating component of streamwise velocity
$\overline{u^2}$	normal stress in X direction
$\overline{u^3}$	streamwise transport of normal stress in X direction
U/U_c	flow intensity
U^+	streamwise velocity U normalised with friction velocity u_τ
U_c	critical velocity of sediment
U_e	maximum velocity of approach flow
$U_e^+ - U^+$	velocity defect
U_j	streamwise contracted jet velocity between wake and sidewall

u_{rms}	streamwise turbulence strength
$(u_{rms})_e$	free-stream streamwise turbulence strength
u_{rms}/u_τ	streamwise turbulence intensity
U_s	streamwise velocity along the separating streamline
$-\overline{uv}$	Reynolds shear stress in XY plane
$\overline{u^2v}$	vertical transport of normal stress in X direction
$\overline{uv^2}$	streamwise transport of normal stress in Y direction
u_τ	shear or friction velocity
V	mean vertical velocity
v	fluctuating component of vertical velocity
$\overline{v^2}$	normal stress in Y direction
$\overline{v^3}$	vertical transport of normal stress in Y direction
v_{rms}	vertical turbulence strength
v_{rms}/u_τ	vertical turbulence intensity
W	mean spanwise velocity
w	fluctuating component of spanwise velocity
w_l	width of horizontal plate
X	streamwise coordinate direction
Y	vertical coordinate direction
y^+	wall distance y normalised by v/u_τ
Z	spanwise coordinate direction
δ	boundary layer thickness
δ_l	depth of flow at which $u_{rms} = (u_{rms})_e$
ε_z	turbulent eddy viscosity in the spanwise direction

κ	von Kármán constant in logarithmic law equation
μ	dynamic viscosity of fluid
ν	kinematic viscosity of fluid
Π	Coles' wake parameter
ρ	density of fluid
σ_g	standard deviation of sediment particle size
τ_b or τ_w	bed or wall shear stress
τ_{bc}	critical bed shear stress of sediment
τ_{xy}	total stress in the XY plane
τ_{xz}	total stress in the XZ plane
Ω	spanwise vorticity

1 INTRODUCTION

1.1 The cost of scour

Scour and erosion have been well-established as leading causes of bridge failures; over half of bridge failures in the United States alone have been attributed to scour (Shirhole & Holt 1991, Wardhana & Hadipriono 2003). Damage to roadway infrastructure due to scour can consist of minor erosion or complete failure of a bridge. Restoration of an overwater bridge of any magnitude can require significant expenditure, cause disruption of local traffic and pose appreciable risk to surrounding ecosystems. In addition to capital for reconstruction, costs include rerouting of traffic and potential erection of temporary service bridges, which can exceed the cost of replacement itself by 50 percent (Melville & Coleman 2000). Furthermore, it has been estimated that indirect losses incurred by the general public, local business and industry are five times greater than reconstruction costs alone (Lagasse et al. 1995). Most crucially, due to the sudden nature of collapses caused by scour, failure of this type can result in loss of life.

In 1987, riprap protection around one pier of the Schoharie Creek Bridge on Interstate 90 over Schoharie Creek in New York failed due to spring flooding (see **Figure 1.1**). The unprotected pier footing failed in tension, causing collapse of the pier and two spans of the bridge, resulting in the death of 10 motorists (LeBeau & Wadia-Fascetti 2007). In 1995, a road bridge on Interstate 5 over Arroyo Pasajero in California collapsed, similarly under flood conditions (see **Figure 1.2**). The collapse resulted in the deaths of seven motorists. After investigation by the Federal Highway Administration (FHWA), the cause of failure was found to be bed degradation due to flooding (Lagasse et al. 1995).

In 2013, a single pier of the Bonnybrook Bridge over the Bow River in Alberta was undermined due to scour during an unprecedented rainfall event, causing derailment of six cars of a passing Canadian Pacific Railway freight train (see **Figure 1.3**). Fortunately, the collapse did not result in any fatalities. The derailed train cars were transporting industrial chemicals (including petroleum product) and flammable liquids, which were contained during the incident (Graveland & Krugel 2013, Government of Canada 2014). A subsequent investigation by the Government of Canada (2014) stated: “If measures are not taken to inhibit local scour, especially at bridges with spread footing foundations, there is an increased risk that high water events will lead to bridge failures.”

1.2 The mechanism of local scour

When a structure such as a circular cylinder is introduced into a fluvial environment, there are several features which are induced in the surrounding flow field. One such feature is the downflow, which is formed when flow decelerates leading up to the upstream face of the cylinder. Due to the nature of the velocity profile of the approach flow in an open channel, the pressure changes along the stagnation line, driving the flow downwards. This feature is known as the downflow, which impinges upon the bed at the base of the cylinder, initiating scour. The strength of the downflow is highly influential on the scouring process.

A horseshoe vortex (HSV) is formed when the downflow rolls up to form a vortex tube at the junction between the base of the cylinder and the bed. The legs of the HSV wrap around the cylinder, extending in the downstream direction and are occasionally broken up and shed. A necklace or collar vortex is formed when the adverse pressure gradient (APG) associated with the stagnation line causes flow separation in the near-bed region. The

boundary layer on the bed surface around the pier separates and the vorticity from the approach flow causes formation of a necklace vortex in the region of maximum shear stress in the vicinity of the cylinder. The necklace vortex is broken up in the wake region by the high bed shear stress and interaction with the wake vortices. The necklace vortex contributes to initiation of scour (Nasif et al. 2015), and the HSV is one of the primary mechanisms by which sediment is removed from around the base of the cylinder. The vortical motion of the HSV entrains sediment from the bed into the flow around the cylinder. The size and strength of the HSV are related to the size of the scour hole around the cylinder, and both will continue to increase until equilibrium is reached. This is the point at which the strength of the HSV is no longer sufficiently high to continue to remove sediment from the bottom of the scour hole, or when the critical shear stress of sediment at the bottom of the scour hole is no longer exceeded.

The vortices in the von Kármán vortex street are formed due to the shear layers which are detached from either side of the cylinder. The wake vortices shed alternately from the cylinder and carry the entrained sediment from the HSV region past the cylinder into the wake region. Downstream of the cylinder, the size of the wake vortices increases, causing them to weaken and deposit the sediment in dune-like formations. From this discussion, it can be inferred that the strength and structure of the downflow, the horseshoe vortex and the wake vortices are unsteady and highly influential on local scour around a cylinder. It is important to make note of the significant variation in structure, strength, and scale of each of the aforementioned turbulence structures.

1.3 Scale effects in hydraulic modelling

Experimental modelling of local scour around a cylinder has been comprehensively explored for an appreciable range of flow, structure and bed material characteristics. Typical scour experiments involve installation of a cylinder in a sediment recess filled with bed material of a prescribed size within a recirculating flume, from which point scour is allowed to progress until equilibrium is reached. The geometry of the scour formation is then measured to varying levels of detail, where the maximum depth of scour d_{se} (typically located near the upstream face of the cylinder) is the primary quantity of interest. Under prototype conditions, this would theoretically be taken as the minimum required foundation head, or the depth below which pier foundations should be placed in order to avoid the possibility of structural failure due to a loss of lateral support from the bed material. In practice, foundation head is determined on the basis of empirical equations, which have been developed by curve-fitting large quantities of laboratory data acquired through experimental methodology similar to what is described above. Dimensional analysis has indicated that the maximum depth of scour normalised with pier diameter d_{se}/D can be evaluated from a set of dimensionless variables, which can be further reduced under certain conditions. For fully turbulent subcritical flow aligned with a circular cylinder in acceptably-graded erodible sediment, relative scour depth d_{se}/D can be evaluated as described in **Equation 1.1**.

Equation 1.1:
$$\frac{d_{se}}{D} = f\left(\frac{U}{U_c}, \frac{h}{D}, \frac{D}{d_{50}}\right)$$

In **Equation 1.1**, U is the velocity of approach flow, U_c is the critical velocity of sediment, h is the depth of flow, D is the cylinder diameter, and d_{50} is the median sediment diameter.

The relationship between each dimensionless parameter and d_{se}/D has been well-established in literature (Melville & Coleman 2000, Ettema et al. 2011). However, analysis has indicated that commonly-used empirical equations in the form of **Equation 1.1** have a tendency to over-estimate d_{se}/D values acquired from laboratory measurements (Williams et al. 2013). Scale effects, which arise due to an imbalance in force ratios between a model and prototype, are certainly partially responsible for this discrepancy. This is particularly obvious in scaling of relative coarseness, D/d_{50} , which cannot be equated between the laboratory and the field. If sediment size were to be scaled similarly to cylinder diameter, the bed material would be in the size range for cohesive sediment, and flow-sediment interactions would not be accurately replicated in the model. Therefore, bed material size in the approximate range of d_{50} in the field is used for modelling, and the experimental value of D/d_{50} is significantly reduced.

There are other model effects to which the poor performance of scour-predicting equations can be attributed. In a laboratory flume experiment, bed sediment is typically well-graded and the approach flow is well-regulated and usually two-dimensional in the central region of flow at the position of the cylinder. These are controlled conditions under which natural river flow rarely, if ever, occurs. Therefore, the differences between a value of d_{se}/D estimated using an equation derived from laboratory results and an actual maximum depth of scour in the field can be understood. It has also been shown that prediction of scour in experiments with similar values of each governing parameter described in **Equation 1.1** yield different values of d_{se}/D , which implies that there are additional significant influences in scour modelling which have not been incorporated into scour estimation (Williams et al. 2016).

1.4 The influence of blockage ratio D/b on local scour

One such influence which has been previously explored in physical scour modelling is blockage ratio, D/b , where b is the channel width. While the effect of D/b on flow around bluff bodies has been widely investigated for a fixed bed condition (e.g. Ramamurthy and Lee 1973, Ramamurthy et al. 1989), the effect of D/b on local scour has not been clearly established. This is partially due to the generally significant relative width in naturally occurring rivers, which mostly eliminates channel blockage as a concern for scour in the field. Nonetheless, in a comprehensive review of pier scour processes, Ettema et al. (2011) stated that estimation of d_{se}/D at a pier can be “complicated” by close channel bank proximity.

The effect of channel blockage in scour experiments has been erroneously defined as negligible when D/b is less than ten percent (Chiew 1984). Laboratory flumes are usually constrained in width by facility size, and pier diameter D is generally chosen such that relative coarseness D/d_{50} is high enough to induce a measurable scour formation. Blockage ratio in experiments is therefore of greater concern than in the field. The influence of blockage ratio on scour around circular cylinders has been investigated by Hodi (2009), D’Alessandro (2013) and Tejada (2014). A review of these investigations, in which scour experiments were conducted for varying D/b , can be found in Williams et al. (2018). The results of this investigation as well as those of both D’Alessandro (2013) and Tejada (2014) reported changes in d_{se}/D when D/b was ten percent or less, which does not agree with the assumed threshold stated above. Examination of literature indicates that there are many experiments for which the effects of blockage have been ignored, despite having $D/b > 0.10$ (see **Figure 1.4**). Since code-specified design equations were derived from such

experiments, a correction factor for the effect of D/b in prediction of d_{se}/D was presented by Williams et al. (2018).

While the conclusions drawn from each investigation are fairly consistent and useful for the specific conditions under which the experiments were carried out, all inferences about the effect of blockage ratio on local scour are based on bed measurements of scour formations only. This is partially due to the difficulty in acquiring measurements in a flow field with sediment transport and bed formations. Point measurements made using Acoustic Doppler Velocimetry (ADV) and Laser Doppler Velocimetry (LDV) are time-consuming, and down-looking ADV probes do not allow for measurements within 5 cm of the free surface. Furthermore, solid features such as bedforms and cylinders will impede optical access in some locations, limiting applicability of techniques such as LDV and Particle Image Velocimetry (PIV). Nevertheless, the influence of channel blockage on the flow field surrounding a cylinder under local scour conditions cannot be fully understood without velocity measurements.

1.5 Use of Particle Image Velocimetry (PIV) in scour experiments in literature

Use of planar Particle Image Velocimetry (PIV) in scour experiments has met with some difficulty, largely due to the practical need for a transparent surface through which image capture can occur. Planar capture is then realistically restricted to the XZ and XY planes, since a reliable method for submerging a PIV camera in flow to capture measurements in the YZ plane (i.e. perpendicular to the main flow direction) has yet to be developed, to the knowledge of the author. Here, X is the streamwise coordinate direction, Y is the vertical coordinate direction and Z is the spanwise coordinate direction. While measurements in the

XZ plane would be possible with orientation of the laser sheet perpendicular to the flume sidewall and positioning of the camera lens in the downward vertical direction atop of the flume, the primary intention of the present experiments was to capture the flow field in the *XY* plane, in which velocity measurements using ADV are commonly presented for scour experiments. The unscoured bed material does impede image capture in the region below the original bed level in this plane; however, PIV measurements were captured in the entire flow field above this location.

Unger and Hager (2007) reported on the characteristics of the downflow and horseshoe vortex around a bridge pier. The authors assumed that the flow field around a half-cylinder placed against a transparent flume sidewall in erodible sediment would be representative of half of the flow field around a full cylinder. PIV measurements were captured in the *XY* plane for this set-up, and as such measurements within the scour hole were obtainable. Practically, however, this configuration describes abutment scour, and cannot really be viewed as intended by the authors. Kirkil et al. (2008) were able to capture streamline patterns at the free surface in the wake region of flow around a circular cylinder with scour using a large-scale Particle Image Velocimetry (LSPIV) system in the *XZ* plane. Zhang et al. (2009) explored local scour around a spur dyke placed against a transparent flume sidewall in a sediment recess. PIV measurements were made in the *XY* and *XZ* planes, and due to the location of the spur dyke, flow field measurements were once again captured within the scour hole. In general, the limitations of PIV use in scour experiments are well-demonstrated in the literature.

1.6 Description of thesis objectives

The present investigation explores blockage effects in local scour experimentally, using planar Particle Image Velocimetry (PIV) to acquire detailed flow field measurements. The method by which the influence of channel blockage on local scour can be isolated in experiments is by alteration of the effective width of flow, b , while holding all other scour-governing parameters constant (i.e. flow intensity U/U_c , flow shallowness h/D , and relative coarseness D/d_{50}). For experiments of this nature, movable PVC walls are installed in the sediment recess and b can be manipulated. In doing so, D/b is altered, but so too is the channel aspect ratio $AR = b/h$. The effect of channel aspect ratio must first be explored in order to establish the role of horizontal confinement (changes in b) and vertical confinement (changes in h) on the approach flow.

Earlier discussion on the prevalence of failure due to scour in the field has similarly established the need for optimization of scour countermeasure methods for long-term infrastructure preservation. As with previous work on blockage effects in scour, the efficacy of scour countermeasures has been primarily explored on the basis of reduction of maximum equilibrium scour depth. While this quantity is of great significance in the context of scour design, the mechanisms by which countermeasures provide protection can be unclear. To this end, exploration of flow field measurements for local scour with countermeasures for mitigation in practice is required.

The objectives of the thesis are as follows:

1. Characterize the role of aspect ratio ($AR = b/h$) on flow characteristics over a porous bed with no scour;

2. Explore the influence of channel blockage ratio (D/b) on the flow field mechanisms surrounding a circular cylinder under equilibrium of local scour;
3. Investigate the effects of two types of scour countermeasures on local scour around a circular cylinder at an equilibrium condition.

1.7 Structure of thesis and scope of experimental work

Table 1.1 shows the structure of chapters for the current investigation. In **Chapter 1**, the scour problem is discussed and background for the problem statement is provided. Project objectives are stated and the thesis is outlined. In **Chapter 2**, the laboratory facility used for experiments is described. A general outline of the experimental program for the thesis is provided. The experimental methodology is discussed and details of the principles of the Particle Image Velocimetry (PIV) system are included. A detailed description of the applicable experimental program is included in each corresponding chapter. **Chapter 3** discusses the results of PIV measurements for straight channel flow over continuous roughness, whose flow dimensions correspond to AR values in the range of 1.90 to 10.2. Analysis of the mean and turbulence properties as well as third-order turbulent moments and quadrant analysis are discussed in order to determine the effects of changes in flow confinement. In **Chapter 4**, PIV results are presented for the flow field around an emergent cylinder for D/b values of 0.05, 0.07 and 0.014. Distribution of time-averaged flow characteristics such as streamwise velocity, Reynolds shear stress and spanwise vorticity are explored for three streamwise-vertical planes (in the centre of the channel, close to the cylinder and between the cylinder and wall) in order to understand the effect of sidewall proximity on local scour at an equilibrium condition. **Chapter 5** discusses changes induced in the flow field surrounding a submerged cylinder under local scour at an equilibrium

condition due to installation of two scour countermeasures, the first of which is a vertical splitter plate and the second of which is a horizontal base plate.

Table 1.1: Description of thesis structure

Chapter	Title
1	Introduction
2	Methodology
3	Role of channel aspect ratio on flow over a porous bed
4	Role of channel blockage ratio on local scour flow field mechanisms
5	Evaluation of flow-altering countermeasures for local scour around a circular cylinder
6	Conclusions and recommendations



Figure 1.1: Schoharie Creek Bridge collapse in NY, 1987 (Croyle 2017)



Figure 1.2: Arroyo Pasajero bridge collapse in CA, 1995 (Richardson 1995)



Figure 1.3: Bonnybrook Bridge collapse in AB, 2013 (Government of Canada 2014)

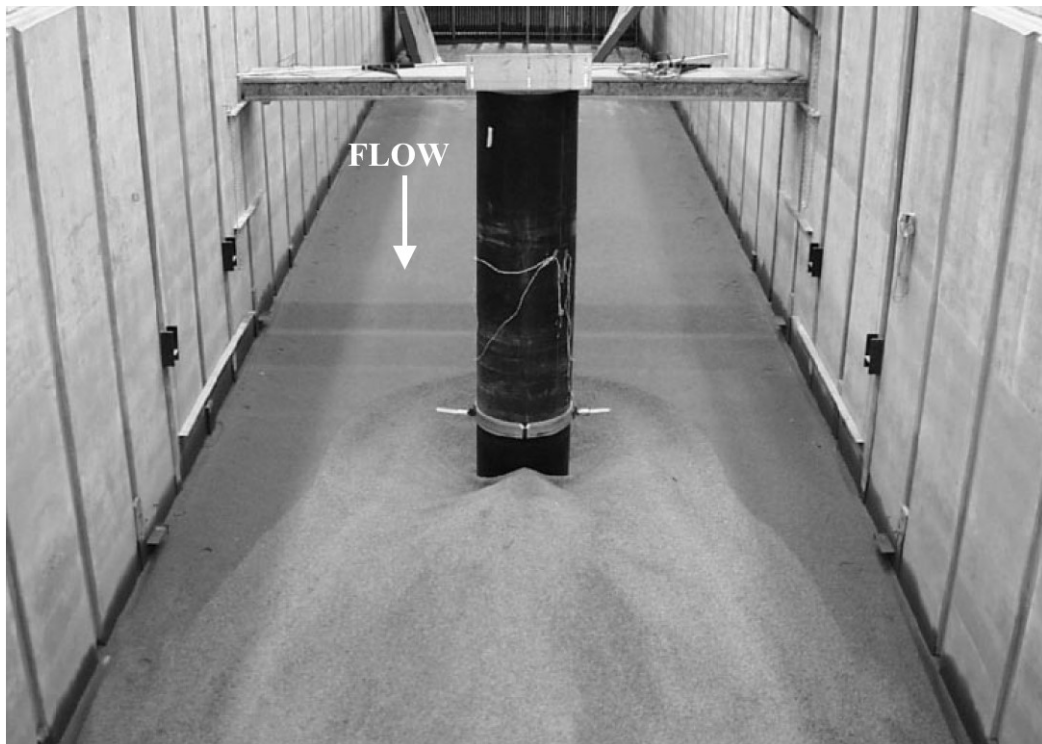


Figure 1.4: Large-scale clear-water scour test with $D = 0.91$ m, $b = 6$ m ($D/b = 0.15$) (Sheppard et al. 2004); figure used with permission from ASCE

1.8 References

1. Chiew, Y. M. (1984). *Local scour at bridge piers*. Doctoral dissertation. University of Auckland, Auckland, New Zealand.
2. Croyle, J. (2017, April 6). On this date: Thruway bridge collapses into Schoharie Creek in 1987. Retrieved September 2, 2019, from newyorkupstate.com website: https://www.newyorkupstate.com/capital-region/2017/04/on_this_date_thruway_bridge_collapses_into_schoharie_creek_in_1987.html
3. D'Alessandro, C. (2013). *Effect of blockage on cylindrical bridge pier local scour*. M.A.Sc. thesis. University of Windsor, Windsor, Canada.
4. Ettema, R., Melville, B. W., & Constantinescu, G. (2011). *Evaluation of bridge scour research: Pier scour processes and predictions*. Washington, DC: Transportation Research Board of the National Academies.
5. Government of Canada (2014, December 17). Railway Investigation Report R13C0069 - Transportation Safety Board of Canada. Retrieved March 8, 2018, from <http://www.bst-tsb.gc.ca/eng/rapports-reports/rail/2013/r13c0069/r13c0069.asp>
6. Graveland, B., & Krugel, L. (2013). Train Derails in Calgary on Bridge, Carries Petroleum Product. *The Canadian Press, Posted, 6(27), 2013*.
7. Hodi, B. (2009). *Effect of blockage and densimetric Froude number on circular bridge pier local scour*. M.A.Sc. thesis. University of Windsor, Windsor, Canada.
8. Kirkil, G., Constantinescu, S. G., & Ettema, R. (2008). Coherent structures in the flow field around a circular cylinder with scour hole. *Journal of Hydraulic*

- Engineering*, 134(5), 572–587. [https://doi.org/10.1061/\(ASCE\)0733-9429\(2008\)134:5\(572\)](https://doi.org/10.1061/(ASCE)0733-9429(2008)134:5(572))
9. Lagasse, P. F., Thompson, P. L., & Sabol, S. A. (1995). Guarding against scour. *Civil Engineering; New York*, 65(6), 56.
 10. LeBeau, K. H., & Wadia-Fascetti, S. J. (2007). Fault tree analysis of Schoharie Creek bridge collapse. *Journal of Performance of Constructed Facilities*, 21(4), 320–326. [https://doi.org/10.1061/\(ASCE\)0887-3828\(2007\)21:4\(320\)](https://doi.org/10.1061/(ASCE)0887-3828(2007)21:4(320))
 11. Melville, B. W., & Coleman, S. E. (2000). *Bridge Scour*. Water Resources Publication.
 12. Nasif, G., Balachandar, R., & Barron, R. M. (2015). Characteristics of flow structures in the wake of a bed-mounted bluff body in shallow open channels. *Journal of Fluids Engineering*, 137(10), 101207. <https://doi.org/10.1115/1.4030537>
 13. Ramamurthy, A. S., Balachandar, R., & Vo, D. N. (1989). Blockage correction for sharp-edged bluff bodies. *Journal of Engineering Mechanics*, 115(7), 1569–1576. [https://doi-org/10.1061/\(ASCE\)0733-9399\(1989\)115:7\(1569\)](https://doi-org/10.1061/(ASCE)0733-9399(1989)115:7(1569))
 14. Ramamurthy, A. S., & Lee, P. M. (1973). Wall effects on flow past bluff bodies. *Journal of Sound and Vibration*, 31(4), 443–451. [https://doi.org/10.1016/S0022-460X\(73\)80259-7](https://doi.org/10.1016/S0022-460X(73)80259-7)
 15. Richardson, E. V. (1995). *I-5 bridge collapse, CA 3/10/95. Original: 12 35mm Slides and 1 p*. Retrieved from <https://mountainscholar.org/handle/10217/170449>
 16. Sheppard, D. M., Odeh, M., & Glasser, T. (2004). Large scale clear-water local pier scour experiments. *Journal of Hydraulic Engineering*, 130(10), 957–963. [https://doi.org/10.1061/\(ASCE\)0733-9429\(2004\)130:10\(957\)](https://doi.org/10.1061/(ASCE)0733-9429(2004)130:10(957))

17. Shirhole, A. M., & Holt, R. C. (1991). Planning for a comprehensive bridge safety program. *Transportation Research Record*, 1290, 39–50.
18. Tejada, S. (2014). *Effects of blockage and relative coarseness on clear water bridge pier scour*. M.A.Sc. thesis. University of Windsor, Windsor, Canada.
19. Unger, J., & Hager, W. H. (2007). Down-flow and horseshoe vortex characteristics of sediment embedded bridge piers. *Experiments in Fluids*, 42(1), 1–19. <https://doi.org/10.1007/s00348-006-0209-7>
20. Wardhana, K., & Hadipriono, F. C. (2003). Analysis of recent bridge failures in the United States. *Journal of Performance of Constructed Facilities*, 17(3), 144–150. [https://doi.org/10.1061/\(ASCE\)0887-3828\(2003\)17:3\(144\)](https://doi.org/10.1061/(ASCE)0887-3828(2003)17:3(144))
21. Williams, P., Balachandar, R., & Bolisetti, T. (2013). Evaluation of local bridge pier scour depth estimation methods. *Proceedings of the 24th Canadian Congress of Applied Mechanics, Saskatoon, SK, Canada*, 2–6.
22. Williams, P., Bolisetti, T., & Balachandar, R. (2016). Evaluation of governing parameters on pier scour geometry. *Canadian Journal of Civil Engineering*, 44(1), 48–58. <https://doi.org/10.1139/cjce-2016-0133>
23. Williams, P., Bolisetti, T., & Balachandar, R. (2018). Blockage correction for pier scour experiments. *Canadian Journal of Civil Engineering*, 45(5), 413–417. <https://doi.org/10.1139/cjce-2017-0563>
24. Zhang, H., Nakagawa, H., Kawaike, K., & Baba, Y. (2009). Experiment and simulation of turbulent flow in local scour around a spur dyke. *International Journal of Sediment Research*, 24(1), 33–45. [https://doi.org/10.1016/S1001-6279\(09\)60014-](https://doi.org/10.1016/S1001-6279(09)60014-7)

2 METHODOLOGY

2.1 Description of experimental facility

Experiments were carried out at the Ed Lumley Centre for Engineering Innovation at the University of Windsor, Canada. The laboratory facility contains a horizontal flume that is 10.5 m in length, 0.84 m in depth and 1.22 m in width. A schematic of the flume is shown in **Figure 2.1**. The flume is fitted with two flow conditioners upstream of the test section, the first of which is constructed out of 0.5-in PVC pipe sections. The second flow conditioner consists of fine polycarbonate honeycomb sections. As shown in **Figure 2.1**, a PVC ramp leads to the test section, which is a sediment recess of 3.68 m in length and 0.23 m in depth, encompassing the width of the flume. The sediment recess is filled with granular material with $d_{50} = 0.74$ mm, $\sigma_g = \sqrt{d_{84}/d_{16}} = 1.34$, $C_u = d_{60}/d_{10} = 1.6$ and $C_c = d_{30}^2/(d_{10} \times d_{60}) = 0.96$. The material is classified as poorly graded sand according to ASTM standards. The critical velocity of sediment (U_c) for the bed material was evaluated using standard methods, which have been detailed in previous works (Williams et al. 2016, 2018).

A boundary layer trip is located at the beginning of the sediment recess. The depth of flow at the cylinder was adjusted by a gate located at the downstream end of the flume, preceding the outlet tank. The flow is serviced by a 60-HP centrifugal pump. The flow was calibrated with 30°, 60° and 90° v-notch weirs, using methods described in the U.S. Department of the Interior Bureau of Reclamation Water Measurement Manual (2001). The Kindsvater-Shen relationship and 8/15 triangular weir equation were used to calculate flow rate and develop the performance curve for the flume pump in the absence of the installed test

section. The orientation of the flume and experimental measurements correspond to X in the streamwise direction, Y in the vertical direction, and Z in the spanwise or transverse direction. The bed level was taken as 0 in the vertical direction for all experiments and the geometric centre of the cylinder was taken as the origin in the XZ plane for local scour tests. The mean velocity components U , V and W correspond to velocity in the X -, Y - and Z -directions respectively; the fluctuating velocity components u , v and w are similarly oriented.

2.2 *Experimental program*

A brief description of the experimental program is provided in **Table 2.1**. Further details for experiments will be included in the corresponding chapters. In **Chapter 3**, PIV measurements were undertaken in flow over the sand bed in order to characterize the approach flow conditions and explore the effect of channel aspect ratio (AR) on a porous bed. Seven experiments (R1 through R6) were conducted at a range of AR between 1.90 and 10.2, six of which were in the central plane (plane A) and one of which was in an off-centre plane (plane C) (see **Figure 2.2**). In **Chapter 4**, the effect of channel blockage on scour around an emergent cylinder was explored. Three tests (B1, B2 and B3) were conducted with constant D (pier diameter), constant h (depth of flow) and similar U (depth-averaged streamwise velocity of approach flow), and movable PVC sidewalls were employed in order to alter blockage ratio (D/b , where b is the channel width) while maintaining all other scour-governing parameters constant. Three additional tests (S1, S2 and S3) were carried out under the same conditions as tests B1, B2 and B3 for a submerged cylinder. PIV measurements for the emergent cylinder scour tests were taken in three planes of interest (**Figure 2.2**).

Table 2.1: Test parameters for experimental program in Chapters 3, 4 and 5

Chapter	Test ID	Plane(s) of interest	b (m)	h (m)	U (m/s)	Cylinder type
Chapter 3 (effect of aspect ratio)	R1	A	0.4	0.12	0.262	-
	R2	A	0.4	0.21	0.252	-
	R3	A	0.8	0.12	0.261	-
	R4	A	0.8	0.24	0.258	-
	R5	A	1.22	0.12	0.254	-
	R6	A	1.22	0.185	0.266	-
	R5-C	C	1.22	0.12	0.272	-
Chapter 4 (effect of blockage ratio)	B1	A, B, C	0.4	0.12	0.262	emergent
	B2	A, B, C	0.8	0.12	0.261	emergent
	B3	A, B, C	1.22	0.12	0.254	emergent
	S1	A	0.4	0.12	0.262	submerged
	S2	A	0.8	0.12	0.261	submerged
	S3	A	1.22	0.12	0.254	submerged
Chapter 5 (scour counter-measures)	E1	A, B, C	0.4	0.12	0.262	submerged
	E2	A, B, C	0.4	0.12	0.262	submerged with vertical splitter plate
	E3	A, B, C	0.4	0.12	0.262	submerged with horizontal base plate

Chapter 5 experiments focused on the efficacy of countermeasures as scour-mitigating techniques for submerged cylinders. Three tests were completed for local scour around a submerged cylinder with $D = 0.056$ m. Test E1 was the control test, i.e. the submerged cylinder did not have any flow-altering attachment. Test E2 was for a submerged cylinder with a vertical splitter plate, whose streamwise length and height were $2D$ and $1.72D$, respectively. For test E3, a submerged cylinder was fitted with a horizontal base plate (i.e. a rectangular collar) whose streamwise length and spanwise width were $2D$ and $7.1D$, respectively.

2.3 Test methodology

Prior to testing, the sediment in the test section was levelled using a trowel. For tests requiring an altered width of the channel (i.e. **Chapters 3** and **4**), movable PVC sidewalls were installed in the sediment recess and adjusted to the desired width (see **Figure 2.3**). For scour tests corresponding to **Chapters 4** and **5**, the necessary pier was installed in the centre of the flume. The flume was then filled with water to the desired depth. A calibration target for PIV image processing was suspended in the flume and calibration images were captured for each field-of-view. After the required calibration images were acquired, the target was removed from the flume and the pump was started and brought up to the required flow rate corresponding to an approximate flow intensity (U/U_c) of 0.85. For the straight channel flow tests described in **Chapter 3**, a flow intensity of 0.85 ensured that no general scour occurred. For tests corresponding to **Chapters 4** and **5**, this flow intensity was used in order to maintain clear-water conditions for local scour.

PIV measurements were then taken for each required field-of-view (FOV). PIV measurements for **Chapter 3** were taken in the central XY plane (plane A) within 30 minutes of starting the pump. The scour tests were left to run for 24 hours before PIV measurements were taken. Prior analysis has indicated that equilibrium of scour was reached within 24 hours, and changes in relative scour depth d_{se}/D were minimal beyond this point (D'Alessandro 2013). Prior to PIV measurements, the flow was seeded with 11- μm spherical glass particles. Measurements were taken in a single field-of-view for the straight channel tests. For each scour test, four fields-of-view were taken in each of planes A, B and C. This was done in order to ensure that the flow field was captured from the upstream extent of the scour hole to the end of the primary deposit in the wake of the

cylinder. During the scour tests, the image capture for each field-of-view was accomplished with a thin glass plate suspended on the free surface in the region of interest in order to eliminate distortion of the laser sheet from perturbations in the free-surface region due to the presence of the cylinder.

After all required PIV data was acquired, the pump was slowed gradually in order to avoid disturbance of the bed material and then shut off. For scour tests, the flume was drained slowly in order to avoid disturbance of the scour formation and a Leica laser distance meter was used to measure bed profiles in the streamwise direction at the location of each plane described in **Figure 2.2** as well as several spanwise profiles (at $X/D = -1.3$, $X/D = 0$ and $X/D = 1.75$) and the contour of the scour profile in the XZ plane. Bed profile measurements were unobtainable very close to the flume sidewall, due to limitations of the traverse system to which the laser distance meter was mounted. However, by observation of photographs taken of the final scour formation, the profiles in this region can be easily inferred. The uncertainty of the acquired bed measurements due to the accuracy of the laser distance meter was determined to be ± 0.05 mm from the resolution of the measurements.

2.4 Particle Image Velocimetry (PIV) system

A schematic of the two-dimensional planar Particle Image Velocimetry (PIV) system is shown in **Figure 2.4**. The PIV system was supplied by TSI and consists of an 8 MP Illunis CCD array camera and a dual pulse Litron L series_ Nd:YAG laser generating at 532 nm wavelength with an output energy of 135 mJ/pulse and a maximum repetition rate of 15 Hz. The laser sheet was expanded through a -15-mm cylindrical lens. The 8 MP camera was used to record images with a resolution of 3312×2488 pixels operating in dual-capture

mode. The camera was fitted with either a 28-105 mm or 50-mm Nikkor lens, depending on the flow dimensions and the distance between the camera and the plane of interest. The laser was mounted on a mechanical traverse system attached to a carriage on top of the flume, and as such could be moved in the spanwise and streamwise directions as required by the experimental program. The CCD array camera was mounted on a manual traverse system comprised of two tripods and a tripod slider on the flume catwalk, all of which was aligned parallel to the flume sidewall and therefore the plane of interest. A TSI PIV LaserPulse synchronizer was used to synchronize image capture for the required exposure time at the corresponding maximum pulse repetition rate (i.e. the time required for exposure and readout of two images) with the timing of the laser pulses for each frame (one pair of images).

The test section for PIV measurements in the sediment recess was located at a distance of 1.5 m downstream of the boundary layer trip. Measurements were obtained in the XY or vertical plane. It was previously determined that between 2000 and 3000 frames captured at a rate of 2 Hz were adequate for time-averaged data acquisition. The optimal pulse separation (Δt , or the time step between two concurrent laser pulses) in the sequence for each field-of-view was determined by adjusting the value of the time step such that the average length of the post-processed vectors (i.e. the displacement of particles) in the region of interest was approximately 8 pixels.

As can be inferred by the above description, there are several components in the PIV system which can result in error in the attained velocity measurements. The positioning of the calibration target, the physical characteristics of the chosen seeding particles, alignment and optical arrangement of the laser sheet, resolution and orientation of the camera, and

choice of post-processing methods all contribute to the total uncertainty of the experimental results. A detailed description of the sources of error and uncertainty analysis for velocity measurements can be found in **Appendix D**. The total propagated uncertainty of the velocity measurements acquired by the PIV system was estimated to be ± 0.015 m/s. The uncertainty analysis was based on the methods described in Park et al. (2008), which were adapted from the Visualization Society of Japan's (2002) guidelines.

PIV measurements for individual fields-of-view were taken and stitched together for the three planes in each test. The extent of each field-of-view is marked by white edges in the following sections. Discontinuities and scatter in any distribution of variables (particularly in the contours for higher-order quantities) can be attributed in part to variability in intensity along the laser sheet in the streamwise direction as well as reflections from the laser sheet on the bed and cylinder. However, there is a strong out-of-plane component in the three-dimensional flow around a cylinder which is not captured by a planar PIV and evaluation of Δt in such areas of cross-stream flow becomes complicated, particularly in the second field-of-view encapsulating the cylinder and near-wake region in the near-cylinder plane. Furthermore, the flow area within the scour hole was not captured due to the physical obstruction by the sediment recess in the field-of-view of the camera. Measurements in the region very close to the free surface were also not obtainable due to the presence of the glass plate in this region.

2.5 PIV processing details

Post-processing of the PIV images was done using PIVlab, a GUI-based open source MATLAB code (Thielicke & Stamhuis 2019). PIVlab uses cross-correlation to determine

displacement of illuminated tracer particles in the flow field. Prior to cross-correlation analysis of the flow field, a background subtraction feature in PIVlab was used to remove reflections and other undesirable features from the raw images. The background subtraction is a two-step process, wherein a background image is first generated from analysis of a set of images, after which the generated background image is subtracted from each image in the set. A high pass filter was also used to suppress low frequency background information and emphasize high frequency information (i.e. illuminated particles). The region of interest for the field-of-view was selected based on the location of the free surface, and the bed area and any solid features (scour formation, cylinder, etc.) were masked where applicable in order to minimize bad vectors in these regions.

In PIVlab, a cross-correlation algorithm is used to determine vectors in the flow field by deriving particle displacement between pairs of captured images. In this method, a “statistical pattern matching technique” is used to correlate the pattern of illuminated particles from a small interrogation area in each image of a pair, yielding a correlation matrix. The discrete cross correlation function is described by **Equation 2.1**:

Equation 2.1:
$$C(m, n) = \sum_i \sum_j A(i, j) B(i - m, j - n)$$

In **Equation 2.1**, A corresponds to the interrogation area in the first image of a frame and B similarly corresponds to the interrogation area from the second image in the same frame. The cross-correlation technique attempts to “locate” the seeding pattern in A in a region with the same pattern in B, and the intensity peak in the generated correlation matrix C (based on the cross-correlation function) is deemed the “most probable” particle displacement between the interrogation areas in each image. The intensity peak is located

by fitting a Gaussian 2·3 point function (i.e. for the adjacent pixels in the vertical and horizontal direction for each point) to the integer contents of the correlation matrix. The principle of the Gaussian 2·3 point function is described as fitting of a one-dimensional Gaussian function to the intensity distribution described by the correlation matrix for each axis (Thielicke & Stamhuis 2014).

The correlation matrix is calculated in the frequency domain using a fast Fourier transform (FFT). Although this method of calculation requires less computation time, its drawbacks include higher levels of noise in the correlation matrix, reduction in accuracy and complication of intensity peak determination. By altering the interrogation area size of the second pass of the FFT using the results of the first pass, this inaccuracy can be mitigated. Vortical flows will also further complicate location of the intensity peak. This is rectified by deformation of the interrogation area in B based on the results of the first pass of the FFT, in which overlap of the interrogation area allows for displacement information to be acquired at nine points within the interrogation area, as opposed to just at its centre. The newly distorted interrogation area B is then correlated with the original interrogation area A, resulting in a stronger intensity peak and higher accuracy (Thielicke & Stamhuis 2014). The calculation was conducted for this present study for two passes, the first with an interrogation area of 64×64 pixels and a 50% overlap. The final interrogation area was 32×32 pixels, which resulted in an area of 16×16 pixels.

After processing of all images, the vectors were converted from pixels per millisecond to metres per second using the externally taken calibrated image. Post-processing was completed in order to remove outliers in the results, using a standard deviation filter with a threshold of seven and a local median filter with a threshold of five. Missing vectors in

the field-of-view were interpolated and incorporated in the results. The mean vectors were calculated for the entire flow field and exported for analysis (Thielicke & Stamhuis 2014).

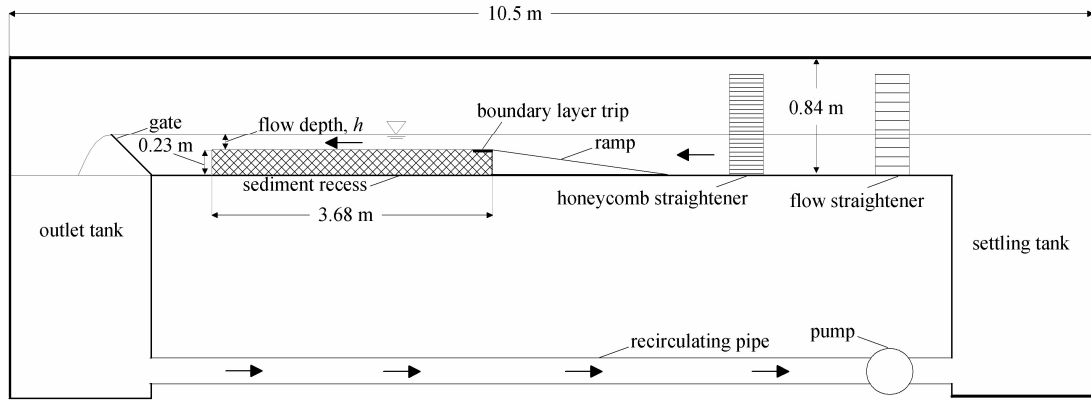


Figure 2.1: Schematic of horizontal laboratory flume used for experimentation

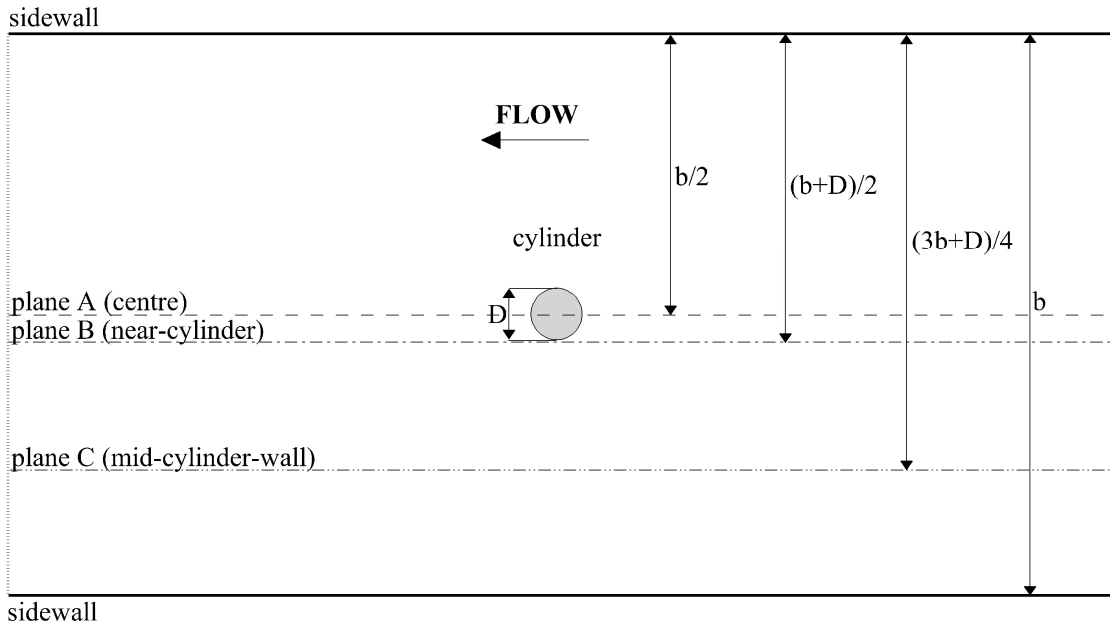


Figure 2.2: Location of planes of interest in local scour experimentation

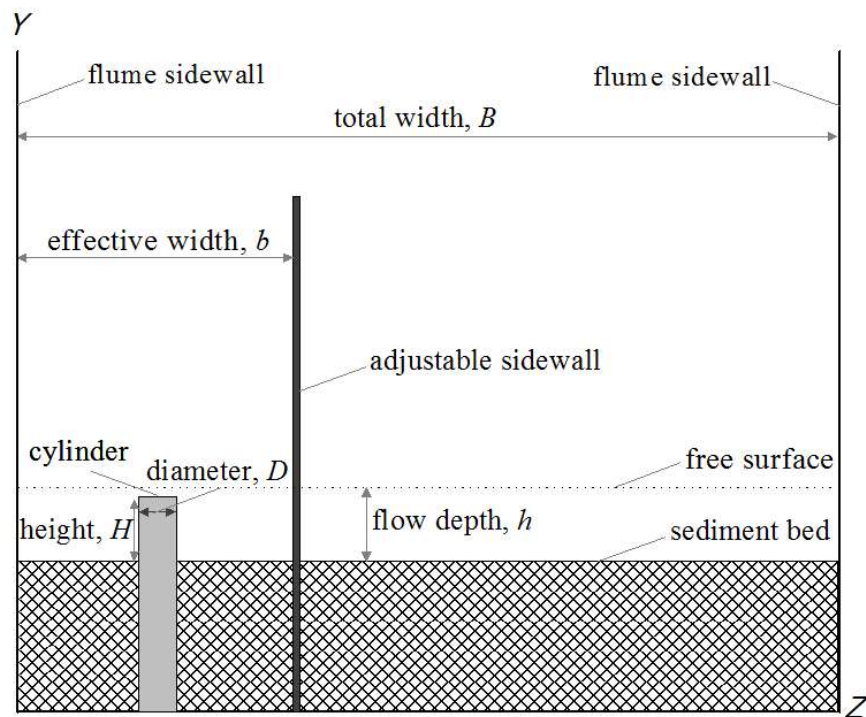
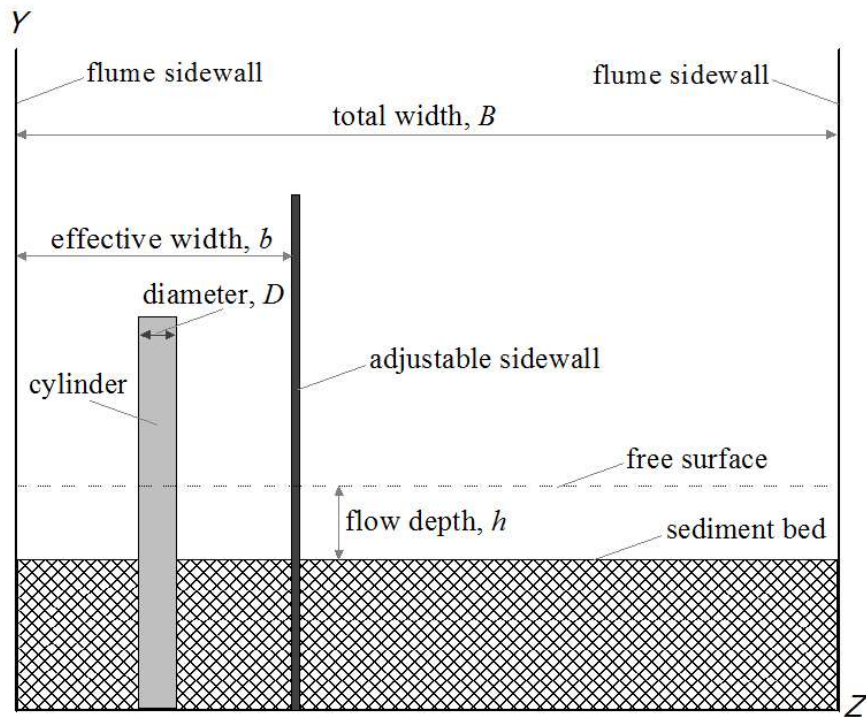


Figure 2.3: Schematic of experimental set-up for local scour experiments around an emergent cylinder (top) and a submerged cylinder (bottom)

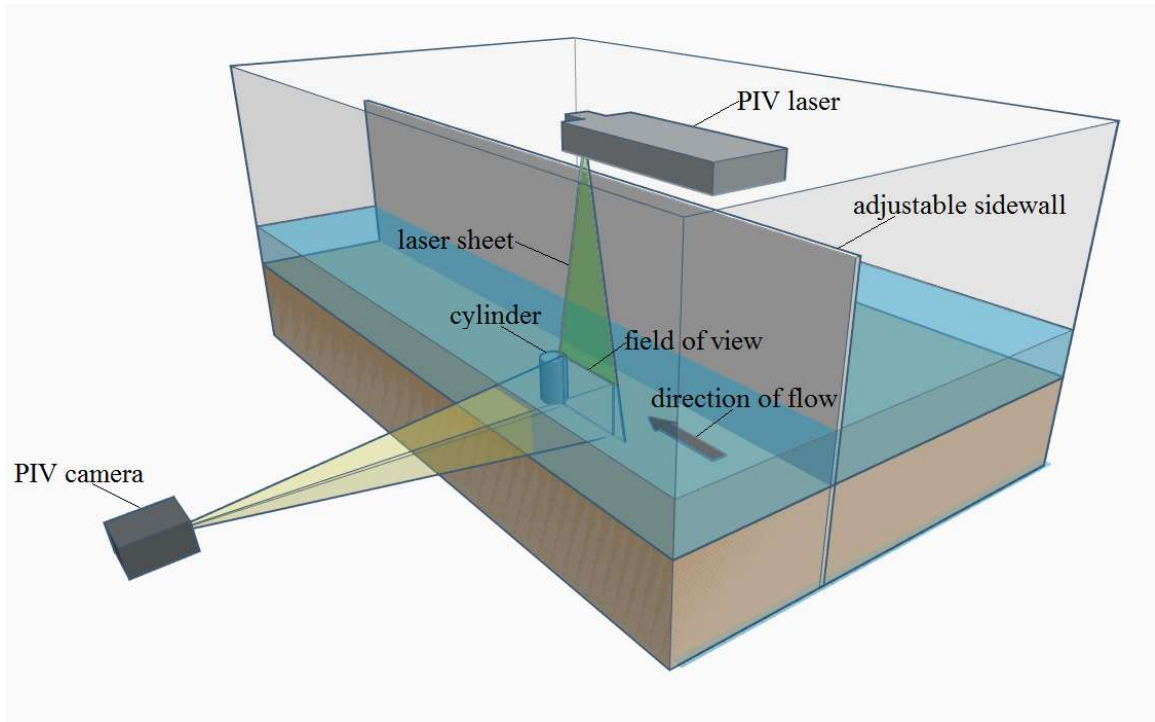


Figure 2.4: Schematic of planar Particle Image Velocimetry (PIV) setup for local scour experiments

2.6 References

1. D'Alessandro, C. (2013). Effect of blockage on cylindrical bridge pier local scour. M.A.Sc. thesis. University of Windsor, Canada.
2. Park, J., Derrandji-Aouat, A., Wu, B., Nishio, S., & Jacquin, E. (2008). Uncertainty analysis: Particle Imaging Velocimetry. *ITTC Recommended Procedures and Guidelines, International Towing Tank Conference (ITTC), Fukuoka, Japan, Sept, 14–20.*
3. United States Department of the Interior Bureau of Reclamation. (2001). *Water measurement manual*. Washington, DC: US Government Printing Office.
4. Thielicke, W., & Stamhuis, E. (2014). PIVlab – Towards User-friendly, Affordable and Accurate Digital Particle Image Velocimetry in MATLAB. *Journal of Open Research Software, 2*(1), e30. <https://doi.org/10.5334/jors.bl>
5. Thielicke, W., & Stamhuis, E. J. (2019, March 1). *PIVlab - Time-Resolved Digital Particle Image Velocimetry Tool for MATLAB*. <https://doi.org/10.6084/m9.figshare.1092508.v12>
6. Visualization Society of Japan. (2002). *Handbook of Particle Image Velocimetry*. Morikita Publishing Co. Ltd. (in Japanese).
7. Williams, P., Bolisetti, T., & Balachandar, R. (2016). Evaluation of governing parameters on pier scour geometry. *Canadian Journal of Civil Engineering, 44*(1), 48–58. <https://doi.org/10.1139/cjce-2016-0133>
8. Williams, P., Bolisetti, T., & Balachandar, R. (2018). Blockage correction for pier scour experiments. *Canadian Journal of Civil Engineering, 45*(5), 413–417. <https://doi.org/10.1139/cjce-2017-0563>

3 ROLE OF CHANNEL ASPECT RATIO ON FLOW OVER A POROUS BED

3.1 Introduction

The study of turbulence in open-channel flow is of interest to the hydraulic engineering community as it can influence the design of hydraulic structures such as bridge piers and abutments, design and maintenance of artificial channels, and prediction of diffusion and dispersion of sediments and contaminants in rivers. The influence of the channel confinement in terms of the aspect ratio (AR), defined as the ratio between channel width (b) and flow depth (h), has been extensively studied in open-channel literature to characterize the structure of turbulence in uniform open-channel flow. The AR in naturally occurring river flow is typically quite large ($b/h > 10$), such that a substantial width allows for a central region of flow which is unaffected by the proximity of the channel banks (Yokosi 1967, Yalin 1992). In the central region of wide open channels, the flow properties of the velocity and turbulence parameters are assumed to be two-dimensional (Nezu & Nakagawa 1993).

The same cannot be said of flow in a small-scale laboratory flume (mostly rectangular in cross-section), which is sized and operated according to facility constraints. Typical rectangular open-channel flumes in hydraulic engineering laboratories are 250 mm to 1 m in width and 250 to 600 mm in height, resulting in an $AR < 10$. As such, AR can severely influence the flow under study. While Nezu and Nakagawa (1993) classified flows with $AR < 5$ as narrow, many of the reported laboratory experiments in the literature are conducted in the intermediate range, for which $5 < AR < 10$ (Rodríguez & García 2008). Many practical applications of fluid-structure interaction problems require accurate

characterization of approach flow (for example, hydraulic structures such as bridge piers in scour-related research) in order to properly evaluate the flow field. Therefore, a clear understanding of the effect of the channel confinement and roughness on flow turbulence is required.

In order to explore the physical significance of the channel confinement and AR in the central region of the flow, it is important to first understand the associated structure of rough open-channel flow. Flow boundaries in open-channels induce anisotropy of turbulence, which in turn generate turbulence-driven secondary flows of Prandtl's second kind (Nezu & Nakagawa 1993). A flow field in which secondary flows exist is described by Prandtl (1926) as "a combination of the main flow with a 'secondary flow' at right angles to it." When studying open-channel flows, the hydraulic engineering community has devoted attention to the effect of the secondary flows over smooth beds and, more recently, over rough beds of gravel and sand with different topographies. The effect of the sidewalls on the flow was originally attributed to the effect of the corner flow as observed in duct flows. In fact, Nezu et al. (1985) demonstrated that these mean secondary flows exist even on a smooth bed and they are both driven and sustained by spatial gradients in the Reynolds stress components. A latter study by Anderson et al. (2015) attributes secondary currents to the imbalance between production and dissipation of turbulent kinetic energy near the bed which feeds the secondary advective velocities. On the other hand, the secondary flows are driven and sustained by the spanwise variation in imposed friction drag from roughness topology. Furthermore, the structure of turbulence (and therefore the mechanism of secondary currents) over continuous (i.e. Nikuradse-type) roughness will differ from that over a porous rough bed (Faruque & Balachandar 2010).

The study of secondary currents over porous beds (i.e. Albayrak & Lemmin 2011) has been limited in literature, and flow over loose gravel has received more attention than erodible sand due to the increased resistance of gravel to particle motion.

Mathematical analysis of the momentum equation in the spanwise direction (normal to the channel sidewalls) illustrates that the highest component of lateral (spanwise) velocity W will occur when the streamwise velocity component U is minimized and the spanwise gradient of the streamwise velocity ($\partial U/\partial z$) is maximized, which occurs at a boundary (Yang et al. 2012). This is illustrated by analysis of the momentum equation in the X -direction (**Equation 3.1**) as described by Yang et al. 2012 (summarized below).

$$\textbf{Equation 3.1:} \quad \frac{\partial(\rho UV - \tau_{xy})}{\partial y} + \frac{\partial(\rho UW - \tau_{xz})}{\partial z} = \rho g S$$

$$\textbf{Equation 3.2:} \quad \tau_{xz} = \mu \frac{\partial U}{\partial z} - \rho \overline{uW}$$

The second term on the LHS of **Equation 3.1** is considered negligibly small relative to the first term. The total shear stress in the XZ plane is defined in **Equation 3.2**. Equating the second term on the LHS of **Equation 3.1** to zero, substituting **Equation 3.2** into the expression and integrating with respect to Z gives **Equation 3.3**.

$$\textbf{Equation 3.3:} \quad UW - \nu \frac{\partial U}{\partial z} + \overline{uW} = 0$$

For fully turbulent flow, the viscous component is considered negligible, which leads to

$$\textbf{Equation 3.4:} \quad -UW - \overline{uW} = 0$$

An approximation of the second component is given by **Equation 3.5**.

Equation 3.5:
$$-\overline{uW} = \varepsilon_z \frac{\partial U}{\partial z}$$

In **Equation 3.5**, ε_z is the transverse turbulent eddy viscosity. Combining **Equation 3.5** with **Equation 3.4** gives

Equation 3.6:
$$W = \frac{\varepsilon_z}{U} \frac{\partial U}{\partial z}$$

From **Equation 3.6**, it can be seen that the spanwise component of velocity (W) is maximized when the streamwise velocity component U is minimized, or when the spanwise gradient of the streamwise velocity is maximized (Yang et al. 2012). Based on this description, secondary flows will occur due to the presence of channel sidewalls for all AR, but their effects may be minimal in the central region as noted by Rodríguez and García (2008). Secondary flow cells in the spanwise direction are formed when low momentum fluid is transported by $\frac{\partial U}{\partial z}$ in the near-sidewall region towards the central region and high momentum fluid is transported from the free surface towards the channel bed (Nezu & Nakagawa 1993). The secondary flows of Prandtl's second kind are considerably weaker relative to the main flow, with a magnitude of approximately 5% (Rodríguez & García 2008) to as low as 1% (Yang et al. 2012) of its streamwise velocity. Nonetheless, secondary flow cells which reach the central region of the channel are still capable of inflicting significant changes to the turbulence structure (Nikora & Roy 2012).

Channel sidewalls, bed roughness (porosity) and the free surface will all contribute to the structure of such secondary currents (Nezu & Nakagawa 1993). Secondary flow cells which have been observed at the corner of duct flow occur in narrow open channel flows as well. A corner bisector, whose slope is a function of flow depth, divides an upper cell

and lower cell, for which turbulent energy is dissipated by the channel sidewall and channel bed, respectively. The size of the upper cell will not change with AR; however, the size of the lower cell increases with AR before reaching constancy (Nezu et al. 1985). In a shallow flow, the location of the maximum velocity will occur below the free surface; this is the well-known velocity ‘dip’ phenomenon, and this phenomenon is attributed to the secondary flows as well (Nezu 2005). It can be concluded that the size and strength of secondary flows, and accordingly the extent to which they influence the flow and turbulence structure in the central region, is thus dictated by the channel dimensions, the flow submergence and the roughness topology.

Nezu et al. (1985) carried out an experimental study into the effects of AR on secondary currents in smooth open-channel flow (OCF). Prior analysis indicated that air duct flow was analogous to smooth OCF close to the sidewalls, with respect to the structure of secondary currents outside of the free surface region. Their experiments were intended to shed light on the initiation mechanism of secondary currents, and it was predetermined that while the presence of the free surface increased the intensity of secondary flow cells in this region, it did not necessarily contribute to their formation. Hot-wire anemometry was employed to acquire flow measurements in one-quarter of the flow cross-sectional area, close to the sidewall and in the lower half of the channel cross-section, near the flat smooth bed. Artificial sidewalls were used to manipulate the channel width, b , in order to attain a range of AR values between 2 and 10. The authors concluded that for $AR > 6$, a central zone of two-dimensional flow was observed in which secondary flow cells were not present, and for $AR = 1$, flow was fully three-dimensional (Nezu et al. 1985).

Although the nature of the turbulence and coherent structures due to the corner and sidewall proximity are not fully understood (Nikora & Roy 2012), there are some established relationships between mean flow and turbulence quantities governing the secondary currents. The secondary currents are generated by the anisotropy of turbulence (Prandtl's secondary flow of the second kind); as such the streamwise vorticity equation has been used to describe their origin (Yang et al. 2012). The origin of secondary currents has been a subject of debate amongst researchers. However, in open channel flow the turbulence anisotropy of the normal stresses (i.e. $\overline{w'w'} - \overline{v'v'}$) dominates the secondary shear stress term near the corners formed by the free surface and the sidewall.

As discussed, the vertical component of flow is influenced by secondary flow cells, and as a result the streamwise velocity distribution may change; however, since the magnitude of secondary flow is relatively small, the general characteristics of the streamwise velocity profile will still follow the log law. Velocity measurements taken for flow with $AR = 10$ in the investigation of Nezu et al. (1985) have shown that the streamwise velocity profile only deviates from the log law very close to the channel sidewall. However, because the spanwise velocity initiates the formation of secondary flow cells, the vertical and streamwise velocity components in the main flow are affected by the redistribution of the momentum (Rodríguez & García 2008) and the Reynolds shear stress $-\overline{u'v'}$ will be influenced by the presence of secondary flows.

To further complicate our understanding, most natural open-channel flows occur on rough beds. It has been established that there exists a distinction between secondary flows in smooth channels and those over rough beds. When roughness is introduced, the upper cell of the corner flow increases in strength while the lower cell decreases in strength, altering

secondary flow cell pattern across the width of flow. This has been demonstrated by the spanwise distribution of bed shear stress, which undulates in the cross-stream direction (Albayrak & Lemmin 2011, Stewart et al. 2019). Yang et al. (2012) similarly stated that the size of roughness does not influence the strength of secondary flows, but uniformity and the roughness pattern can have an effect. This is mainly due to the roughness difference between a smooth channel sidewall (especially in a laboratory flume) and a bed with any roughness type. However, since it is the anisotropy between the vertical and transverse velocity fluctuations which generates secondary currents, and these fluctuations are influenced by boundary conditions (i.e. boundary roughness), the presence of roughness will influence the secondary flow cells. For statistically homogeneous roughness in the streamwise direction, the dispersive stresses are related to the roughness effects as well as to the effect of the secondary currents (Nikora et al. 2019). On a smooth bed, these secondary currents must be related to the corner flow only.

In general, there is a consensus that the above constraints established for classification of AR are not necessarily applicable for flow over a rough bed. Secondary flow cells in flows over a rough bed have been found to extend over the entire spanwise cross-section of flow for AR up to a value of 20. The number of secondary flow cells has also been found to change with bed roughness when AR is held constant (Nikora & Roy 2012). The maintenance of secondary flows across the entire width of flow has been attributed to the difference in roughness between the sidewall and channel bed and therefore the aforementioned increase in strength of the upper cell of corner flow (Belcher & Fox 2009). Blanckaert et al. (2010) carried out detailed ADV measurements in the cross-stream plane in order to explore secondary flows over gravel beds for a range of AR between 6.2 and

11.9. The authors reported that secondary currents were found to be present throughout the entire width of flow for all values of AR, but that the strength of the secondary flow cells did weaken with increasing distance from the channel sidewall. The distribution of secondary currents in the cross-stream plane was also found to “considerably” influence the distribution of the Reynolds shear stress $-\overline{uv}$ (Blanckaert et al. 2010). Furthermore, secondary flow cells are generally more stable for rough bed flows than for smooth bed flows (Nezu & Nakagawa 1993). The majority of investigations in literature pertaining to secondary currents over rough beds employ fixed continuous roughness (e.g. Blanckaert et al. 2010, Rodríguez & García 2008) as opposed to an erodible porous bed (e.g. Albayrak & Lemmin 2011).

The present study investigates the effect of changing aspect ratio on streamwise turbulence in flow over a porous bed. The objective here is to consistently modify the turbulence by changing the AR as well as to keep the effect of the roughness minimal. In doing so, the roughness of the porous bed is held closer to the hydraulic condition of a smooth wall, where the shift of the velocity is small. It is expected that the friction will be influenced only by the roughness function ΔU^+ .

PIV measurements were undertaken in a horizontal flume with a test section comprising of a porous sand bed under varying values of AR. Many investigations in the literature have been conducted using gravel beds, in order to attain a higher value of Reynolds number while avoiding sediment transport due to general scour and to investigate the effect of the roughness that is in the hydraulically rough regime. These experiments have also primarily altered the value of AR by changing flow depth h while maintaining constant channel width b (Rodríguez & García 2008, Belcher & Fox 2009, Albayrak & Lemmin 2011). The present

investigation incorporated the use of artificial channel sidewalls in the test section in order to change the width of the channel as well as the depth of flow, also allowing for comparison of flow properties in tests with similar values of AR, but differing channel dimensions. By changing b and h for each test, the effect of horizontal and vertical confinement of flow on various mean velocity and turbulence properties are explored in order to establish the influence of AR on open-channel flow over a porous bed.

3.2 Background

Knowledge of the structure of the turbulent boundary layer (TBL) over a smooth wall is well-documented and is often used in comparison with the TBL over roughness of varying types, topologies and magnitudes. The structure of the TBL consists of an inner layer (dominated by viscous effects) and an outer layer (dominated by turbulence). The inner layer of the TBL is scaled with the friction velocity, u_τ (which is equal to $\sqrt{\tau_w/\rho}$) and the associated viscous length, ν/u_τ , where ν is the kinematic viscosity of the fluid. The outer layer is scaled with either u_τ or maximum flow velocity, U_e , and the boundary layer thickness, δ . The streamwise velocity U normalised with u_τ is known as U^+ , and the wall distance y normalised by ν/u_τ is denoted as y^+ . These quantities, known as inner variables, allow for distinction between the various regions of the TBL. The viscous sublayer, close to the smooth wall, is a region of small thickness for which $y^+ < 5$ and throughout which the mean velocity distribution is described by $U^+ = y^+$. The buffer layer is located in the region for which $5 < y^+ < 30$, and there is no universal expression which defines the mean velocity distribution in this layer. The overlap layer is characterized by both viscous forces and turbulence, and it is located in the region for which $y^+ > 30$ for smooth beds. In the overlap region, the well-known logarithmic law, which takes the form of **Equation 3.7**,

describes the mean velocity distribution in the region above the buffer layer and up to the point at which $y/h < 0.2$ (Nezu & Nakagawa 1993) or $y/\delta < 0.15$ (Jiménez 2004).

Equation 3.7:
$$\frac{U}{u_\tau} = \frac{1}{\kappa} \ln \left(\frac{yu_\tau}{\nu} \right) + B$$

In **Equation 3.7**, κ and B are taken as constant, where κ has been theoretically derived and experimentally confirmed, and B has been experimentally determined for various canonical flow conditions. The values of $\kappa = 0.41$ and $B = 5.0$ (Hinze 1959) are used for the current investigation. In the outer layer, the velocity deficit expression [**Equation 3.8**] shows the deviation from log law [**Equation 3.7**] which is described by the wake function (Coles 1956), where Π is the Coles' wake parameter.

Equation 3.8:
$$\frac{U_e - U}{u_\tau} = -\frac{1}{\kappa} \ln \left(\frac{y}{\delta} \right) + \frac{2\Pi}{\kappa} \cos^2 \left(\frac{\pi y}{2\delta} \right)$$

Although analysis of a smooth wall TBL is imperative for establishment of the above relationships, understanding of flow over roughness elements is more applicable in the field. This is particularly true of open-channel flow in rivers, where natural channel beds often consist of some type of sand grain or gravel roughness. Turbulent boundary layer theory is commonly applied to open-channel flow as well. The flow depth for open-channel flow (OCF) is also divided into an inner and outer region, each with a distinct characteristic velocity and length scale. However, the spanwise and vertical boundaries imposed by the channel sidewalls and presence of the free surface in OCF can impact the flow field. Like the channel sidewalls, the free surface represents a flow boundary at which anisotropy of turbulence is induced (Rodríguez & García 2008). The influence of the free surface will

also increase as flow depth decreases (Mahananda et al. 2018). The turbulence distribution in OCF is similarly influenced by the presence of the free surface.

While the turbulence structure for OCF over smooth beds has been investigated in greater detail than that over rough walls, there are still some established changes in OCF due to roughness. Physically, the viscous sublayer becomes partially or completely destroyed due to protrusion of roughness elements from the wall surface. Furthermore, since the buffer layer is highly active in terms of turbulence production, any interference in this region due to increasingly large roughness elements will further influence viscous effects (Nakagawa et al. 1975, Jiménez 2004). The wall can be characterized as hydraulically smooth, transitionally rough, or fully rough based on the size of the roughness elements and therefore the significance of the protrusion into the viscous sublayer. By way of comparison, flow over a completely smooth wall will have no roughness effects in the wall region, but flow over a completely rough wall will have no viscous effects, and a transitionally rough wall will induce both viscous forces and roughness effects (Nezu & Nakagawa 1993).

In general, both the mean and fluctuating components of velocity are affected by surface roughness in OCF (Bergstrom et al. 2002). In terms of the mean velocity distribution, the profiles are less “full” over a rough wall than a smooth wall due to friction drag (Krogstad et al. 1992, Tachie et al. 2000). Similarly, the intensity of turbulence in the streamwise direction, u_{rms}/u_{τ} , decreases in the wall region with increasing roughness due to the formation of a ‘quasi-separated layer’ of retarded fluid over the roughness elements. Turbulence intensity in the wall-normal or vertical direction, v_{rms}/u_{τ} , will increase as roughness size increases and the ability of the wall to suppress eddy growth decreases. In

effect, the tendency towards turbulence isotropy in the near-wall region increases with roughness (Nezu & Nakagawa 1993). When normalised by friction velocity, turbulence intensities for both smooth and rough walls should not display any differences outside the roughness sublayer (according to Townsend’s wall similarity hypothesis), where the roughness sublayer is the region in which the applicable length scale is associated with roughness size. However, many investigations have indicated that roughness effects are evident in the outer region when the roughness “strength” is significant, i.e. the ratio of inner layer thickness to roughness height k is less than 40. This could be due to destruction of the log-law region by appreciably large elements of roughness (Jiménez 2004, Flack et al. 2005).

Although descriptions of roughness type and distribution are variable and difficult to quantify (Stewart et al. 2019), it is generally accepted that the length scale for the inner region of flows over a rough wall is k_s^+ , which is equal to $k_s u_\tau / \nu$, where k_s is the equivalent sand roughness height. Jiménez (2004) describes the value of k_s as “a convenient way of characterizing the drag increment due to roughness;” its value is determined based on the roughness function, ΔU^+ , which is representative of the downward shift in U^+ due to the effect of roughness. For flows over rough surfaces, the length scale for the inner layer can be taken as k_s^+ . The value of roughness function ΔU^+ can be determined based on k_s^+ and vice versa using **Equation 3.9**.

Equation 3.9:
$$\Delta U^+ = \frac{1}{\kappa} (k_s^+) + B - 8.5$$

The constant 8.5 in **Equation 3.9** is based on the fully rough regime in literature. The value of k_s^+ is also used to classify flow over a surface as hydraulically smooth ($k_s^+ < 5$), fully

rough ($k_s^+ > 70$), or transitionally rough ($5 \leq k_s^+ \leq 70$), as previously described. Flow over the porous bed used in the current investigation is classified as transitionally rough, so the following discussion will pertain to flows over this type of surface. In the transitionally rough regime, turbulence quantities are expected to collapse with smooth wall quantities outside the roughness sublayer (Flack et al. 2005). As discussed, the transitionally rough flow regime experiences both viscous forces and roughness effects. While the value of k_s and accordingly the geometric size of the roughness elements are used to classify the flow regime in terms of hydraulic roughness, Jiménez (2004) reported that gradation of bed material (i.e. distribution of grain size) can alter the conditions under which flow is considered to be transitionally rough. This is related to the reduction and production of skin friction relating to form drag. Form drag increases over roughness elements, thereby increasing the skin friction; conversely, the viscous generation cycle is disrupted by any type of roughness, which decreases skin friction. Furthermore, sparsely distributed roughness elements will cause an increase in form drag as k_s increases, indicating that uniformly rough surfaces reduce drag most efficiently (Jiménez 2004).

This is further confirmed by comparison of the roughness function for a mesh surface roughness with that of sandpaper roughness by Flack et al. (2005); although the value of k (the height of the roughness elements) was higher for the sandpaper than for the mesh, ΔU^+ was shown to be higher for the mesh than for the sandpaper. Therefore, the roughness height alone does not fully describe the effect of roughness (Flack et al. 2005), since roughness geometry will result in different drag coefficients as well (Djenidi et al. 2018).

From the above discussion, it can be seen that turbulence structure is dependent on the shape and distribution of wall roughness. However, bed permeability will also affect flow

turbulence. For example, flow over a wall with sandpaper roughness of a certain grain size will not be identical to flow over a natural sand (i.e. porous) bed with a similar grain size. Faruque and Balachandar (2010) reported the effects of various roughness types on turbulence characteristics, including continuous, Nikuradse-type roughness (sand grains glued to a smooth surface) and a porous sand bed. The streamwise velocity distribution for $Re = 47500$ showed that the roughness function was higher for flow over the bed with continuous roughness when compared with the porous bed. The streamwise turbulence intensity distribution also showed a greater deviation from the smooth wall distribution for the porous bed. In addition, the magnitude of Q2 ejection and Q4 sweep events was shown to be higher for a porous bed in the near-wall region below $y/h \approx 0.2$ (Faruque & Balachandar 2010).

3.3 *Results and discussion*

As discussed above, many studies in literature have adjusted the value of AR in flow over rough beds by changing the value of flow depth, h , and maintaining a constant channel width, b . The present study has employed the use of movable sidewalls to change b as well as h , in order to isolate the influence of the ratio AR (as opposed to just the influence of flow depth) on flow characteristics at the centre of the channel. The dimensions b and h for each test were chosen in order to investigate the largest range of AR values possible based on laboratory constraints, and in order to compare tests with similar values of AR and differing dimensions (e.g. tests R1 and R4 as seen in **Table 3.1**).

3.3.1 Distribution of streamwise velocity, velocity deficit and turbulence intensities

As described in **Table 3.1**, tests R1, R3 and R5 have a flow depth of $h = 0.12$ m, but each has a varying channel width, b , resulting in a change in AR. Reynolds number based on flow depth for each of these tests is approximately 3.3×10^4 . In effect, all of the controllable parameters for this group of tests are identical, with the exception of channel width b , and therefore AR. **Figure 3.1** shows the distribution of normalised mean streamwise velocity (U^+), the velocity defect ($U_e^+ - U^+$), streamwise turbulence intensity (u_{rms}/u_τ) and vertical turbulence intensity (v_{rms}/u_τ) over the wall distance normalised with boundary layer thickness, y/δ , for tests R1, R3 and R5. **Figure 3.1(a)** shows the distribution of U^+ over y^+ for tests R1, R3 and R5 as well as other tests from literature. Measurements for tests S1, S2 and S3 were carried out over a smooth bed for varying values of AR by Roussinova et al. (2008). Tests FS1, FR1 and FR2 are from an experimental water tunnel investigation into turbulent boundary layers by Flack et al. (2005), where the profile FS1 is for flow over a smooth wall and profiles FR1 and FR2 are for flows over fully rough sandpaper and woven mesh walls, respectively. The channel dimensions in m are indicated in the legend for each test. The dashed line represents the logarithmic law for a smooth wall.

The details of each flow field can be found in **Table 3.1**. Overall, the full range of bed conditions starting from hydraulically smooth to fully rough is shown in the figure. The downward and y^+ -positive shift from the smooth logarithmic law line for tests FR1 and FR2 is significant relative to the shifts for test R1, R3 and R5, demonstrating the appreciable influence of wall roughness on the streamwise velocity distribution. Tests S1, S2, S3 and FS1 collapse well with one another and with the logarithmic law, which corresponds to a roughness function ΔU^+ of zero, as expected. In **Figure 3.1(a)** it can also

be seen that the value of the roughness increases with increasing AR for the transitionally rough tests R1, R3 and R5. From **Table 3.1**, it can be seen that the value of k_s^+ increases with increasing AR. This infers that the drag increment due to roughness is increasing as channel width increases.

Figure 3.1(b) shows the distribution of the velocity deficit, $U_e^+ - U^+$, over the flow depth normalised with boundary layer thickness, y/δ . The profiles for all tests, including tests FS1, FR1 and FR2, show good collapse. This indicates that AR does not influence the velocity deficit outside of the roughness sublayer, which is in agreement with literature. The velocity deficit approaches zero asymptotically around the edge of the boundary layer. This is reasonable since δ was taken as the wall distance at which U/U_e first reached a value of 0.99. The collapse shows good agreement with results from literature, supporting the hypothesis of a uniform defect profile for smooth and transitionally rough walls (Flack et al. 2005). There is slight separation between the profiles of the current investigation and the profiles of Flack et al. (2005) in the region $y/\delta < 0.2$ (shown by the dotted line). The inset in the figure shows the same profiles with a log scale on the horizontal axis, in order to better illustrate the separation in profiles below $y/\delta \approx 0.2$. The near-wall peaks observed for the profiles FS1, FR1 and FR2 are higher and closer to the wall than the peak for the transitionally rough profiles, which is reasonable since the Reynolds number and k_s^+ for the literature tests are significantly higher than the current investigation.

Figure 3.1(c) and **Figure 3.1(d)** show the distribution of the turbulence intensities in the streamwise and vertical directions for tests R1, R3 and R5 only. The profiles of streamwise turbulence intensity, u_{rms}/u_τ , collapse well over the outer layer, before separating in the free-stream region where the values become constant. At the edge of the boundary layer,

the streamwise turbulence intensity magnitude increases with increasing AR. Such increase of the streamwise free-stream turbulence suggests increase of the intermittency at the turbulent non-turbulent interface associated with the larger AR = 10.2. The vertical turbulence intensity collapses over the boundary layer and the free-stream region, indicating that sidewall proximity does not influence the magnitude of velocity fluctuations in the vertical direction throughout the depth of flow. The value of AR, and therefore changes in spanwise confinement of the flow, appears to influence the streamwise turbulence intensity at the inner (near-wall) extent of the boundary layer and in the free-stream region, but has no influence on the vertical turbulence intensity throughout the boundary layer.

Table 3.1: Parameters for flume experiments of the current investigation and in literature

Test ID	b m	h m	b/h	U m/s	u_τ m/s	Π	U_e m/s	δ mm	ΔU^+	k_s^+	C_f $\times 10^{-3}$	δ^* mm	θ mm	Re $\times 10^4$	Re_θ
R1	0.4	0.12	3.33	0.262	0.0135	0.332	0.280	47.6	1.33	7.2	4.65	7.03	5.41	3.35	1508
R2	0.4	0.21	1.90	0.252	0.0129	0.303	0.268	64.5	1.22	6.9	4.67	7.77	6.07	5.60	1620
R3	0.8	0.12	6.67	0.261	0.0147	0.346	0.280	48.3	3.34	16.5	5.48	8.09	6.05	3.34	1686
R4	0.8	0.24	3.33	0.258	0.0142	0.326	0.273	63.5	3.67	18.9	5.43	9.73	7.31	6.52	1983
R5	1.22	0.12	10.17	0.254	0.0149	0.374	0.275	54.9	4.48	26.4	5.84	7.93	5.65	3.29	1548
R6	1.22	0.185	6.59	0.266	0.0127	0.240	0.273	53.0	0.70	5.6	4.35	8.96	6.89	5.02	1870
R5-C	1.22	0.12	10.17	0.272	0.0146	--	0.292	52.3	1.92	9.2	5.03	7.75	5.85	3.48	1700
S1	0.61	0.061	10.00	0.451	0.0220	0.157	0.507	54.3	--	--	3.76	6.41	5.09	3.08	2572
S2	0.61	0.081	7.53	0.455	0.0214	-0.097	0.503	64.5	--	--	3.62	7.63	6.02	4.06	3018
S3	0.61	0.102	5.98	0.459	0.0212	-0.319	0.496	73.4	--	--	3.64	7.42	5.98	5.04	2517
FS1	0.4	0.4	1.00	--	0.1410	--	3.770	26.4	--	--	2.80	3.20	2.53	75.1	9500
FR1	0.4	0.4	1.00	--	0.1850	--	3.770	31.9	7.70	98.7	4.82	5.05	3.64	75.1	13668
FR2	0.4	0.4	1.00	--	0.1960	--	3.810	31.1	8.50	137.0	5.29	5.03	3.66	75.9	13889

To investigate the effect of the vertical confinement (flow depth), the value of AR was held constant, and the variation of the streamwise and vertical turbulence intensities was investigated. **Figure 3.2(a)** and **(b)** show the streamwise and vertical turbulence intensities for tests R1 and R4, both of which correspond to an $AR = 3$. Although the values of AR are identical for both, the channel width and depth of flow differs for each test. In fact, the flow depth and width for test R4 are exactly double those of test R1. The value of the Reynolds number based on flow depth Re is greater than 10^4 and the value of the Reynolds number based on momentum thickness Re_θ is similar for all tests as shown in **Table 3.1**. However, an experimental investigation by Mahananda et al. (2018) into the effect of AR on flow characteristics over a rough bed indicated that Reynolds number does not have an effect on the distribution of streamwise or vertical turbulence intensities in fully developed flow conditions.

Analysis of the current approach flow conditions indicated that flow properties at the location of measurements are similar over the field-of-view under consideration. Furthermore, inspection of the Reynolds shear stress profiles for the present investigation (to be detailed in a later section) indicates that the distribution is similar to those acquired under fully developed conditions. Therefore, it can be assumed that any differences in the turbulence intensities between tests R1 and R4 can be attributed to changes in flow depth and not the change in Reynolds number. For the same AR, the streamwise turbulence intensity is higher throughout the depth of flow, and the vertical turbulence intensity, which was previously unchanged with changing AR, is now higher in the outer region of the boundary layer and in the free-stream region for test R4. This is similarly demonstrated in **Figure 3.2(c)** and **(d)**, which show the turbulence intensity distribution for tests R3 and

R6, both of which have a value of $AR \approx 6.6$. The flow depth for test R6 is approximately 1.5 times higher than that of test R3. Again, it can be seen that the channel with the greater cross-sectional area has higher streamwise turbulence intensity throughout the depth of flow. The influence of the bed roughness becomes important with the decrease of the depth. A recent study by Nikora et al. (2019) shows that the contribution of friction due to the secondary currents increases with increase of the relative submergence. The same authors reported that this increase is balanced by the relative decrease of the friction due to the turbulent stresses. At large relative submergence, the secondary flow cells become less organized and their vertical extent does not scale with the flow depth as previously reported by Nezu and Nakagawa (1993).

The vertical turbulence intensity for test R6 is also higher than test R3 throughout the depth of flow, which differs from tests R1 and R4. One may recall that the results of **Figure 3.1(c)** and **(d)** indicated that changes in channel width only influence the streamwise turbulence intensity, and do not influence the vertical turbulence intensity at all. Therefore, it is possible that the discrepancies in streamwise and vertical turbulence intensities shown in **Figure 3.2** can be attributed to changes in the structure of the secondary cells that is dependent on the flow depth. It is conjectured that at a larger flow depth, the events originating from the bed are responsible for the increase of the intermittency of the turbulent non-turbulent (TNT) interface, increasing the streamwise turbulence fluctuations. In the present study, although the roughness is expected to be randomly distributed over the bed, the flow might be prone to preferential pathways due to the porous nature of the bed, which may cause secondary currents (Nikora et al. 2019).

Figure 3.3 shows a comparison of the streamwise and vertical turbulence intensities for tests R1 and R2 ($b = 0.4$ m), R3 and R4 ($b = 0.8$ m) and R5 and R6 ($b = 1.22$ m). In **Figure 3.3(a)** and **(b)**, it can be seen that the streamwise turbulence intensity is higher for test R2 throughout the depth of flow when compared with test R1, and the vertical turbulence intensity is higher from the inner edge of the boundary layer upwards. Similar observations can be made when comparing tests R3 and R4 as well as tests R5 and R6. In each pair having a constant channel width, streamwise turbulence intensity is higher for the deeper test throughout the depth of flow. Interestingly, as b increases, the difference in u_{rms}/u_τ in the free-stream region between the pair of tests decreases. For $b = 0.4$ m, the difference in u_{rms}/u_τ in the free-stream region for tests R1 and R2 is 70%, which decreases to 57% between tests R3 and R4, and finally reduces to 26% between tests R5 and R6.

Furthermore, as b increases, the differences in vertical turbulence intensity extend across the entire depth of flow as opposed to existing only in the free-stream region (as for the channel of smallest width), and the discrepancy in v_{rms}/u_τ in the free-stream region is also reduced. In general, it appears that lesser vertical confinement of the flow (i.e. greater flow depth) allows for higher streamwise turbulence intensity throughout the depth of flow, but this effect is less pronounced with reduced horizontal confinement (i.e. greater channel width). Similarly, lesser vertical confinement results in higher vertical turbulence intensity, the effect of which extends towards the wall from the free-stream region as horizontal confinement is reduced. As is seen **Figure 3.2**, the effect of flow dimensions on turbulence intensities in either direction cannot be strictly defined by the magnitude of AR, i.e. the ratio of flow dimensions. **Figure 3.3** allows for examination of the effects of changes in h and b separately.

Figure 3.4 shows the distribution of the streamwise and vertical turbulence intensity normalised with the free-stream streamwise turbulence intensity $(u_{rms})_e$ over the flow depth normalised by δ_I , the location at which $u_{rms} = (u_{rms})_e$. This scaling was introduced by Balachandar and Patel (2002). The free-stream streamwise turbulence intensity $(u_{rms})_e$ appears to be the proper velocity length scale in the free-stream region, but not in the boundary layer region. Like **Figure 3.3** (which shows the distribution of turbulence intensities with different velocity and length scales), **Figure 3.4** points to the influences of both h and b on the turbulence intensities. Before the free-stream turbulence intensity is reached, the distributions of $u_{rms}/(u_{rms})_e$ shows a near-wall peak with a steady decrease until the point at which $y/\delta_I \approx 0.75$. The distributions of $v_{rms}/(u_{rms})_e$ increase from the wall region to a maximum, beyond which point the values decrease before reaching constancy around $y/\delta_I \approx 1.0$. The values of both $u_{rms}/(u_{rms})_e$ and $v_{rms}/(u_{rms})_e$ are higher for the test in each pair with the lesser depth of flow before the free-stream value of u_{rms} is reached. However, the difference between each pair decreases with increasing channel width. This indicates once again that the influence of water depth on both the streamwise and vertical turbulence intensities is dependent on channel width.

In **Figure 3.5**, the distribution of v_{rms}/u_{rms} is shown for tests R1 and R2, R3 and R4 and R5 and R6. For all measurements, it can be seen that the magnitude of v_{rms} is lower than the magnitude of u_{rms} . All distributions of v_{rms}/u_{rms} for tests R1, R3 and R5 (i.e. $h = 0.12$ m) show an increase from the wall before decreasing in the free-stream region and eventually reaching constancy. However, tests R1 and R3 show a peak (i.e. an increase in v_{rms}) at the edge of the boundary layer, by which it is shown that the tendency towards turbulence isotropy is at a maximum at this point. The distribution of v_{rms}/u_{rms} for tests R2, R4 and R6

(i.e. $h > 0.12$ m) similarly increases from the wall, but a peak is reached very close to the wall before decreasing steadily and reaching constancy in the free-stream region. In each pair of tests, it can be seen that the value of v_{rms}/u_{rms} increases with increasing vertical confinement. While this is true over the entire depth of flow for test R1, the value of v_{rms}/u_{rms} dips below the profile of test R4 (for test R3) and below test R6 (for test R5). As seen in **Figure 3.3**, the vertical turbulence intensity is unchanged with increasing vertical confinement in the boundary layer. Therefore, the changes in v_{rms}/u_{rms} can be attributed to the streamwise turbulence intensity. As horizontal confinement decreases, the efficacy of vertical confinement in reducing anisotropy of turbulence decreases.

3.3.2 Distribution of third-order turbulent moments

Figure 3.6 shows the distribution of third-order turbulent moments for tests R1, R3 and R5. At a glance, it can be seen that across and just outside of the boundary layer, the absolute values of the fluxes of normal stresses $\overline{u^2}$ and $\overline{v^2}$ in either the streamwise or vertical direction increases as AR decreases. In effect, the transport of the Reynolds stresses in the boundary layer increases as sidewall proximity increases. **Figure 3.6(a)** shows the distribution of $\overline{u^3}$. Very close to the wall, there is a sharp increase in streamwise transport of $\overline{u^2}$ for all tests. In the region for which $y/\delta < 0.15$, the sign of $\overline{u^3}$ changes for test R5 only. From **Table 3.1**, the value of k_s^+ is highest for test R5. Flack et al. (2005) reported a change in sign for $\overline{u^3}$ in flow over fully rough walls when compared with smooth walls. Therefore, the magnitude of $\overline{u^3}$ close to the wall becomes positive as roughness increases. The transport of $\overline{u^2}$ in the positive streamwise direction then decreases up to $y/\delta \approx 0.5$, before increasing steadily and reaching constancy just outside of the boundary layer. In

this region of constant $\overline{u^3}$, the magnitude for each test is close to zero but the curves do not collapse on each other completely, unlike the distributions in **Figure 3.6(b)** through **(d)**, which show good collapse in the free-stream region for all other third-order turbulent moments. The free-stream $\overline{u^3}$ is highest for test R5 with $b = 1.22$ m and decreases with channel width; this corresponds to the distribution of u_{rms}/u_τ shown for test R1, R3 and R5 in **Figure 3.1(c)**, where the free-stream turbulence intensity in the streamwise direction is highest for $b = 1.22$ m and decreases with decreasing b . Therefore, streamwise transport of $\overline{u^2}$ as well as streamwise turbulence intensity are suppressed in the free-stream region by sidewall proximity.

Figure 3.6(b) shows the distribution of $\overline{v^3}$. The distribution of this quantity is more straightforward and shows a closer collapse than for the profiles of $\overline{u^3}$. The transport of $\overline{v^2}$ in the positive vertical direction increases from the wall before reaching a peak around the middle of the boundary layer. The peak for test R1, for which sidewall proximity is highest, is particularly prominent. In general, the distribution shown in **Figure 3.6(b)** for $\overline{v^3}$ indicates that the vertical transport of the normal stress in the vertical direction are not influenced as strongly by changes in channel width when compared with $\overline{u^3}$ for tests with $h = 0.12$ m, which is also consistent with the distributions of u_{rms}/u_τ and v_{rms}/u_τ shown in **Figure 3.1(c)** and **(d)**, where the vertical turbulence intensities are similarly unaffected by sidewall proximity.

Figure 3.6(c) shows the distribution of the flux of $\overline{u^2}$ in the vertical direction. The profiles of $\overline{u^2 v}$ for all three tests show a sharp decrease to a local minimum with increasing distance from the bed. Very close to the wall, the transport of normal stress $\overline{u^2}$ away from the wall

increases and the sharp drop which follows extends to the same approximate location as the peak in the transport of $\overline{u^2}$ in the positive streamwise direction. Therefore, a region of increase in transport of $\overline{u^2}$ in the positive streamwise direction corresponds to a region of decrease in transport of $\overline{u^2}$ in the positive vertical direction, below $y/\delta \approx 0.2$.

Figure 3.6(d) shows the distribution of the transport of $\overline{v^2}$ in the streamwise direction. For tests R1 and R3, there is a peak very close to the wall before a decrease to a minimum which is located about halfway between the wall and the edge of the boundary layer. The location of the peak is further from the wall for test R1 (at $y/\delta \approx 0.2$) than for test R3. From all of the profiles of the higher-order moments, it appears that transport of normal stresses in all directions reaches its extreme at the same point in the boundary layer, around $y/\delta \approx 0.5$. The transport of $\overline{u^2}$ is in the negative streamwise and positive vertical direction at this point. The transport of $\overline{v^2}$ is also in the negative streamwise and positive vertical direction at the same point. As previously described, the absolute values of the triple-order moments are highest for the test with lowest value of AR. These findings are consistent with the results of Roussinova et al. (2008), in which the effect of AR on the turbulence structure was investigated for OCF over a smooth bed. In this investigation, the distribution of $\overline{u^2v}$ and $\overline{uv^2}$ showed the highest peaks in the test for which AR was the lowest.

In earlier discussion, it was established that the distribution of turbulence intensities is not solely reliant upon the value of AR, but rather is somewhat dependent on both flow depth and channel width independently. **Figure 3.7**, **Figure 3.8** and **Figure 3.9** show the distribution of third-order turbulent moments for tests R1 and R2 ($b = 0.4$ m), R3 and R4 ($b = 0.8$ m) and R5 and R6 ($b = 1.22$ m). In **Figure 3.7**, the absolute values of normal stress

transport in any direction is higher for test R2 (with a higher depth of flow), in the region for which $0.35 < y/\delta < 0.85$ for transport of $\overline{u^2}$ and $0.2 < y/\delta < 0.85$ for transport of $\overline{v^2}$. Outside of these specified regions, the absolute magnitude of third-order moments is either close or less for R2 than R1. **Figure 3.8** shows an increase in all third-order quantities within $0.35 < y/\delta < 0.85$ for transport of $\overline{u^2}$ and $0.2 < y/\delta < 0.85$ for transport of $\overline{v^2}$ for tests R3 and R4 with $b = 0.8$ m, although the magnitude of the difference is less than what is shown between tests R1 and R2 with $b = 0.4$ m.

In **Figure 3.9**, it appears that the transport of normal stresses in either direction is greater for test R6 (with a greater depth of flow) than for test R5 throughout the boundary layer. Unlike the comparison for tests R1 and R2 (with $b = 0.4$ m), the absolute magnitude of the higher-order moments is higher for test R6 than test R5 throughout the boundary layer, as opposed to just within a certain region of the boundary layer (as shown in **Figure 3.7**). Furthermore, the difference between the profiles of $\overline{u^3}$ in the free-stream region are smaller than the difference in profiles between tests R1 and R2 (for which the channels are narrower). The value of $\overline{u^3}$ in the free-stream region is still higher for test R6 (with the greater depth of flow), which is also consistent with **Figure 3.7**. In general, it appears that, for a given b , a higher flow depth enhances transport of normal stresses in both streamwise and vertical directions. This is consistent for all b , but is restricted to specific regions of the boundary layer for a narrow channel.

3.3.3 Distribution of normalised Reynolds shear stress $-\overline{uv}/u_\tau^2$

Figure 3.10 shows the distribution of Reynolds shear stress $-\overline{uv}/u_\tau^2$ over the flow depth normalised by the boundary layer thickness. Transitionally rough tests R1 through R6 are

included, as well as smooth test FS1 from a water tunnel investigation by Flack et al. (2005). The Reynolds shear stress does not appear to be significantly affected by channel width, as the profiles show good collapse over the majority of the boundary layer ($0.5 < y/\delta < 1$) before reaching constancy at a value of zero just outside of the boundary layer around $y/\delta \approx 1.25$. The near-wall peak is higher and closer to the wall for FS1 which is reasonable for a flow over a hydraulically smooth surface. It can be seen that $-\overline{uv}/u_\tau^2$ does not deviate significantly from the theoretical line for a 2D channel shown, which confirms that flow at the location of measurements behaves similarly to fully developed flow (Mahananda et al. 2018). For the transitionally rough tests R1 through R6, the role of AR on $-\overline{uv}/u_\tau^2$ appears to be minimal, if any exists.

Quadrant analysis was developed in order to appreciate the contribution of positive and negative streamwise and vertical velocity fluctuations to the total Reynolds shear stress, $-\overline{uv}$. The method used for analysis was first introduced by Lu and Willmarth (1973), in which the contribution to $-\overline{uv}$ from a quadrant Q_i is given by

Equation 3.10:
$$(uv)_{Q_i} = \lim_{T \rightarrow \infty} \frac{1}{T} \int_0^T u(t)v(t)I(t)dt \quad \text{for } i = 1 - 4$$

Equation 3.11:
$$I(t) = \begin{cases} 1 & \text{when } |uv|_Q \geq Hu'v' \\ 0 & \text{otherwise} \end{cases}$$

In **Equation 3.11**, H is the Reynolds shear stress magnitude parameter used to filter stronger events.

Q2 events ($u < 0, v > 0$) correspond to intermittent bursting motions from the wall, known as ejections. Ejection events play a significant role in the vertical transport of momentum in the positive direction, as well as the production of turbulent kinetic energy in the wall

region. Q4 events ($u > 0, v < 0$), known as sweeps, are related to large-scale motions in the negative vertical direction at small angles relative to the wall. In the near-wall region, the contribution of the Q2 events to the Reynolds shear stress is greater than the contribution of the Q4 events; as the distance from the wall increases, the relative strength of the Q4 events increases and overtakes the strength of the Q2 events. Q1 ($u > 0, v > 0$) and Q3 ($u < 0, v < 0$) events are known as outward and inward interactions, respectively. The total value of the Reynolds shear stress is mostly comprised of the contributions from ejection and sweep events; the contributions from the outward and inward interactions are smaller. In addition, the time scales for Q2 and Q4 events are typically larger than those for Q1 and Q3 events (Wallace 2016).

Figure 3.11 shows distribution of contributions for each quadrant over y/δ for $H = 0$ (i.e. all events) for tests R1, R3 and R5. The magnitude and distribution of the contributions to $-\overline{uv}$ from Q1 and Q3 events for tests R1, R3 and R5 are similar over the boundary layer, showing a decrease from the wall to a minimum at $y/\delta \approx 0.2$. At this negative peak, R1 shows the greatest magnitude of contribution to the Reynolds shear stress. All profiles decrease steadily after the common peak at $y/\delta \approx 0.2$ and reach constancy outside of the boundary layer. Inside the edge of the boundary layer and in the free-stream region, the contributions from Q1 (corresponding to positive fluctuations in the streamwise and vertical directions) and Q3 (corresponding to negative fluctuations in the streamwise and vertical directions) increase with decreasing AR (or decreasing channel width). The distribution of u_{rms}/u_τ (**Figure 3.1(c)**) similarly indicates an increase in the same region with increasing AR.

Figure 3.11(b) and **(d)** show the distributions for the Q2 ejection and Q4 sweep contributions to $-\overline{uv}$ for $H = 0$. For Q2 events, the profiles for all tests are quite similar throughout the depth of flow; with the contributions in test R1 shown as slightly higher in the region close to the bed. For Q4 events, the profiles are nearly identical for all three tests in the region where $y/\delta > 0.3$. In the near wall region, however, distribution of the magnitude of the sweep events is significantly influenced by sidewall proximity. For test R1, the magnitude of the sweep motions is high near the wall, before decreasing to a local minimum and then increasing once again to peak at the point at which $y/\delta \approx 0.3$. There is no peak immediately adjacent to the wall for tests R3 and R5, but the maximum magnitude of the sweeps is located nearer to the wall for both than for test R1.

Figure 3.12 shows the distribution of contributions for Q1 through Q4 for tests R1 and R4 with $AR = 3.33$. Unlike tests R1, R3 and R5 in **Figure 3.11**, the profiles differ throughout most of the depth of flow. Contributions from the Q1 and Q3 events are close for both tests below $y/\delta = 0.2$, and contributions from the Q2 and Q4 events are similarly close below $y/\delta = 0.3$. Beyond these points, however, the inward and outward contributions are greater for test R1 (with greater horizontal and vertical confinement of flow), and the ejection and sweep event contributions are greater for test R4 (with lesser horizontal and vertical confinement of flow). **Figure 3.13** similarly compares the distribution of contributions for tests R3 and R6 with $AR \approx 6.6$. As with the comparison between tests R1 and R4, the contributions from Q1 and Q3 are greater for test R3 (greater confinement), and Q2 and Q4 are greater for test R6 (lesser confinement). Unlike tests R1 and R4, however, the differences are shown throughout the depth of flow for all quadrants; there is no collapse in the near-wall region.

In **Figure 3.14**, **Figure 3.15** and **Figure 3.16**, the contributions for R1 and R2 ($b = 0.4$ m), R3 and R4 ($b = 0.8$ m) and R5 and R6 ($b = 1.22$ m) are shown. **Figure 3.14** shows that the Q1 and Q3 contributions are higher for test R1 (smaller depth of flow, i.e. greater vertical confinement) and the Q2 and Q4 motions are higher for test R2 (greater depth of flow, i.e. lesser vertical confinement). Examination of the profiles in **Figure 3.15** and **Figure 3.16** show a similar effect of flow depth. Like the comparison of turbulence intensities (**Figure 3.3**) and third-order turbulent moments (**Figure 3.6**), the difference in profiles due to flow depth decrease as channel width increases.

The profiles for the stronger events (with $H = 1$) for each quadrant are shown in **Figure 3.17** through **Figure 3.20**. In **Figure 3.17(a)**, it can be seen that the magnitude of the relatively stronger Q1 events is once again highest close to $y/\delta = 1.0$ and in the free-stream region for the most narrow channel, and then decreases as channel width increases (and therefore horizontal confinement decreases). This is also true for the Q3 events as shown in **Figure 3.17(c)**, although this can only be seen outside the boundary layer in the free-stream region. There is appreciable scatter in the near-wall region and throughout most of the boundary layer for Q1 and Q3 profiles for all tests, with no noticeable prominence for any channel width. For the Q2 ejection and Q4 sweep events, the distribution is very similar between $H = 0$ and the stronger events for which $H = 1$. The magnitude of Q2 ejection events is once again higher over the remainder of the boundary layer for test R1, while the events for tests R3 and R5 show good collapse over most of the flow. Once again, profiles for all three tests collapse in the free-stream region. In **Figure 3.17(d)**, the profiles for all three tests collapse over the majority of the flow and in the free-stream region, with differences contained to the region close to the wall. The peak for the strong Q4 sweep

events is highest for test R5, as opposed to those for which $H = 0$, where the highest peak was seen for test R1. Comparison of contributions to Q1 through Q4 for tests R1 and R2, R3 and R4 and R5 and R6 are shown in **Figure 3.18**, **Figure 3.19**, and **Figure 3.20**. The differences between the distribution for each quadrant for $H = 1$ is similar to the differences shown in **Figure 3.14**, **Figure 3.15** and **Figure 3.16** for $H = 0$. The magnitude of the contributions in Q1 and Q3 is higher for the test with the greater vertical confinement for each pair, and the magnitude of the contributions in Q2 and Q4 are higher for the test with lesser horizontal confinement for each pair. The difference in the magnitude for all comparisons once again decreases as channel width, b , increases.

The number of events for each quadrant with $H = 1$ normalised by the total number of events can be seen in **Figure 3.21** (for tests R1, R3 and R5) and **Figure 3.22** (for tests R2, R4 and R6). **Figure 3.21(a)** shows the number of stronger Q1 events over the depth of flow. While the number of Q1 events is at a minimum and is constant throughout most of the boundary layer, this quantity begins to increase just after the midway point in the boundary layer for test R5, and closer to the edge of the boundary layer for test R1 and R3. Once this increase begins, the number of Q1 events is higher for the highest AR value and then decreases with decreasing AR. Towards the free surface, the number of Q1 events in test R3 begins to approach the number for test R5. In **Figure 3.21(c)**, it can be seen that the number of Q3 events is, like the number of Q1 events, at a minimum close to the wall. However, there is no region of constancy for the number of Q3 events, which increases steadily for all tests until just inside the boundary layer. At this point, the number of Q3 events for test R5 becomes higher than for either test R1 and R3, before the profile for test R3 once again approaches the profile for test R5 near the free surface region. **Figure**

3.21(b) shows that the number of Q2 ejection events is not significantly affected by AR. The profiles for all three tests are very similar throughout the depth of flow, with a slight increase in the number of ejection events just inside the boundary layer for test R1.

Figure 3.21(d) shows the distribution of the number of Q4 sweep events. Although there is a slight peak for test R5 close to the wall, there is little difference between the profiles for the three tests over the majority of the boundary layer. Just inside the boundary layer, however, the number of sweep events suddenly drops for test R1 with the smallest channel width, before increasing sharply and reaching constancy in the free-stream region. The number of sweep events for test R3, with a greater channel width than test R1, also experiences a drop (albeit one of lesser magnitude) at the edge of the boundary layer before similarly increasing and reaching constancy beyond $y/\delta = 1$. In contrast, the number of sweep events for test R5, with the highest channel width, does not experience a drop but instead becomes constant in the same region. The number of events in the free-stream region where constancy is attained for all tests shows that the number of sweep events increases as channel width decreases.

For the tests R2, R4 and R6 ($h > 0.12$ m) in **Figure 3.22**, the differences in the number of events in each quadrant are suppressed. The number of Q1 and Q3 events is quite consistent for all tests throughout the depth of flow, with a slight increase in Q1 events occurring in the free-stream region just outside the boundary layer for test R2. The number of Q2 events for all tests of greater flow depth is quite consistent over the depth of flow, with a slight dip for test R2 just outside the edge of the boundary layer. The number of Q4 events is also relatively constant in the near-wall region, with a slight separation between tests R4 and tests R2 and R6 at the edge of the boundary layer. In comparison with **Figure 3.21**, this

indicates that the effect of horizontal confinement on the number of events is enhanced by increased vertical confinement.

A summary of the findings in the experiment results is found in **Table 3.2**.

Table 3.2: Summary of the effect of horizontal and vertical confinement on flow characteristics

Region of flow	General observations	
Near-wall ($0 < y/\delta < 0.2$)	<ul style="list-style-type: none"> • $\overline{u^3}$ has a peak • $\overline{u^2v}$ has a local minima • $\overline{uv^2}$ has a peak • Q1 and Q3 events have a peak • Q4 increases with increasing HC in this region 	
	Effect of increasing horizontal confinement (HC)	Effect of increasing vertical confinement (VC)
Outer layer ($0.2 < y/\delta < 1.0$)	<ul style="list-style-type: none"> • $\overline{u^3}$, $\overline{v^3}$, $\overline{u^2v}$ and $\overline{uv^2}$ increase • v_{rms}/u_{rms} reaches a peak ($y/\delta \approx 1.0$ only) • Q2 increases • Number of Q2 events increase ($y/\delta \approx 1.0$ only) • Number of Q4 events decrease ($y/\delta \approx 1.0$ only) 	<ul style="list-style-type: none"> • $\overline{u^3}$, $\overline{v^3}$, $\overline{u^2v}$ and $\overline{uv^2}$ decrease • v_{rms}/u_{rms} increases
Free-stream ($1.0 < y/\delta < 2.0$)	<ul style="list-style-type: none"> • u_{rms}/u_τ decreases • $\overline{u^3}$ decreases • Q1/Q3 decreases • Number of Q1/Q3 events decreases • Number of Q4 events increases 	<ul style="list-style-type: none"> • $\overline{u^3}$ decreases • v_{rms}/u_{rms} decreases
Entire depth of flow ($0 < y/\delta < 2.0$)	<ul style="list-style-type: none"> • drag increment due to roughness decreases • no change in v_{rms}/u_τ 	<ul style="list-style-type: none"> • u_{rms}/u_τ and v_{rms}/u_τ decrease (percent difference due to increasing VC decreases with decreasing HC and the percentage of the boundary layer over which the difference is seen increases with decreasing HC) • $\overline{u^3}$, $\overline{v^3}$, $\overline{u^2v}$ and $\overline{uv^2}$ decrease in the boundary layer (in addition, the percent of the boundary layer over which difference occurs increases with decreasing HC) • Q1 and Q3 increase and Q2 and Q4 events decrease (in addition, the percent difference due to increasing VC increases with decreasing HC)

3.3.4 Effect of sidewall proximity on mean and turbulence properties

Figure 3.23 shows the distribution of the mean streamwise velocity, the Reynolds shear stress $-\overline{uv}/u_\tau^2$, and the streamwise and vertical turbulence intensities u_{rms}/u_τ and v_{rms}/u_τ over the wall distance normalised with the boundary layer thickness, y/δ for test R5 (AR = 10.17). Profiles are shown for the central plane (where $Z = 0$, used for analysis in the previous sections) and also for an off centre plane for which $Z = 0.32$ m (i.e. close to the midpoint between the central plane and the sidewall). Measurements were taken in the off-centre plane, called R5-C, in order to explore the effect of sidewall proximity on the mean and turbulence properties.

Figure 3.23(a) shows the distribution of U/U_e and U^+ for tests R5 and R5-C. It can be seen that the normalised streamwise velocity is slightly higher for test R5-C than for test R5 in the boundary layer, and vice versa in the free-stream region. This can likely be attributed to the secondary flow cell structure in the spanwise direction. The location of plane C, where measurements were taken for test R5-C, is in greater proximity to the flume sidewall. In this near-sidewall location, it is probable that secondary flow cells are still present. If the measurements were then taken in a region of upwelling or downwelling flow associated with such a structure, the distribution of the mean streamwise velocity would also be affected, particularly since secondary currents tend to be larger closer to the bed and magnitude of upflow is generally greater than the magnitude of downflow (Nezu et al. 1985). The value of U^+ is higher over the entire depth of flow in the inset. However, the increase in U^+ corresponds to a decrease in u_τ in the spanwise direction, as described by Nezu et al. (1985). Flow measurements in the spanwise (z) direction for an air flow (shown to be analogous to open-channel flow) indicated a sidewall-normal variation of u_τ , the

nature of which was dependent on the value of channel AR. For an AR = 10 (recall that AR for R5 and R5-C is 10.2), it was determined that the value of u_τ is constant in the two-dimensional central zone of flow, and then begins to decrease as the sidewall was approached (Nezu et al. 1985). This finding is consistent with the values of u_τ for R5 (0.01487 m/s) compared with R5-C (0.01462 m/s), and the shift in the roughness function shown in **Figure 3.23(a)** can therefore be attributed to the spanwise variation in shear velocity due to secondary currents.

Figure 3.23(b) shows $-\overline{uv}/u_\tau^2$ for R5 and R5-C, which show good collapse over most of the depth of flow. **Figure 3.23(c)** and **(d)** show the distribution of u_{rms}/u_τ and v_{rms}/u_τ . **Figure 3.23(c)** indicates that the streamwise turbulence intensity at the inner edge of the boundary layer and in the free-stream region is reduced as sidewall proximity increases. This is consistent with the findings in **Figure 3.1(c)**, in which u_{rms}/u_τ decreased in the same region with an increase in horizontal confinement (i.e. with an increase sidewall proximity). The vertical turbulence intensity is unaffected by sidewall proximity here, which is also consistent with the conclusions drawn from **Figure 3.1(d)**, stated in **Table 3.2**.

3.4 Conclusions and recommendations

Analysis of the experimental results of the present investigation indicates that open-channel flow over a porous bed cannot be characterized by the value of AR (b/h) alone, as is presently done in literature. The distribution of streamwise velocity, streamwise and vertical turbulence intensities, triple-order turbulent moments and contributions of quadrants to the Reynolds shear stress have been identified based on increasing vertical confinement (i.e. decreasing h) and increasing horizontal confinement (i.e. decreasing b).

These effects have also been found to vary with spanwise location. This implies that careful examination of the approach flow conditions is required for various applications of open-channel flow modelling. Further experimentation on the nature of secondary flow over an erodible porous bed is also required. Scour modelling in laboratory flumes is particularly affected, since laboratory constraints often result in flow that is highly constrained both vertically and horizontally. Re-examination of hydraulic modelling practices is required for future experimentation and applicability of previously acquired results must be re-considered.

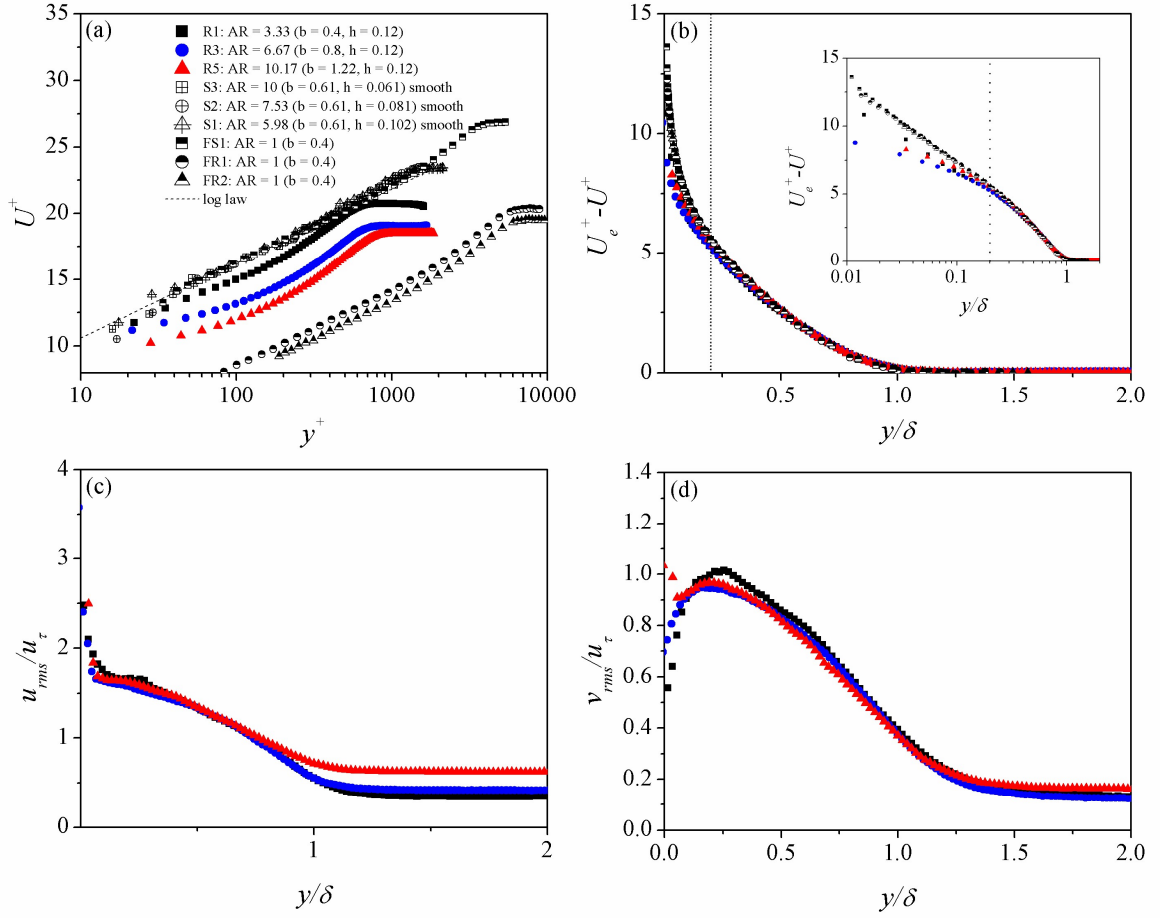


Figure 3.1: Distribution of (a) U^+ vs. y^+ (b) $U_e^+ - U^+$ vs. y/δ (inset with logarithmic scaling included), (c) streamwise turbulence intensity u_{rms}/u_τ vs. y/δ and (d) vertical turbulence intensity v_{rms}/u_τ vs. y/δ for tests R1, R3 and R5 (present investigation), S1, S2 and S3 (Roussinova et al. 2008) and FS1, FR1 and FR2 (Flack et al. 2005)

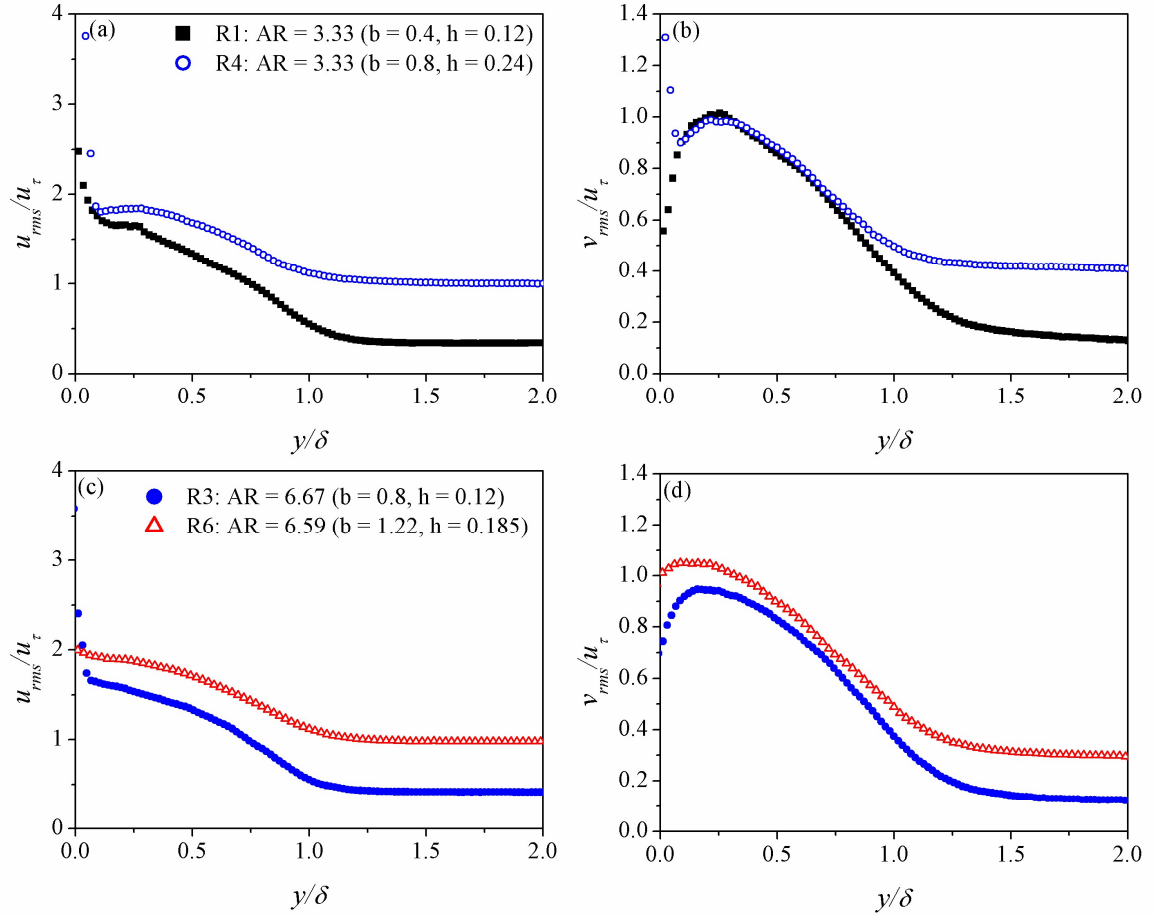


Figure 3.2: Distribution of (a) streamwise turbulence intensity u_{rms}/u_τ for tests R1 and R4 (AR = 3.3), (b) vertical turbulence intensity v_{rms}/u_τ for tests R1 and R4 (AR = 3.3), (c) streamwise turbulence intensity u_{rms}/u_τ for tests R3 and R6 (AR = 6.6) and (d) vertical turbulence intensity v_{rms}/u_τ for tests R3 and R6 (AR = 6.6) over flow depth y normalised by boundary layer thickness δ

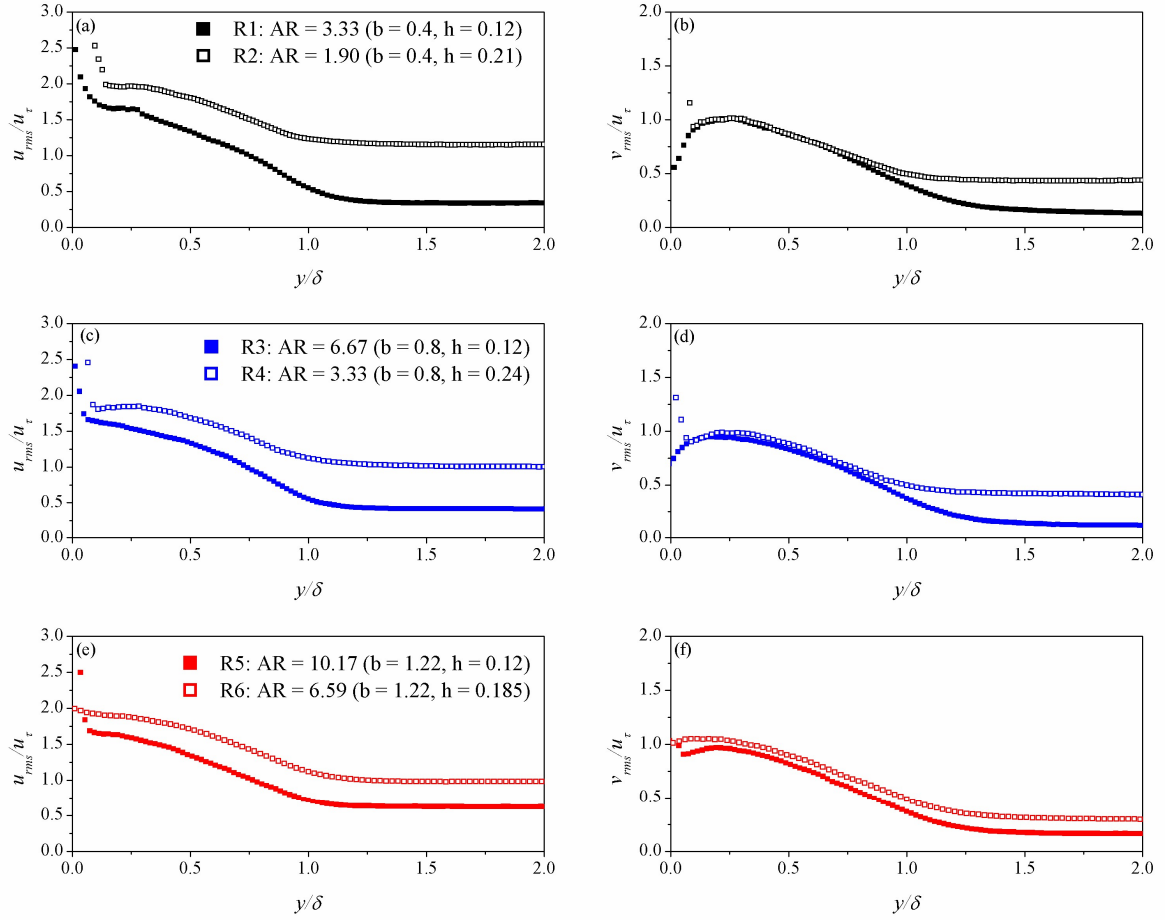


Figure 3.3: Distribution of (a) streamwise turbulence intensity u_{rms}/u_{τ} and (b) vertical turbulence intensity v_{rms}/u_{τ} for tests R1 and R2 ($b = 0.4$ m), (c) streamwise turbulence intensity u_{rms}/u_{τ} and (d) vertical turbulence intensity v_{rms}/u_{τ} for tests R3 and R4 ($b = 0.8$ m), (e) streamwise turbulence intensity u_{rms}/u_{τ} and (f) vertical turbulence intensity v_{rms}/u_{τ} for tests R5 and R6 ($b = 1.22$ m) over flow depth normalised by boundary layer thickness y/δ

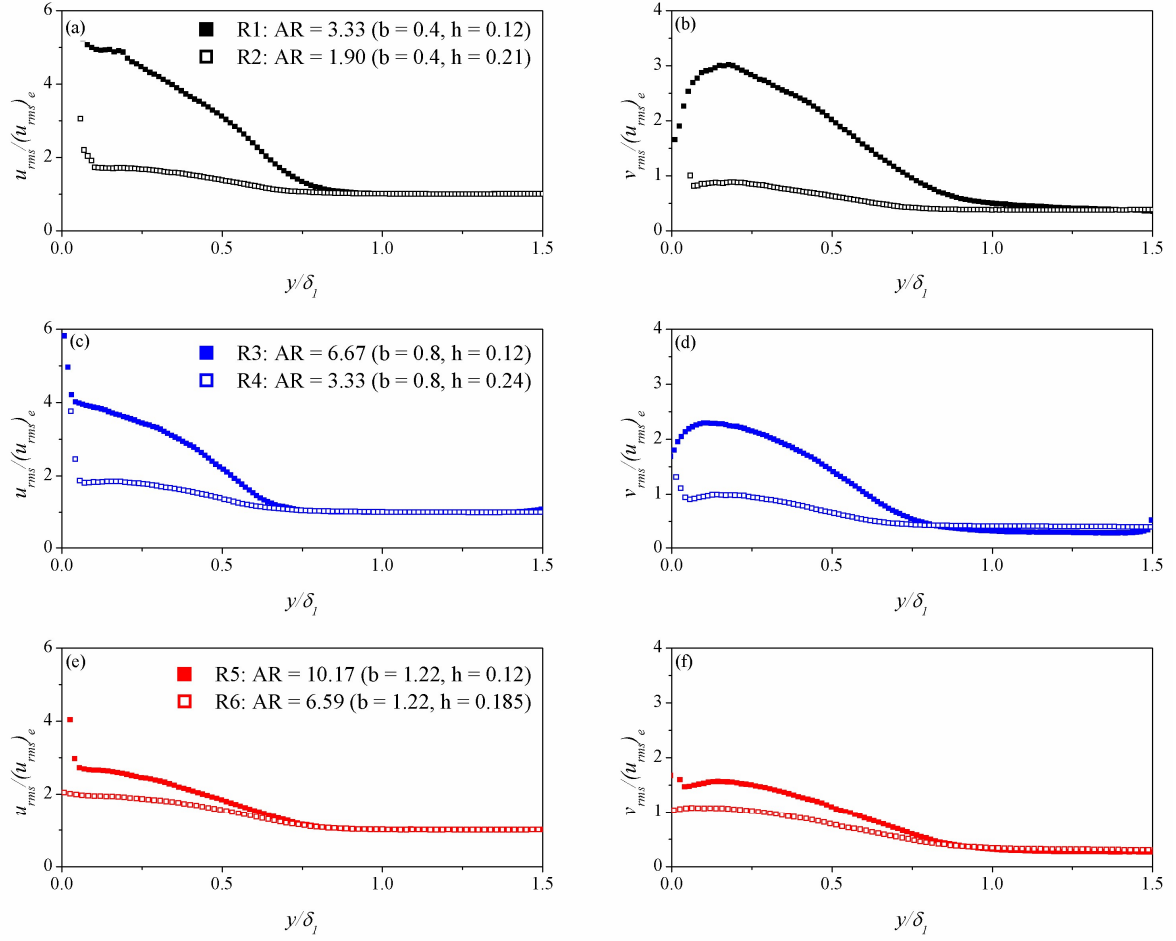


Figure 3.4: Distribution of (a) streamwise turbulence intensity $u_{rms}/(u_{rms})_e$ and (b) vertical turbulence intensity $v_{rms}/(u_{rms})_e$ for tests R1 and R2 ($b = 0.4$ m), (c) streamwise turbulence intensity $u_{rms}/(u_{rms})_e$ and (d) vertical turbulence intensity $v_{rms}/(u_{rms})_e$ for tests R3 and R4 ($b = 0.8$ m), (e) streamwise turbulence intensity $u_{rms}/(u_{rms})_e$ and (f) vertical turbulence intensity $v_{rms}/(u_{rms})_e$ for tests R5 and R6 ($b = 1.22$ m) over y/δ_l , where y is flow depth and δ_l is the location at which u_{rms} reaches the free-stream streamwise turbulence intensity $(u_{rms})_e$

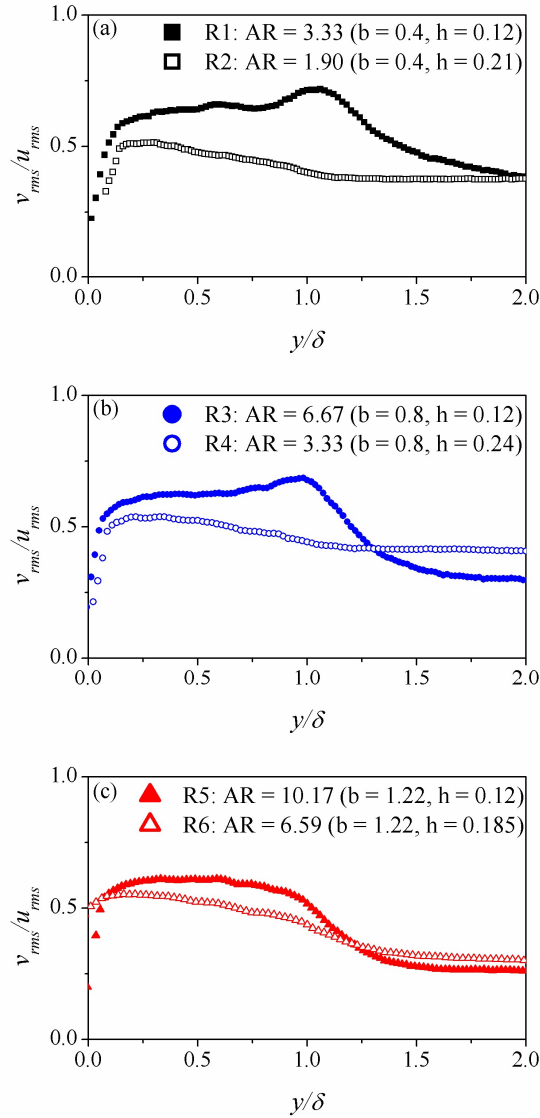


Figure 3.5: Distribution of the ratio of streamwise turbulence intensity to vertical turbulence intensity v_{rms}/u_{rms} for (a) tests R1 and R2 ($b = 0.4$ m), (b) tests R3 and R4 ($b = 0.8$ m) and (c) tests R5 and R6 ($b = 1.22$ m) over flow depth normalised by boundary layer thickness y/δ

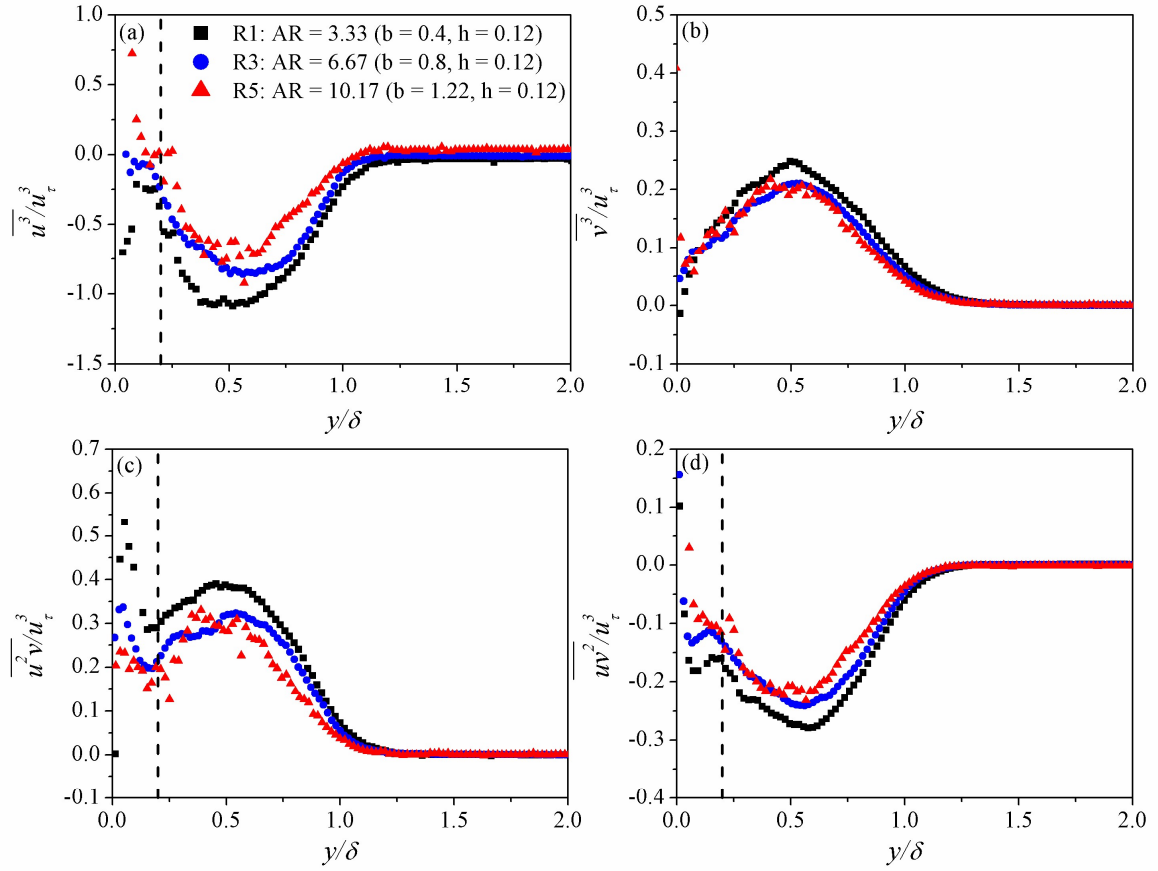


Figure 3.6: Distribution of (a) streamwise transport of the streamwise component of normal stress $\overline{u^3}$, (b) vertical transport of the vertical component of normal stress $\overline{v^3}$, (c) vertical transport of the streamwise component of normal stress $\overline{u^2v}$ and (d) the streamwise transport of the vertical component of normal stress $\overline{uv^2}$ for tests R1, R3 and R5 ($h = 0.12$ m) over flow depth normalised by boundary layer thickness y/δ

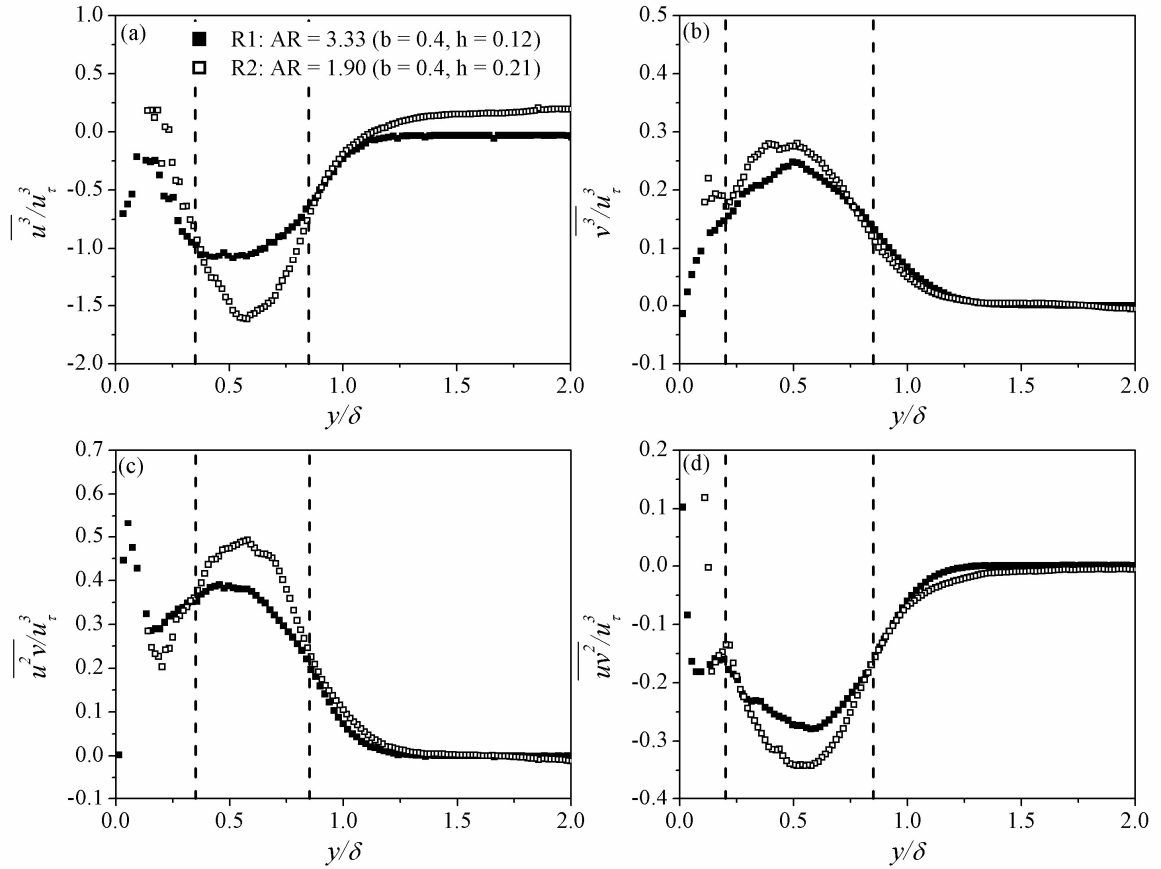


Figure 3.7: Distribution of (a) streamwise transport of the streamwise component of normal stress $\overline{u^3}$, (b) vertical transport of the vertical component of normal stress $\overline{v^3}$, (c) vertical transport of the streamwise component of normal stress $\overline{u^2v}$ and (d) the streamwise transport of the vertical component of normal stress $\overline{uv^2}$ for tests R1 and R2 ($b = 0.4$ m) over flow depth normalised by boundary layer thickness y/δ

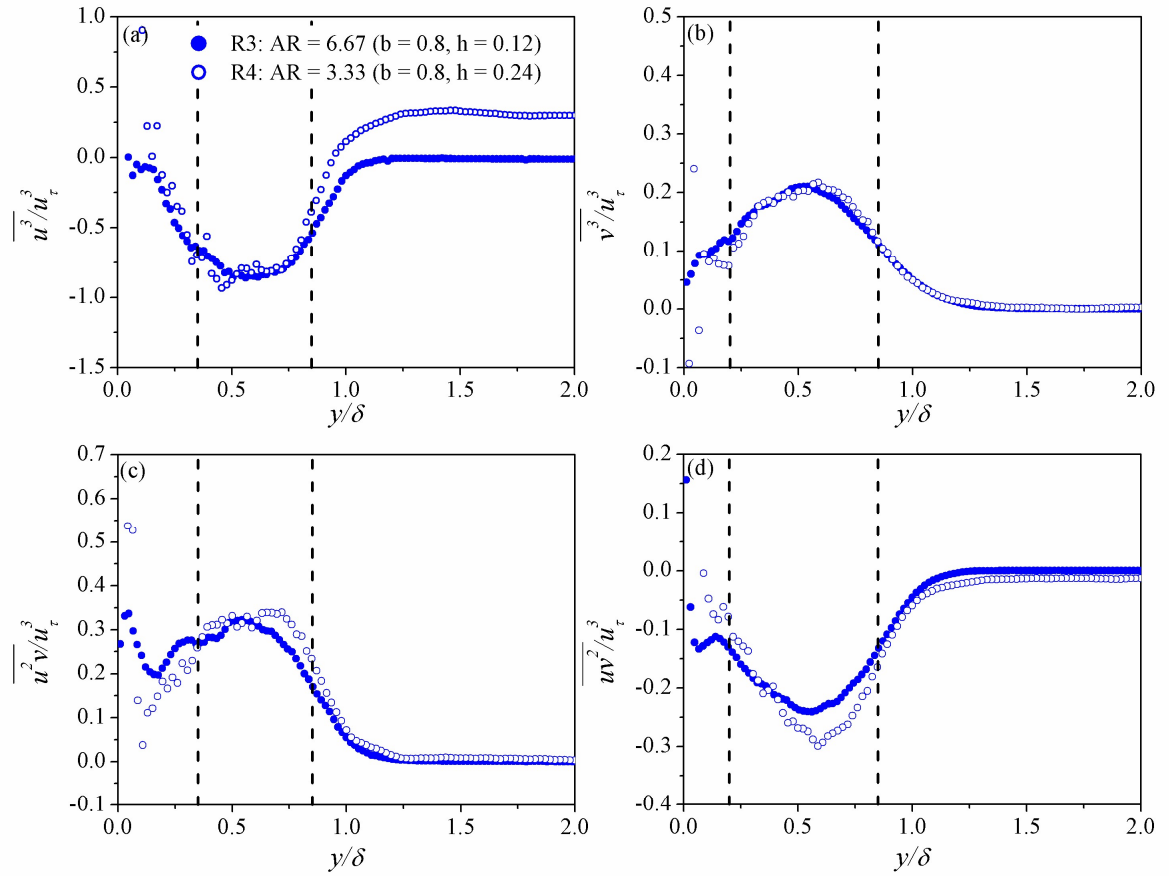


Figure 3.8: Distribution of (a) streamwise transport of the streamwise component of normal stress $\overline{u^3}$, (b) vertical transport of the vertical component of normal stress $\overline{v^3}$, (c) vertical transport of the streamwise component of normal stress $\overline{u^2v}$ and (d) the streamwise transport of the vertical component of normal stress $\overline{uv^2}$ for tests R3 and R4 ($b = 0.8$ m) over flow depth normalised by boundary layer thickness y/δ

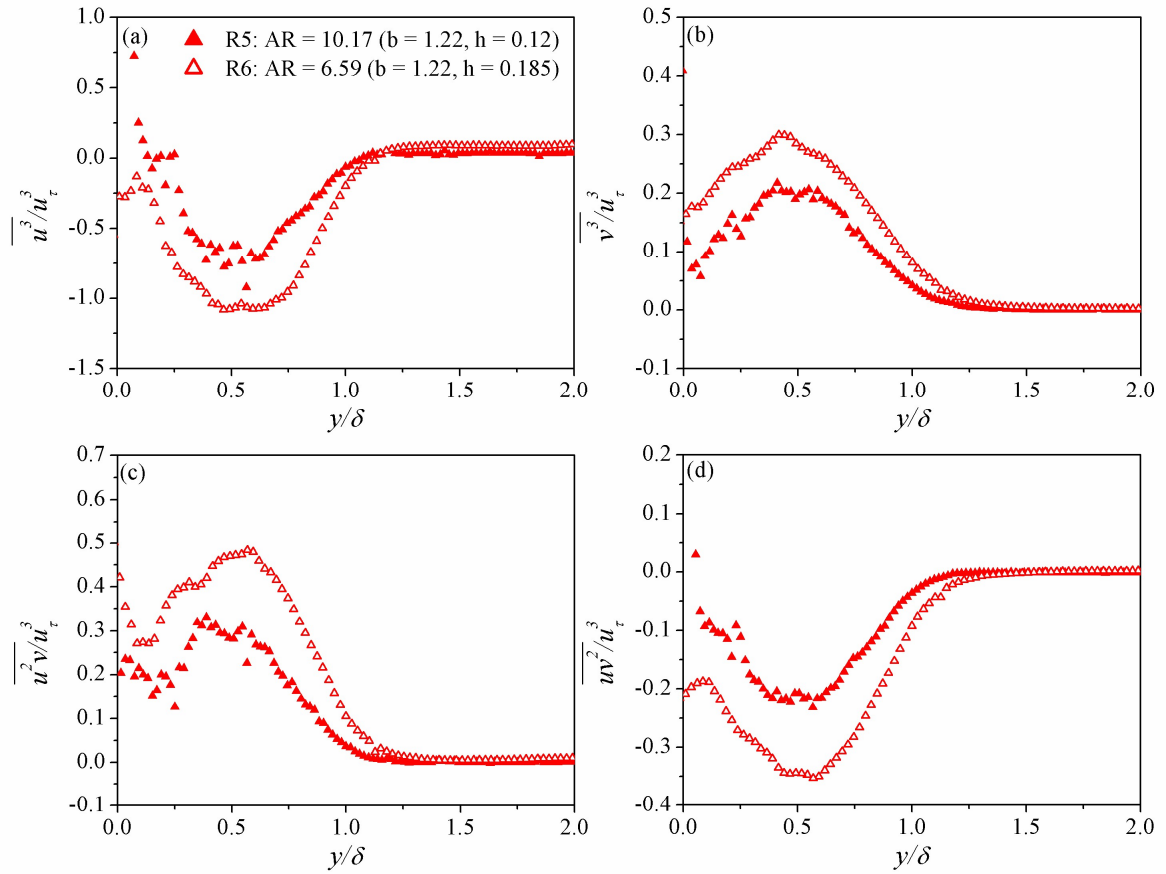


Figure 3.9: Distribution of (a) streamwise transport of the streamwise component of normal stress $\overline{u^3}$, (b) vertical transport of the vertical component of normal stress $\overline{v^3}$, (c) vertical transport of the streamwise component of normal stress $\overline{u^2v}$ and (d) the streamwise transport of the vertical component of normal stress $\overline{uv^2}$ for tests R5 and R6 ($b = 1.22$ m) over flow depth normalised by boundary layer thickness y/δ

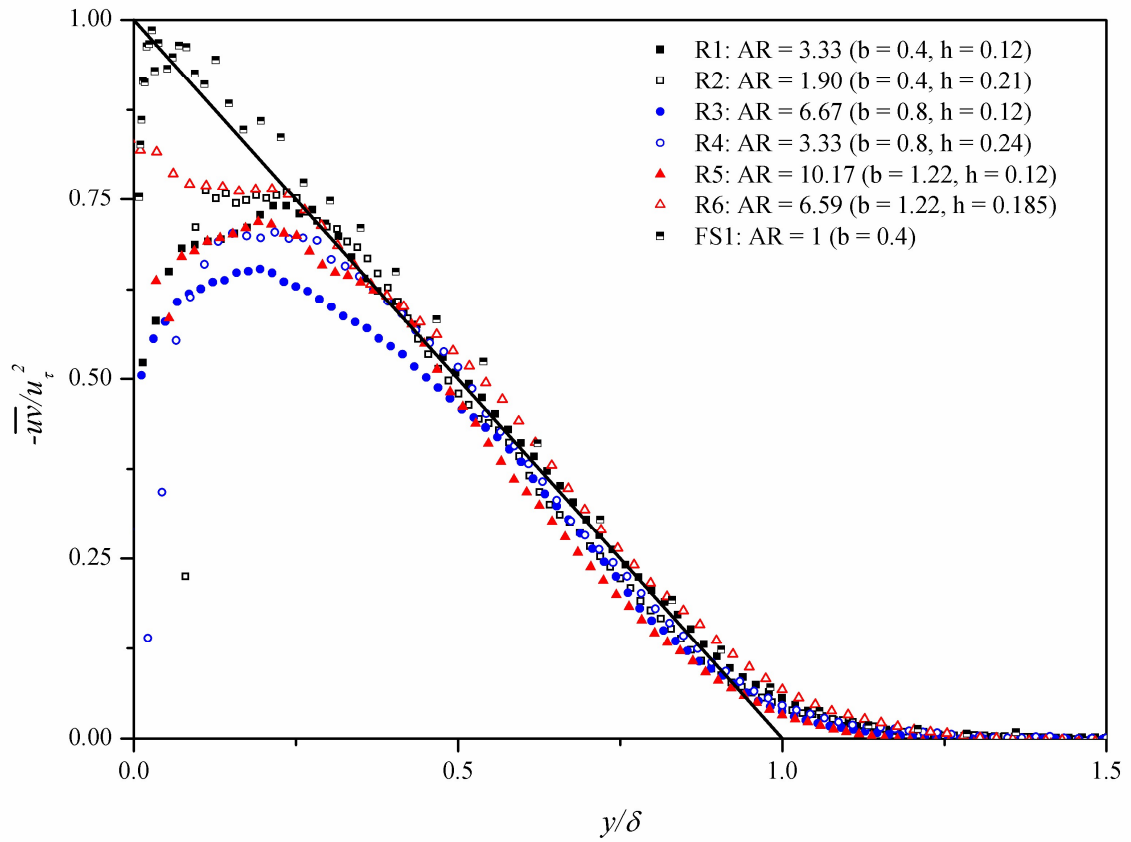


Figure 3.10: Distribution of the Reynolds shear stress normalised with friction velocity $-\overline{uv}/u_\tau^2$ for tests R1 – R6 (present investigation) and FS1 (Flack et al. 2005) over flow depth normalised by boundary layer thickness y/δ

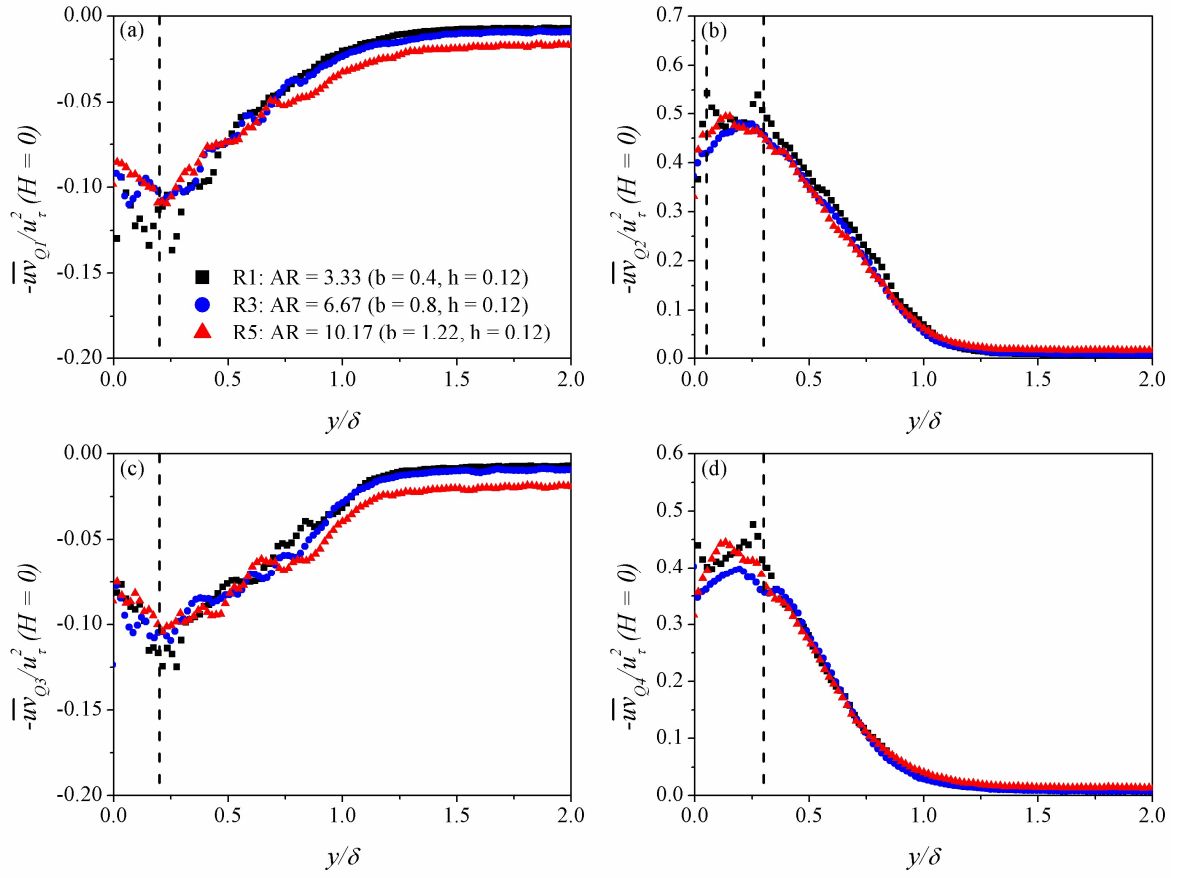


Figure 3.11: Distribution of the contributions of (a) Q1 outward interactions ($u > 0, v > 0$), (b) Q2 ejection events ($u < 0, v > 0$), (c) Q3 inward interactions ($u < 0, v < 0$) and (d) Q4 sweep events ($u > 0, v < 0$) for which $H = 0$ to the total Reynolds shear stress $-\overline{u'v'}$ for tests R1, R3 and R5 ($h = 0.12$ m) over flow depth normalised by boundary layer thickness y/δ

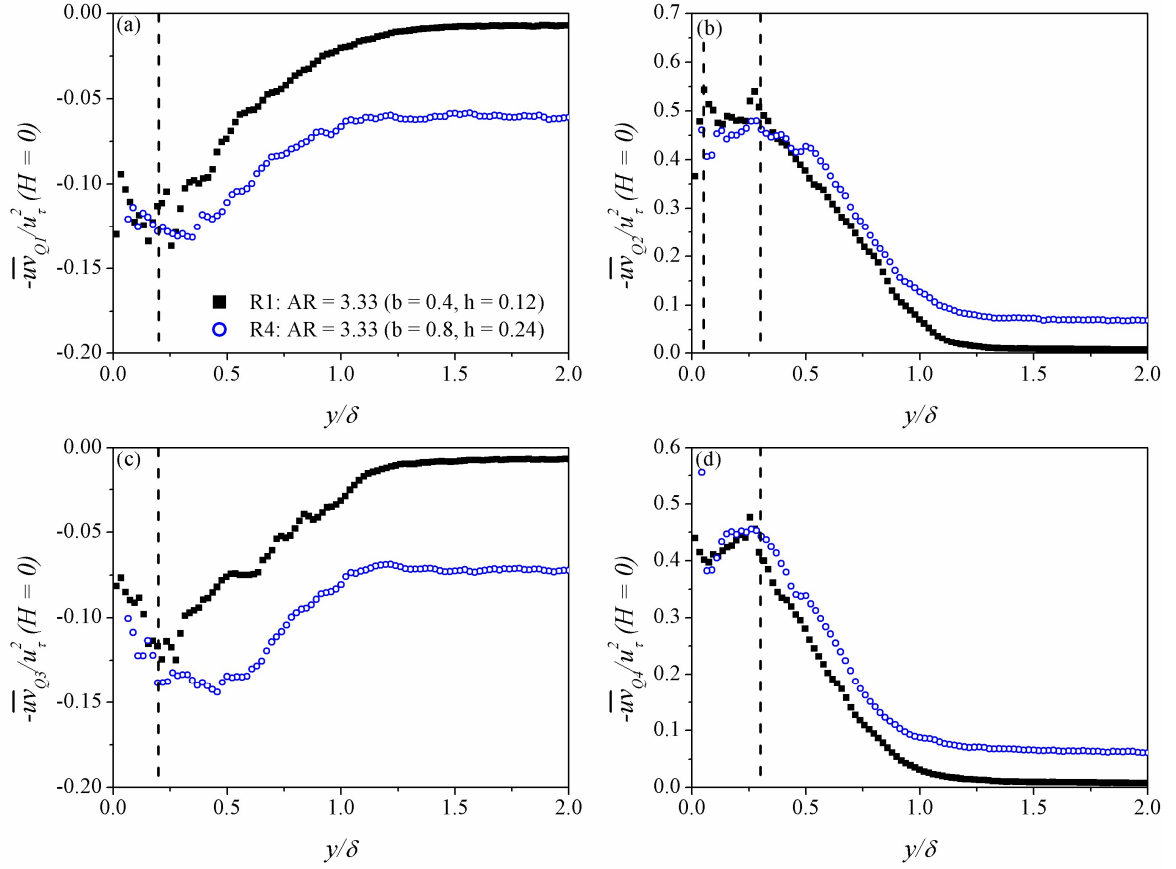


Figure 3.12: Distribution of the contributions of (a) Q1 outward interactions ($u > 0, v > 0$), (b) Q2 ejection events ($u < 0, v > 0$), (c) Q3 inward interactions ($u < 0, v < 0$) and (d) Q4 sweep events ($u > 0, v < 0$) for which $H = 0$ to the total Reynolds shear stress $-\overline{u'v'}$ for tests R1 and R4 ($AR = 3.3$) over flow depth normalised by boundary layer thickness y/δ

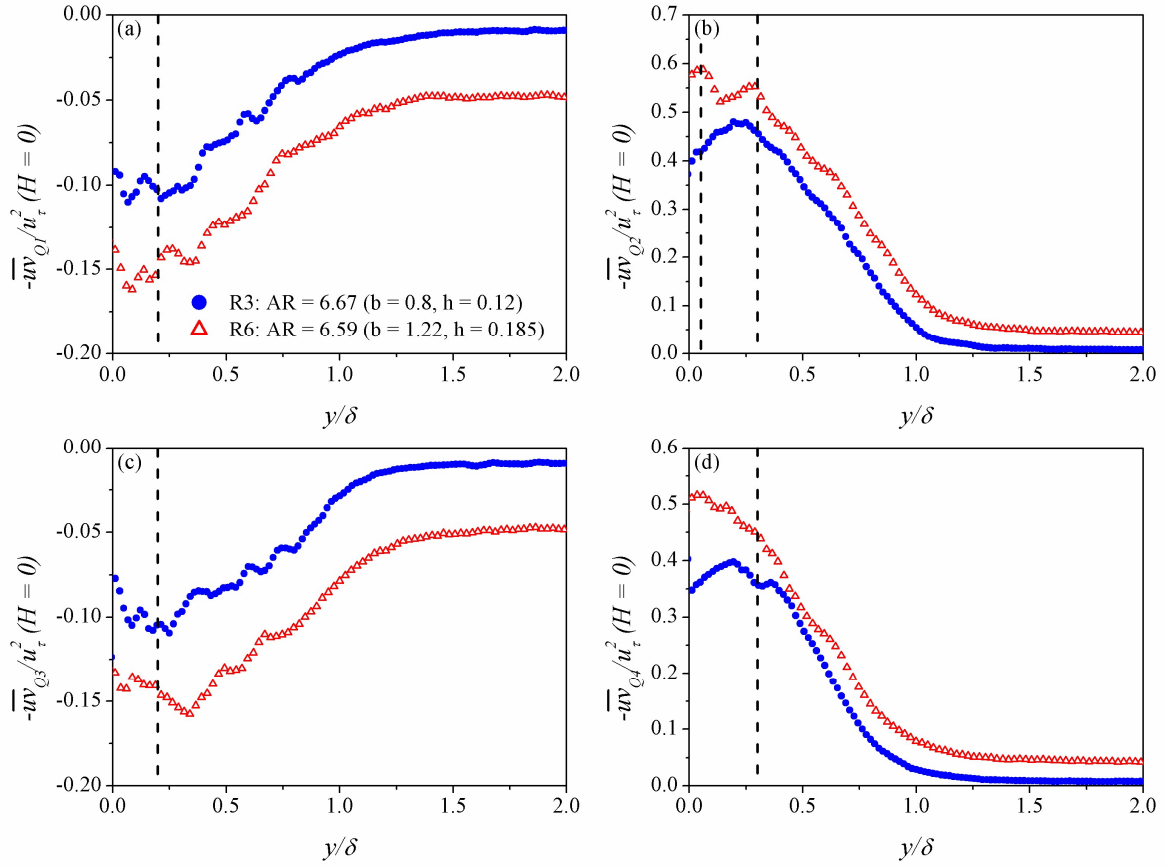


Figure 3.13: Distribution of the contributions of (a) Q1 outward interactions ($u > 0, v > 0$), (b) Q2 ejection events ($u < 0, v > 0$), (c) Q3 inward interactions ($u < 0, v < 0$) and (d) Q4 sweep events ($u > 0, v < 0$) for which $H = 0$ to the total Reynolds shear stress $-\overline{u'v'}$ for tests R3 and R6 (AR = 6.6) over flow depth normalised by boundary layer thickness y/δ

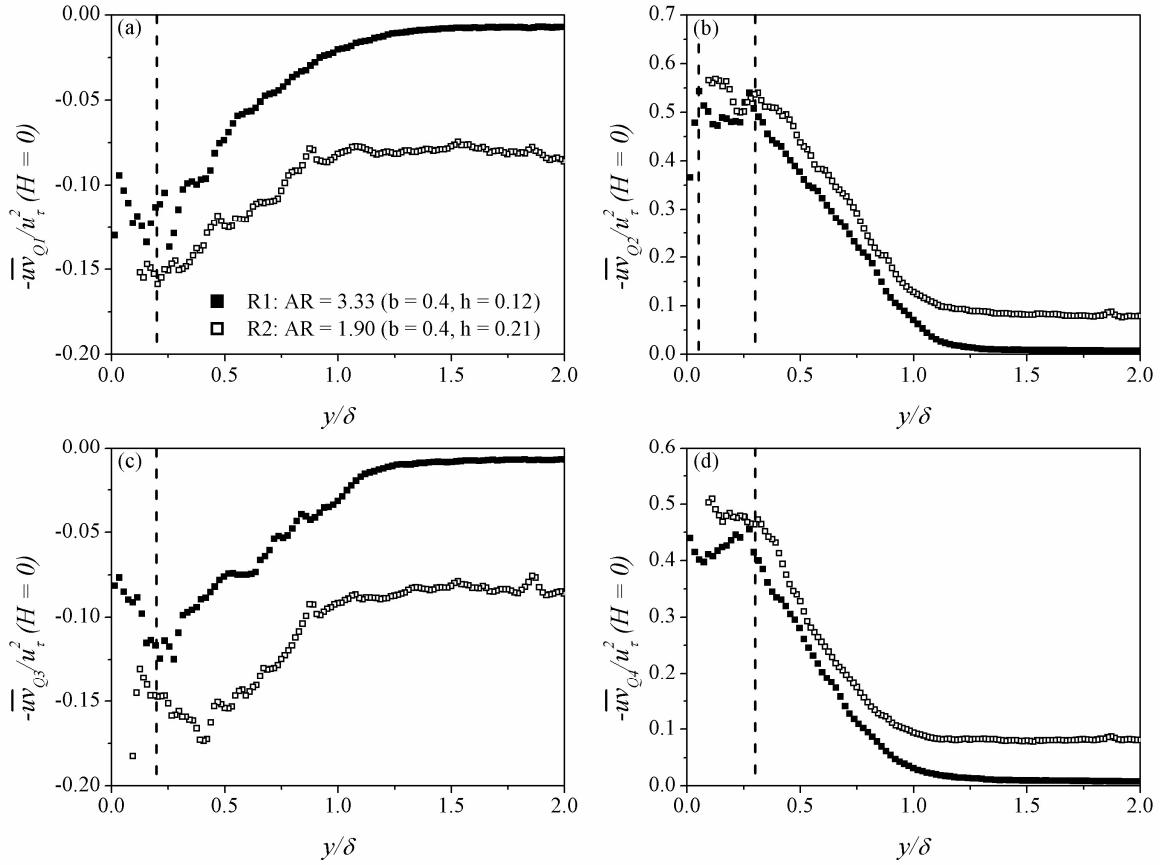


Figure 3.14: Distribution of the contributions of (a) Q1 outward interactions ($u > 0, v > 0$), (b) Q2 ejection events ($u < 0, v > 0$), (c) Q3 inward interactions ($u < 0, v < 0$) and (d) Q4 sweep events ($u > 0, v < 0$) for which $H = 0$ to the total Reynolds shear stress $-\overline{uv}$ for tests R1 and R2 ($b = 0.4$ m) over flow depth normalised by boundary layer thickness y/δ

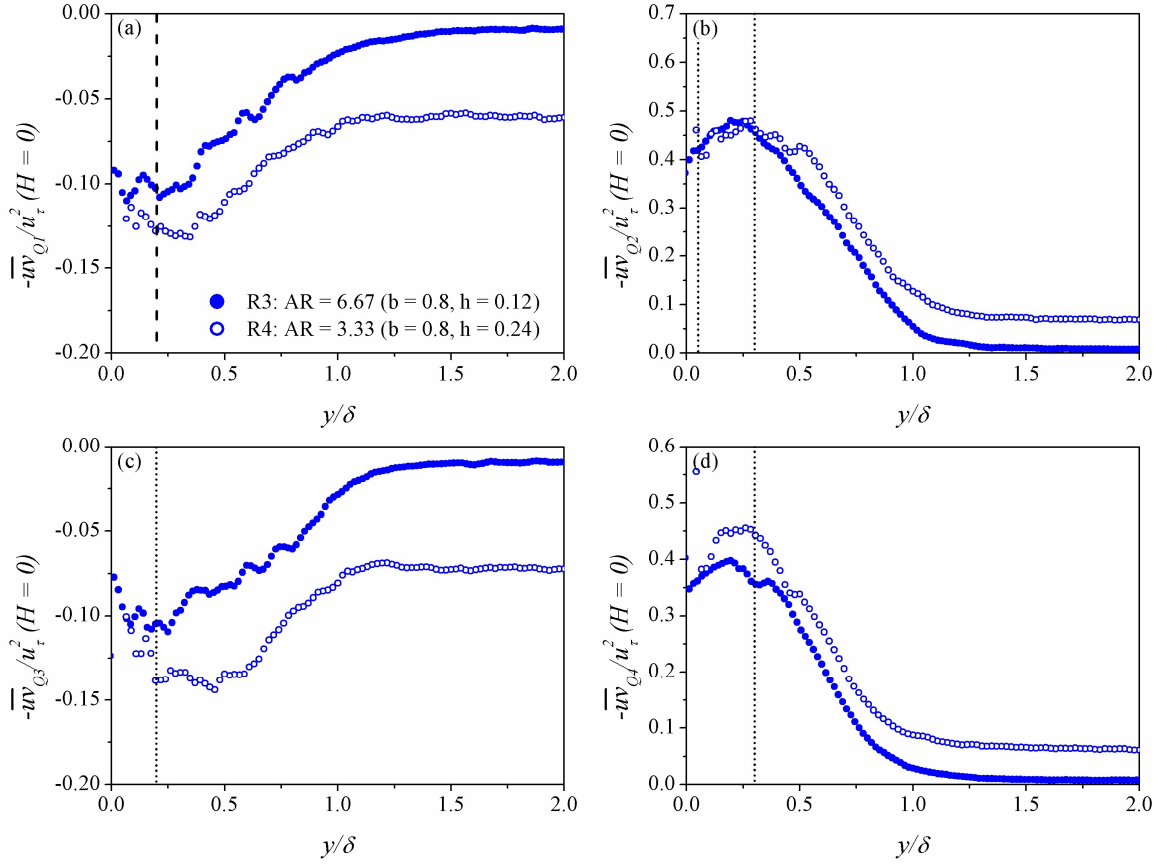


Figure 3.15: Distribution of the contributions of (a) Q1 outward interactions ($u > 0, v > 0$), (b) Q2 ejection events ($u < 0, v > 0$), (c) Q3 inward interactions ($u < 0, v < 0$) and (d) Q4 sweep events ($u > 0, v < 0$) for which $H = 0$ to the total Reynolds shear stress $-\overline{u'v'}$ for tests R3 and R4 ($b = 0.8$ m) over flow depth normalised by boundary layer thickness y/δ

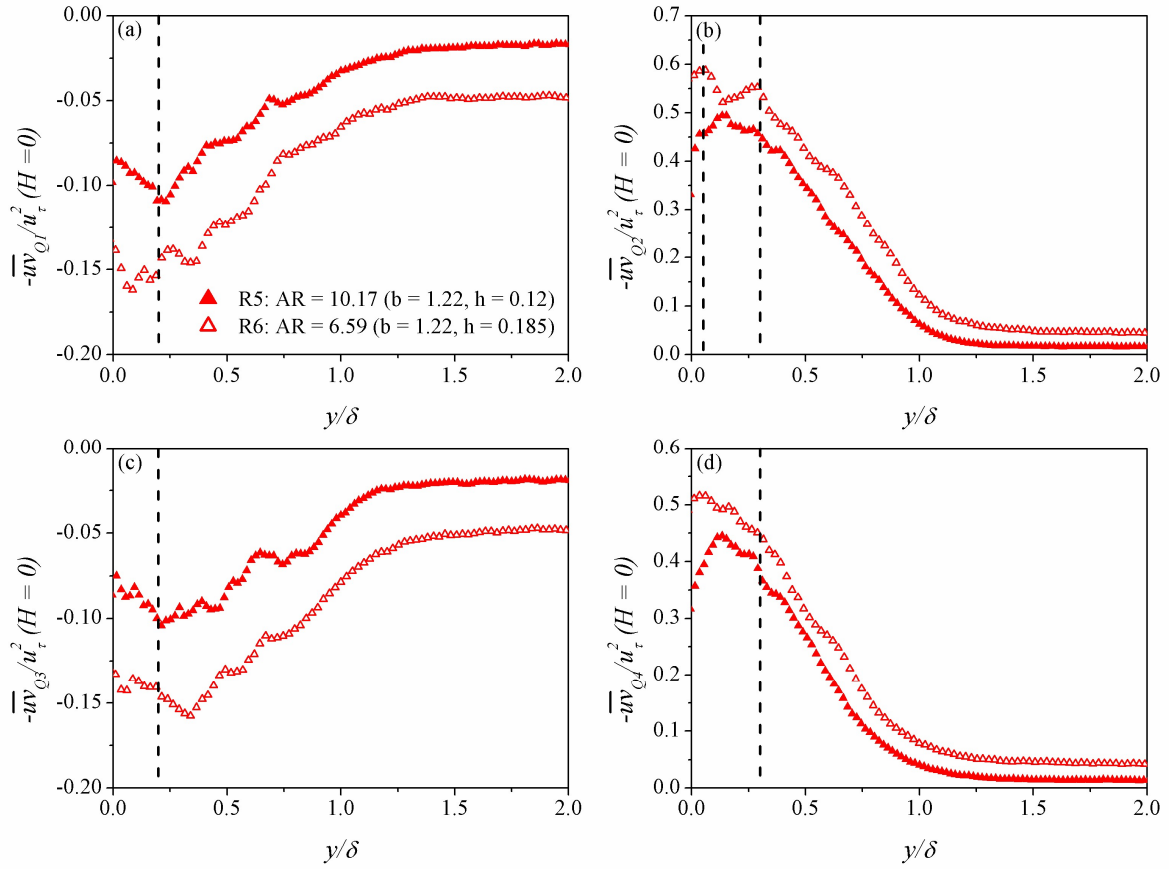


Figure 3.16: Distribution of the contributions of (a) Q1 outward interactions ($u > 0, v > 0$), (b) Q2 ejection events ($u < 0, v > 0$), (c) Q3 inward interactions ($u < 0, v < 0$) and (d) Q4 sweep events ($u > 0, v < 0$) for which $H = 0$ to the total Reynolds shear stress $-\overline{u'v'}$ for tests R5 and R6 ($b = 1.22$ m) over flow depth normalised by boundary layer thickness y/δ

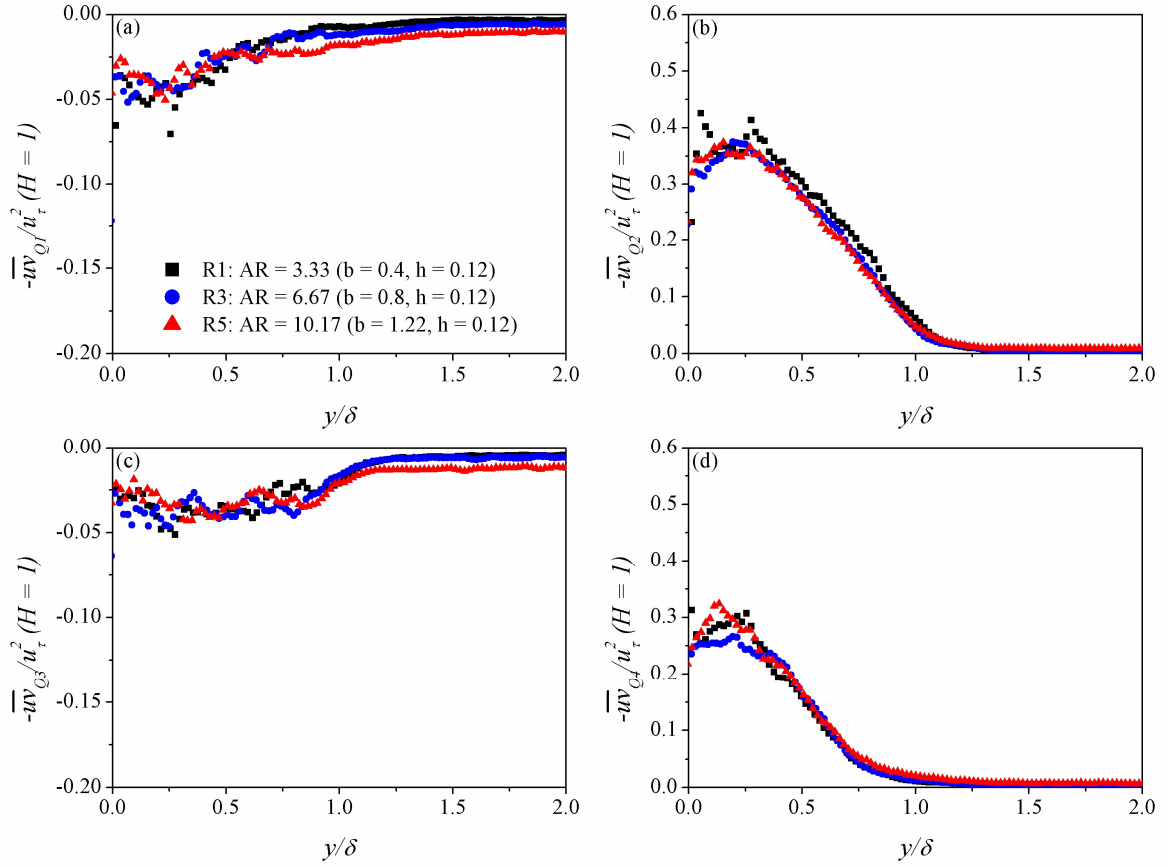


Figure 3.17: Distribution of the contributions of (a) Q1 outward interactions ($u > 0, v > 0$), (b) Q2 ejection events ($u < 0, v > 0$), (c) Q3 inward interactions ($u < 0, v < 0$) and (d) Q4 sweep events ($u > 0, v < 0$) for which $H = 1$ to the total Reynolds shear stress $-\overline{uv}$ for tests R1, R3 and R5 ($h = 0.12$ m) over flow depth normalised by boundary layer thickness y/δ

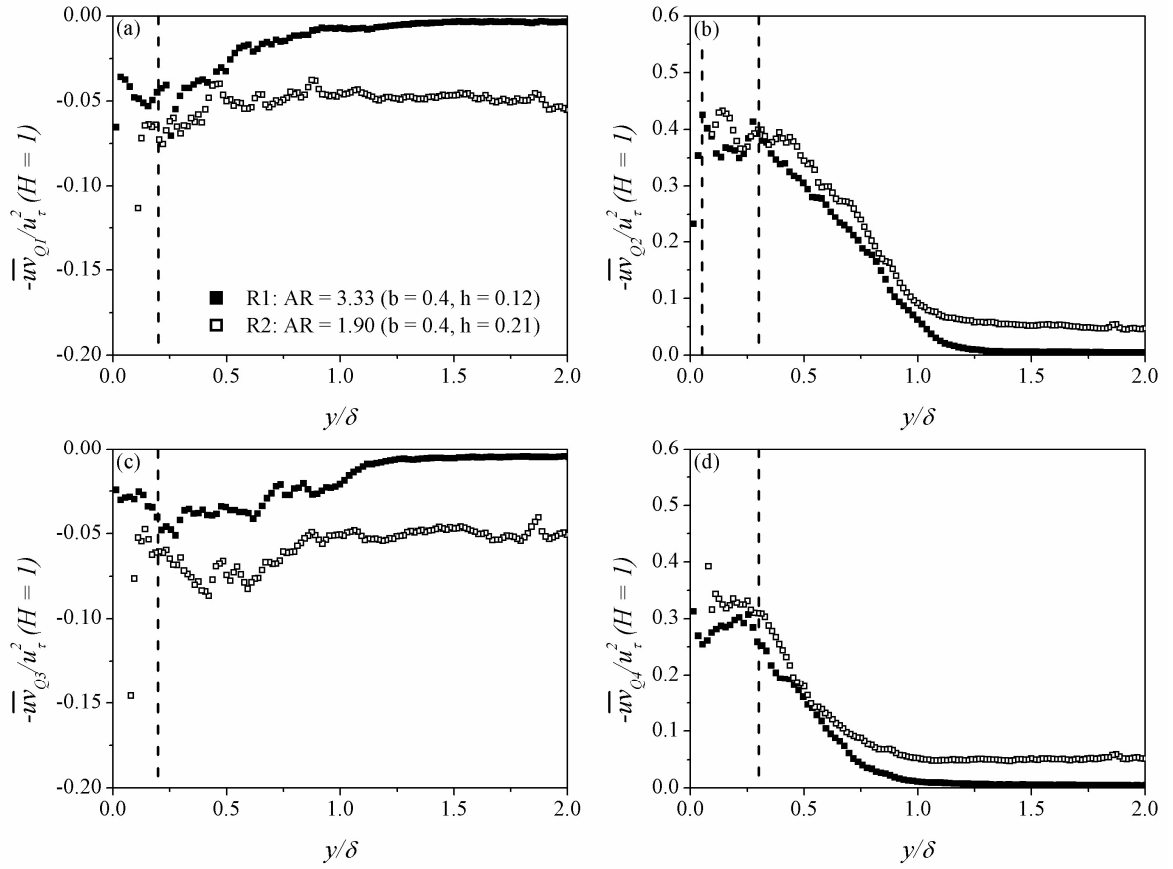


Figure 3.18: Distribution of the contributions of (a) Q1 outward interactions ($u > 0, v > 0$), (b) Q2 ejection events ($u < 0, v > 0$), (c) Q3 inward interactions ($u < 0, v < 0$) and (d) Q4 sweep events ($u > 0, v < 0$) for which $H = 1$ to the total Reynolds shear stress $-\overline{u'v'}$ for tests R1 and R2 ($b = 0.4$ m) over flow depth normalised by boundary layer thickness y/δ

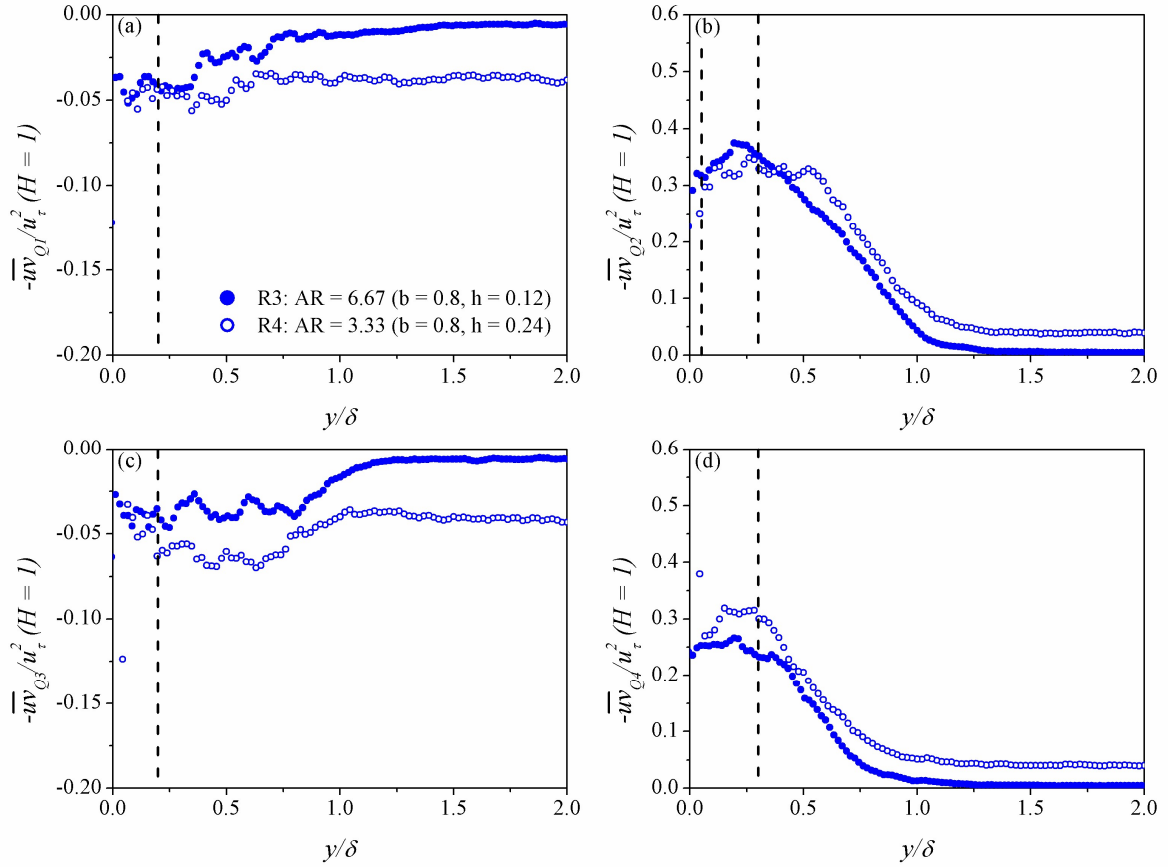


Figure 3.19: Distribution of the contributions of (a) Q1 outward interactions ($u > 0, v > 0$), (b) Q2 ejection events ($u < 0, v > 0$), (c) Q3 inward interactions ($u < 0, v < 0$) and (d) Q4 sweep events ($u > 0, v < 0$) for which $H = 1$ to the total Reynolds shear stress $-\overline{uv}$ for tests R3 and R4 ($b = 0.8$ m) over flow depth normalised by boundary layer thickness y/δ

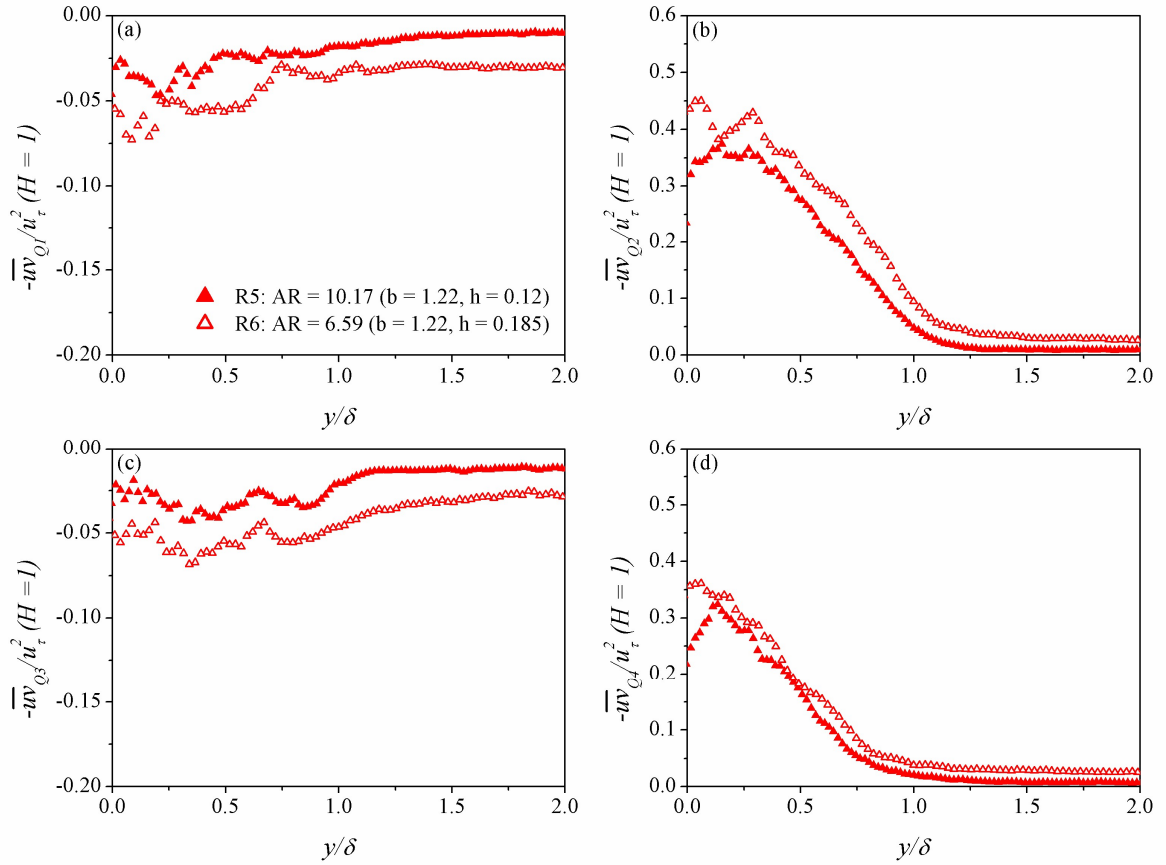


Figure 3.20: Distribution of the contributions of (a) Q1 outward interactions ($u > 0, v > 0$), (b) Q2 ejection events ($u < 0, v > 0$), (c) Q3 inward interactions ($u < 0, v < 0$) and (d) Q4 sweep events ($u > 0, v < 0$) for which $H = 1$ to the total Reynolds shear stress $-\overline{u'v'}$ for tests R5 and R6 ($b = 1.22$ m) over flow depth normalised by boundary layer thickness y/δ

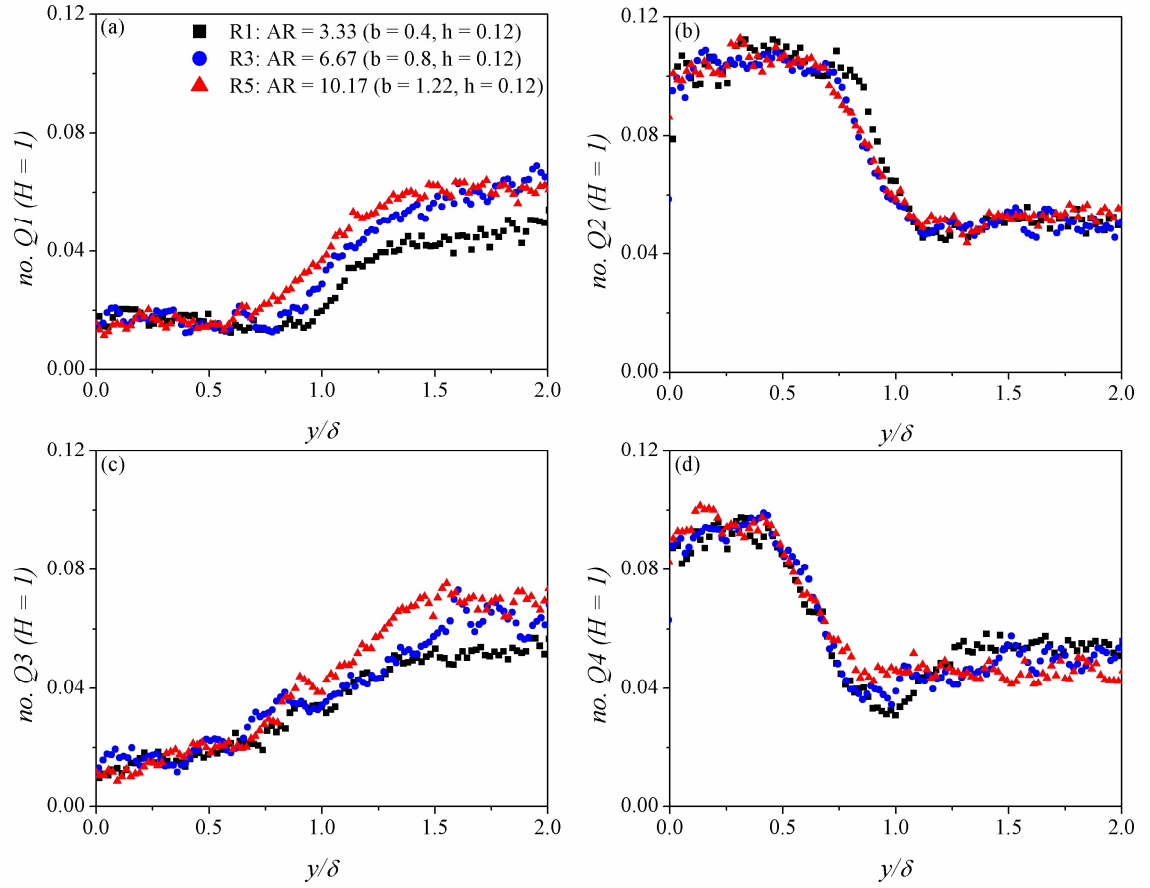


Figure 3.21: Distribution of the number of (a) Q1 inward interactions ($u > 0, v > 0$), (b) Q2 ejection events ($u < 0, v > 0$), (c) Q3 outward interactions ($u < 0, v < 0$) and (d) Q4 sweep events ($u > 0, v < 0$) normalised with the total number of events with $H = 1$ for tests R1, R3 and R5 ($h = 0.12$ m) over the flow depth y normalised with boundary layer thickness δ

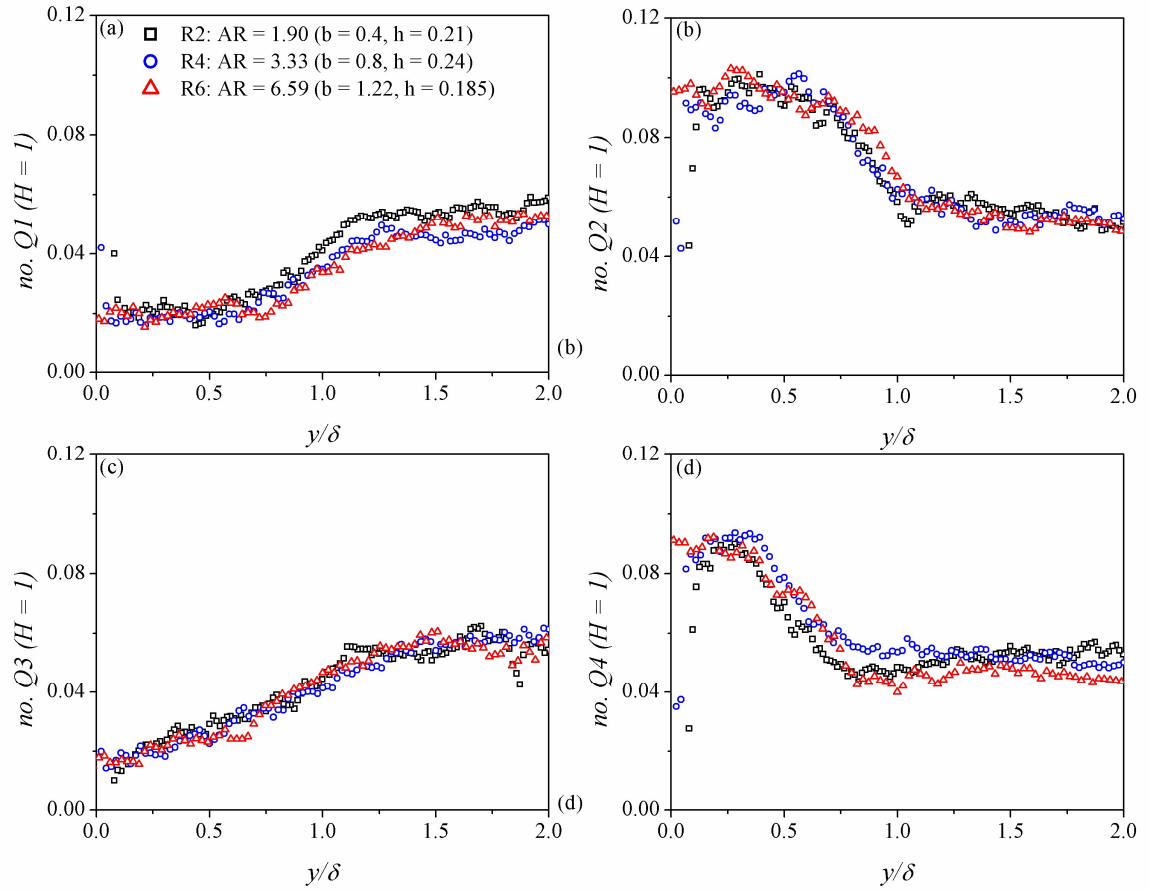


Figure 3.22: Distribution of the number of (a) Q1 inward interactions ($u > 0, v > 0$), (b) Q2 ejection events ($u < 0, v > 0$), (c) Q3 outward interactions ($u < 0, v < 0$) and (d) Q4 sweep events ($u > 0, v < 0$) normalised with the total number of events with $H = 1$ for tests R2, R4 and R6 ($h > 0.12$ m) over the flow depth y normalised with boundary layer thickness δ

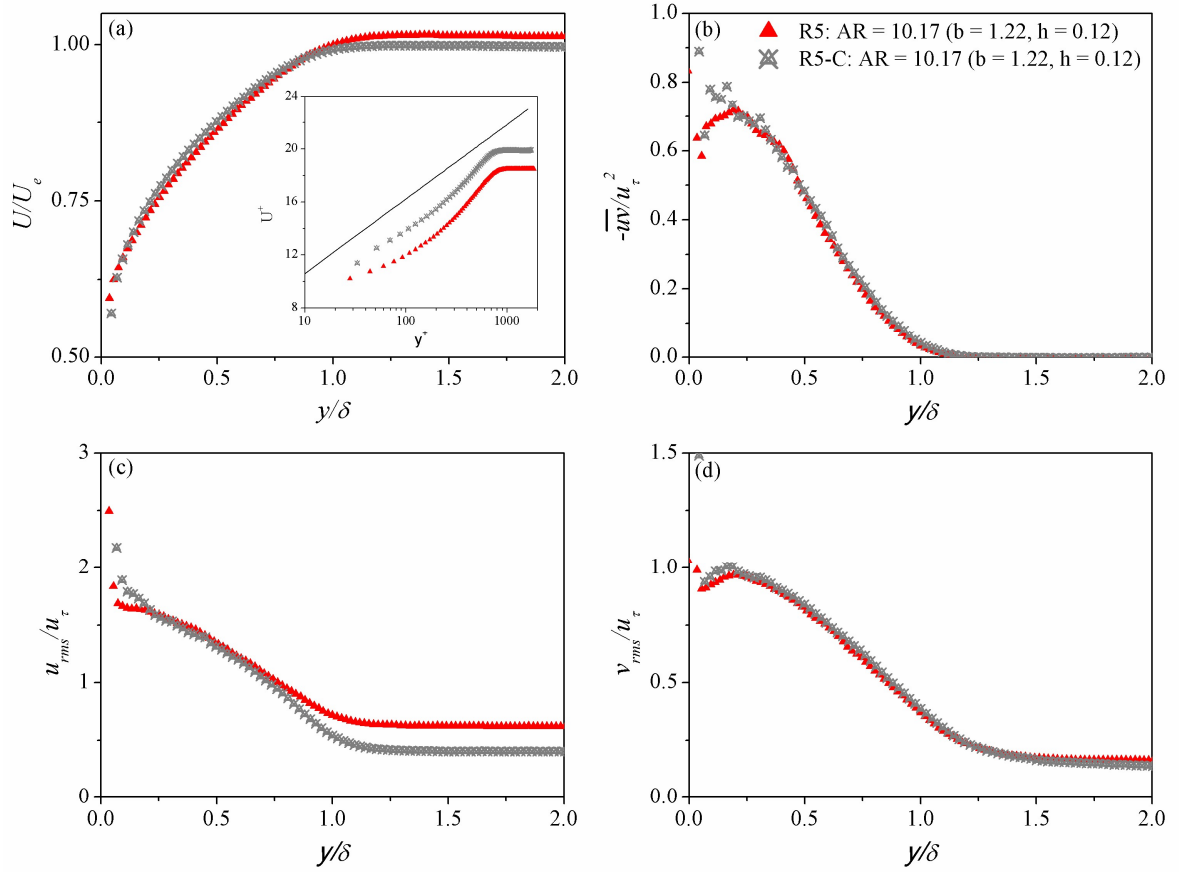


Figure 3.23: Distribution of (a) U/U_e (inset with U^+ vs. y^+ included), (b) Reynolds shear stress normalised with shear velocity $-\overline{u'v'}/u_\tau^2$ (c) streamwise turbulence intensity u_{rms}/u_τ and (d) vertical turbulence intensity v_{rms}/u_τ for tests R5 ($Z = 0$) and R5-C ($Z = 0.32$ m) over the flow depth y normalised with boundary layer thickness δ

3.5 References

1. Albayrak, I., & Lemmin, U. (2011). Secondary currents and corresponding surface velocity patterns in a turbulent open-channel flow over a rough bed. *Journal of Hydraulic Engineering*, 137(11), 1318–1334.
[https://doi.org/10.1061/\(ASCE\)HY.1943-7900.0000438](https://doi.org/10.1061/(ASCE)HY.1943-7900.0000438)
2. Anderson, W., Barros, J. M., Christensen, K. T., & Awasthi, A. (2015). Numerical and experimental study of mechanisms responsible for turbulent secondary flows in boundary layer flows over spanwise heterogeneous roughness. *Journal of Fluid Mechanics*, 768, 316–347. <https://doi.org/10.1017/jfm.2015.91>
3. Balachandar, R., & Patel V. C. (2002). Rough wall boundary layer on plates in open channels. *Journal of Hydraulic Engineering*, 128(10), 947–951.
[https://doi.org/10.1061/\(ASCE\)0733-9429\(2002\)128:10\(947\)](https://doi.org/10.1061/(ASCE)0733-9429(2002)128:10(947))
4. Belcher, B. J., & Fox, J. F. (2009). Laboratory measurements of 3-D flow patterns and turbulence in straight open channel with rough bed. *Journal of Hydraulic Research*, 47(5), 685–688. <https://doi.org/10.1080/00221686.2009.9522050>
5. Bergstrom, D. J., Kotey, N. A., & Tachie, M. F. (2002). The effects of surface roughness on the mean velocity profile in a turbulent boundary layer. *Journal of Fluids Engineering*, 124(3), 664–670. <https://doi.org/10.1115/1.1493810>
6. Blanckaert, K., Duarte, A., & Schleiss, A. J. (2010). Influence of shallowness, bank inclination and bank roughness on the variability of flow patterns and boundary shear stress due to secondary currents in straight open-channels. *Advances in Water Resources*, 33(9), 1062–1074. <https://doi.org/10.1016/j.advwatres.2010.06.012>

7. Coles, D. (1956). The law of the wake in the turbulent boundary layer. *Journal of Fluid Mechanics*, 1(2), 191–226. <https://doi.org/10.1017/S0022112056000135>
8. Djenidi, L., Talluru, K. M., & Antonia, R. A. (2018). Can a turbulent boundary layer become independent of the Reynolds number? *Journal of Fluid Mechanics*, 851, 1–22. <https://doi.org/10.1017/jfm.2018.460>
9. Faruque, M. A. A. (2009.). *Smooth and rough wall open channel flow including effects of seepage and ice Cover*. Doctoral dissertation. University of Windsor, Windsor, Canada.
10. Faruque, M. A. A., & Balachandar, R. (2010). Roughness effects on turbulence characteristics in an open channel flow. *Canadian Journal of Civil Engineering*, 37(12), 1600–1612. <https://doi.org/10.1139/L10-098>
11. Flack, K. A., Schultz, M. P., & Shapiro, T. A. (2005). Experimental support for Townsend’s Reynolds number similarity hypothesis on rough walls. *Physics of Fluids*, 17(3), 035102. <https://doi.org/10.1063/1.1843135>
12. Hinze, J. (1959). *1975 Turbulence*. McGraw-Hill.
13. Jiménez, J. (2004). Turbulent Flows Over Rough Walls. *Annual Review of Fluid Mechanics*, 36(1), 173–196.
<https://doi.org/10.1146/annurev.fluid.36.050802.122103>
14. Krogstad, P.-Å., Antonia, R. A., & Browne, L. W. B. (1992). Comparison between rough- and smooth-wall turbulent boundary layers. *Journal of Fluid Mechanics*, 245(1), 599–617. <https://doi.org/10.1017/S0022112092000594>

15. Lu, S. S., & Willmarth, W. W. (1973). Measurements of the structure of the Reynolds stress in a turbulent boundary layer. *Journal of Fluid Mechanics*, 60(3), 481–511. <https://doi.org/10.1017/S0022112073000315>
16. Mahananda, M., Hanmaiahgari, P. R., & Balachandar, R. (2018). Effect of aspect ratio on developing and developed narrow open channel flow with rough bed. *Canadian Journal of Civil Engineering*, 45(9), 780–794. <https://doi.org/10.1139/cjce-2017-0458>
17. Nakagawa, H., Nezu, I., & Ueda, H. (1975). Turbulence of open channel flow over smooth and rough beds. *Proceedings of the Japan Society of Civil Engineers*, 1975(241), 155–168. https://doi.org/10.2208/jscej1969.1975.241_155
18. Nezu, I., Nakagawa, H., & Tominaga, A. (1985). Secondary currents in a straight channel flow and the relation to its aspect ratio. In *Turbulent shear flows 4* (pp. 246–260). Springer, Berlin, Heidelberg. https://doi.org/10.1007/978-3-642-69996-2_20
19. Nezu, I. (2005). Open-channel flow turbulence and its research prospect in the 21st century. *Journal of Hydraulic Engineering*, 131(4), 229–246. [https://doi.org/10.1061/\(ASCE\)0733-9429\(2005\)131:4\(229\)](https://doi.org/10.1061/(ASCE)0733-9429(2005)131:4(229))
20. Nezu, I., & Nakagawa, H. (1993). Turbulence in open-channel flows, IAHR monograph series. *AA Balkema, Rotterdam*, 1–281.
21. Nezu, I., & Nakagawa, H. (1984). Cellular Secondary Currents in Straight Conduit. *Journal of Hydraulic Engineering*, 110(2), 173–193. [https://doi.org/10.1061/\(ASCE\)0733-9429\(1984\)110:2\(173\)](https://doi.org/10.1061/(ASCE)0733-9429(1984)110:2(173))

22. Nikora, V., & Roy, A. G. (2012). Secondary flows in rivers: Theoretical framework, recent advances, and current challenges. *Gravel-Bed Rivers: Processes, Tools, Environments*, 3–22.
23. Nikora, V., Stoesser, T., Cameron, S. M., Stewart, M., Papadopoulos, K., Ouro, P., McSherry, R., Zampiron, A., Marusic, I., & Falconer, R. A. (2019). Friction factor decomposition for rough-wall flows: theoretical background and application to open-channel flows. *Journal of Fluid Mechanics*, 872, 626–664. <https://doi.org/10.1017/jfm.2019.344>
24. Nikuradse, J. (1933). Laws of flow in rough pipes. *VDI Forschungsheft*, 361.
25. Prandtl, L. (1926). Über die Ausgebildete Turbulenz. In Meissner, E., editor, *2e Internationaler Kongress der Technischen Mechanik, Verhandlung*. Zurich. English Translation: NACA Tech. Memo, 62–75.
26. Rodríguez, J. F., & García, M. H. (2008). Laboratory measurements of 3-D flow patterns and turbulence in straight open channel with rough bed. *Journal of Hydraulic Research*, 46(4), 454–465. <https://doi.org/10.3826/jhr.2008.2994>
27. Roussinova, V. (2009.). *Turbulent structures in smooth and rough open channel flows: effect of depth*. Doctoral dissertation. University of Windsor, Windsor, Canada.
28. Roussinova, V., & Balachandar, R. (2011). Open channel flow past a train of rib roughness. *Journal of Turbulence*, 12, N28. <https://doi.org/10.1080/14685248.2011.591399>

29. Roussinova, V., Biswas, N., & Balachandar, R. (2008). Revisiting turbulence in smooth uniform open channel flow. *Journal of Hydraulic Research*, 46(sup1), 36–48. <https://doi.org/10.1080/00221686.2008.9521938>
30. Roussinova, V., Shinneeb, A.-M., & Balachandar, R. (2010). Investigation of fluid structures in a smooth open-channel flow using Proper Orthogonal Decomposition. *Journal of Hydraulic Engineering*, 136(3), 143–154. [https://doi.org/10.1061/\(ASCE\)HY.1943-7900.0000155](https://doi.org/10.1061/(ASCE)HY.1943-7900.0000155)
31. Roussinova, V., Balachandar, R., & Biswas, N. (2009). Reynolds stress anisotropy in open-channel flow. *Journal of Hydraulic Engineering*, 135(10), 812–824. [https://doi.org/10.1061/\(ASCE\)HY.1943-7900.0000076](https://doi.org/10.1061/(ASCE)HY.1943-7900.0000076)
32. Stewart, M. T., Cameron, S. M., Nikora, V. I., Zampiron, A., & Marusic, I. (2019). Hydraulic resistance in open-channel flows over self-affine rough beds. *Journal of Hydraulic Research*, 57(2), 183–196. <https://doi.org/10.1080/00221686.2018.1473296>
33. Tachie, M. F., Bergstrom, D. J., & Balachandar, R. (2000). Rough wall turbulent boundary layers in shallow open channel flow. *Journal of Fluids Engineering*, 122(3), 533. <https://doi.org/10.1115/1.1287267>
34. Wallace, J. M. (2016). Quadrant analysis in turbulence research: history and evolution. *Annual Review of Fluid Mechanics*, 48, 131–158. <https://doi.org/10.1146/annurev-fluid-122414-034550>
35. Yalin, M. S. (1992). *River Mechanics*. Elsevier.
36. Yang, S.-Q., Tan, S. K., & Wang, X.-K. (2012). Mechanism of secondary currents in open channel flows: secondary currents, sand ridges, flows. *Journal of*

Geophysical Research: Earth Surface, 117(F4).

<https://doi.org/10.1029/2012JF002510>

37. Yokosi, S. (1967). The structure of river turbulence. *Bulletin of the Disaster Prevention Research Institute*, 17(2): 1 – 29.

4 ROLE OF CHANNEL BLOCKAGE RATIO ON LOCAL SCOUR FLOW FIELD MECHANISMS

4.1 Introduction

In a National Cooperative Highway Research Program (NCHRP) evaluation of the landscape of pier scour research, Ettema et al. (2011) stated that “several important aspects of pier scour processes remain inadequately understood and not yet incorporated into design methods.” The parametric framework for scour estimation has been well-established through dimensional analysis, examination of the flow field mechanisms which drive the scouring process and exploration of experimental data. For a turbulent subcritical flow aligned with a circular cylinder in cohesionless, well-graded sediment, prediction of relative scour depth d_{se}/D is commonly based on a function of flow intensity U/U_c , flow shallowness h/D and relative coarseness D/d_{50} . The influence of each of the so-called primary parameters on d_{se}/D have been explored experimentally and defined for ranges attainable under laboratory conditions. Prior analysis has indicated that many commonly-used design equations overestimate d_{se}/D (Williams et al. 2013). Interestingly, tests with common values of U/U_c , h/D , and D/d_{50} still show discrepancies in scour formation (Williams et al. 2016).

Scale effects in hydraulic modelling (described in **Chapter 1**) have been well-reviewed in a paper by Heller (2011). Scale effects are defined as distorted model outputs due to an imbalance in force ratios between a model in the laboratory and a prototype in the field. The review reiterates that scale effects are always present in modelling, but their impact on experimental results can be minimized under certain conditions. The importance of Froude

number similarity between model and prototype in scour modelling is described, as well as some stated thresholds under which scale effects due to certain phenomenon can be neglected. As an example, the vorticity of large-scale structures induced by the presence of the cylinder increases as cylinder size decreases, resulting in disproportionately high depths of scour in experiments (Ettema et al. 2006). Therefore, it is recommended that D be greater than 0.4 m in order to avoid scale effects related to large-scale turbulence (Heller 2011). Similarly, it is recommended that bed material is selected such that median sediment diameter d_{50} is greater than approximately 0.80 mm in order to avoid viscous effects (Oliveto & Hager 2005) and 0.60 mm in order to avoid formation of ripples (Richardson et al. 1990). At the same time, it is desirable to achieve the highest value of relative coarseness D/d_{50} possible, in order to approach the range in which field values lie and reduce scale effects due to the associated disruption of geometric similitude. In effect, cylinder diameter D is further maximized since d_{50} has a minimum size requirement.

Furthermore, D must be large enough to produce flow field structures which induce a measurable scour pattern. The culmination of these restrictions in scour modelling leads to tests with cylinders which are sized such that they pose appreciable blockage to the open-channel flow in a laboratory flume, which are typically half to one metre in width. This results in high values of blockage ratio, D/b , where b is channel width. These are typical conditions under which scour data is acquired, and such data has been used for development of many methods of scour estimation. The role of D/b in scour must therefore be established, both in order to provide correction to previously acquired results where applicable, and to define the conditions under which blockage effects on scour formation can be neglected.

It is important to note that the influence of D/b on scour in the field is usually considered negligible. Naturally occurring rivers are typically wide enough such that channel banks do not affect the formation of local scour at piers. However, in certain cases, the proximity of piers to channel banks can alter scour geometry, complicating scour estimation for design (Ettema et al. 2011). Closely-spaced piers or piers located near bridge abutments may be similarly affected (Laursen & Toch 1956, Ramamurthy & Lee 1973, Oben-Nyarko & Ettema 2011).

Prior analysis on the effect of channel aspect ratio on the distribution of velocity and turbulence in straight channel flow has been carried out. It has been determined that increasing horizontal confinement and vertical confinement on open-channel flow over a transitionally rough porous bed has distinct influences on the distribution of mean streamwise velocity, streamwise and vertical turbulence intensities, third-order turbulent moments and quadrant contributions to Reynolds shear stress. In the present chapter, the effect of horizontal confinement is explored for local scour around an emergent circular cylinder at an equilibrium condition. Previous investigations on blockage effects in scour have focused on equilibrium scour formation only. A closer examination of the flow field surrounding the cylinder under scour conditions is required in order to establish the role of sidewall proximity on the mechanism of local scour.

4.2 *Background*

4.2.1 **The effect of blockage ratio D/b on flow around cylinders**

Blockage effects, as defined by blockage ratio D/b , are a common phenomenon in experimental flow around bluff bodies. Zdravkovich (1997a) described blockage as a

steady disturbance in which the presence of sidewalls in wind and water tunnels confine the disturbed flow and result in imposition of an additional pressure gradient on the flow field surrounding the cylinder. The force imposed by the flow on the cylinder is already dependent on the dynamic pressure of the approach flow and the projected area upon which the approach flow is inflicted. Addition of a pressure gradient in the spanwise direction further complicates the flow field mechanisms surrounding a cylinder. The pressure distribution on the downstream face of the cylinder is particularly affected, which is reflected in changes to the drag coefficient C_D . The conditions under which blockage effects are negligible have been established for flow around a circular cylinder on a fixed bed. For $D/b < 0.1$, blockage effects are generally ignored. When $0.1 < D/b < 0.6$, correction factors should be applied in order to account for modification of flow. If $D/b > 0.6$, the sidewall proximity has a significant impact on the flow field and correction would be insufficient. However, quantification of the effects of changing D/b also depends on Reynolds number Re , cylinder shape and channel configuration (Zdravkovich 1997a, 1997b).

Ramamurthy and Lee (1973) conducted a study on the effects of sidewall proximity in flow past bluff bodies. For various cylinder shapes and configurations, the effect of D/b on the pressure distribution around a cylinder was investigated. The authors analyzed the flow field surrounding a cylinder and determined that wall interference would induce an increase in streamwise velocity near the cylinder body and outside of the wake region, resulting in a decrease in pressure in the wake region and an increase in the drag force on the cylinder. They also made note of the additional pressure gradient in the spanwise direction. For most confined flows, the contracted jet velocity in the region between the wake and the sidewall,

U_j (**Figure 4.1**), has been deemed to be a close approximation of the velocity along the separating streamline, U_s . The value of k , equal to the ratio between U_s and the approach flow velocity U , was found to increase with increasing D/b for all cylinder shapes. The pressure distribution for a circular cylinder with $D/b = 0.6$ was unchanged around the sides of the cylinder for Re values of 6.9×10^4 , 11.7×10^4 , 14.8×10^4 and 20.4×10^4 . In the wake of the cylinder, the pressure coefficient increased with increasing Re , and became constant over the two highest values of Re . Slight changes were observed in the location of the separation point as well. The drag coefficient C_D was also found to increase slightly with D/b , but the drag coefficient normalised by U_j was found to be nearly constant with changing D/b . The observed changes in drag force due to increasing sidewall proximity were similar to changes in drag force induced by decreasing gap width between adjacent cylinders (Ramamurthy & Lee 1973).

Ramamurthy et al. (1989) conducted a similar experimental investigation in order to establish a correction factor for sharp-edged bluff bodies (a flat plate and an equilateral prism). The authors identified the necessity for appreciably-sized bluff bodies in models (similar to the minimum cylinder diameter requirement for scour modelling) for measurement accuracy, and the conflicting need for reduction of wall interference due to sidewall proximity. In concurrence with the results of Ramamurthy and Lee (1973), the experimental results indicated that k and C_D increased with increasing D/b and an expression for correction of C_D based on D/b was presented (Ramamurthy et al. 1989).

4.2.2 Blockage effects in scour literature

The blockage problem has been identified since the introduction of scour modelling in laboratory experiments. An early investigation on local scour around piers and abutments by Laursen and Toch (1956) pointed to the effect of contraction in flow due to alignment of multiple cylinders in the cross-stream direction. As stated by Ramamurthy and Lee (1973), this effect is often taken as analogous to wall interference. It was postulated that the contraction would be expected to result in an increase in the streamwise velocity, and therefore relative scour depth d_{se}/D , in the vicinity of the cylinders. Furthermore, Laursen and Toch (1956) stated that scour depth would be likely governed by h/D (where h is the depth of flow) if the gap between adjacent cylinders is acceptably larger than D . As the gap between cylinders decreases, scour depth will be related to the gap width. Here, the described contraction effect is related to the gap between adjacent cylinders. The authors concluded that an accurate model of a prototype pier would require a very large channel width b or a very small cylinder diameter D . However, it was stated that b did not need to be optimized based on gap width since contraction in the model could be ‘distorted’ with minimal error (Laursen & Toch 1956).

Chiew (1984) conducted an extensive experimental and analytical investigation of local scour at piers. The experiments were conducted such that D/b was held below 0.1 (i.e. 10 percent). This threshold, below which maximum sidewall effects were deemed insignificant, was established from a previous investigation by Shen et al. (1966). In this paper, it was reported that a D/b of 0.125 produced a ‘significant’ wall effect. Many investigations in literature include scour data under testing conditions for which D/b exceeds 10 percent. Details for examples of such investigations are shown in **Table 4.1**,

including the maximum value of blockage ratio in the experimental program $(D/b)_{max}$. It can be seen that blockage effects have largely been ignored in much of the scour literature published in the past.

The effect of proximity between a bridge abutment and adjacent pier has been explored experimentally by Oben-Nyarko and Ettema (2011). Although this effect is not exactly analogous to channel blockage since the abutment is located near only one side of the flow field surrounding the pier, the investigation provides further confirmation that the mechanism of local scour is affected by lateral proximity to a solid boundary. Scale experiments were carried out in order to establish the effect of abutment proximity on pier scour, and it was reported that scour depth at the pier increased significantly as proximity to the abutment increased (Oben-Nyarko & Ettema 2011).

Table 4.1: Description of literature experiments with large blockage ratio D/b

Author(s)	Year	b (m)	D (m)	$(D/b)_{max}$
Raudkivi and Ettema	1983	1.5	0.102	0.068
Johnson and Torrico	1995	1.8	0.254	0.141
Sheppard et al.	2004	6.1	0.91	0.149
Ettema et al.	2006	3.0	0.406	0.135

4.2.3 Previous investigations on the influence of blockage ratio D/b on relative scour depth d_{se}/D

Hodi (2009) carried out an experimental investigation into the effects of D/b on scour geometry. Experiments were conducted in two flumes with varying channel widths and cylinder diameter values. Blockage ratio D/b was held in the range of 0.022 to 0.05 and it was determined that over the range considered, d_{se}/D increased with increasing D/b .

D'Alessandro (2013) altered the width of flow with movable sidewalls installed in a sediment recess of fixed median sediment diameter d_{50} , in order to isolate the effects of blockage ratio. The range of D/b for this investigation was 0.025 to 0.112. The sidewall proximity was adjudged to influence both the depth and width of the scour hole. For a fixed D/d_{50} , it was reported that an increase in D/b resulted in an increase in d_{se}/D , in agreement with the results of Hodi (2009).

Tejada (2014) carried out similar experiments with implementation of movable sidewalls, but also used four types of bed material in order to determine if blockage effects are influenced by changes in d_{50} . The range of blockage for this investigation was $0.05 < D/b < 0.15$. The author reported that D/b was less influential on d_{se}/D when relative coarseness D/d_{50} was less than 100 (Tejada 2014). Williams et al. (2018) reported similar findings for two types of bed material. For d_{50} values of 0.51 mm and 0.77 mm, d_{se}/D was found to increase with increasing blockage ratio and the scour formation reached the sidewalls at further distance downstream when the flow was less constrained by the sidewalls (see **Figure 4.2**). The differences between the scour formations due to changes in D/b were found to decrease with decreasing D/d_{50} , which is in agreement with the results reported in Tejada (2014). Finally, a new parameter k_c , the ratio between U_s and U_c , was defined. A new scour estimation method based on k_c and h/D was established and validated using results from literature (Williams et al. 2018).

While such prior investigations have provided a general idea of how blockage ratio D/b influences the maximum relative scour depth d_{se}/D , the impact of wall interference on the flow field mechanisms surrounding a cylinder under scour conditions still lacks clarity. In order to appropriately incorporate blockage correction into scour estimation methods,

understanding of the flow field under horizontal confinement must be improved. The present investigation discusses bed profile measurements and Particle Image Velocimetry (PIV) measurements which have been taken for local scour at an equilibrium condition around an emergent cylinder under varying horizontal confinement (i.e. varying D/b). The results of the investigation described in **Chapter 3** indicated that increasing horizontal confinement (i.e. decreasing channel width b) affects the magnitude and distribution of mean streamwise velocity, streamwise turbulence intensity, third-order turbulent moments and the magnitude and quantity of quadrant events in straight channel flow over a porous bed in the absence of the cylinder. In the boundary layer region ($0.2 < y/\delta < 1.0$), all third-order turbulent moments increased with decreasing b . In the free-stream region, the streamwise turbulence intensity and the streamwise transport of the normal stress $\overline{u^2}$ decrease with decreasing b . These aspects need to be taken into consideration when analyzing the flow field with local scour, particularly in view of the understanding that changes in approach flow turbulence will influence the mechanism of scour (Kirkil et al. 2008).

4.3 Methodology

Three tests were conducted under varying D/b for an emergent circular cylinder and nominally the same approach flow. Cylinder diameter D was constant at 0.056 m in all tests and so D/d_{50} based on the test sediment with $d_{50} = 0.74$ mm was 76. Flow depth h was 0.12 m and corresponded to a flow shallowness h/D of 2.14. A flow shallowness h/D greater than 1.4 corresponds to the narrow range of cylinders, which is the range in which the majority of scour experiments fall (Ettema et al. 2011). Flow intensity U/U_c was approximately 0.85 for all tests, such that clear-water conditions were maintained. Flow

intensity is typically held between 0.75 and 0.90 in order to ensure flow is in the clear-water regime while still obtaining a measurable scour pattern. Three additional tests (S1, S2 and S3) were carried out for a submerged cylinder with $D = 0.056$ m under the same flow conditions as tests B1, B2 and B3 (see **Table 4.2**).

Table 4.2: Test parameters for local scour experiments

Test ID	Cylinder type	b (m)	b/h	D/b	U (m/s)	U_e (m/s)	u_τ (m/s)	ΔU^+	Re
B1	E	0.4	3.33	0.14	0.262	0.28	0.0135	1.33	33500
B2	E	0.8	6.67	0.07	0.261	0.28	0.0147	3.34	33400
B3	E	1.22	10.2	0.05	0.254	0.275	0.0149	4.48	32900
S1	S	0.4	3.33	0.14	0.262	0.28	0.0135	1.33	33500
S2	S	0.8	6.67	0.07	0.261	0.28	0.0147	3.34	33400
S3	S	1.22	10.2	0.05	0.254	0.275	0.0149	4.48	32900

Movable sidewalls were installed in the flume as required in order to alter channel width b while holding all other scour-governing parameters constant, therefore isolating the effect of horizontal confinement on both scour geometry and the surrounding flow field. For all tests, the cylinder was located in the middle of the channel ($Z/D = 0$). PIV measurements were taken in the central plane A, near-cylinder plane B and mid-cylinder-wall plane C (see **Figure 2.2**). Details for the approach flow characteristics for each test are given in **Table 4.2**.

During the local scour tests, the flow was circulated in the flume for 24 hours prior to acquisition of PIV data. Prior experimentation indicated that an acceptable equilibrium condition of scour was obtained within 24 hours, after which changes in the maximum

scour depth were minimal (D'Alessandro 2013, Williams 2014). Select tests were repeated and bed profile measurements were compared in order to assure repeatability.

It is important to make note of the approach flow conditions for local scour tests in the present investigation. In previous studies (Hodi 2009, D'Alessandro 2013, Tejada 2014, Williams et al. 2018), flowrate Q was held constant for all tests and it was assumed that the velocity profiles for all tests were similar. No velocity profiles were measured. For the current investigation, the flowrate Q was mildly adjusted in order to attain the same value of the depth Reynolds number for all tests.

4.4 Results and discussion

4.4.1 Approach flow conditions

The approach flow conditions for tests B1, B2 and B3 are shown in **Figure 4.3** and **Figure 4.4**. **Figure 4.3** shows the distribution of streamwise velocity U at two stations in a single field-of-view taken in the central plane in the absence of the cylinder. The velocity profiles in **Figure 4.3** indicate that the distribution of U is similar over a single-field-of-view. **Figure 4.4(a)** shows profiles of U and the Reynolds shear stress $-\overline{uv}/U_e^2$ over the depth of flow. The value of U is very close for test B1 and B2 in the free-stream region and the magnitude of U is slightly higher for test B1 within the boundary layer. U is slightly lower throughout the depth of flow for test B3, which is reflected in the lower depth-averaged velocity and maximum velocity U_e given in **Table 4.2**. **Figure 4.4(b)** shows that the Reynolds shear stress $-\overline{uv}/U_e^2$ is higher in the near-bed region for test B3 than tests B1 and B2. While the Reynolds shear stress is quite similar for tests B1 and B2 in the free-stream region, $-\overline{uv}/U_e^2$ is slightly higher for test B2 than B1 in the near-bed region.

Therefore, increasing channel width b causes an increase in Reynolds shear stress in the near-bed region. **Figure 4.4** has established how increasing channel width affects flow properties for straight-channel flow in the absence of a cylinder, which is applied to analysis of flow properties in the following sections.

4.4.2 Comparison of bed profiles

Figure 4.5 shows photographs taken from upstream of the cylinder for each test. The extent of the scour hole surrounding the cylinder can be seen for each test. In the wake of the cylinder, the primary deposit is also indicated. The primary deposit is the dune formed by deposition of sediment by the wake vortices as they advect away from the cylinder in the downstream direction. The location of the undisturbed sand bed on either side of the scour formation is marked by ‘A’ and ‘A’ for each test.

In **Figure 4.6**, the bed profile measurements in the XZ plane ($Y/D = 0$) are given for tests B1, B2 and B3. The profiles for test B1 are shown by the black square symbols, test B2 is shown by the blue circular symbols and test B3 is shown by the red triangular symbols. In the vicinity of the cylinder, the size of the scour hole is shown to increase with decreasing D/b . The width of the scour formation downstream of the scour hole increases for tests B2 and B3 (‘A’). The width of scour in test B1 increases further as the formation progresses downstream (‘B’). However, the lateral progression is smaller for test B1 than for tests B2 and B3 (see **Figure 4.5**). This could be an effect of horizontal confinement, where the increase in sidewall proximity in the narrow channel for test B1 confines the von Kármán vortex street. Since the wake vortices in the von Kármán vortex street are responsible for transport and deposition of the sediment, confinement of the wake would result in a narrower scour formation.

The scour formation for test B1 reaches the sidewalls around $X/D = 7$, and so the scour formation downstream of this point encompasses the width of the flume. In contrast, the scour formations for tests B2 and B3 do not reach the sidewalls at all. However, the scour formation for test B2 shows fewer undulations than that for test B3 (see **Figure 4.5**). This indicates that even when the scour formation does not progress to the sidewalls, increasing horizontal confinement can still influence the mechanism of sediment transport and deposition.

Figure 4.7 shows bed profile measurements of the equilibrium scour formation in the XY plane for (a) the central plane A ($Z/D = 0$), (b) the near-cylinder plane B ($Z/D \approx 0.5$) and the mid-cylinder-wall plane C (Z/D is variable). The flow direction in the figures is denoted as the positive X -direction. The original bed level is shown by the dotted line along $Y/D = 0$, and the location of the cylinder is shown by the filled grey area. In **Figure 4.7(a)**, the classical scour profile is shown in each test, with a scour hole in the vicinity of the cylinder and a primary deposit in the form of a dune with a crest in the downstream region. In general, the maximum scour depth near the upstream face of the cylinder increases as D/b decreases. As seen in the photographs in **Figure 4.5**, the scour formation occupies the entire width of the flume downstream of the scour hole for test B1. Since the flow is subcritical and the control is located downstream, there will be corresponding changes to the velocity distribution further upstream, around the cylinder. Consequently, there is reduction in velocity in the vicinity of the cylinder, thereby reducing the size of the scour hole in test B1 compared to tests B2 and B3. Details of the velocity contours are discussed in a forthcoming section.

In **Figure 4.7(a)**, the bed profiles also indicate that differences in the scour depth between tests B2 ($D/b = 0.07$) and B3 ($D/b = 0.05$) are very small in the scour hole and increase in the downstream region over the dune and at its crest. The length of the dune is taken as the point from which the scour profile crosses the horizontal axis downstream of the cylinder to the point at which the profile returns to the original bed level. The length of the dune is longer for test B2 ($X/D \approx 6$) than for tests B1 ($X/D \approx 5$) and B3 ($X/D \approx 4.5$).

In **Figure 4.7(b)**, the bed measurements in plane B indicate that the depth of scour increases with decreasing D/b . The scour profiles for tests B2 and B3 are very similar along the entire near-cylinder plane, except in the region immediately adjacent to the cylinder and at the crest of the dune. This indicates that the effect of the sidewalls on scour around the cylinder is amplified when $D/b = 0.14$ for the range of D/b in the present investigation. This is in agreement with Zdravkovich (1997b), whose analysis indicated that correction factors must be applied to the flow field when $D/b > 0.10$ for flow around circular cylinders with a fixed bed.

In **Figure 4.7(c)** which gives bed measurements along plane C, only tests B1 and B2 are shown because the scour formation did not extend as far as this plane for test B3. In **Figure 4.6**, the location of plane C for each test is indicated by the dashed lines. Plane C was taken along the midpoint between the side of the cylinder ($Z/D = 0.5$) and the channel sidewall. Therefore, when the channel width b was increased for test B2 and B3 and the gap between the cylinder and the sidewall were subsequently increased, the location of plane C was also changed. While the profile for test B1 shows an appreciable depth of scour in plane C close to the cylinder, only a small portion of the downstream extent of scour reached this plane for test B2.

Figure 4.8 shows bed profile measurements for tests S1, S2 and S3. In **Figure 4.8(a)**, it can be seen that the size of the scour hole increases with decreasing D/b for a submerged cylinder, which is in agreement with the relationship between scour hole size and D/b for an emergent cylinder seen in **Figure 4.6**. In **Figure 4.8(b)**, the scour holes are very similar for all tests; the greatest differences are seen in the dune region. As with test B2, the dune for test S2 (both having $D/b = 0.07$) are longer than the dunes for the other tests. This comparison provides validation for the bed profiles for tests B1, B2 and B3.

To further understand the changes in the scour formations, velocity profiles in plane B were analyzed for tests B1, B2 and B3. The distribution of the mean streamwise velocity U/U_e , mean vertical velocity V/U_e and Reynolds shear stress $-\overline{uv}/U_e^2$ are provided at several streamwise locations in plane A (**Figure 4.9**) and plane B (**Figure 4.10**), starting at the location of the scour hole. The location where each profile was extracted in plane B is shown by the dashed lines in **Figure 4.7(b)**. The following analysis focuses on plane B as the profiles in the two planes are qualitatively similar.

The distribution of U/U_e is shown in the top row of **Figure 4.10**. At $X/D = -2.0$, profiles are taken in the region above the scour hole. The corresponding approach flow conditions for each test in the absence of the cylinder are also provided for comparison. The mean streamwise velocity is less than the magnitude of the approach flow for all tests. It can be seen that U/U_e for test B3 is closest to the approach flow magnitude, and U/U_e for test B1 is lowest. Near the free surface, perturbations due to the presence of the cylinder also appear to cause a reduction in U/U_e for tests B2 and B3. Within the scour hole ($Y/D < 0$), the mean velocity also decreases for all tests due to separation of flow from the leading edge of the hole. At $X/D = -0.5$ (i.e. the location of the upstream face of the cylinder), U/U_e

clearly decreases with increasing D/b throughout the depth of flow. Along the side of the cylinder ($X/D = 0$), U/U_e is also lowest for test B1. Close to the bed, the velocity for test B3 decreases, dropping below that of test B2. In the mid-depth region, B3 approaches B2. In the upper region of flow, the velocity for B3 increases and becomes constant, decreasing only very near the free surface. The streamwise velocity decreases sharply around $Y/D = 1.8$ for both tests B1 and B2.

At the location of the downstream face of the cylinder ($X/D = 0.5$), U/U_e is higher for test B3 than tests B1 and B2. Close to the bed, U/U_e is very similar for tests B2 and B3, and lower for test B1. For tests B1 and B2, U/U_e shows a decrease in the positive vertical direction until $Y/D \approx 1.5$. However, the magnitude of U/U_e is constant in the region between $0.5 < Y/D < 1.5$ for test B3. In the upper region of flow, there is a sharp decrease below the free surface. This dip in the velocity is closer to the free surface for test B3 than for tests B1 and B2. Downstream of the cylinder close to the leading edge of the dune for all tests ($X/D = 2.0$), the velocity for tests B1 and B2 is very similar and the magnitude is higher for test B3 throughout the depth. Further downstream at $X/D = 7.0$, the dune has ended for test B1 but flow at this location is still over the dune for tests B2 and B3. Nonetheless, the magnitude of U/U_e above $Y/D = 0.5$ (i.e. the height of the dune for all tests) is very similar. Below $Y/D = 0.5$ for test B1, the region of very low velocity corresponds to the separated flow in the wake of the dune.

The middle row of profiles in **Figure 4.10** gives the distribution of the normalised vertical velocity V/U_e . Around the start of the scour hole ($X/D = -2.0$), the vertical velocity distribution is very similar for all three tests and directed downwards through most of the depth. At $X/D = -0.5$, the negative component of V for all tests is shown to increase as the

original bed level is approached, which is reasonable since it is expected that a significant component of flow would be entering the scour hole at this location. Along the side of the cylinder at $X/D = 0$, the vertical velocity distribution for all tests collapses between $1.0 < X/D < 1.5$. It appears that the profiles show a tendency towards positive V in all three tests close to the free surface. The component of negative vertical velocity increases close to the bed as flow continues to be diverted into the scour hole. At the downstream edge of the cylinder ($X/D = 0.5$), the velocity distribution is similar to that at $X/D = 0$. There is a decrease in negative V/U_e below $Y/D = 0$ at this location, which corresponds to acceleration of the flow up along the downstream slope of the scour hole. The vertical velocity is lowest for test B3 throughout most of the depth. In the mid-depth region, the profiles for B1 and B2 are similar in magnitude.

At the leading edge of the dune ($X/D = 2.0$), the distribution of V/U_e is similar for all tests. There is a local minima around $Y/D = 1.5$, which is lowest for test B3. The magnitude of the vertical velocity decreases with decreasing D/b at this location. Further downstream ($X/D = 7.0$), the profiles show good collapse in the region near the end of the dune. For test B1, this profile is located downstream of the crest the dune. This location can be viewed as a backward-facing step and the increase in V/U_e close to the bed corresponds to the expected recirculating region in its wake.

The distribution of the Reynolds shear stress $-\overline{uv}/U_e^2$ is similar for all tests between $-2.0 < X/D < 0$. There are some small changes close to the bed and near the free surface, but the profiles are largely unchanged throughout most of the depth. At $X/D = 0.5$, $-\overline{uv}/U_e^2$.for tests B1 and B2 increases in magnitude in the mid-depth region, while the Reynolds shear stress is close to zero through most of the depth for test B3 ('A') at the smallest D/b .

Additional tests with an acrylic flat plate around the base of the cylinder (to prevent the formation of the scour hole) indicate that the bed shear stress between $-0.5 < X/D < 0$ in plane B is of the order of 2.5 to 3 times the critical shear stress required for sediment motion. This is indicative of the potential for initiation of scour at the sides of the cylinder. From $2.0 < X/D < 7.0$, the shape of the profiles for $-\overline{uv}/U_e^2$ is similar for all tests.

Graf and Istiarto (2002) presented Acoustic Doppler Velocity Profiler (ADVP) measurements in the central plane of flow around a circular cylinder at equilibrium of local scour. The authors similarly reported profiles of streamwise velocity, vertical velocity and Reynolds shear stress at several streamwise locations upstream and downstream of the cylinder. The results of the present investigation are in good qualitative agreement with the ADVP measurements presented therein.

In order to appreciate the contribution of positive and negative streamwise and vertical velocity fluctuations to the total Reynolds shear stress, quadrant analysis was carried at $X/D = -0.5$ and $X/D = 0.5$ in plane B. The method used for analysis was introduced by Lu and Willmarth (1973), in which the contribution to $-\overline{uv}$ from a given quadrant Q_i is determined by **Equation 4.1** and **Equation 4.2**.

Equation 4.1:
$$(uv)_{Q_i} = \lim_{T \rightarrow \infty} \frac{1}{T} \int_0^T u(t)v(t)I(t)dt \quad \text{for } i = 1 - 4$$

Equation 4.2:
$$I(t) = \begin{cases} 1 & \text{when } |uv|_Q \geq Hu'v' \\ 0 & \text{otherwise} \end{cases}$$

In **Equation 4.2**, H is the Reynolds shear stress magnitude parameter used to filter stronger events. The distribution of Q2 events ($u < 0, v > 0$), known as ejections, and Q4 events ($u > 0, v < 0$), known as sweeps, are given in **Figure 4.11** and **Figure 4.12**, respectively. Note

that the average Reynolds shear stress contribution for each quadrant $-\overline{uv}_{Qi}$ was obtained by dividing by the total number of events for each quadrant, which differs from the method used to determine the quadrant contributions calculated in **Chapter 3**. Analysis was carried out for $H = 0$ and $H = 1.75$, where $H = 1.75$ corresponds to the extreme events which contribute significantly to the total shear stress. Profiles are given for $X/D = -0.5$ and $X/D = 0.5$ (i.e. the locations of the upstream and downstream faces of the cylinder).

In **Figure 4.11(a)**, the magnitude of the Q2 contributions with $H = 0$ at $X/D = -0.5$ is shown to be close to zero for all tests throughout most of the depth. Closer to the original bed level ($Y/D \approx 0.5$), the magnitude of the ejections begins to increase for all tests; the magnitude of the contributions becomes greater for tests B2 and B3 in this region. **Figure 4.11(b)** shows that the magnitude of the ejection events has increased at $X/D = 0.5$. For tests B1 and B2, the profiles increase above the original bed level, reaching a local maxima around $Y/D \approx 0.5$ before decreasing towards the free surface. The magnitude of the Q2 events is higher for test B2 between $0.5 < Y/D < 1.75$. For test B3, the magnitude of the Q2 events is very low close to the original bed level, increasing slightly around $Y/D \approx 0.25$. The profile then shows a sharp increase towards the free surface at $Y/D \approx 1.75$. The magnitude of the profile for test B3 is less than tests B1 and B2 throughout the depth of flow except in the region near the free surface ($Y/D > 1.75$). In **Figure 4.11(c)**, the distribution of Q2 ejection events for $H = 1.75$ at $X/D = -0.5$ is shown to be similar to the distribution for $H = 0$. The profiles for all tests are close to zero and there is an increase around $Y/D \approx 0.75$, below which the magnitude is greater for tests B1 and B2 than test B3. At $X/D = 0.5$ (**Figure 4.11(d)**), the magnitude of the ejections is higher throughout the depth of flow when $H = 1.75$ when compared to the distribution for $H = 0$. The strength of the Q2 events is higher

above $Y/D \approx 1.0$ for test B2 when compared with B1, and B3 is also lower than either test except close to the free surface ($Y/D > 1.5$).

In **Figure 4.12(a)**, the magnitude of the Q4 contributions with $H = 0$ at $X/D = -0.5$ is shown to be similar to the distribution of the Q2 contributions. At the location of the downstream face of the cylinder ($X/D = 0.5$), **Figure 4.12(b)** shows that the distribution of the magnitude of the sweep events is similar for tests B1 and B2, showing an increase between $0.5 < Y/D < 1.75$. As with the Q2 contributions, the magnitude of the Q4 contributions is lower for test B3 than tests B1 and 2, except close to the free surface ($Y/D > 1.75$). **Figure 4.12(c)** gives the distribution of Q4 contributions for which $H = 1.75$ at $X/D = -0.5$, which is also similar to the distribution of the Q2 contributions with $H = 0$ at the same location. In **Figure 4.12(d)**, the distribution of the magnitude of the Q4 contributions at $X/D = 0.5$ is shown to be similar for tests B1 and B2, but the magnitude is higher for test B2 throughout the depth of flow. The distribution for test B3 is still lower than tests B1 and B2 throughout the depth, except in the region close to the free surface ($Y/D > 1.75$).

In general, the quadrant decomposition indicates that the distribution and magnitude of both sweep and ejection events is affected by changes in D/b . At the location of the upstream face of the cylinder ($X/D = -0.5$), the magnitude of the Q2 and Q4 contributions is reduced near the bed when $D/b = 0.14$ for $H = 0$ and $H = 1.75$. At the location of the downstream face of the cylinder, the Q2 and Q4 contributions with $H = 0$ are enhanced in the middle of the depth when D/b is high ($0.07 < D/b < 0.14$) compared with $D/b = 0.05$. The distribution of magnitude of the stronger ejections and sweeps ($H = 1.75$) is similar for all D/b at $X/D = 0.5$. When compared with tests for which D/b is 0.05 and 0.14, the magnitude of the stronger ejection events becomes higher for $D/b = 0.07$ at $Y/D \approx 1.0$, and

the magnitude of the stronger sweep events for $D/b = 0.07$ is highest throughout the depth of flow. From the bed profiles, this corresponds to an increased potential in sediment removal over the dune downstream of the cylinder and therefore a greater dune length for test B2.

Spanwise profiles of scour are shown in **Figure 4.13** for the YZ plane (a) upstream of the cylinder ($X/D = -1.3$), (b) at the spanwise centreline ($X/D = 0$) and (c) downstream of the cylinder ($X/D = 1.75$). The effect of D/b shown in the spanwise profiles shares similarities with the effects seen in the streamwise profiles. In **Figure 4.13(a)**, the profile of scour along $X/D = -1.3$ is indicative of the frustum shape of the scour hole upstream of the cylinder, and once again shows that scour depth in this region increases with decreasing D/b . The profiles of scour along $X/D = 0$ in **Figure 4.13(b)** confirm that decreasing D/b increases scour. The differences in scour depth between test B2 ($D/b = 0.07$) and test B3 ($D/b = 0.14$) are smaller than the differences shown at $X/D = -1.3$ in **Figure 4.13(a)**. **Figure 4.13(c)**, which shows scour along $X/D = 1.75$, confirms that there is almost no difference at all between the scour profiles for tests B2 and B3 at the downstream edge of the scour hole. For $D/b = 0.07$ and 0.05 , it can be seen that the effect of horizontal confinement is stronger far away from the pier (i.e. near the crest of the primary deposit and in the scour hole upstream of the cylinder) than in the vicinity of the pier. This indicates that the effect of the sidewalls is less influential on the flow field mechanisms driving scour near the cylinder (i.e. the horseshoe vortex) and more influential on the wake vortices, which control the scour formation in the region of the primary deposit.

In general, the equilibrium scour profiles indicate that increasing horizontal confinement reduces the depth of the scour hole, but the overall bed formation downstream of the hole

is different at each D/b . This contradicts the conclusions of the small number of investigations on the effect of D/b on d_{se}/D , in which increasing D/b was mostly shown to increase d_{se}/D (Hodi 2009, D'Alessandro 2013, Tejada 2014, Williams et al. 2018). From analysis of the bed measurements and velocity profiles, it appears that the dune in the wake region is most significantly affected by sidewall proximity. The correlation of this finding with the flow field will be discussed in the following section.

4.4.3 Distribution of normalised mean streamwise velocity U/U_e

In **Figure 4.14(a)**, the distribution of U/U_e for plane A in test B1 is shown. Upstream of the cylinder, an adverse pressure gradient is indicated by the decrease in streamwise velocity in the region leading to the stagnation line at the upstream face of the cylinder ('A'). Near the leading edge of the scour hole, a region of low velocity is visible ('B'), which corresponds to separated flow within the hole. In the near-wake region downstream of the cylinder, there is a region of low and negative U/U_e ('C'); in the same region, there is an upwash of flow indicated by the vector field. The flow is shown to accelerate out of the scour hole in the downstream direction over the dune ('D'), exceeding the maximum velocity in the approach flow. The flow separates over the peak of the dune and forms a shear layer which emanates from its crest ('E').

Features B and C were also observed by Graf and Istiarto (2002). Similar features were also reported in Dey et al. (2008), by whom Acoustic Doppler Velocimetry (ADV) measurements were presented in the central plane for an equilibrium scour formation which had been fixed with resin spray. In the present investigation, the flow field within the scour hole was not captured due to restriction of optical access. However, Large Eddy Simulation (LES) and Detached Eddy Simulation (DES) investigations on the flow field surrounding

a cylinder under equilibrium of local scour have been carried out by Kirkil et al. (2008, 2009). The experimental results include distribution of the flow field characteristics below the original bed level. The results, along with the experimental data of Graf and Istiarto (2002) and Dey et al. (2008), can be viewed as a qualitative indication of the structure of the HSV within the scour hole.

A very similar distribution of the streamwise flow in the central plane can be seen for tests B2 in **Figure 4.14(b)** and B3 in **Figure 4.14(c)**. Overall, the magnitude of U/U_e increases with decreasing D/b throughout the central plane. The approach flow in the absence of the cylinder was described by **Figure 4.3** and **Figure 4.4** and it has been established that the depth-averaged streamwise velocity, U , was very similar for all tests. This indicates that changes in the magnitude of streamwise velocity upstream of the cylinder can only have been induced changes in the flow field from the presence of the cylinder, and the variation in the shape of the dune for each test. Since the flow is subcritical, changes in the depth of flow due to the shape of the dune downstream will have implications for the velocity distribution upstream of the cylinder. This effect is observed by the increase in U/U_e upstream of the cylinder for tests B2 and B3. From the dark red contour at $X/D < -2.0$ in **Figure 4.14(c)**, it can be seen that the magnitude of the streamwise velocity in the approach flow increases with decreasing D/b , thereby contributing to the increase in scour depth.

Figure 4.15 shows that a similar trend in the distribution of U/U_e can be seen in the near-cylinder plane for which $Z/D \approx 0.5$. For test B1 shown in **Figure 4.15(a)**, the deceleration of flow upstream of the cylinder ('A') is also observed in plane B. There is a region of high streamwise velocity at the side of the cylinder ('B'), along which acceleration is expected due to separation of flow from the cylinder surface. Close to the free surface near the

downstream face of the cylinder, there is a small region of low streamwise velocity ('C'). As is seen in the central plane, flow accelerates out of the scour hole and over the dune ('D') and separates over the crest of the dune ('E'). The distribution of the noted features in plane B for test B2 in **Figure 4.15(b)** and test B3 in **Figure 4.15(c)** are very similar. It can be seen that as the horizontal confinement decreases, feature 'B' increases in size, extending to the free surface for test B3. At this location, the depth of scour is also shown to increase. Therefore, the sediment transport mechanism close to the cylinder is dependent on the characteristics of feature 'B.' Similarly, features 'C' and 'D' increase in magnitude for tests B2 and B3. Feature 'D' in particular appears to have a significant effect on the shape of the dune. As 'D' increases in length for test B2 when compared with tests B1 and B3, so too does the length of the dune for B2.

For plane C, **Figure 4.16** shows the distribution of U/U_e for all tests. As established by the scour profiles, the scour formation did not reach plane C for test B3 and so there is no bed profile shown in **Figure 4.16(c)**. In any case, the distribution of U/U_e for tests B1 and B2 can be viewed essentially as a distortion of the approach flow. For test B1, U/U_e in plane C increases in the region adjacent to the location of the cylinder. Since the U/U_e contours in plane C for test B3 indicate that the flow field at this location is undisturbed by the cylinder or the sidewall, analysis of plane C for other flow field quantities will be restricted to tests B1 and B2 for the remaining discussion.

4.4.4 Distribution of normalised Reynolds shear stress $-\overline{uv}/U_e^2$

The distribution of the normalised Reynolds shear stress $-\overline{uv}/U_e^2$ is shown in **Figure 4.17** through **Figure 4.19**. In the central plane (**Figure 4.17**), the distribution of the Reynolds

shear stress upstream of the cylinder for all tests includes a region of increased shear stress below $Y/D = 0$ at the leading edge of the scour hole ('A') where flow has separated. The distribution of the Reynolds shear stress downstream of the cylinder is characterized by a patch of high shear stress in the wake region ('B') and a region of low shear stress ('C') inclined over the dune close to the edge of the scour hole. There is a shear layer emanating from the crest of the dune ('D') for each test as well. The magnitude of $-\overline{uv}/U_e^2$ is slightly higher for both features 'B' and 'C' as sidewall proximity decreases. Once again, this is consistent with the approach flow analysis, in which it was determined that the Reynolds shear stress was higher in the boundary layer for a greater channel width b .

In the near-cylinder plane (**Figure 4.18**), there is a region of high Reynolds shear stress approximately midway between the original bed level and the free surface ('B'). In this region, $-\overline{uv}/U_e^2$ is significantly higher for tests B1 and B2 when compared with test B3, and the region is located further downstream as channel width increases. The distribution of $-\overline{uv}/U_e^2$ in plane B also consists of large negative region ('C') which extends over most of the scour hole and towards the dune. In **Figure 4.19**, the distribution of $-\overline{uv}/U_e^2$ is shown in plane C for tests B1 and B2. The magnitude of the Reynolds shear stress is significantly lower in plane C than planes A or B. For test B1, the distribution of $-\overline{uv}/U_e^2$ shows a region of high shear stress emanating from the scour hole and extending over the dune ('A') as well as a region of negative shear stress close to the free surface ('B'). For test B2, $-\overline{uv}/U_e^2$ is fairly similar throughout the plane.

4.4.5 Distribution of spanwise vorticity Ω

The distribution of the spanwise vorticity, Ω , is shown in **Figure 4.20**. The distribution for all tests in the central plane shows high positive vorticity within the scour hole ('A'). The vorticity distribution is characterized by a region of negative vorticity at the upstream face of the cylinder ('B') and in the wake very close to the cylinder ('C'). There are two regions of positive vorticity in the wake of the cylinder, emanating from the scour hole in the downstream region ('D') and near the free surface close to the downstream face of the cylinder ('E'). There is also a region of high vorticity close to the free surface downstream of the cylinder ('F') for all tests. The region of low vorticity at the upstream face of the cylinder for all tests can be associated with the orientation of the downflow. The size of features 'A,' 'E,' 'D' and 'F' (i.e. all regions of positive vorticity) are smaller for test B3 than for tests B1 and B2, indicating that increased sidewall proximity enhances vorticity in the spanwise direction. Similarly, features 'B' and 'C' are smaller for test B3 when compared with tests B1 and B2.

4.5 Conclusions and recommendations

The experimental results indicate that sidewall proximity influences the equilibrium scour formation, including the size of the scour hole and the length, width and height of the dune downstream of the cylinder. The bed profile measurements show that the primary deposit becomes increasingly narrow as D/b increases, indicating that the width of the wake is confined with increasing sidewall proximity. The size and shape of the dune are heavily influenced by the flow field mechanisms in the wake region. The dune for test B1 is of shorter length and greater height than that of test B3, and the dune for test B2 has the

greatest length and smallest height, although the width of the dune for test B3 is highest. For shallow flows, the dimensions of the dune are likely to have a significant effect on the flow field in the wake region. Downstream of the primary deposit, the scour formation occupies the entire width of the flume for the largest blockage ratio. Because the flow is subcritical, the control is downstream, and these effects will be felt upstream of the cylinder as well. This has resulted in an increase in the streamwise velocity upstream of the cylinder, as shown by the acquired PIV measurements. As the magnitude of U/U_e in the approach flow is increased, the depth of the scour hole in the vicinity of the cylinder also increases.

The results of this investigation have implications for future development of scour estimation methods and design of scour countermeasures. Considering the complicated nature of blockage effects in local scour modelling, implementation of a correction factor for scour data acquired under high values of D/b may not be sufficient. As demonstrated by the differences in the experimental results between local scour at an equilibrium condition with $D/b = 0.14$ and $D/b = 0.05$, channel blockage significantly influences the scour formation and the flow field surrounding the cylinder. For a smaller range of D/b ($0.07 < D/b < 0.05$), significant changes in the dune region are still observed. This implies that further experimentation is required under highly controllable conditions in which channel blockage is minimized. Detailed analysis of approach flow conditions must also be considered prior to experimentation, in order to minimize blockage effects and develop scour prediction methods.

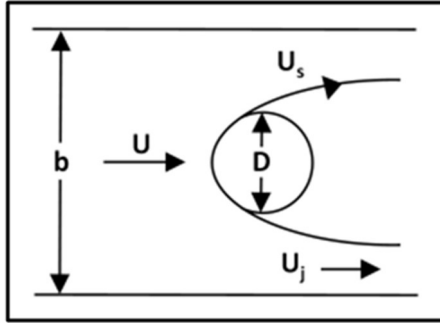


Figure 4.1: Description of channel flow around a circular cylinder with blockage ratio D/b

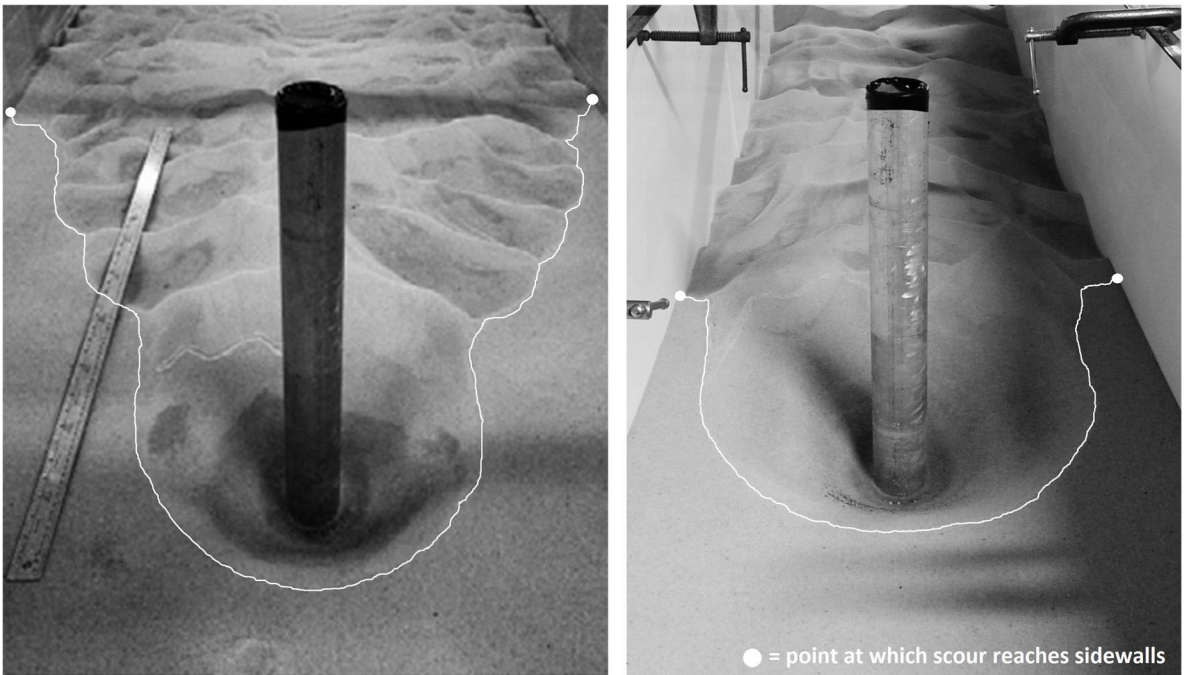


Figure 4.2: Photographs of equilibrium scour profiles with $D/b = 0.05$ (left) and $D/b = 0.10$ (right) (Williams et al. 2018)

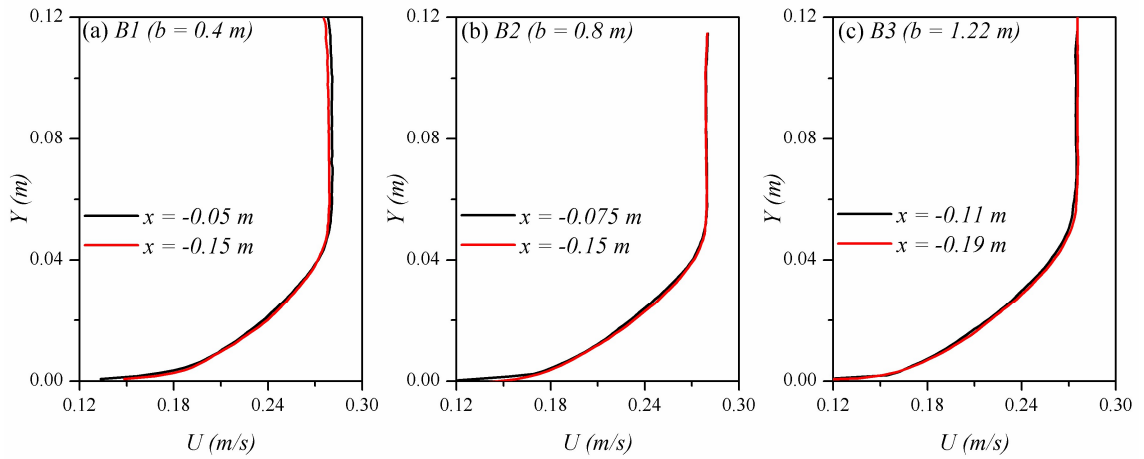


Figure 4.3: Distribution of streamwise velocity U (m/s) for two streamwise locations in the central plane ($Z/D = 0$) in the absence of the cylinder for (a) test B1 ($b = 0.4$ m), (b) B2 ($b = 0.8$ m) and (c) B3 ($b = 1.22$ m)

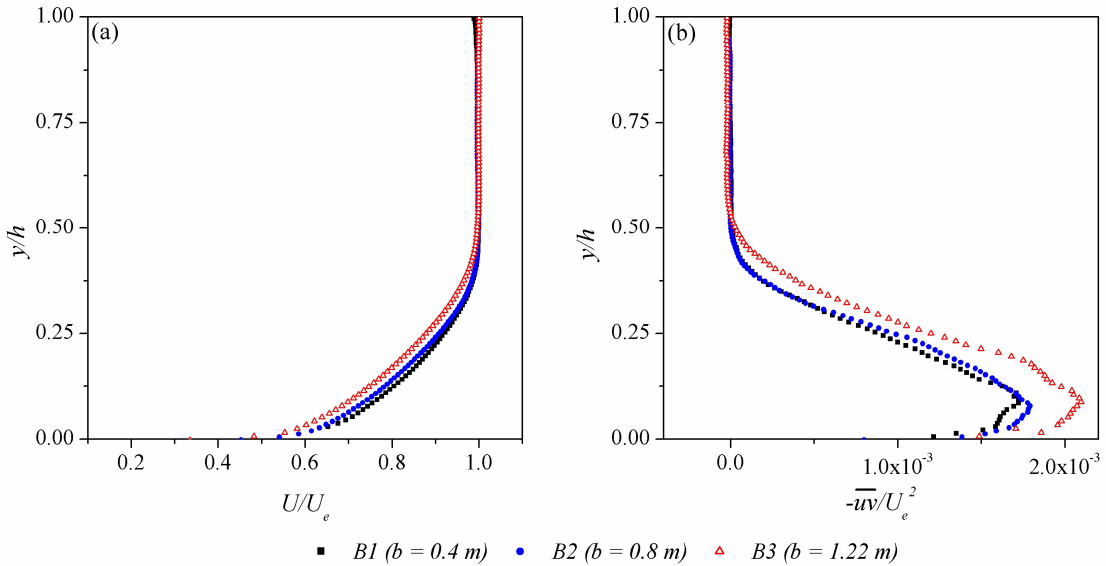


Figure 4.4: Distribution of (a) streamwise velocity U , (b) Reynolds shear stress $-\overline{u'v'}/U_e^2$, (c) streamwise turbulence strength u_{rms} and (d) vertical turbulence strength v_{rms} for approach flow of tests B1, B2 and B3 in the absence of the cylinder

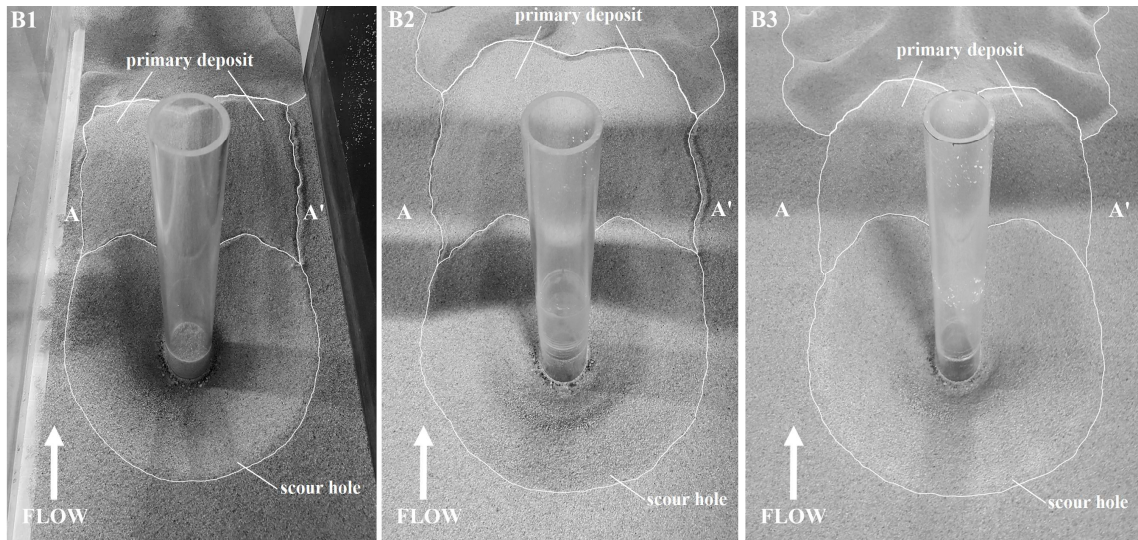


Figure 4.5: Photographs of equilibrium scour formation for test B1 ($D/b = 0.14$, left), test B2 ($D/b = 0.07$, middle) and test B3 ($D/b = 0.05$, right)

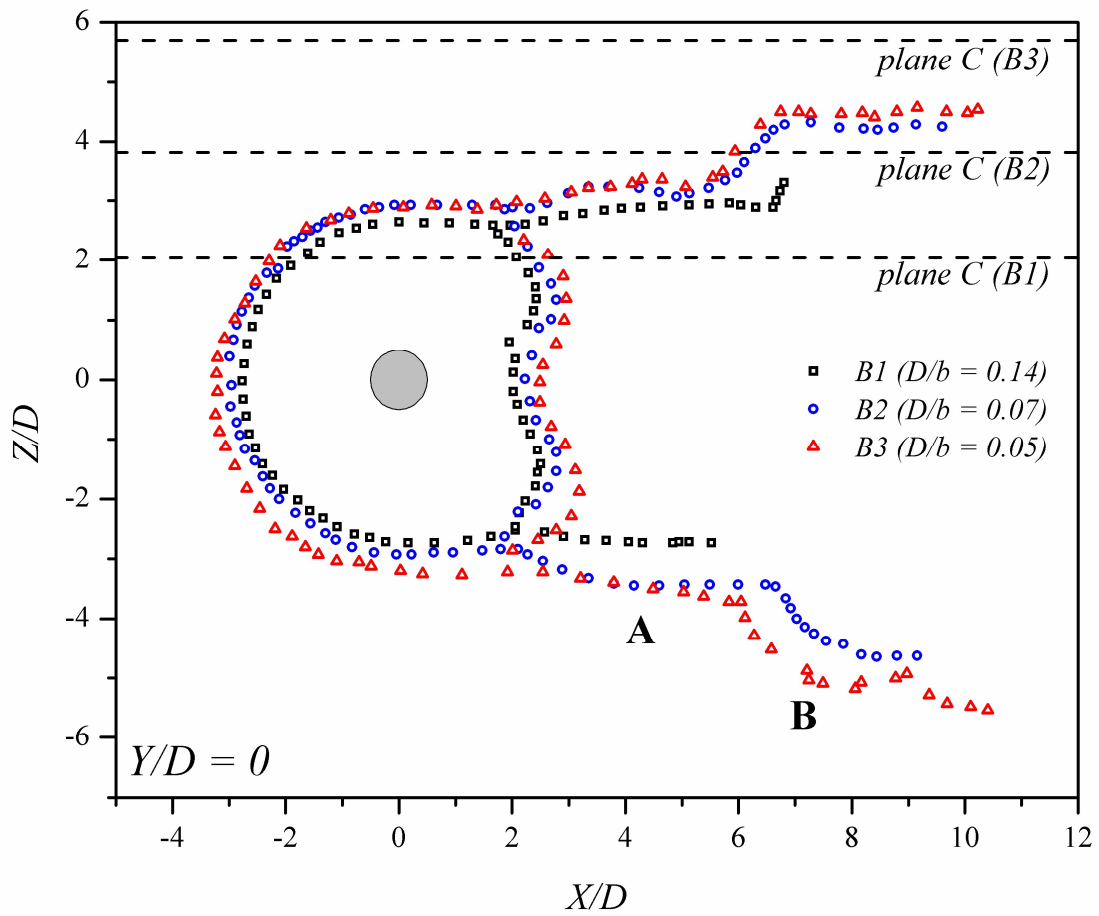


Figure 4.6: Plan-view profile measurements of equilibrium scour formation for tests B1, B2 and B3 in XZ plane

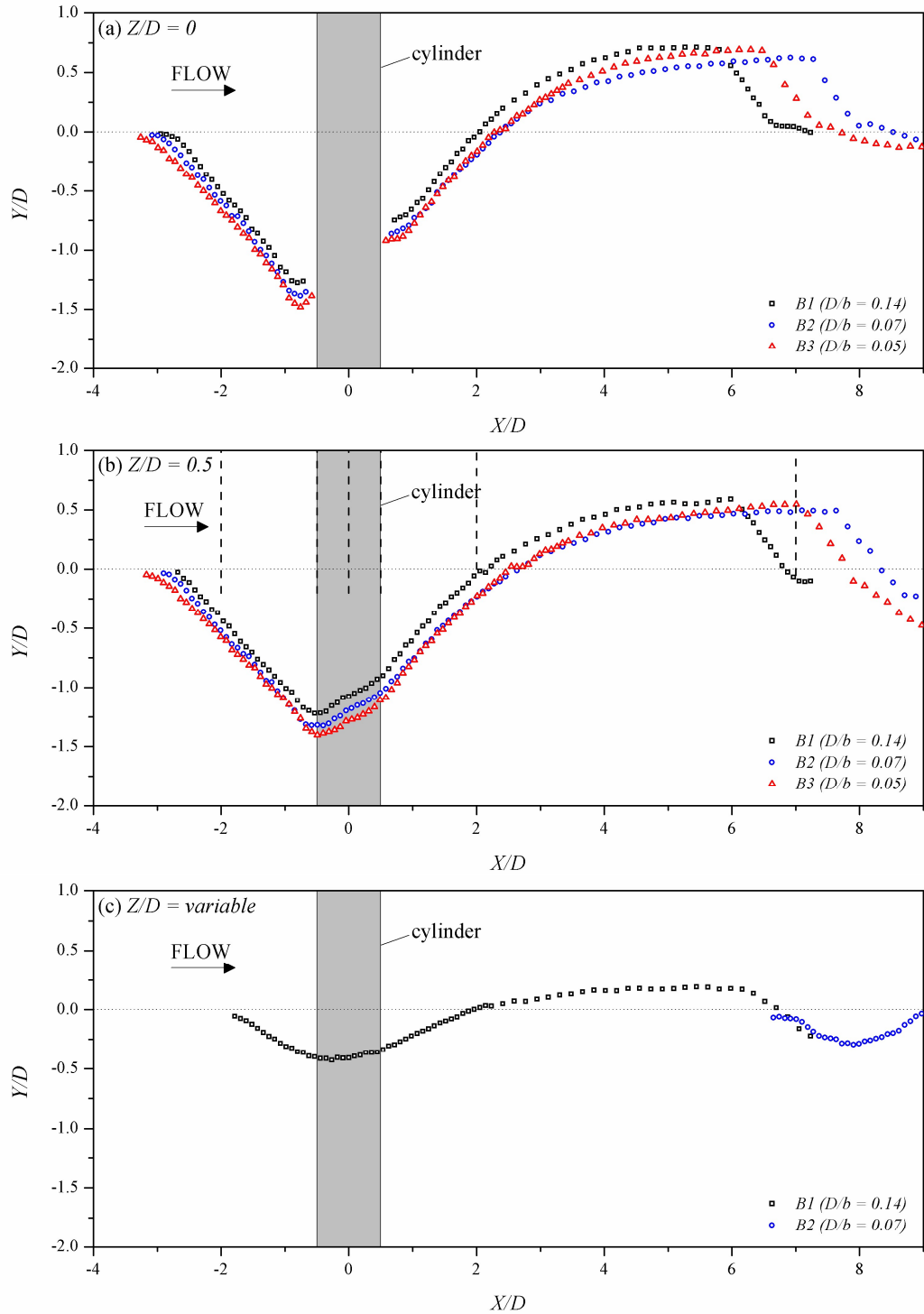


Figure 4.7: Bed profile measurements of equilibrium scour formation for tests B1, B2 and B3 in XY plane along (a) the central plane with $Z/D = 0$, (b) the near-cylinder plane with $Z/D \approx 0.5$ and (c) the mid-cylinder-wall plane with variable Z/D

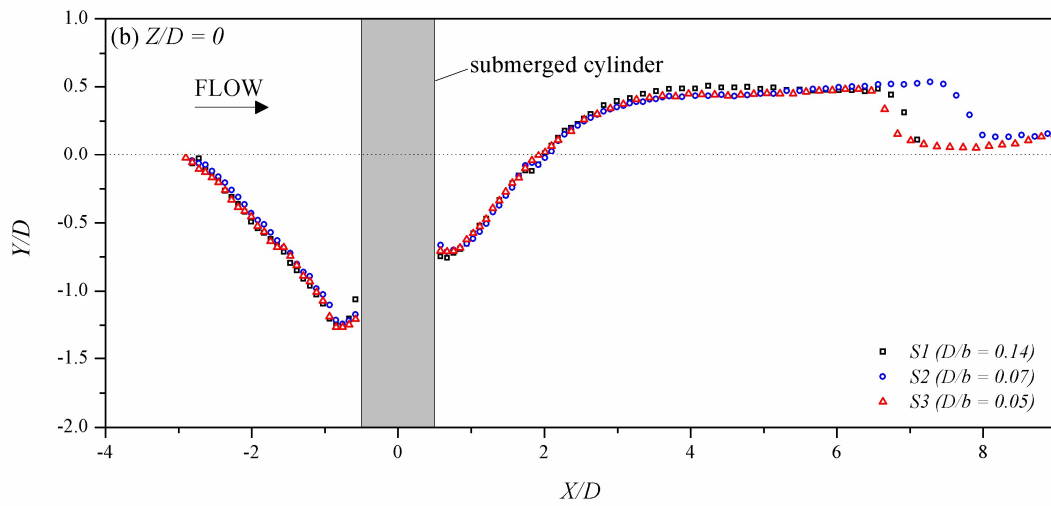
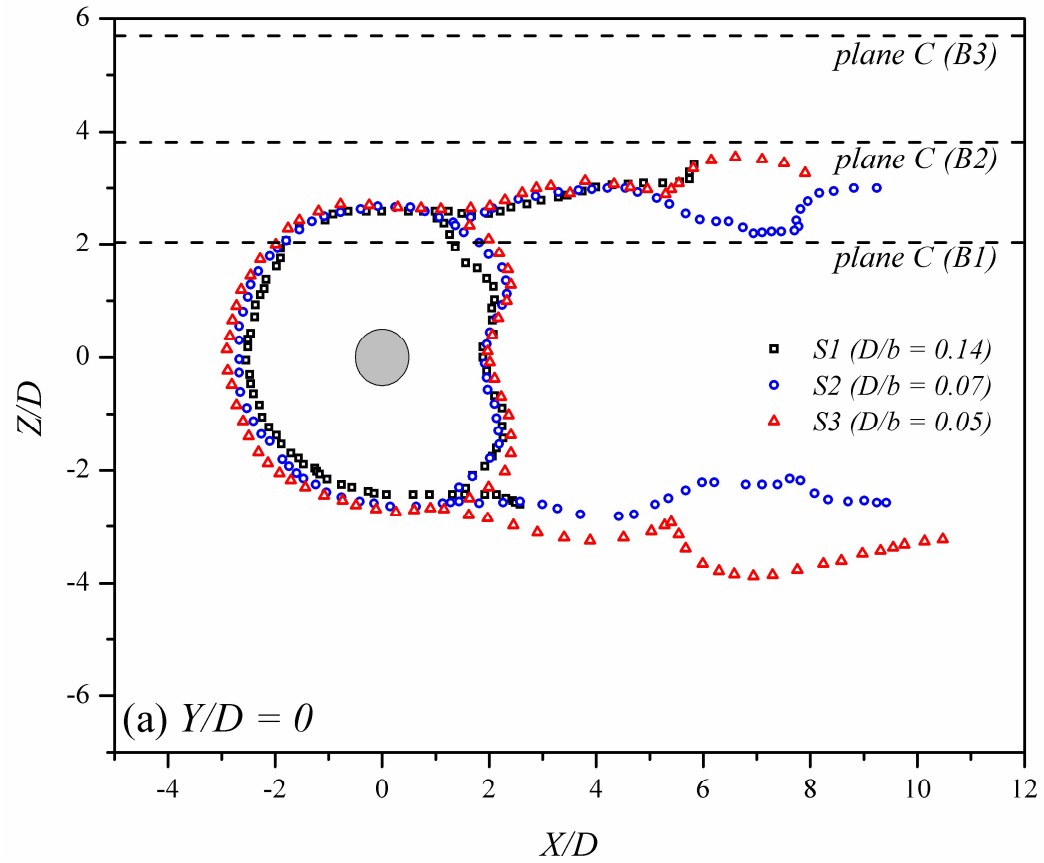


Figure 4.8: Bed profile measurements in (a) the XZ plane at $Y/D = 0$ and (b) the XY plane at $Z/D = 0$ for tests $S1 (D/b = 0.14)$, $S2 (D/b = 0.07)$ and $S3 (D/b = 0.05)$

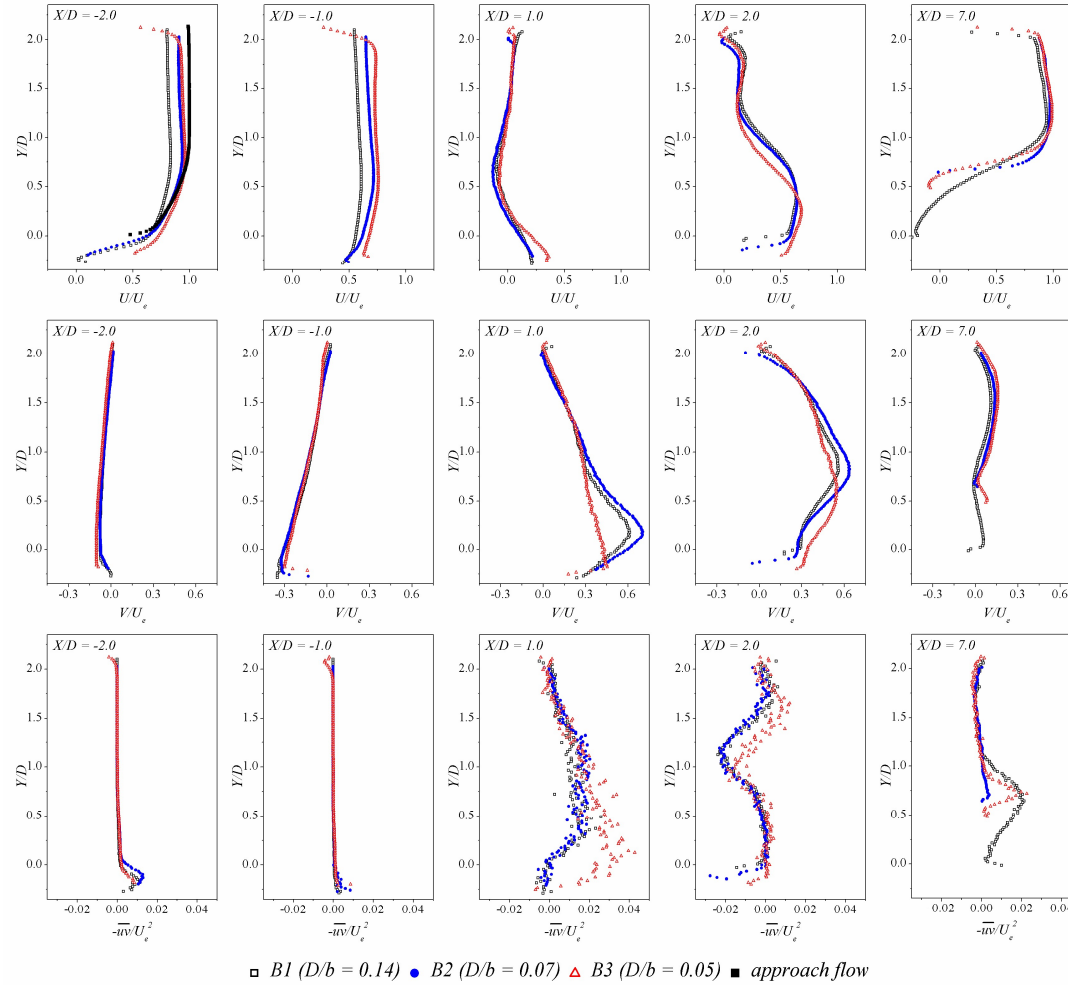


Figure 4.9: Distribution of mean streamwise velocity U/U_e , mean vertical velocity V/U_e and Reynolds shear stress $-\overline{uv}/U_e^2$ over the depth of flow in plane A ($Z/D = 0$) for $X/D = \{-2.0, -1.0, 1.0, 2.0, 7.0\}$

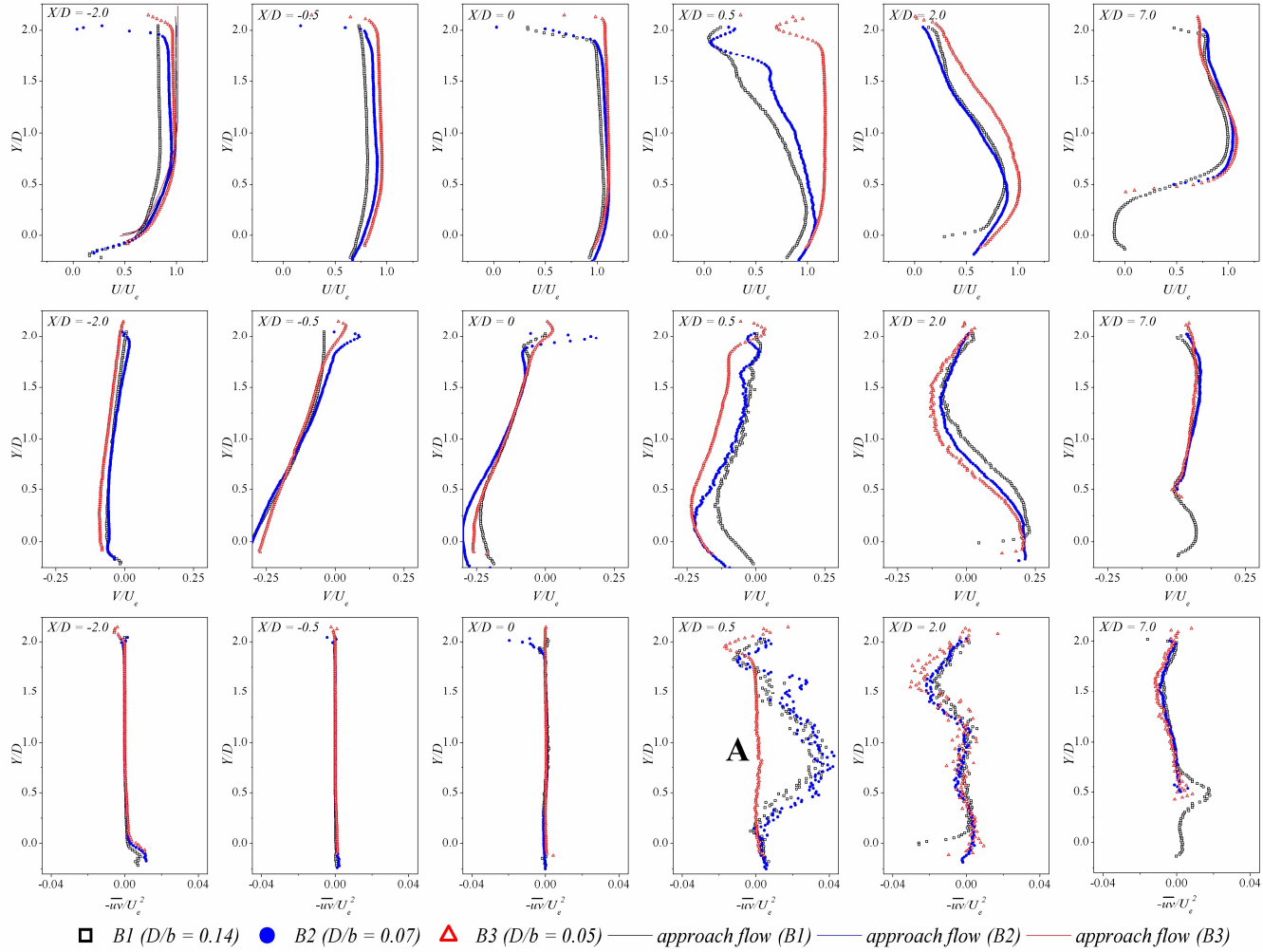


Figure 4.10: Distribution of mean streamwise velocity U/U_e , mean vertical velocity V/U_e and Reynolds shear stress $-\overline{uv}/U_e^2$ over the depth of flow in plane B ($Z/D \approx 0.5$) for $X/D = \{-2.0, -0.5, 0, 0.5, 2.0, 7.0\}$

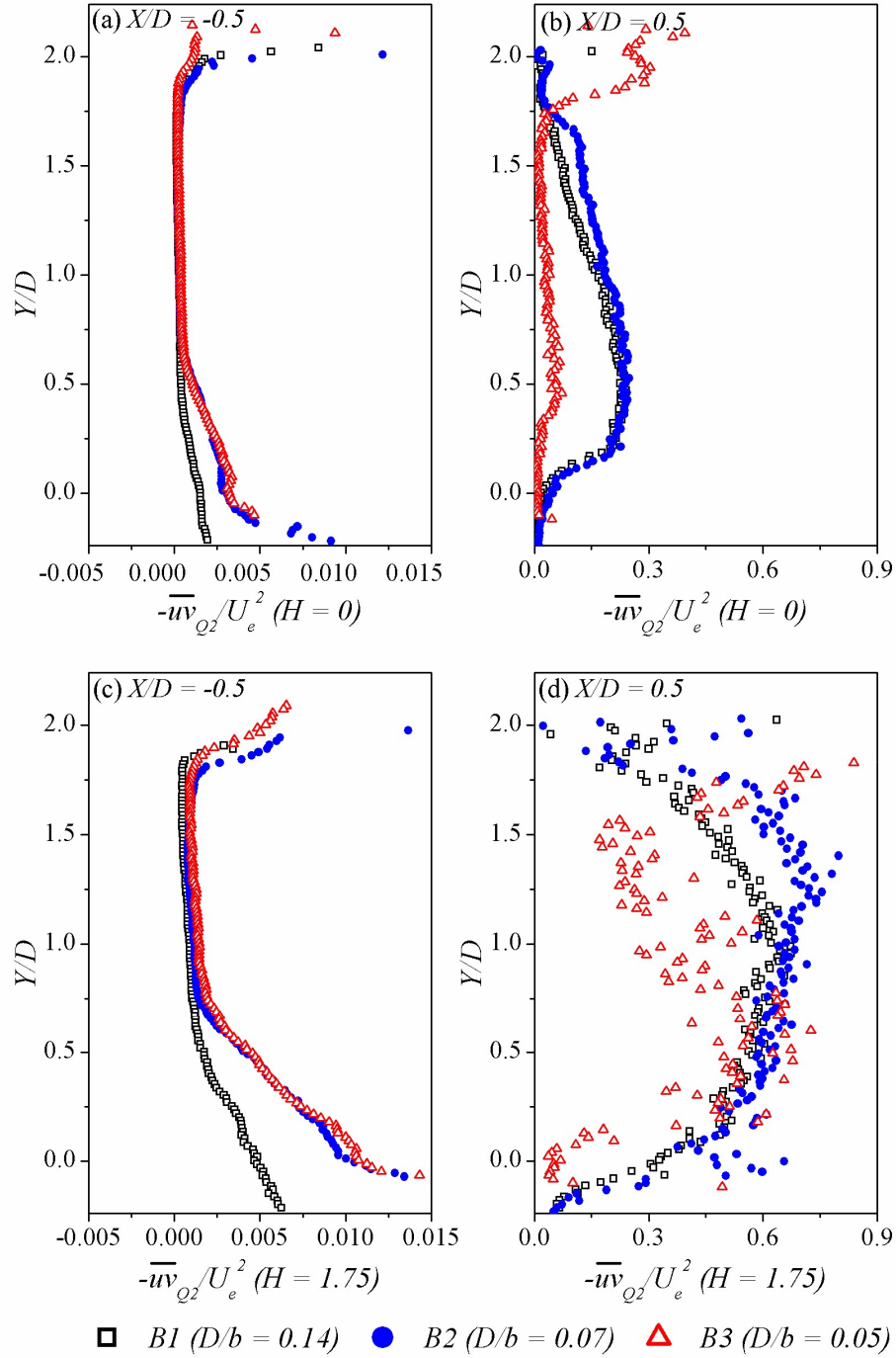


Figure 4.11: Distribution of the contribution of Q2 ejection events ($u < 0, v > 0$) at (a) $X/D = -0.5$ for $H = 0$, (b) $X/D = 0.5$ for $H = 0$, (c) $X/D = -0.5$ for $H = 1.75$ and (d) $X/D = 0.5$ for $H = 1.75$

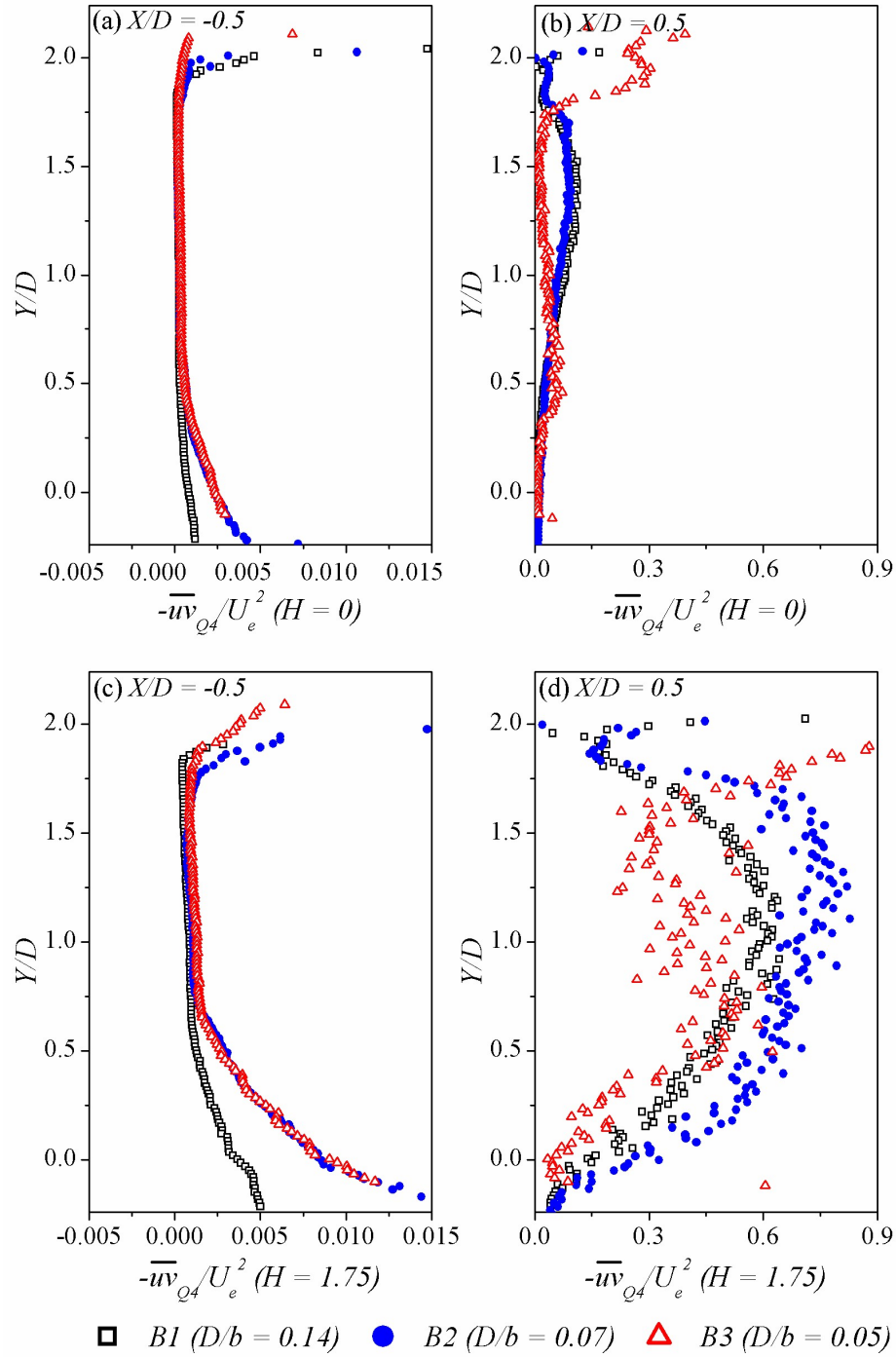


Figure 4.12: Distribution of the contribution of Q4 sweep events ($u > 0, v < 0$) at (a) $X/D = -0.5$ for $H=0$, (b) $X/D = 0.5$ for $H = 0$, (c) $X/D = -0.5$ for $H = 1.75$ and (d) $X/D = 0.5$ for $H = 1.75$

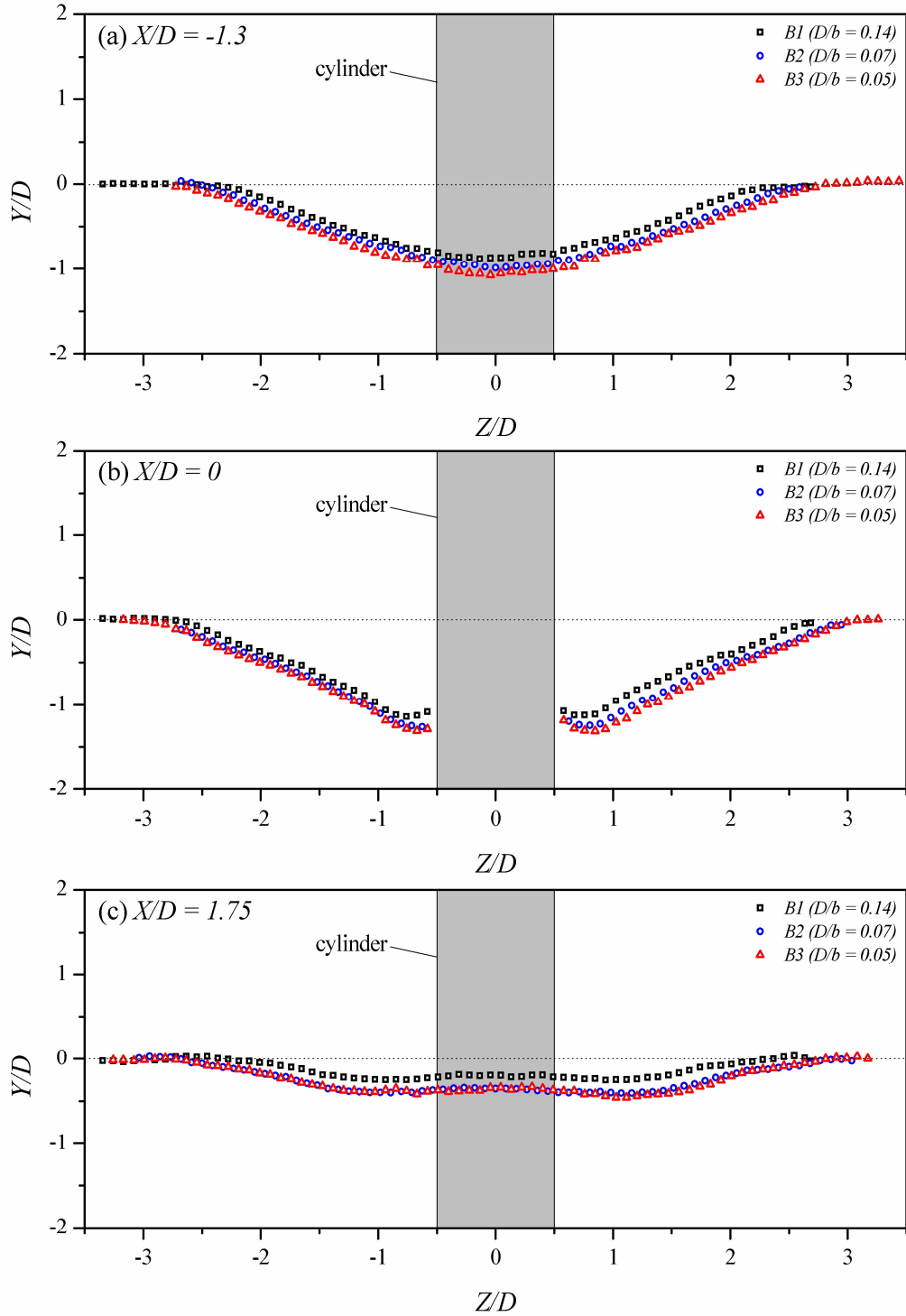


Figure 4.13: Bed profile measurements of equilibrium scour formation for tests B1, B2 and B3 in YZ plane along (a) the upstream spanwise plane ($X/D = -1.3$), (b) the spanwise central plane ($X/D = 0$) and (c) the downstream spanwise plane ($X/D = 1.75$)

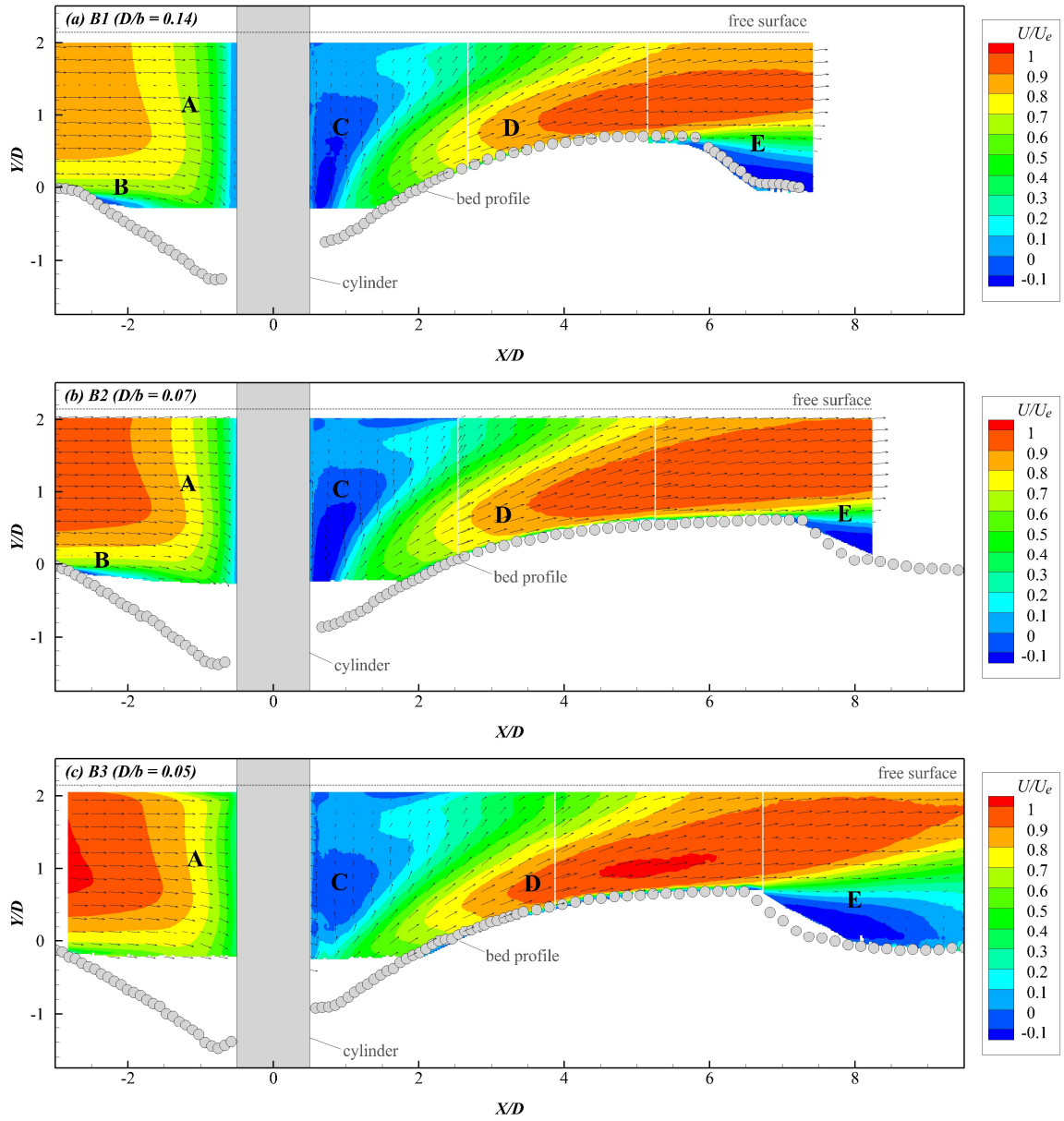


Figure 4.14: Distribution of normalised streamwise velocity U/U_e in the central plane (plane A, $Z/D = 0$) for (a) test B1 ($D/b = 0.14$), (b) test B2 ($D/b = 0.07$) and (c) test B3 ($D/b = 0.05$)

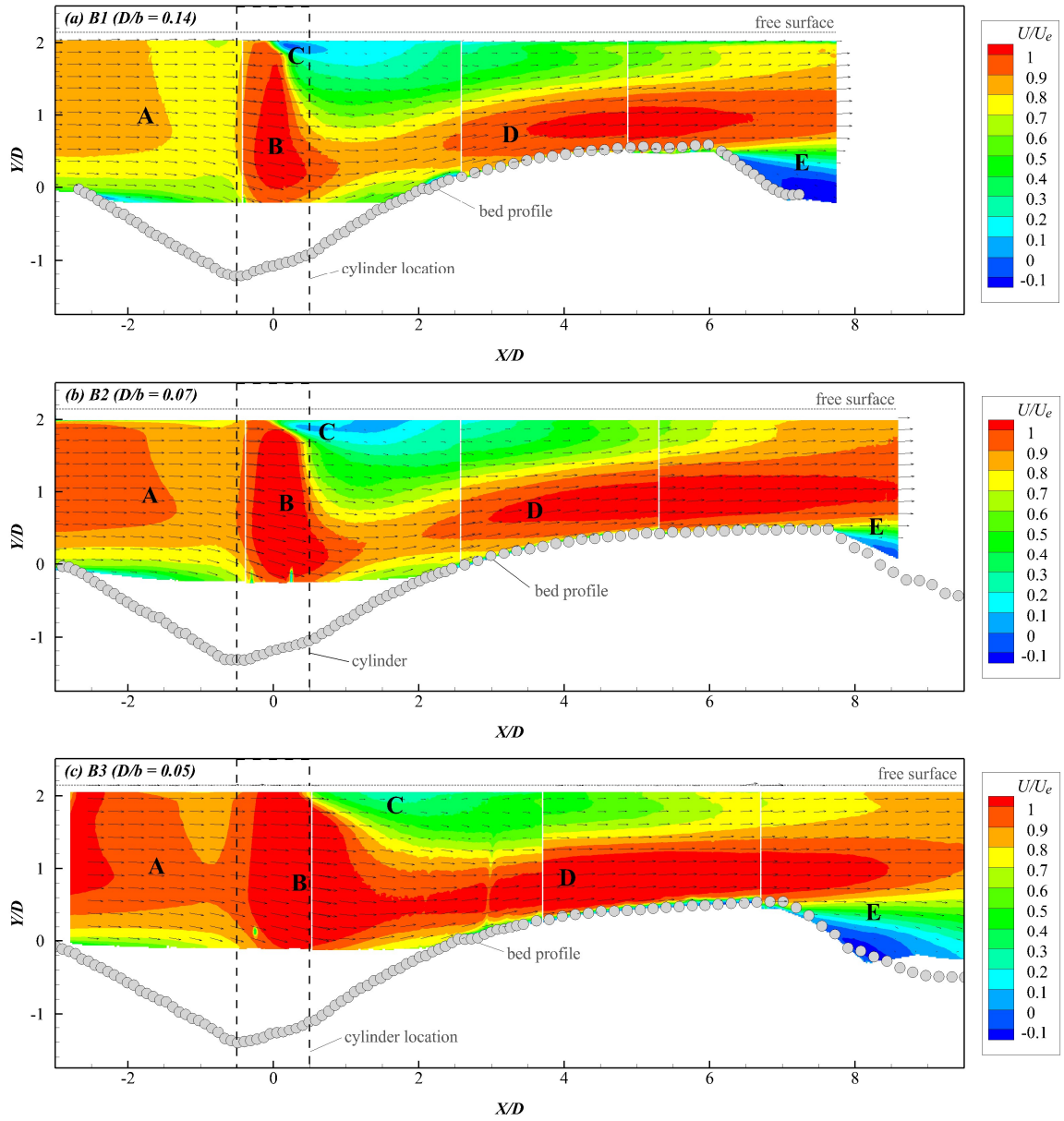


Figure 4.15: Distribution of normalised streamwise velocity U/U_e in the near-cylinder plane (plane B, $Z/D \approx 0.5$) for (a) test B1 ($D/b = 0.14$), (b) test B2 ($D/b = 0.07$) and (c) test B3 ($D/b = 0.05$)

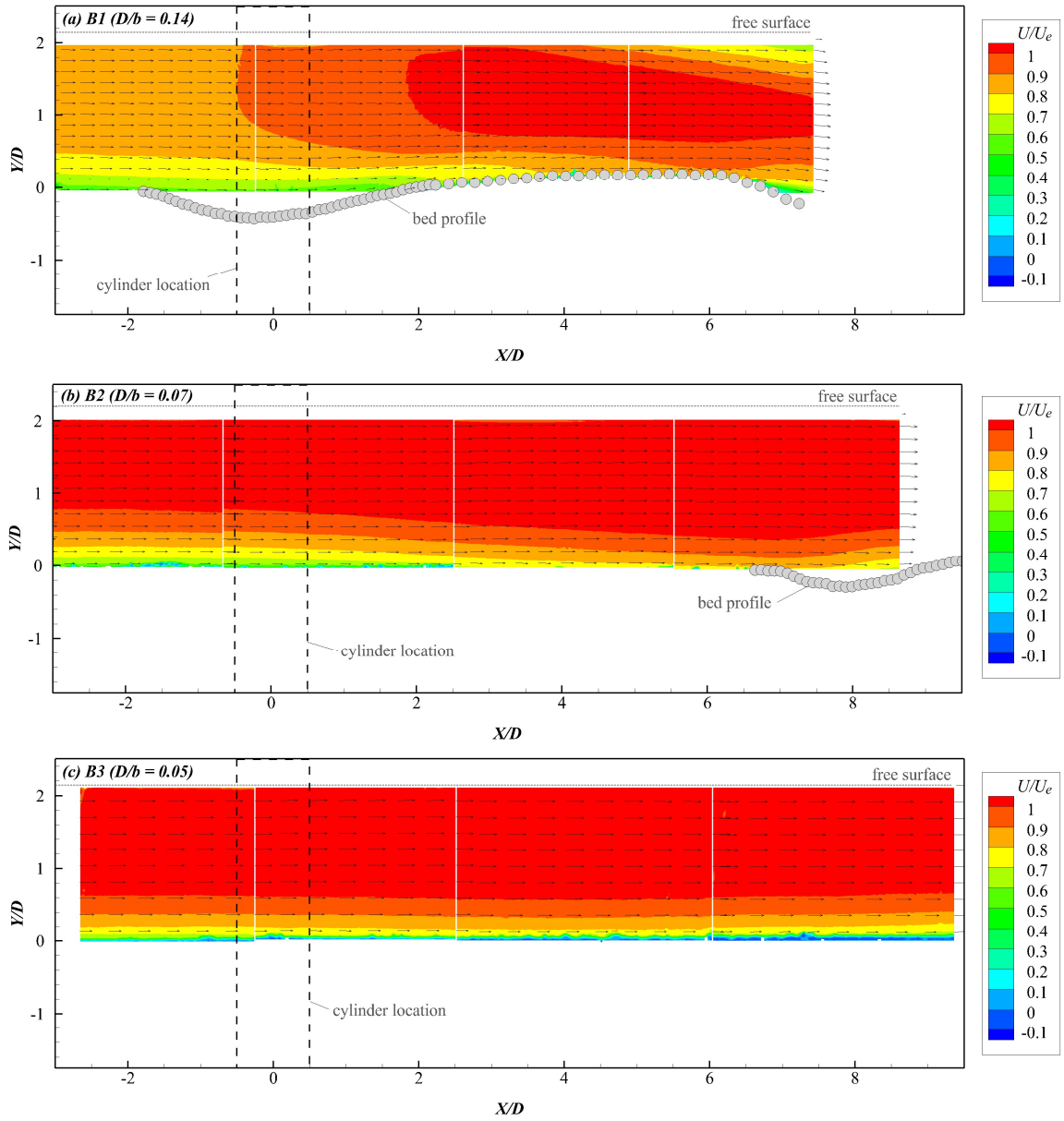


Figure 4.16: Distribution of normalised streamwise velocity U/U_e in the mid-cylinder-wall plane (plane C, $Z/D = \text{variable}$) for (a) test B1 ($D/b = 0.14$), (b) test B2 ($D/b = 0.07$) and (c) test B3 ($D/b = 0.05$)

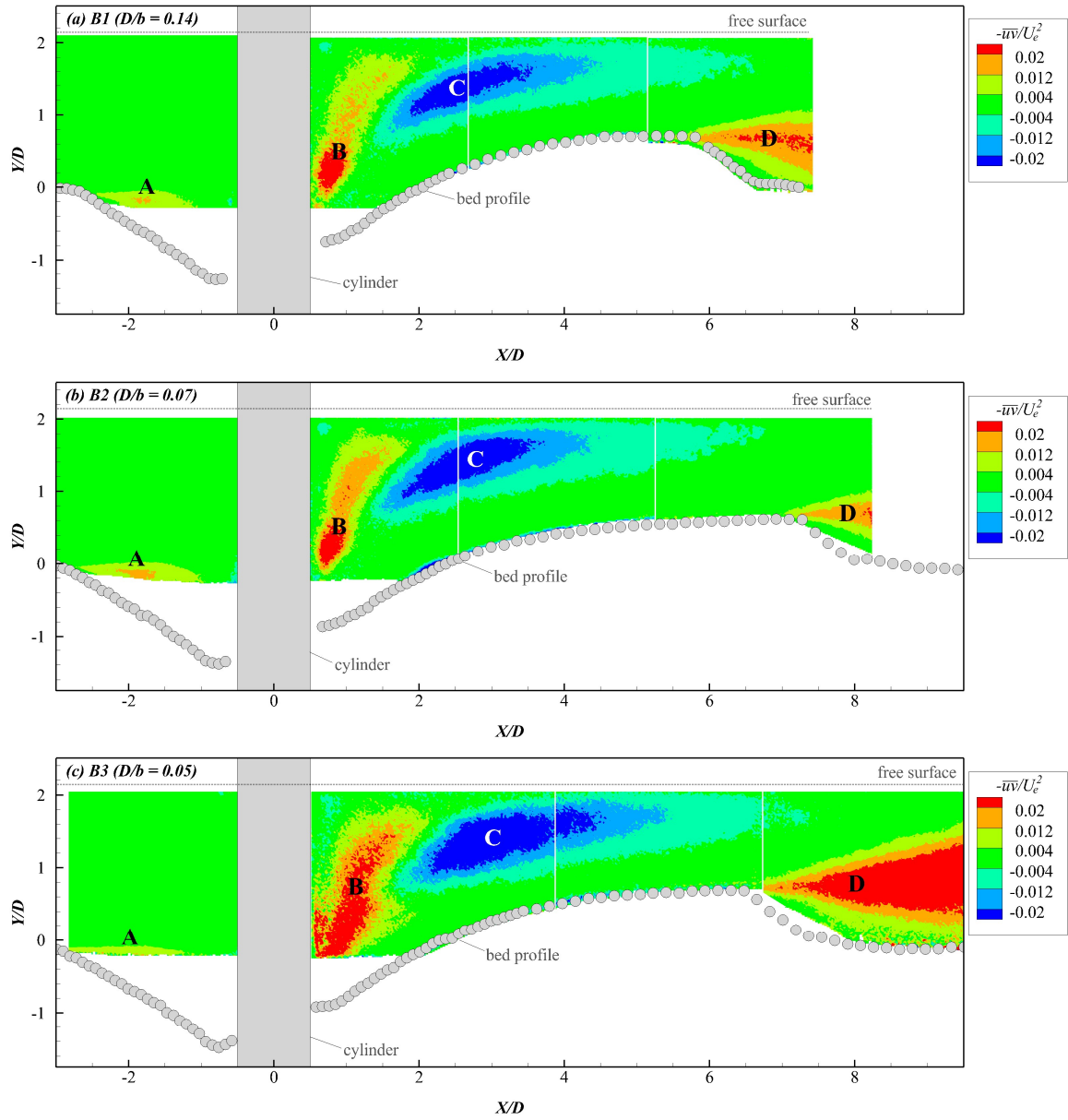


Figure 4.17: Distribution of the normalised Reynolds shear stress $-\overline{uv}/U_e^2$ in the central plane (plane A, $Z/D = 0$) for (a) test B1 ($D/b = 0.14$), (b) test B2 ($D/b = 0.07$) and (c) test B3 ($D/b = 0.05$)

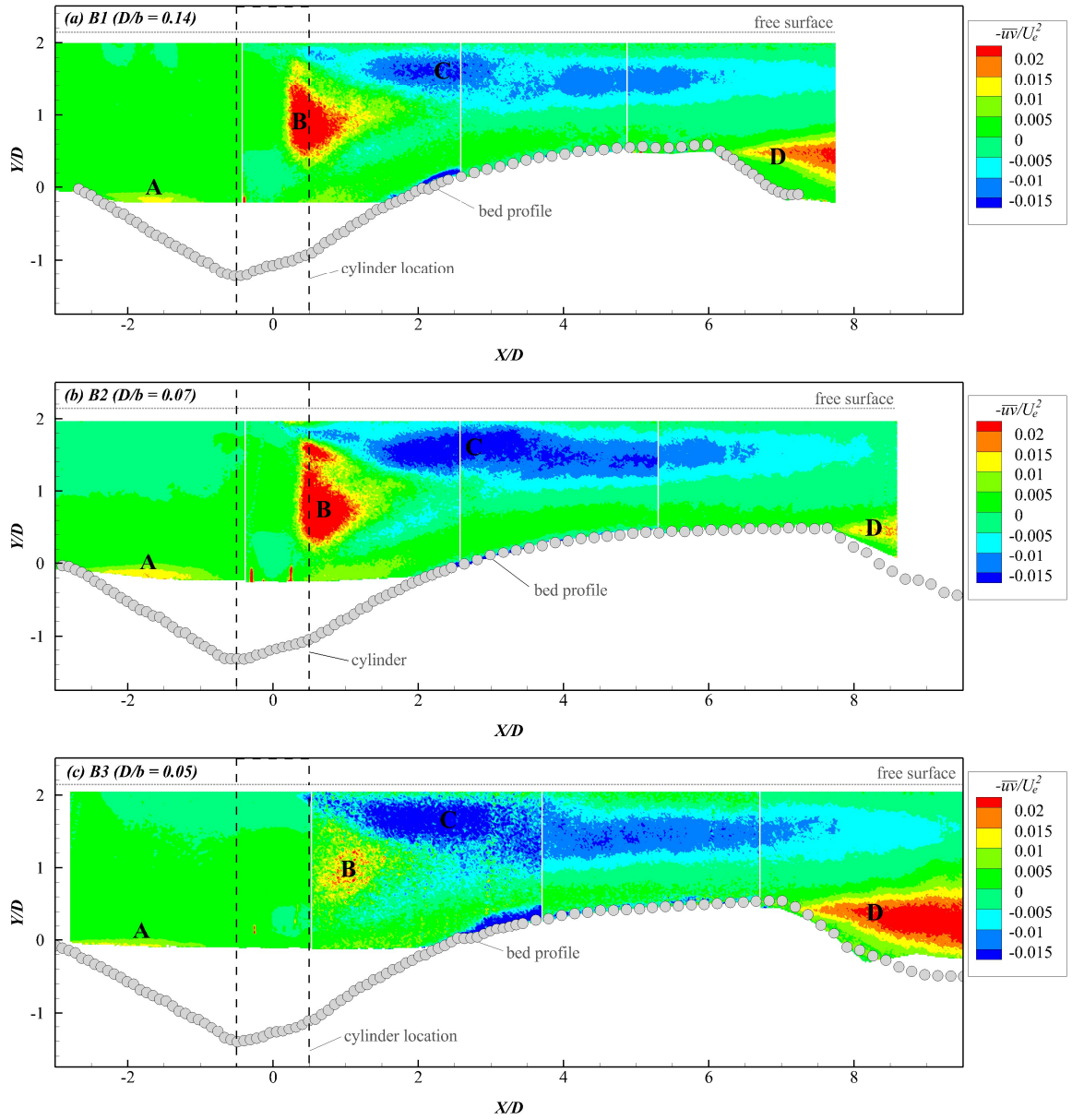


Figure 4.18: Distribution of the normalised Reynolds shear stress $-\overline{u'v'}/U_e^2$ in the near-cylinder plane (plane B, $Z/D \approx 0.5$) for (a) test B1 ($D/b = 0.14$), (b) test B2 ($D/b = 0.07$) and (c) test B3 ($D/b = 0.05$)

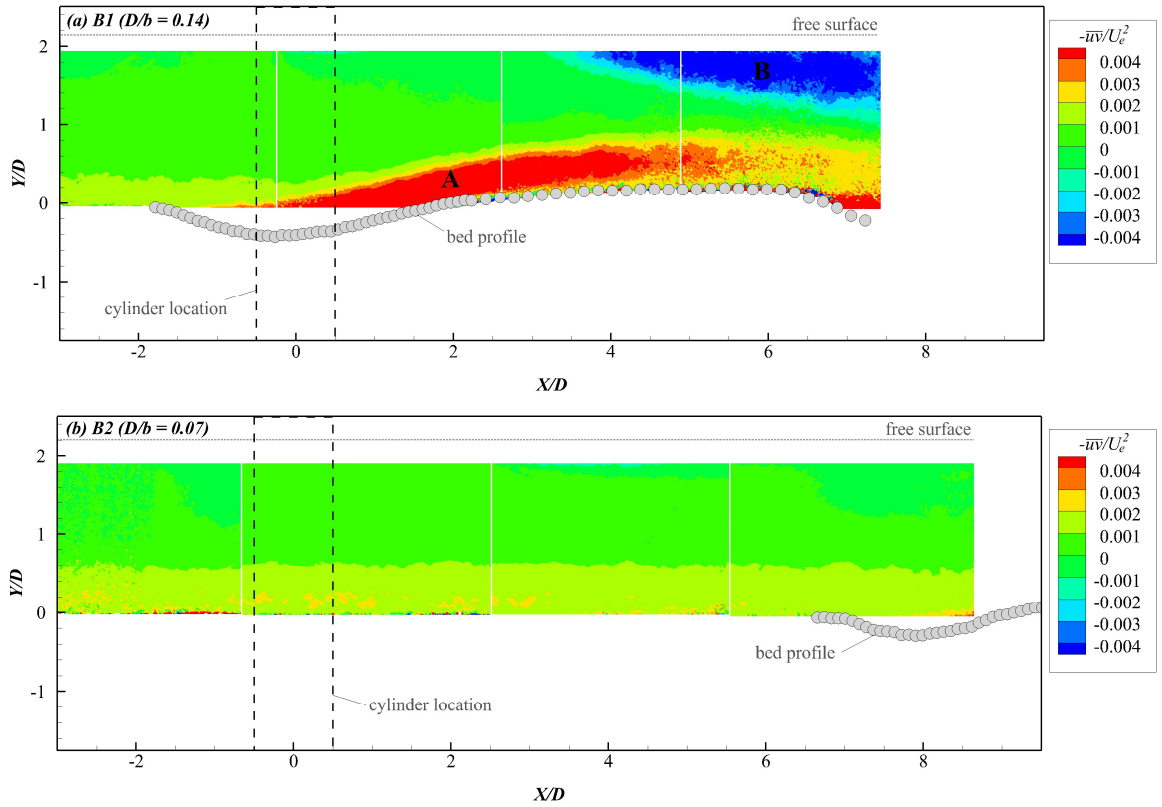


Figure 4.19: Distribution of the normalised Reynolds shear stress $-\overline{uv}/U_e^2$ in the mid-cylinder-wall plane (plane C, variable Z/D) for (a) test B1 ($D/b = 0.14$) and (b) test B2 ($D/b = 0.07$)

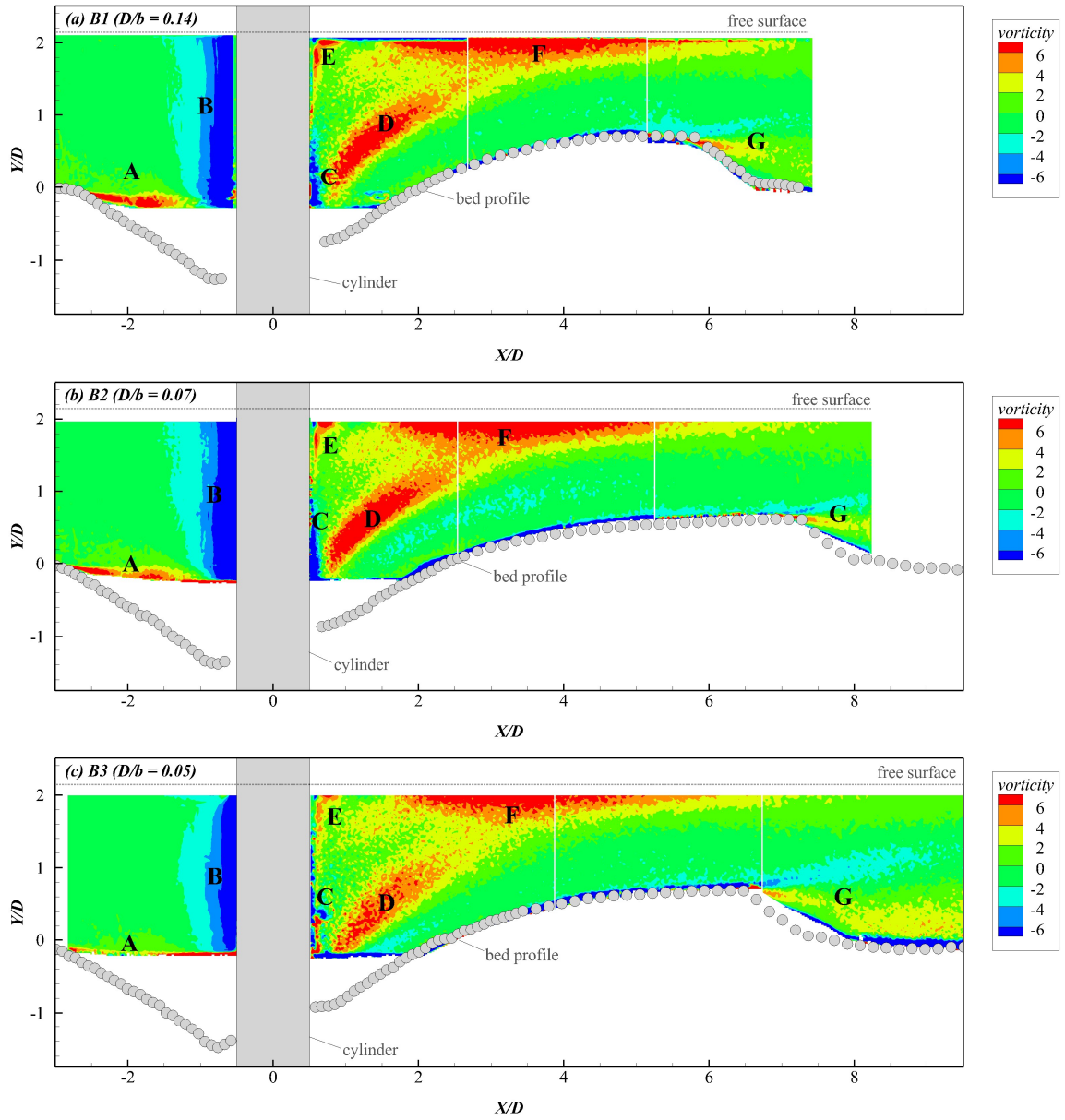


Figure 4.20: Distribution of the spanwise vorticity Ω in the central plane (plane A, $Z/D = 0$) for (a) test B1 ($D/b = 0.14$), (b) test B2 ($D/b = 0.07$) and (c) test B3 ($D/b = 0.05$)

4.6 References

1. Chiew, Y. M. (1984). *Local scour at bridge piers*. Doctoral dissertation. University of Auckland, Auckland, New Zealand.
2. D'Alessandro, C. (2013). *Effect of blockage on cylindrical bridge pier local scour*. M.A.Sc. thesis. University of Windsor, Windsor, Canada.
3. Dey, S., Raikar, R. V., & Roy, A. (2008). Scour at submerged cylindrical obstacles under steady flow. *Journal of Hydraulic Engineering*, 134(1), 105–109. [https://doi.org/10.1061/\(ASCE\)0733-9429\(2008\)134:1\(105\)](https://doi.org/10.1061/(ASCE)0733-9429(2008)134:1(105))
4. Ettema, R., Kirkil, G., & Muste, M. (2006). Similitude of large-scale turbulence in experiments on local scour at cylinders. *Journal of Hydraulic Engineering*, 132(1), 33–40. [https://doi.org/10.1061/\(ASCE\)0733-9429\(2006\)132:1\(33\)](https://doi.org/10.1061/(ASCE)0733-9429(2006)132:1(33))
5. Ettema, R., Melville, B. W., & Constantinescu, G. (2011). *Evaluation of bridge scour research: Pier scour processes and predictions*. Washington, DC: Transportation Research Board of the National Academies.
6. Graf, W. H., & Istiarto, I. (2002). Flow pattern in the scour hole around a cylinder. *Journal of Hydraulic Research*, 40(1), 13–20. <https://doi.org/10.1080/00221680209499869>
7. Heller, V. (2011). Scale effects in physical hydraulic engineering models. *Journal of Hydraulic Research*, 49(3), 293–306. <https://doi.org/10.1080/00221686.2011.578914>
8. Hodi, B. (2009). *Effect of blockage and densimetric Froude number on circular bridge pier local scour*. M.A.Sc. thesis. University of Windsor, Windsor, Canada.

9. Johnson, P. A., & Torrico, E. F. (1994). Scour around wide piers in shallow water. *Transportation Research Record*, (1471), 66-70.
10. Kirkil, G., Constantinescu, G., & Ettema, R. (2008). Coherent structures in the flow field around a circular cylinder with scour hole. *Journal of Hydraulic Engineering*, 134(5), 572–587. [https://doi.org/10.1061/\(ASCE\)0733-9429\(2008\)134:5\(572\)](https://doi.org/10.1061/(ASCE)0733-9429(2008)134:5(572))
11. Kirkil, G., Constantinescu, G., & Ettema, R. (2009). Detached Eddy Simulation investigation of turbulence at a circular pier with scour hole. *Journal of Hydraulic Engineering*, 135(11), 888–901. [https://doi.org/10.1061/\(ASCE\)HY.1943-7900.0000101](https://doi.org/10.1061/(ASCE)HY.1943-7900.0000101)
12. Laursen, E. M., & Toch, A. (1956). *Scour around bridge piers and abutments* (Vol. 4). Iowa Highway Research Board Ames, IA.
13. Lu, S. S., & Willmarth, W. W. (1973). Measurements of the structure of the Reynolds stress in a turbulent boundary layer. *Journal of Fluid Mechanics*, 60(3), 481–511. <https://doi.org/10.1017/S0022112073000315>
14. Oben-Nyarko, K., & Ettema, R. (2011). Pier and abutment scour interaction. *Journal of Hydraulic Engineering*, 137(12), 1598–1605. [https://doi.org/10.1061/\(ASCE\)HY.1943-7900.0000446](https://doi.org/10.1061/(ASCE)HY.1943-7900.0000446)
15. Oliveto, G., & Hager, W.H. (2005). Further results to time-dependent local scour at bridge elements. *Journal of Hydraulic Engineering*, 131(2), 97–105. [https://doi.org/10.1061/\(ASCE\)0733-9429\(2005\)131:2\(97\)](https://doi.org/10.1061/(ASCE)0733-9429(2005)131:2(97))
16. Ramamurthy A. S., Balachandar R., & Vo, D. N. (1989). Blockage correction for sharp-edged bluff bodies. *Journal of Engineering Mechanics*, 115(7), 1569–1576. [https://doi.org/10.1061/\(ASCE\)0733-9399\(1989\)115:7\(1569\)](https://doi.org/10.1061/(ASCE)0733-9399(1989)115:7(1569))

17. Ramamurthy, A. S., & Lee, P. M. (1973). Wall effects on flow past bluff bodies. *Journal of Sound and Vibration*, 31(4), 443–451. [https://doi.org/10.1016/S0022-460X\(73\)80259-7](https://doi.org/10.1016/S0022-460X(73)80259-7)
18. Raudkivi, A.J., & Ettema, R. (1983). Clear-water scour at cylindrical piers. *Journal of Hydraulic Engineering*, 109(3), 338–350. [https://doi.org/10.1061/\(ASCE\)0733-9429\(1983\)109:3\(338\)](https://doi.org/10.1061/(ASCE)0733-9429(1983)109:3(338))
19. Richardson, E. V., Simons, D. B., & Julien, P. Y. (1990). *Highways in the river environment: participant notebook*. Federal Highway Administration, Washington, DC.
20. Shen, H. W., Schneider, V. R., & Karaki, S. S. (1966). *Mechanics of local scour*. Colorado State University Engineering Research Center, Fort Collins, CO.
21. Sheppard, D. M., Odeh, M., & Glasser, T. (2004). Large scale clear-water local pier scour experiments. *Journal of Hydraulic Engineering*, 130(10), 957–963. [https://doi.org/10.1061/\(ASCE\)0733-9429\(2004\)130:10\(957\)](https://doi.org/10.1061/(ASCE)0733-9429(2004)130:10(957))
22. Tejada, S. (2014). *Effects of blockage and relative coarseness on clear water bridge pier scour*. M.A.Sc. thesis. University of Windsor, Windsor, Canada.
23. Williams, P., Balachandar, R., & Bolisetti, T. (2013). Evaluation of local bridge pier scour depth estimation methods. *Proceedings of the 24th Canadian Congress of Applied Mechanics, Saskatoon, SK, Canada*, 2–6.
24. Williams, P., Bolisetti, T., & Balachandar, R. (2016). Evaluation of governing parameters on pier scour geometry. *Canadian Journal of Civil Engineering*, 44(1), 48–58. <https://doi.org/10.1139/cjce-2016-0133>

25. Williams, P., Bolisetti, T., & Balachandar, R. (2018). Blockage correction for pier scour experiments. *Canadian Journal of Civil Engineering*, 45(5), 413–417.
<https://doi.org/10.1139/cjce-2017-0563>
26. Williams, P. (2014). *Scale effects on design estimation of scour depths at piers*. M.A.Sc. thesis. University of Windsor, Windsor, Canada.
27. Zdravkovich, M. M. (1997a). *Flow Around Circular Cylinders: Volume 1: Fundamentals*. OUP Oxford.
28. Zdravkovich, M. M. (1997b). *Flow Around Circular Cylinders: Volume 2: Applications*. OUP Oxford.

5 EVALUATION OF FLOW-ALTERING COUNTERMEASURES FOR LOCAL SCOUR AROUND A CIRCULAR CYLINDER

5.1 *Introduction*

5.1.1 **A review of scour countermeasures**

Scour countermeasure systems are commonly introduced to existing bridge structures which are vulnerable to scour failure. Countermeasures are defined by the National Cooperative Highway Research Program (Lagasse et al. 2007) as “measures incorporated into a highway-stream crossing system to monitor, control, inhibit, change, delay or minimize stream instability and bridge scour problems.” Countermeasures are categorized as one of two types: armoring, in which a physical barrier is placed around the base of the pier in order to increase the resistance of the bed material to scouring; and flow alteration, in which various accessories are strategically placed in the vicinity of the pier in order to reduce the strength of the flow field features which cause scouring. Examples of armoring countermeasures are riprap protection, Gabion mattresses and cable-tied blocks. Flow-altering countermeasures include collars, slots, vanes, sacrificial piles, helical threading and splitter plates (Chiew 1992, Dey et al. 2006, Lagasse et al. 2007, Khwairakpam & Mazumdar 2009, Tafarojnoruz et al. 2010). Flow-altering countermeasures can be further classified as one of four types: openings through piers (e.g. slots); pier attachments (helical threading, collars); bed attachments (sacrificial piers, vanes and sills); and other devices such as suction applied to a pier, modification of pier shape, etc. (Tafarojnoruz et al. 2010).

Although there are many types of countermeasures, in practice they are often difficult to incorporate into design. Not all countermeasures have well-defined design methodology,

and the variability of conditions in the field further complicates selection of site-appropriate countermeasures. Although flow-altering countermeasures are considered less expensive than armoring, both types of protection can require significant capital and as a result, optimal efficiency in terms of performance and costs is prioritized. Despite these pitfalls, newly constructed bridges often include some type of countermeasure (Lagasse et al. 2007).

Parker et al. (1998) explored the efficacy of several flow-altering devices. Sacrificial piles, vanes, submerged permeable sheet piles and collars were investigated and it was found that many of these devices were not effective countermeasures, and in some cases could even enhance scour. Collars were found to be the exception and were shown to prevent scour entirely with large enough dimensions; however, this was adjudged to be impractical and, similar to other devices, could worsen scour if not implemented properly. Six flow-altering countermeasures were also evaluated by Tafarjnoruz et al. (2012), and the authors established that each design alternative explored was not particularly efficient in terms of scour reduction on its own, but that combining two or more of the six alternatives may improve effectiveness. The authors also stated that “the best [effectiveness] can be achieved only when the flow conditions match those for which the countermeasure was designed,” further highlighting the complication of effective countermeasure design and implementation (Tafarjnoruz et al. 2012). This is emphasized by the same authors in an investigation into the use of combined flow-altering devices, who stated that “... an improper combination of two countermeasures may be less effective than each individual countermeasure” (Gaudio et al. 2012).

5.1.2 Circular and rectangular collars

Notwithstanding, there have been many experimental investigations into flow-altering countermeasures for emergent cylinders, particularly with collars. Chiew (1992) observed that scour depth is reduced in shallow flow due to the associated weakening of the downflow; as flow depth decreases, the downward momentum of the fluid at the upstream face of the cylinder decreases accordingly, resulting in lesser scour. Circular collars (disc-shaped plates around the cylinder in a plane parallel to the original bed) were used as a barrier between the downflow and the underlying scour-susceptible bed sediment. Both clear-water and live-bed conditions were investigated experimentally, and it was determined that the formation and migration of bedforms under live-bed conditions may undermine the effect of collars and reduce their scour-mitigating capacity. Slots in the cylinder were also investigated, as openings in the cylinder reduce the effective depth of flow, thereby reducing the strength of the downflow. Collars were found to be effective for scour reduction under clear-water conditions, and a combination of a slot in the cylinder near the bed with a collar of diameter $2D$ (where D is the cylinder diameter) was found to eliminate scour altogether (Chiew 1992).

Kumar et al. (1999) carried out a similar investigation into the use of slots and circular collars for scour reduction. The vertical location of the collar with respect to the original bed level was altered for each test, and the effectiveness of the collar for scour reduction was found to depend on the location of the collar as well as the size. It was found that the deepest scour occurred at the upstream face of the pier for smaller-sized collars placed at higher elevations, and in the wake for larger-sized collars placed at lower elevations. The most effective configuration was found to be a collar of diameter $4D$ located at bed level,

which eliminated scour entirely upstream of the cylinder, while inducing higher scour in the wake region. The authors of the investigation stated that mitigation of scour upstream and at the sides of the cylinder would obviously eliminate sediment entrainment and therefore deposition downstream of the cylinder, which would explain the increase in scour in the wake region. An expression was developed which determined the ratio of scour depth at a cylinder with a collar to scour depth at a cylinder without a collar as a function of vertical location of the collar with respect to the free surface, flow depth, cylinder diameter and collar width (Kumar et al. 1999). Moncada-M et al. (2009) also concluded that a combination of a collar and slot reduced scour most efficiently. Experiments were also performed using collars alone, and the optimal vertical location of a circular collar was determined to be at or below the original bed level. Similar to previous studies, a collar of diameter $2D$ reduced scour while a collar of diameter $3D$ eliminated scour entirely. However, the collar size was determined to be less crucial for scour reduction as flow depth decreased (Moncada-M et al. 2009). Despite the efficacy displayed by a combination of collars and slots in literature, it is important to note that use of slots in the field may not be practical, due to the risk of blockage by debris carried in the flow.

Jahangirzadeh et al. (2014) carried out both experimental and numerical investigations on the effect of collar shape. The authors concluded that the optimal location for both circular and rectangular collars of any size was at or below bed level, which is in agreement with other research reported in the literature. However, rectangular collars were found to be more effective for scour depth reduction. The maximum decrease in scour depth for a rectangular collar of optimal configuration was 79% compared with 71% for a circular collar of optimal configuration (Jahangirzadeh et al. 2014).

The use of collars in conjunction with other countermeasures has also been explored experimentally. Zarrati et al. (2006) investigated the use of a combination of circular collars at bed level and riprap protection to reduce scour, and found that as collar width increased, scour depth decreased. However, concerns were raised about the applicability of this finding under prototype conditions, since a cost-optimal design of collars with a diameter greater than $3D$ may not be achievable. The authors also found that scour was not eliminated entirely upstream of the cylinder, even for a collar of diameter $3D$. It was observed that the wake vortices induced scour on either side of the collar in the wake region and migrated around and under the front edge of the collar. Therefore, undermining of even a comparatively wide collar is still a concern in design (Zarrati et al. 2006).

5.1.3 Splitter plates

While collars are used to mitigate the ability of the downflow and horseshoe vortex (HSV) to induce scour, they are not intended to specifically disrupt the wake vortices, which are also a scour-inducing flow field feature. The use of splitter plates for inhibiting the vortex shedding mechanism in the wake region has been occasionally investigated for local scour. The motivation for incorporation of this countermeasure stems from an experimental investigation by Roshko (1954) on the wake region of flow around circular cylinders. Roshko inferred that installation of a vertical splitter plate on the downstream face of the cylinder would disrupt the periodic vortex formation and affect the pressure on the base of the cylinder. It was determined that the streamwise length of the splitter plate as well as the inclusion of a gap between the plate and the cylinder would also specifically influence both characteristics. A short splitter plate ($l = 1D$) was found to have a slight influence on the frequency of vortex shedding, while not disrupting vortex formation (Roshko 1954).

Gerrard (1966) carried out a similar investigation of the formation of vortices in the wake of a circular cylinder, showing that the Strouhal number (related to the frequency of vortex shedding from the cylinder) decreased as the length of the splitter plate increased. The length of the vortex formation region (the end of which is described as the point at which “fluid from outside the wake first crosses the axis”) in the wake was also found to increase with inclusion of a splitter plate. In general, Gerrard (1966) described the disruption of the crossflow in the wake region (characteristic of the vortex shedding from either side of the cylinder) as responsible for an increase in production of circulation in the rear of the cylinder and weakening of the vortex strength. A comprehensive review of the use of the splitter plates in the wake region of cylinders can be found in Wu et al. (2018).

Dey et al. (2006) used splitter plates in both the front and back of a circular cylinder to inhibit local scour under waves, finding that this method resulted in an average reduction of scour depth of 62%. The authors stated that splitter plates would not be an effective flow-altering device for steady currents, since the plate would effectively turn the circular cylinder into a semi-circular abutment. Wu et al. (2018) carried out an experimental investigation on the use of both front splitter plates and back (vertical) splitter plates fitted to emergent cylinders, while varying the heights of both types of plate with and without gaps between the cylinder and plate. A back splitter plate was shown to have no influence on the scour profile upstream of the cylinder. In the wake of the cylinder, a splitter plate with a length of $2D$ (**Figure 5.1**) did reduce scour more efficiently than a splitter plate with length $1.33D$. Back splitter plate height was not found to have a significant influence on scour in the wake region. The length of the back splitter plate was found to influence the height of the dune in the wake region, but in general, the presence of a back splitter plate

was not particularly effective for scour depth reduction, particularly in the region of highest concern at the upstream face of the cylinder (Wu et al. 2018).

5.1.4 Scour at submerged cylinders

Practical examples of flow past submerged cylinders include well foundations of bridge piers, piers which are submerged during flooding, structures in floodplains during flood events, structures submerged in offshore or coastal tides or currents (Dey et al. 2008), such as sub-sea caissons, platform foundations and submerged cylindrical breakwaters (Zhao et al. 2010), and submerged vegetation in natural streambeds (Dey et al. 2008).

The flow structures in the region surrounding a submerged cylinder are similar to those around an emergent cylinder with the addition of a trailing vortex which is formed at the top of the cylinder due to flow separation. For a submerged cylinder, the strength of the downflow on the upstream face is reduced compared with an emergent cylinder under the same flow conditions, since the surface along which it is formed is also reduced (Dey et al. 2008). The strength of the wake vortices in the von Kármán vortex street downstream of the cylinder is also diminished as the height of the cylinder decreases (Zhao et al. 2010).

5.1.5 Motivation and problem background

Recently, Lachaussée et al. (2018) presented their analysis of two competing erosion patterns in flow past a submerged circular cylinder. The authors stated that local scour can be classified as horseshoe scour (controlled by the HSV) and wake scour (controlled by the wake vortices), and that the geometry of scour is related to the dominance of horseshoe scour over wake scour. Bed profile images for local scour tests around a submerged cylinder from this investigation are shown in **Figure 5.2**. When the flow intensity (U/U_c ,

where U is the free-stream velocity and U_c is the critical velocity required to initiate sediment motion) was sufficiently low such that the onset of scour was just reached, the wake scour development resulted in formation of two symmetrical troughs in the wake region. Although the horseshoe vortex was formed and some horseshoe scour around the cylinder did develop, the local scour region associated with horseshoe scour did not interfere with the region associated with wake scour (**Figure 5.2(b)**). As the flow intensity increased, the local scour pattern was dominated by the horseshoe scour and the scour hole around the cylinder became the dominant feature in the local scour geometry, although wake troughs were still observed in the region downstream of the cylinder (**Figure 5.2(d)**). In order to investigate the development of wake scour without the influence of horseshoe scour at a higher flow intensity, a horizontal plate was placed around the base of the cylinder (**Figure 5.2(c)**). This plate (a rectangular collar) inhibited horseshoe scour, and it was established that the wake scour pattern was formed as a result of the wake vortices. It was concluded that the horseshoe scour is not affected by wake scour but an increase in the horseshoe scour does influence wake scour, and the wake troughs occur due to the wake scour mechanism (Lachaussée et al. 2018).

The results presented by Wu et al. (2018) and Lachaussée et al. (2018) have indicated that the introduction of scour countermeasures can affect the geometry of local scour around a cylinder. The present investigation was conducted in order to further explore the effects of flow-altering countermeasures on local scour around a submerged cylinder. A control test was first completed for a submerged cylinder with no flow-altering attachment. Two further experiments were carried out in order to determine the effects of a horizontal rectangular collar (plate mounted at the original bed level) and a vertical back splitter plate

on local scour geometry. PIV measurements were undertaken in several planes surrounding the cylinder to explore the influence of each device on the flow characteristics that are known predictors of scour.

5.2 Methodology

The test parameters and approach flow characteristics for the experiments are provided in **Table 5.1**. Three tests were completed for local scour around a submerged cylinder with height of $1.88D$, embedded in a channel of width $7.14D$. Test E1 was the control test, i.e. the submerged cylinder did not have any flow-altering attachment (see **Figure 5.3**). Test E2 was for the submerged cylinder with a vertical splitter plate having streamwise length and vertical height of $2D$ and $1.72D$, respectively. For test E3, the submerged cylinder was fitted with a horizontal base plate (i.e. a rectangular collar) whose streamwise length and spanwise width were $2D$ and $7.14D$, respectively. Bed profile measurements are included in analysis for local scour around an emergent cylinder (test B1), for which all other characteristics of flow were identical to test E1. The experimental conditions, including scour-governing parameters (see **Table 5.1**), were held constant for all tests so that the effects of each countermeasure on local scour geometry and the surrounding flow field could be isolated. Flow intensity U/U_c was maintained at 0.85 in order to ensure clear-water conditions while still obtaining a measurable scour pattern. Flow shallowness h/D was held at 2.14 so that the pier classification was narrow. Narrow piers comprise the majority of laboratory experiments in the literature (Ettema et al. 2011). The relative sand coarseness D/d_{50} was held at 76 such that $D/d_{50} > 25$. For $D/d_{50} < 25$, the relationship between relative scour depth d_{se}/D and D/d_{50} changes. The majority of experiments

reported in the literature are conducted for $D/d_{50} > 25$ in order to simulate field conditions (Lee & Sturm 2009).

Experiment E3 was modelled after a similar local scour experiment conducted by Lachaussée et al. (2018) (**Figure 5.2**). The blockage ratio D/b in their experiment was 0.20. Channel blockage has been previously found to have a significant effect on local scour even when $D/b < 0.10$ (Hodi 2009, D’Alessandro 2013, Tejada 2014, Williams et al. 2018). In order to minimize the effects of blockage while still considering the conditions under which the results of Lachaussée et al. (2018) were obtained, a value of $D/b = 0.14$ was selected for the present experiments.

Table 5.1: Experimental conditions for tests E1, E2 and E3

Parameter notation, description	Magnitude
D , pier diameter	0.056 m
h , flow depth	0.12 m
b , effective channel width	0.40 m
U , depth-averaged velocity of approach flow	0.262 m/s
u_τ , friction velocity of approach flow	0.0135 m/s
d_{50} , median sediment diameter	0.74 mm
AR , aspect ratio	3.33
h/D , flow shallowness	2.14
D/b , blockage ratio	0.14
D/d_{50} , relative coarseness	76
U/U_c , flow intensity	0.85

Previous analysis has indicated that changes in the approach flow channel geometry affect the distribution of mean streamwise velocity U , the Reynolds shear stress $-\overline{uv}/U_e^2$, streamwise turbulence intensity u_{rms}/u_τ and vertical turbulence intensity v_{rms}/u_τ . Here, U_e is

the maximum velocity in the approach flow in the absence of the cylinder. These quantities (particularly the Reynolds shear stress) have a significant influence on local scour. As a result, the approach flow characteristics for tests E1, E2 and E3 were held constant. The distribution of the mean streamwise velocity of the approach flow in addition to $-\overline{uv}/U_e^2$, u_{rms}/u_τ and v_{rms}/u_τ are shown in **Figure 5.4**. From the roughness function ΔU^+ acquired from the distribution of U^+ (mean streamwise velocity normalised with friction velocity), the value of k_s^+ (length scale for inner region of flow over a rough wall) was determined to be 7.25. The roughness of the bed in the current investigation falls in the category of transitional roughness, for which $5 < k_s^+ < 70$ (Nezu and Nakagawa 1993). The shear velocity u_τ was calculated from extrapolation of the Reynolds shear stress to the bed. The Reynolds number based on the approach flow depth, Re_h , and based on the cylinder diameter, Re_D , were 33473 and 15621, respectively.

Experiments were conducted for a period of 24 hours, after which equilibrium of local scour was reached and PIV measurements were taken for the flow field at the equilibrium state. Prior experimentation indicated that changes in d_{se}/D (where d_{se} is the maximum scour depth in the vicinity of the cylinder) after 24 hours were less than five percent and so equilibrium was considered to have been attained under the present testing conditions. Similar testing conditions were applied in previous investigations and the details of the progression of scour with time can be found therein (D'Alessandro 2013, Williams 2014).

5.3 Results and discussion

5.3.1 Comparison of bed profiles

Figure 5.5 shows plan-view pictures of the equilibrium scour formations for tests E1, E2 and E3. Tests E1 and E2 exhibit many similarities, with the formation of a scour hole around the cylinder and a primary deposit. For test E3, two adjacent wake troughs form symmetrically downstream of the cylinder. The primary deposit is quite different from that noticed in tests E1 and E2. It can be noted that the scour formation seen for test E2 is qualitatively similar to the formation observed by Wu et al. (2018), and the formation for test E3 is similar to that seen by Lachaussée et al. (2018).

Figure 5.6 shows the contour of the scour profiles in the XZ plane at $Y/D = 0$. The origin of the coordinate system is located at the geometric centre of the cylinder at the original bed level. The X -coordinate is in the streamwise direction, the Y -coordinate is in the vertical direction and the Z -coordinate is in the spanwise direction. For all bed measurement figures, the profiles for control test E1 are denoted by black square symbols, the profiles for test E2 with a vertical plate are shown by blue circular symbols, and the profiles for test E3 with a horizontal plate are shown by red triangular symbols. The profiles for test B1 with an emergent cylinder are shown by the filled black square symbols. The locations of the vertical and horizontal plates are shown with dashed-dotted open area and small-dashed open area, respectively. The location of the original bed is shown by the dotted line at $Y/D = 0$.

In **Figure 5.6**, the scour holes for tests E1 and E2 are shown to be comparable in size, with the size of the scour hole for test E2 being slightly larger. The scour hole for test B1 with

an emergent cylinder is larger than test E1 with a submerged cylinder, which is to be expected since the downflow is weakened for a submerged cylinder. Furthermore, the location relative to the cylinder differs slightly; while the scour hole has formed equally upstream and downstream of the cylinder for test E1, the scour hole is located further upstream relative to the cylinder location for test E2. Relative to test E1, the scour hole in test E2 is smaller in the wake region. This points to a weakening of the erosive action by the wake vortices in this region, caused by the presence of the vertical plate.

Anderson and Szewczyk (1997) reported the effect of splitter plate length on the wake characteristics of flow around a circular cylinder. The effect of a splitter plate on the interaction of the shear layers shed from either side of the cylinder is illustrated in **Figure 5.7**. In the control case of flow around a circular cylinder with no plate, the shear layers interacted through transverse oscillations, which were in phase with the shedding of the von Kármán vortices. When a splitter plate longer than $1.5D$ was fitted to the cylinder, the transverse oscillations were reduced and the interaction between the shear layers was decreased. However, there was additional interaction between the splitter plate and the shear layers. The presence of a splitter plate did not change the location of flow separation from the cylinder. As also described by Roshko (1954) and Gerrard (1966), a splitter plate of length greater than $1.5D$ reduced the frequency of vortex shedding in the wake of the cylinder. If the frequency of vortex shedding is reduced, the transport processes in the wake of the cylinder change. The conservation of mass and conservation of momentum would then dictate a corresponding adjustment in the flow conditions upstream of the cylinder, resulting in an increase in local scour shown by the shaded region G' (**Figure 5.6**). Since the wake vortices are the mechanism by which sediment is transported downstream from

the sides of the cylinder, it is reasonable that the scour hole for control test E1 is larger than the scour hole for test E2 in the wake region. For both tests E1 and E2, it can be seen that the scour formation reaches the sidewalls on either side, which is likely due to the blockage effect. However, the width of scour in the wake region is greater in test E1 than in test E2. This is also in agreement with the findings of Anderson and Szewczyk (1997), who reported that the width of the wake is reduced by the dampening of the transverse oscillations in the presence of the splitter plate.

As one would expect, there is no scour upstream of the cylinder in test E3 due to the presence of the horizontal plate. The contour profile for E3 also shows that the wake troughs reach the sidewalls in the wake and extend to $4D$ downstream of the cylinder. The extent of the scour is farther downstream compared to the scour holes in tests E1 and E2. Therefore, the horizontal plate results in a greater downstream extension of scour than for a cylinder fitted with a splitter plate or for an unprotected cylinder, which may be cause for concern for groups of piers.

Figure 5.8 shows the bed profile for equilibrium scour for tests E1, E2 and E3 in the XY plane along (a) $Z/D = 0$, (b) $Z/D \approx 0.5$ and (c) $Z/D = 2.0$. **Figure 5.8(a)** demonstrates that the bed profile shapes upstream of the cylinder for tests E1 and E2 are very similar in the central plane. For the reasons described earlier, the scour hole commences further upstream in test E2. In the wake region, test E1 shows the classical scour hole and dune formation pattern, with a crest located around $X/D = 6.75$. Upstream of the cylinder, it can be seen that the depth of scour for both a submerged (test E1) and emergent cylinder (test B1) is similar. The scour hole is slightly deeper for test B1, which is reasonable since extension of the cylinder height would also increase the strength of the downflow (Dey et al. 2008).

Downstream of the cylinder, the dune for test E1 is shown to be longer and flatter than the dune for test B1 due to the influence of the flow separating from the top edge of the submerged cylinder and interacting with the dune. The effect of the flow separation will be discussed in a forthcoming section. In general, the bed profiles at all locations show that the depth of scour is slightly greater for test B1 when compared with test E1. The bed profiles for test B1 are included for comparison only and will not be discussed further as the focus of the present investigation is not flow submergence.

In **Figure 5.8(a)**, the scour profile in the central plane for test E2 is only available after $X/D = 2.5$ due to the presence of the vertical plate, but the profile does show a dune that is of slightly greater height and similar length to the dune for test E1. However, the dune for test E2 has a more rounded shape than the dune for test E1. The vertical splitter plate does not appear to have significantly influenced the depth of scour, which is in agreement with Wu et al. (2018). One should note that although the test setup used by Wu et al. (2018) (shown in **Figure 5.1**) for an emergent cylinder is similar to that of test E2, the scour-governing parameters D/d_{50} , h/D and D/b are quite different (see **Table 5.2**). Comparison of the bed profiles of the scour formation between test E2 and the results of Wu et al. (2018) must be solely on a qualitative basis.

In **Figure 5.8(b)**, the scour profiles along the near-cylinder plane ($Z/D \approx 0.5$) show that the scour hole upstream of the cylinder is slightly deeper for test E2 than test E1. At the location of the cylinder and downstream of $X/D = -0.5$, the scour hole is slightly deeper for test E1. This can once again be attributed to the weakening of the wake vortices by the splitter plate; the ability of these vortices to remove entrained sediment from the sides of the cylinder appears to have diminished, resulting in less erosion in the near-cylinder region,

where shedding of vortices is initiated. However, as indicated by the deeper scour upstream of the cylinder, there is a greater volume of sand to be deposited downstream. Since the dunes are comparable in length, the dune height for test E2 with the splitter plate is greater than for the dune height for test E1 without the splitter plate. However, the classical dune shape with a crest can now be seen, and from **Figure 5.5**, the picture for profile E2 indicates that there is a small divot in the dune in the wake of the vertical plate, leading to the rounded shape seen in **Figure 5.8(a)**. On either side of the plate, the dune resumes the expected shape, and the crest is allowed to form. **Figure 5.8(c)** will be discussed in a forthcoming paragraph.

Table 5.2: Comparison of experimental conditions with tests from literature

Parameter (unit)	Cylinder with vertical splitter plate		Cylinder with horizontal (base) plate	
	E2	Wu et al. (2018)	E3	Lachaussée et al. (2018)
Cylinder type	submerged	emergent	submerged	submerged
D , pier diameter (m)	0.056	0.062	0.056	0.02
h , flow depth (m)	0.12	0.15	0.12	0.16
b , effective channel width (m)	0.4	1.22	0.4	0.1
H , cylinder height (m)	0.107	-	0.107	0.09
U , velocity of approach flow (m/s)	0.26	0.22	0.26	0.25
u_{τ} , approach flow friction velocity (mm/s)	13.51	-	13.51	19.2
d_{50} , median bed material diameter (mm)	0.74	0.51	0.74	0.27
AR , aspect ratio	3.33	8.1	3.33	0.63
h/D , flow shallowness	2.14	2.42	2.14	8.0
D/b , blockage ratio	0.14	0.051	0.14	0.2
D/d_{50} , relative coarseness	76	122	76	74
U/U_c , flow intensity	0.85	0.85	0.85	0.92
d_{se}/D , relative scour depth	1.2	1.3	-	-
l , length of splitter plate	$2D$	$2D$	-	-
H_l , height of splitter plate	$1.72D$	$1.2D$	-	-
w_l , width of horizontal plate	-	-	b	b
l_l , length of horizontal plate	-	-	$2D$	$2D$

To further understand the evolution of the scour profiles, typical velocity profiles in plane B ($Z/D \approx 0.5$) were analyzed. To this end, the distribution of the mean streamwise velocity U/U_e , mean vertical velocity V/U_e and Reynolds shear stress $-\overline{uv}/U_e^2$ are provided in **Figure 5.9** at several streamwise locations starting at the location of the scour hole and ending downstream of the dune crest. The location where each profile was extracted is shown by the dashed lines in **Figure 5.8(b)**. The location of the top of the cylinder in **Figure 5.9** is shown by the horizontal dotted line for all profiles. For reference, corresponding velocity profiles in plane A are provided in **Figure 5.10**. However, the following analysis will focus on plane B as the profiles in the two planes are qualitatively similar.

The distribution of U/U_e for the approach flow in the absence of the cylinder is shown in the top row of **Figure 5.9** along with other profiles at $X/D = -2.0$. The classical streamwise velocity profile in an open channel is observed in the absence of the cylinder. The streamwise velocity distribution has a decreased magnitude for all tests compared to the approach flow profile, with the profile for test E3 exhibiting the greatest change. For tests E1 and E2, the profiles at $X/D = -2.0$ are located in the scour hole region. Inside the scour hole ($Y/D < 0$), the streamwise velocity shows a decrease. For test E3, flow at $X/D = -2.0$ is over the horizontal plate. There is also a reduction in velocity in the region around the top of the cylinder ($Y/D = 1.88$) for all tests, but the decrease is enhanced for test E3. At $X/D = -0.5$, the streamwise velocity has increased for tests E1 and E2 closer to the bed. Due to the local changes in the scour hole profile, there is an acceleration of flow. In the absence of any scour upstream of the horizontal plate, the distribution for E3 is very similar between $-2.0 < X/D < -0.5$.

At $X/D = 0$, the magnitude of U/U_e is still very similar throughout the depth for tests E1 and E2. However, U/U_e has increased for test E3 in the upper region of flow, adjusting to the separation at the top edge of the cylinder. The magnitude of the increase in U/U_e between test E3 and the other tests is about 11% at $Y/D = 1.88$. There is also an increase in the mean velocity along the edge of the cylinder for test E3 through most of the depth ($Y/D > 0.5$). This indicates that the horizontal plate influences flow separation from the surface of the cylinder, causing it to occur further upstream for test E3 than for tests E1 and E2. This would imply that the width of the wake is greater for test E3. This is corroborated by the profiles at the downstream edge of the cylinder ($X/D = 0.5$), where U/U_e has decreased significantly for test E3 and only slightly for tests E1 and E2. At this location, the separating streamline (along which U is maximum) is closer to plane B for tests E1 and E2 than for test E3. This is illustrated by the inset in **Figure 5.8(b)**.

For test E2, there is no flow interaction between the two shear layers emanating from the sides of the cylinder at $X/D = 0.5$. The flow accelerates along the sides of the splitter plate and therefore the magnitude of U/U_e is higher than that for test E1 at this location. The effect of flow separation from the top of the cylinder is also seen from the increased velocity for all three tests at $Y/D = 1.88$. At $X/D = 2.0$, the profiles for test E1 and E2 are located at the leading edge of the dune. The increase in U/U_e as flow accelerates over the dune at this location is also higher for test E2 due to the acceleration of flow along the sides of the splitter plate. The profile for test E3 at $X/D = 2.0$ is located over the wake trough in which flow has separated, which corresponds to the decrease in U/U_e below $Y/D = 0$. At $X/D = 7.0$, flow separation from the dune crest causes a decrease in velocity close to the

bed. The streamwise velocity at this location is similar for test E1 and E2, and slightly lower for test E3.

The distribution of normalised vertical velocity, V/U_e , is shown in the middle row in **Figure 5.9**. In the undisturbed approach flow, the magnitude of the vertical velocity is close to zero throughout the depth of flow. As with the distribution of U/U_e at $X/D = -2.0$, V/U_e for E3 is mostly unchanged from the approach flow conditions. For tests E1 and E2, there is an increase in negative (downward component) V/U_e which increases towards the bed as the flow enters the scour hole. It should be noted that the vertical component of velocity in the negative direction increases from the approach flow conditions up to $Y/D = 2.14$ for tests E1 and E2, indicating that the effect of the scour hole is felt throughout the depth of flow. This negative vertical velocity is shown to have an increase in magnitude at $X/D = -0.5$, where the depth of scour has also increased. For test E3, the streamwise velocity component was mostly unchanged between $-2.0 < X/D < -0.5$. However, the vertical component of velocity in the negative direction changes quite significantly between these two stations. This indicates that upstream of the cylinder, the flow has already begun to incline downwards towards the approaching wake trough.

At $X/D = 0$, the negative vertical velocity for test E3 is nearly as high as that seen for tests E1 and E2. At $X/D = 0.5$, the reduction in negative V/U_e for test E1 relative to tests E2 and E3 corresponds to an increase in the depth of scour for the control test at this location. At the leading edge of the dunes for tests E1 and E2 ($X/D = 2.0$), the distribution of V/U_e is characterized by a positive vertical component near the bed as flow accelerates up and over the dune. For test E3, $X/D = 2.0$ is within the wake trough and so there is still an appreciable component of negative V/U_e at this location as flow enters the trough. Downstream of the

dune crests ($X/D = 7.0$), V/U_e is very small in all cases. There is an increase in the positive direction for tests E1 and E2 close to the bed (possibly due to recirculation in the downstream of the dune), and an increase in the negative direction for test E3 as flow accelerates down the slope in the wake of the dune.

From $-2.0 < X/D < 0$, the distribution of the Reynolds shear stress $-\overline{uv}/U_e^2$ (**Figure 5.9**, bottom row) is very similar and close to zero throughout the depth. There are slight increases in $-\overline{uv}/U_e^2$ close to the bed and near the free surface for all three tests, but significant changes are not observed until $X/D = 0.5$. At $X/D = -0.5$, a peak in $-\overline{uv}/U_e^2$ is observed very close to the horizontal plate for test E3. The magnitude of the bed shear stress τ_b calculated from the Reynolds shear stress at this location was found to be more than 2.5 times greater than the critical bed shear stress of sediment τ_{bc} . A similar peak in the Reynolds shear stress is located near the surface of the horizontal plate at $X/D = 0$ (i.e. the side of the cylinder). The magnitude of τ_b at this location was determined to be over $3\tau_{bc}$. Therefore, τ_{bc} was exceeded between $-0.5 < X/D < 0$ for test E3.

This is in agreement with the results of Large Eddy Simulation (LES) and Detached Eddy Simulation (DES) investigations of flow around an emergent cylinder under local scour equilibrium by Kirkil et al. (2008, 2009), in which the bed shear stress was shown to be high along the sides of the cylinder. It is well known that local scour is initiated at the sides of an unprotected cylinder. The Reynolds shear stress at the location of the horizontal plate for test E3 ($-1.5 < X/D < 0.5$) can therefore be viewed as a base case of flow around a cylinder without scour, and the distributions for tests E1 and E2 are illustrative of the effects of the exceeded bed shear stress on the scour profile.

At $X/D = 0.5$, $-\overline{uv}/U_e^2$ shows an increase close to the free surface for all tests, due to the flow which has separated from the top of the cylinder. The Reynolds shear stress is still quite low for test E3 in the mid-region of the flow. The magnitude of the Reynolds shear stress is significantly higher for test E1 in the mid-depth of flow, indicating that the vertical splitter plate in test E2 and the horizontal plate in test E3 aid to reduce $-\overline{uv}/U_e^2$ particularly effectively at this location. The depth of scour downstream of $X/D = 0.5$ is less for tests E2 and E3 when compared with test E1, indicating that a reduction in the Reynolds shear stress close to the cylinder is a desirable outcome of scour-countermeasure implementation. The Reynolds shear stress shows a significant increase close to the horizontal plate for test E3 due to the impending separation at the edge of the plate. Further downstream, the change in the Reynolds shear stress profile between $0.5 < X/D < 2.0$ in the upper region of the flow is indicative of the downward inclination of the separated flow from the top of the cylinder, which is clearly stronger for test E3. At $X/D = 7.0$, $-\overline{uv}/U_e^2$ is small throughout most of the depth of flow, with an increase at the expected location of a shear layer emanating from the crest of the dune for tests E1 and E2.

Figure 5.8(c) shows the scour profiles in the XY plane at $Z/D = 2.0$. Once again, it can be seen that scour for test E2 is greater than that for test E1 upstream of the cylinder, and then lesser than test E1 downstream of the cylinder. The length and height of the dune in this plane are also greater for test E2 than for test E1 in the wake region. For test E3, the formation of the adjacent wake troughs can be seen in both planes B and C. The absence of scour in the vicinity of the scour hole shows the efficacy of the horizontal plate in suppressing horseshoe scour. The wake scour has been permitted to progress unimpeded in the wake region. This bed formation was also reported by Lachaussée et al. (2018) and

qualitatively compares well with the present results. Quantitative comparison would not be meaningful, because changes between the profiles for the two tests could be attributed to changes in approach flow conditions, Reynolds number, D/b , b/h or D/d_{50} .

In plane B, the dune in the wake of test E3 decreases in height while maintaining approximately the same length as the dunes for tests E1 and E2. For plane C, the dune is considerably shorter in length than the dune for tests E1 and E2, and a trough preceding a secondary deposit can be seen. Although the scour downstream of the cylinder for test E3 beyond $X/D \approx 1.5$ is deeper than the scour for tests E1 and E2 in plane B and the same is true beyond $X/D \approx 1$ in plane C, the maximum depth of scour for test E3 in either case is still significantly smaller than the maximum scour depth upstream of the cylinder for tests E1 and E2, indicating that the horizontal plate is a promising flow-altering countermeasure. The foundation head required for serviceability would be significantly less for a cylinder with a rectangular collar of similar configuration, than for an unprotected cylinder or one employing a back splitter plate.

Figure 5.11 shows the scour profiles in the YZ plane for the streamwise locations of (a) $X/D = -1.3$ (b) $X/D = 0$ (i.e. the spanwise centreline of the cylinder) for tests E1 and E2 and $X/D = 0.5$ for test E3, and (c) $X/D = 1.75$. In general, the scour profiles for all tests show good symmetry. In **Figure 5.11(a)**, upstream of the cylinder at $X/D = -1.3$, the scour profiles for E1 and E2 are once again nearly identical. This is consistent with the distribution of the flow field characteristics from $-2.0 < X/D < -0.5$ shown in **Figure 5.9** and **Figure 5.10**. In **Figure 5.11(b)**, the profile for test E3 is shown at $X/D = 0.5$, since the horizontal plate extends to $X/D = 0.5$. In the spanwise centreline of this figure, it can be seen that there is still very little difference in the scour holes for tests E1 and E2. The scour

profile for test E3 at $X/D = 0.5$ shows that the wake troughs are beginning to form just at the edge of the horizontal plate, and the narrow dune shown in the XY plane profiles between the adjacent wake troughs is observed as well. Downstream of the cylinder, at $X/D = 1.75$, **Figure 5.11(c)** shows that the scour holes for tests E1 and E2 have nearly progressed to the original bed level. However, the wake troughs formed for test E3 can be seen to span nearly the entire width of the channel and are deeper in this region. Again, the depth of the wake troughs is still smaller than the maximum scour depth at $X/D = 0$ for tests E1 and E2. This confirms that the wake scour and horseshoe scour work together for tests E1 and E2, but the wake scour is the only prevailing mechanism as the HSV does not contribute to scour in test E3.

In general, the profiles shown in **Figure 5.8** through **Figure 5.11** indicate that while the splitter plate does not significantly change the formation of scour in the vicinity of the cylinder, the horizontal plate has a greater effect. The cause for these changes in scour geometry will be explored in greater detail in the following section, through analysis of the flow field at an equilibrium condition for each test.

5.3.2 Distribution of normalised mean streamwise velocity U/U_e

Figure 5.12 shows the distribution of mean streamwise velocity normalised by U_e , the maximum velocity of the undisturbed approach flow, in the central plane ($Z/D = 0$) for tests E1, E2 and E3. The location of the vertical and horizontal plates for tests E2 and E3 are shown by the filled dark grey areas, and the cylinder location is indicated by the filled light grey area. Many features which are expected in the flow field surrounding a cylinder at an equilibrium scour condition can be visualised in the distribution of U/U_e for the control test E1 (**Figure 5.12(a)**). In region marked 'A' in the figure, the adverse pressure gradient

induced by the stagnation line on the cylinder causes deceleration of the streamwise velocity in the approach flow leading up to the upstream face of the cylinder. In the field-of-view captured by the PIV, there is a region of low streamwise velocity ('B') due to separation of flow from the leading edge of the hole. This points to the clockwise rotation of the horseshoe vortex (HSV), the majority of which is located within the portion of the scour hole uncaptured by the PIV measurements. Dey et al. (2008) presented Acoustic Doppler Velocimetry (ADV) measurements in the central plane for local scour around a submerged cylinder. The distribution of the velocity vectors is similar to those presented in the central plane for test E1, and so the rotation of the HSV presented therein can be viewed as a general representation of the flow field within the scour hole. The separating flow emanating from the top of the cylinder ('C'), which is characteristic of flow over a submerged cylinder, is shown by the region of high streamwise velocity above the cylinder (from about $-0.5 < X/D < 2.0$). This feature was also noted by Dey et al. (2008).

The region of low and negative streamwise velocity in the immediate wake of the cylinder (denoted as 'D' in **Figure 5.12(a)**) is typical of a cylinder wake. The vector field in this area indicates an upward vertical component of flow as well. Following the near-wake region ($X/D < 1.0$), there is a strong upwash as indicated by the vector field, which can aid in the removal and transport of sediment. This feature was also observed by Graf and Istiarto (2002), who acquired Acoustic Doppler Velocimetry (ADV) measurements in the central plane for local scour equilibrium around an emergent cylinder.

The region of low streamwise velocity appears to weaken around $X/D = 2.0$, or approximately where the primary deposit begins. The primary deposit is formed when sediment is deposited by weakening wake vortices, which increase in radial size and

decrease in strength as they advect away from the cylinder in the downstream direction. The flow also accelerates out of the scour hole and over the surface of the primary deposit (region 'E' in **Figure 5.12(a)**) and separates over the crest to form a shear layer emanating in the downstream direction. The dune can be viewed as a backward-facing step, characterized by the recirculating region immediately downstream of the crest ('F').

Figure 5.12(b) shows the distribution of U/U_e in the central plane for test E2 for a submerged cylinder fitted with a vertical splitter plate. For most part, the approach flow is very similar to test E1 in the region $-3 < X/D < -2.5$, with some minor differences. In fact, the velocity contours in the vicinity of the scour hole are very similar to those seen in the distribution of U/U_e for test E1 (regions 'A' and 'B' in the contours). The separating flow over the submerged cylinder is also unaffected by the vertical splitter plate, showing similar size and magnitude to that seen for test E1 ('C'). While the wake region flow is not visible in the central plane due to the presence of the vertical plate, a similar acceleration of flow over the primary deposit is noted ('E'). However, the strength of this accelerating flow is higher than what is shown for test E1. This can likely be attributed to disruption of the vortex shedding mechanism due to the presence of the vertical splitter plate. When flow accelerates from the stagnation line around the sides of a cylinder, it reaches a point of separation and alternately sheds vortices in the wake region, as previously described. Since the interaction of the vortices is impeded by the presence of the vertical plate, some flow reattaches to the plate itself and accelerates along its sides in the downstream direction. There is also an increase in U/U_e immediately downstream of the vertical splitter plate close to the bed ('E'). This flow joins with the flow accelerating out of the scour hole on either side of the plate and increases transport of mass and momentum over the primary

deposit ('E'). This could also be an effect of the interaction between the shear layers on either side of the wake, which is mitigated by the splitter plate for $X/D < 2.0$. The streamwise flow over the dune is of significantly higher magnitude and is distributed over the entire depth of flow for test E2 when compared with flow in the same region for test E1. Referring to **Figure 5.5**, the crest of the dune is suppressed in the central plane (A'), which is reflected in the bed profile in **Figure 5.12(b)**. The flow gradually negotiates the shape of the dune without a large-scale recirculating region which was visible in test E1.

Figure 5.12(c) shows that the approach flow in the immediate vicinity of the cylinder ('A') for test E3 is similar to that of test E1 and is mostly unaffected by the presence of the horizontal plate at the base of the cylinder. Close to the base of the cylinder, a small region of recirculating flow is indicative of the HSV which has formed on the surface of the horizontal plate ('B'). Over the top of the cylinder, the region of separating flow is the same approximate size and magnitude as that seen in tests E1 and E2 ('C'). The von Kármán vortex street that is shed from the cylinder is expected to have the same characteristics as test E1, since unlike the vertical splitter plate, the horizontal plate would not physically disrupt the shedding of vortices. However, the area of very low and negative streamwise velocity associated with the wake region ('D') is longer than that seen in test E1. Furthermore, the streamwise velocity is negative and the flow has a very small vertical component. Whereas in test E1, one could notice that the vectors were more prone to be directed upwards in this region. As is seen for flow over the dune in tests E1 and E2, there is acceleration in region E for test E3, albeit with a very small magnitude. The recirculating region following the crest of the dune is also smaller when compared with test E1 ('F').

In **Figure 5.13**, the distribution of U/U_e for tests E1, E2 and E3 in the near-cylinder plane ($Z/D \approx 0.5$) is shown. In **Figure 5.13(a)**, the distribution of U/U_e for control test E1 shows a region of high streamwise velocity along the side of the cylinder, which is an indication of the characteristic acceleration of flow along the sides of the cylinder and separation of flow from around the cylinder surface ('B'). The influence of the flow separating from the top of the cylinder seen in the central plane is also reflected in the near-cylinder plane ('C'). There is a region of lower flow velocity in the wake of the cylinder close to the free surface ('D'). Flow accelerates over the dune as in the central plane ('E'), and the recirculating region ('F') emanating from the dune crest is smaller than what was seen in the central plane.

In **Figure 5.13(b)**, a very similar distribution for U/U_e is observed for test E2. Interestingly, the approach flow, similar to that noticed in **Figure 5.13(b)**, is higher in magnitude for test E2 when compared with test E1 ('A'), indicating that the splitter plate influences the flow upstream of the cylinder. This is reasonable, since the flow is subcritical and the flow control is located downstream (i.e. disturbances in the flow can propagate upstream). In the discussion of the bed profile measurements, it was established that the splitter plate reduces the frequency of vortex shedding in the wake of the cylinder. The conservation of mass and momentum then requires that the flow field upstream of the cylinder is strengthened, which is observed here. This was also reflected in an increase in local scour upstream of the cylinder for test E2 when compared with test E1 (**Figure 5.8(b)**).

Region B seen in **Figure 5.13(b)** is elongated due to disruption of the wake vortex shedding by the splitter plate and reattachment of flow on the plate. The width of the wake is greater for test E1 than test E2 (see **Figure 5.6**). As a result, the separating streamline (along which

U is highest) is closer to plane B for test E2 than test E1 (see inset in **Figure 5.8(b)**) and the streamwise velocity is enhanced. Similarly, the region of lower velocity beneath the separating flow ('D') is smaller for test E2 when compared with the same region for test E1. Because of the acceleration along the sides of the plate, the acceleration over the dune in test E2 is significantly stronger than the same acceleration in test E1 (region 'E'). Because the crest of the dune has re-formed at this location, a recirculating region ('F') can be observed in the wake of the crest, which was not seen in the central plane (**Figure 5.12(b)**).

Figure 5.13(c) shows the distribution of U/U_e for test E3 with a horizontal plate. The horizontal plate does not seem to have a significant influence on the distribution of approach flow upstream of the cylinder ('A') since the distribution is very similar to what is seen in the same region for test E2 and overall the magnitude of U/U_e is slightly lower in the same region in test E1. The region of high streamwise velocity (coloured red in the contour plot) at the side of the cylinder extends nearly to the free surface and does not extend as far downstream as seen in test E1 (region 'B'), indicating that the point of flow separation from the cylinder is located further upstream along the cylinder surface for test E3 than for tests E2 and E1. Because there is no redirection of flow into the scour hole for test E3, the acceleration along the sides of the cylinder is enhanced and causes flow to separate from the cylinder further upstream. The separating flow ('C') over the cylinder is very similar to tests E1 and E2 and is therefore unaffected by the presence of the horizontal plate. In the wake of the cylinder, the region of low flow velocity ('D') is significantly lower than for tests E1 and E2. There is a small recirculating region which has formed in the wake trough downstream of the horizontal plate ('D'). For test E3, flow also accelerates

over the dune. However, since the wake is likely to be wider in this region for test E3 than for tests E1 and E2 and the shallowness of the trough at this location reduces the volume of flow accelerating over the dune, the magnitude of the acceleration is of significantly less magnitude than for tests E1 and E2.

In **Figure 5.14**, the distributions of U/U_e in the mid-plane between the cylinder and the side wall (plane C, where $Z/D = 2.0$) for tests E1, E2 and E3 are provided. The streamwise flow in this plane for tests E1 and E2 is characterized by a decrease close to the bed near the scour hole followed by a region of high U/U_e in the downstream region over the dune. The distribution of U/U_e is very similar for both tests in plane C, although the magnitude of streamwise velocity is slightly higher throughout the plane for test E2. For test E3, flow in this plane is similarly higher in the downstream region, but decreases as flow is redirected into the wake trough. Because the differences observed in plane C are minimal for all tests, further discussions will focus on planes A and B.

5.3.3 Distribution of normalised Reynolds shear stress $-\overline{uv}/U_e^2$

The distribution of the Reynolds shear stress $-\overline{uv}/U_e^2$ is given in **Figure 5.15** and **Figure 5.16** for planes A and B, respectively. The distribution of $-\overline{uv}/U_e^2$ for test E1 (**Figure 5.15(a)**) shows that the Reynolds shear stress in the approach flow is low compared to the highly sheared regions elsewhere in the flow. In region A, there is a slight increase in $-\overline{uv}/U_e^2$, which corresponds to flow separation from the leading edge of the scour hole. In the near-wake region, a region of high Reynolds shear stress appears to be emanating from the scour hole ('B'). This could be due to the interaction of flow accelerating around the sides of the cylinder with flow recirculating in the scour hole. The location of feature 'B'

also corresponds to a region of vertical flow (see **Figure 5.8(a)**). Region ‘B’ extends to the approximate vertical location of the surface of the dune before the magnitude decreases near the top of the cylinder. Downstream of the cylinder, there is a region of high Reynolds shear stress close to the free surface (‘C’) near the edge of the submerged cylinder, between $0.5 < X/D < 2.5$. There is a large region of negative $-\overline{uv}/U_e^2$ over the dune (‘D’), which begins within the scour hole and extends throughout the plane. This region nearly reaches the free surface between $4.0 < X/D < 5.0$. Downstream of the crest of the dune, a shear layer is shown by an increase in $-\overline{uv}/U_e^2$ (‘E’).

In **Figure 5.15(b)**, the distribution of $-\overline{uv}/U_e^2$ shows that the shear stress in the approach flow is very similar between tests E1 and E2. The Reynolds shear stress is very low in the region upstream of the scour hole, and an increase due to flow separation at the leading edge of the hole is once again visible (‘A’). The region of high $-\overline{uv}/U_e^2$ due to the separation of flow from the top of the cylinder (‘C’) is approximately the same size as the same feature in test E1 ($0.5 < X/D < 2.5$). Downstream of the splitter plate, the region of negative Reynolds shear stress (‘D’) is smaller than the corresponding region in test E1. The shear layer caused by separation of flow from the crest is also visible from the region of high Reynolds shear stress at this location (‘E’). For test E3, distribution of the Reynolds shear stress (**Figure 5.15(c)**) is characterized by a larger region (‘C’) of high $-\overline{uv}/U_e^2$ downstream of cylinder close to the free surface, extending from $0.5 < X/D < 3.5$. Feature ‘D’ is located at a further distance downstream than for tests E1 and E2.

The distribution of $-\overline{uv}/U_e^2$ in the near-cylinder plane is given in **Figure 5.16** for tests E1, E2 and E3. For test E1 (**Figure 5.16(a)**), the Reynolds shear stress in the approach flow is similar to that in the central plane. The recirculating region within the scour hole (‘A’) is

also visible in plane B. There is a region of high $-\overline{uv}/U_e^2$ in the middle of the depth of flow near the cylinder ('B'), which likely corresponds to the location of flow separation. Feature 'B' could be confined to the mid-depth of flow due to the separation of flow over the top of the cylinder and flow within the scour hole. The large region of high $-\overline{uv}/U_e^2$ ('C') due to flow separation over the top of the cylinder is longer in plane B, extending from $0.5 < X/D < 3.5$. As in the central plane, there is a region of negative Reynolds shear stress over the dune ('D'). In the near-cylinder plane, this feature extends upstream past the edge of the cylinder. The shear layer at the crest of the dune is also seen in plane B ('E').

In **Figure 5.16(b)**, the upstream features are similar to those seen in test E1. Downstream of the cylinder, the feature 'B' has been significantly reduced in size by the splitter plate. This indicates that flow separation around the sides of the cylinder is disrupted by the vertical splitter plate, which was also illustrated by the scour formation in **Figure 5.8(b)** and the distribution of U/U_e (**Figure 5.13(b)**). The region of high Reynolds shear stress extending downstream from the top of the cylinder ('C') is also smaller for test E2 ($0.5 < X/D < 2.5$). The region 'D' extends as far upstream as the cylinder for test E2, as with test E1.

Figure 5.16(c) shows changes in the distribution of Reynolds shear stress due to the presence of the horizontal plate. Feature 'C' in particular is much larger than the same feature seen in tests E1 and E2, extending from $0.25 < X/D < 4.5$. Similarly, the region of negative Reynolds shear stress over the dune ('D') is larger for test E3, extending down towards the edge of the plate and upwards in the vicinity of the cylinder. In the wake trough,

in the region of flow acceleration over the leading edge of the dune, there is an area of high $-\overline{uv}/U_e^2$ ('D') which is not seen in the scour holes for tests E1 and E2.

5.4 *Conclusions and recommendations*

The experimental results indicate that the vertical splitter plate and horizontal base plate induce changes in the equilibrium scour geometry and the distribution of velocity field characteristics in the vicinity of the cylinder. The splitter plate reduces the frequency of vortex shedding, causing an increase in local scour upstream of the cylinder and a decrease downstream of the cylinder. The width of the wake is also reduced by the presence of the splitter plate, and the streamwise velocity downstream of the plate is increased by acceleration along either side of the plate. The Reynolds shear stress is also reduced close to the cylinder. However, the changes induced by the vertical splitter plate in the flow field do not significantly influence the formation of scour (as indicated by the bed profile measurements) and are therefore less consequential for the purposes of scour mitigation.

The horizontal base plate eliminates scour entirely upstream of the cylinder. Analysis of the Reynolds shear stress distribution indicates that the bed shear stress at the surface of the horizontal plate near the sides of the cylinder exceeds the critical shear stress of the sediment by a factor between 2.5 and 3, providing a base case at the location of the plate for flow around a cylinder without scour. Without the presence of the scour hole and the horseshoe vortex contained therein, the wake characteristics are significantly altered in test E3. The streamwise velocity and the Reynolds shear stress in the wake of the cylinder close to the bed are also reduced by the horizontal plate. Other flow-altering devices which maximize reduction of U/U_e and $-\overline{uv}/U_e^2$ in the wake of the cylinder should be explored

in order to reach an optimal countermeasure design. Furthermore, while changes in the flow field due to the presence of the splitter plate and the horizontal plate are evident in the central plane and near-cylinder plane, the flow field in the mid-cylinder-wall plane was shown to be mostly unchanged by the presence of either countermeasure. This indicates that the width of the plate itself could be reduced with no associated increase in scour near the cylinder, and this effect should be further explored in order to reduce potential for high costs associated with larger collar width.

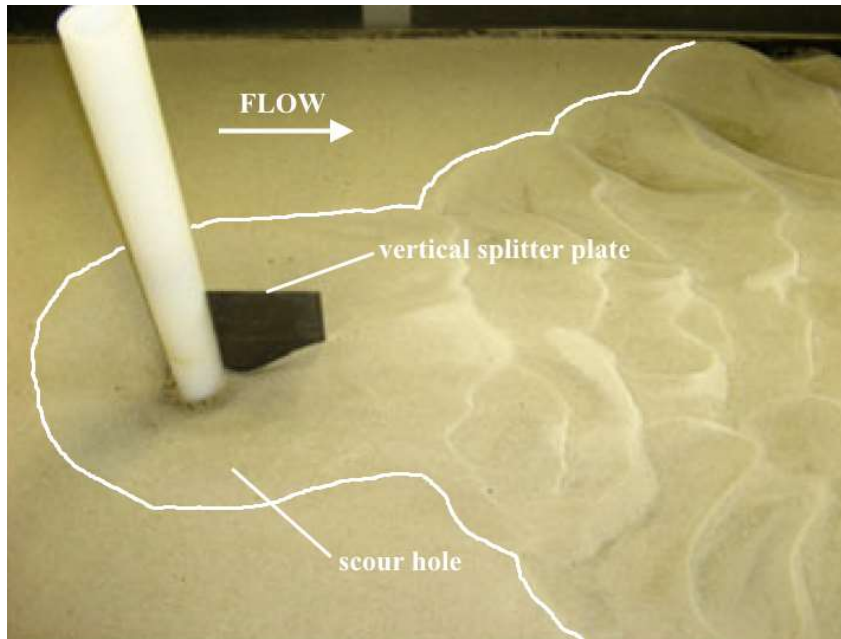


Figure 5.1: Scour formation for flow around a circular cylinder ($D = 0.062$ m) with a back splitter plate of length $2D$ and height $1.2D$, from Wu et al. (2018); figure used with permission from Wiley

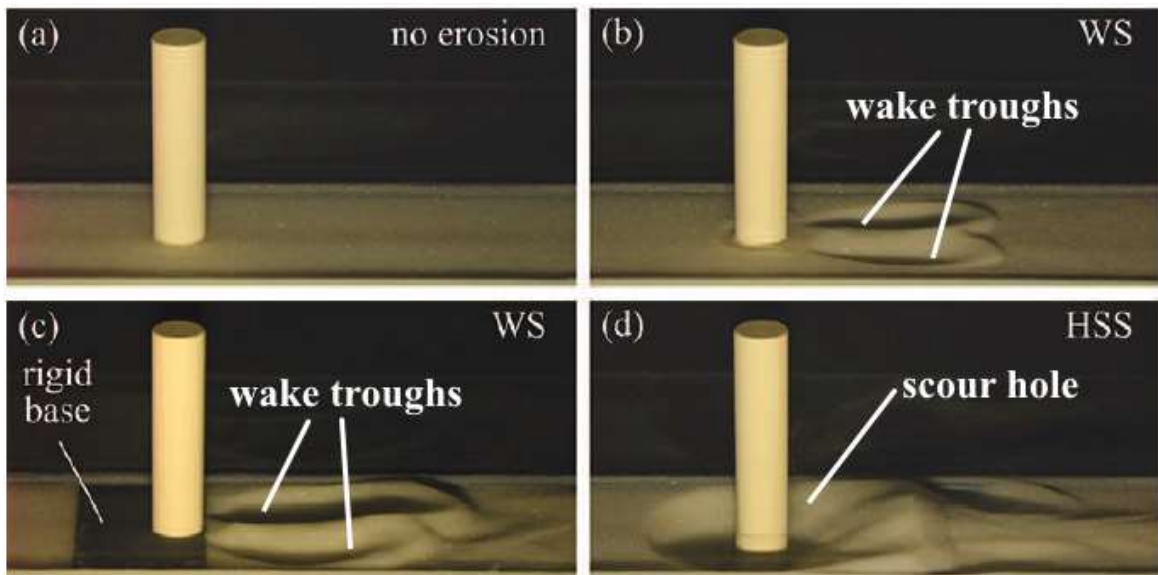


Figure 5.2: Bed profile images from Lachaussee et al. (2018) for a submerged cylinder with (a) no scour ($Re_D \approx 1000$), (b) low U/U_c , ($Re_D \approx 2100$) (c) high U/U_c ($Re_D \approx 3200$) with horizontal base plate and (d) high U/U_c ($Re_D \approx 3200$) with no base plate (WS = wake scour, HSS = horseshoe scour); figure used with permission from APS

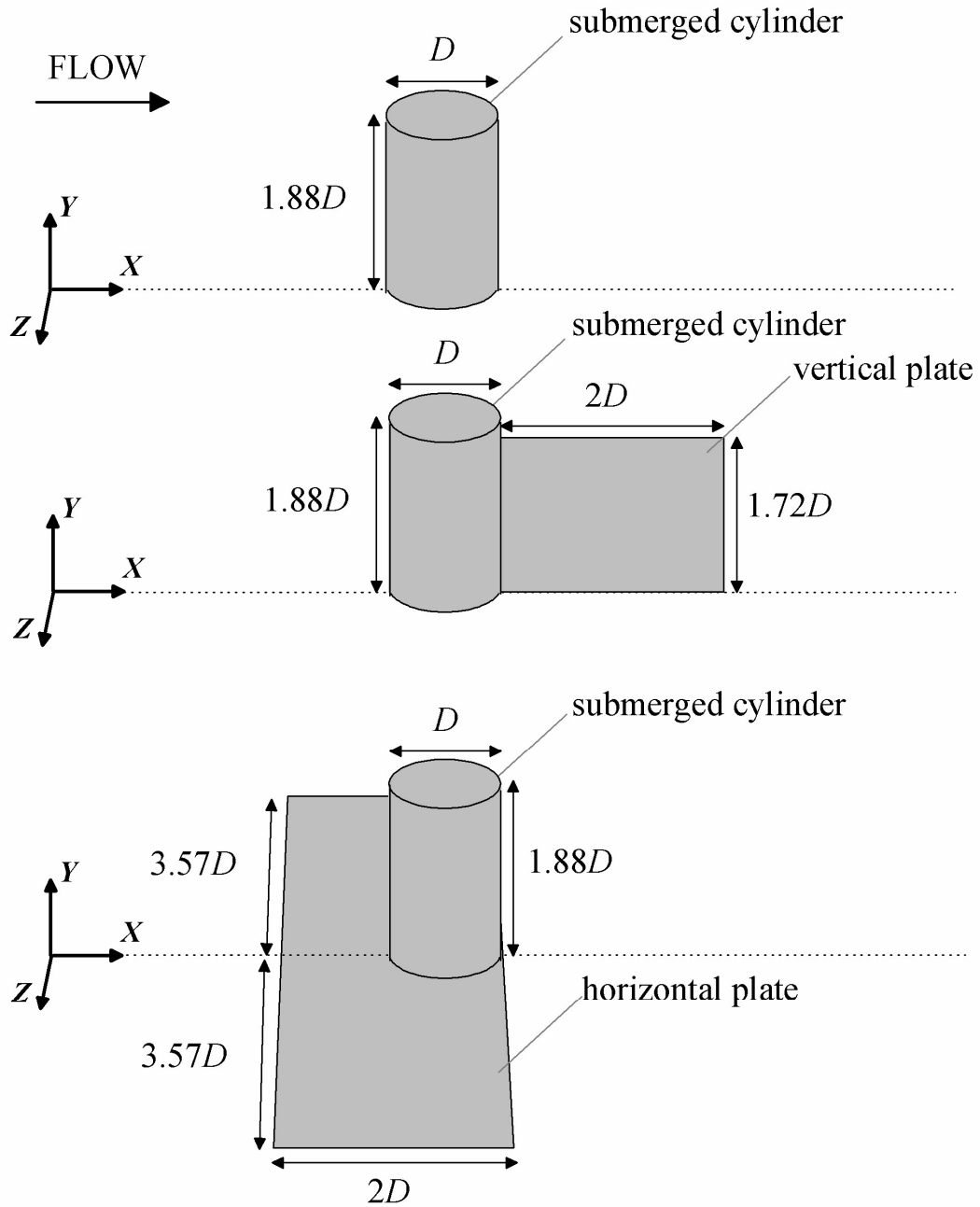


Figure 5.3: Schematic of submerged cylinder and countermeasure configuration for tests E1 (no countermeasure), E2 (cylinder with vertical plate) and E3 (cylinder with horizontal plate)

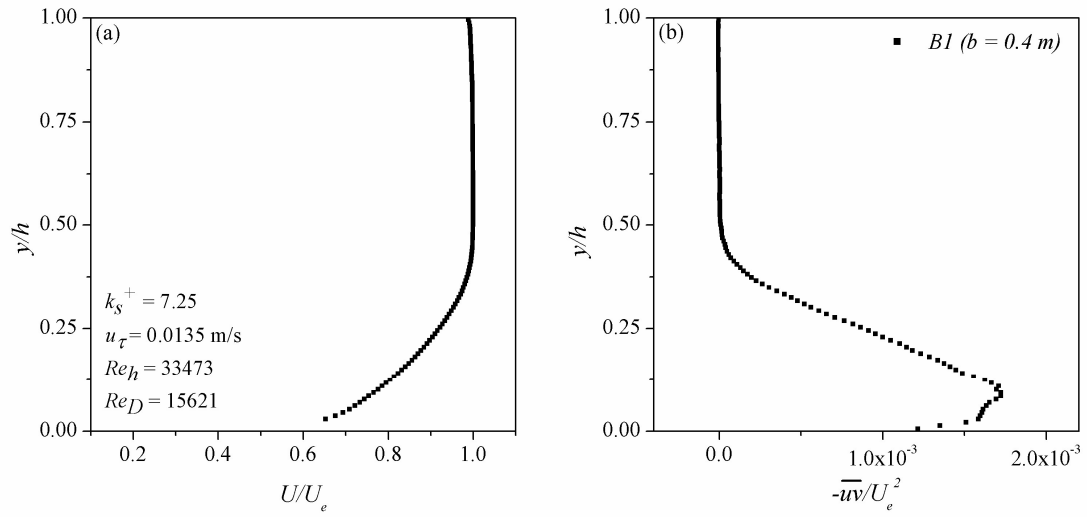


Figure 5.4: Approach flow velocity characteristics used for tests E1, E2 and E3, including (a) mean streamwise velocity and (b) Reynolds shear stress $-\overline{u'v'}/U_e^2$

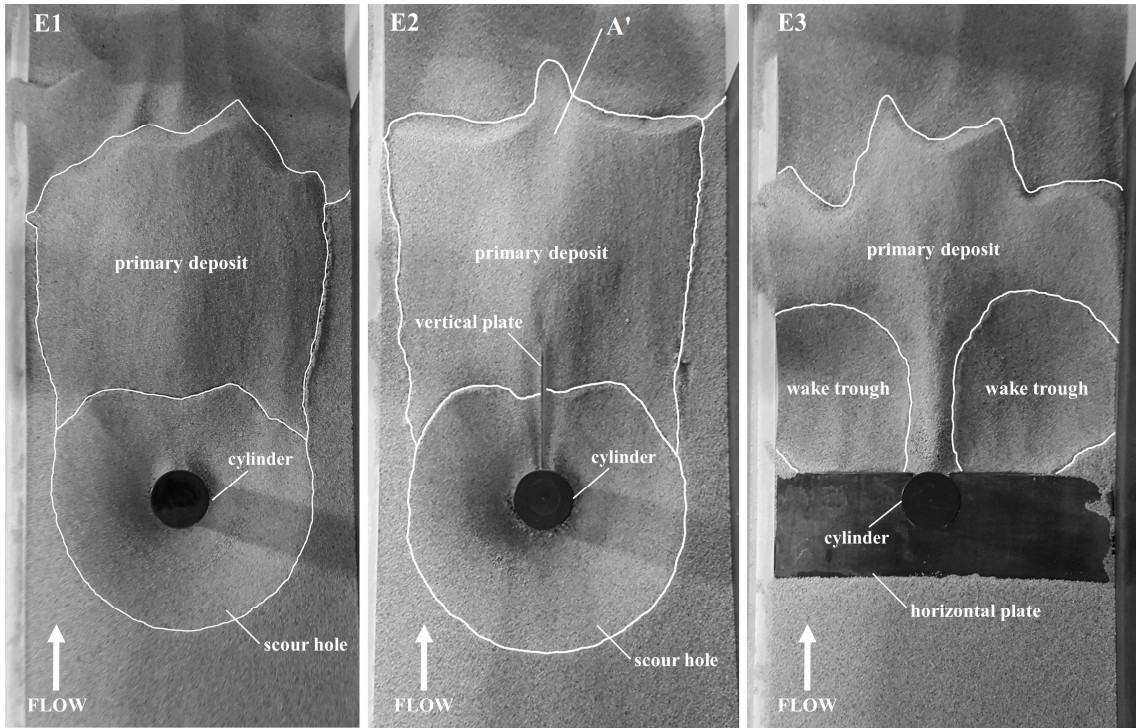


Figure 5.5: Plan-view photographs of tests E1 (submerged cylinder), E2 (submerged cylinder with vertical plate) and E3 (submerged cylinder with horizontal plate)

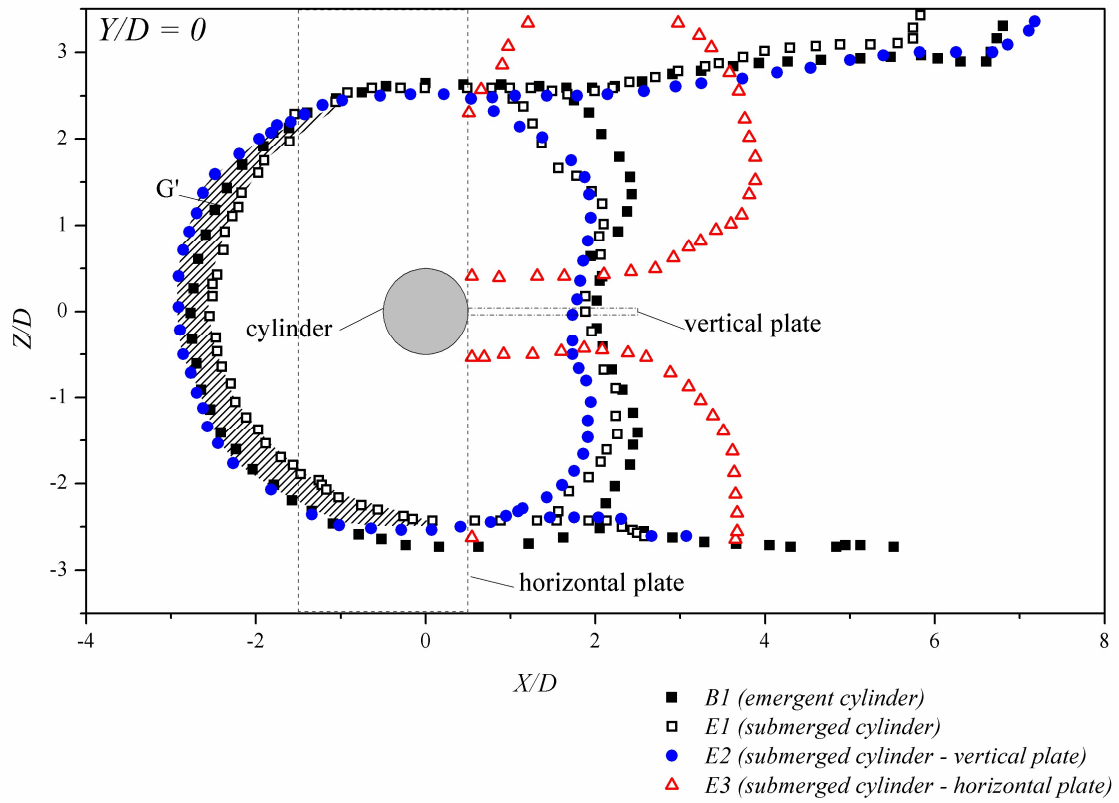


Figure 5.6: Plan view profile measurements of equilibrium scour formation for tests B1, E1, E2 and E3 in XZ plane ($Y/D = 0$)

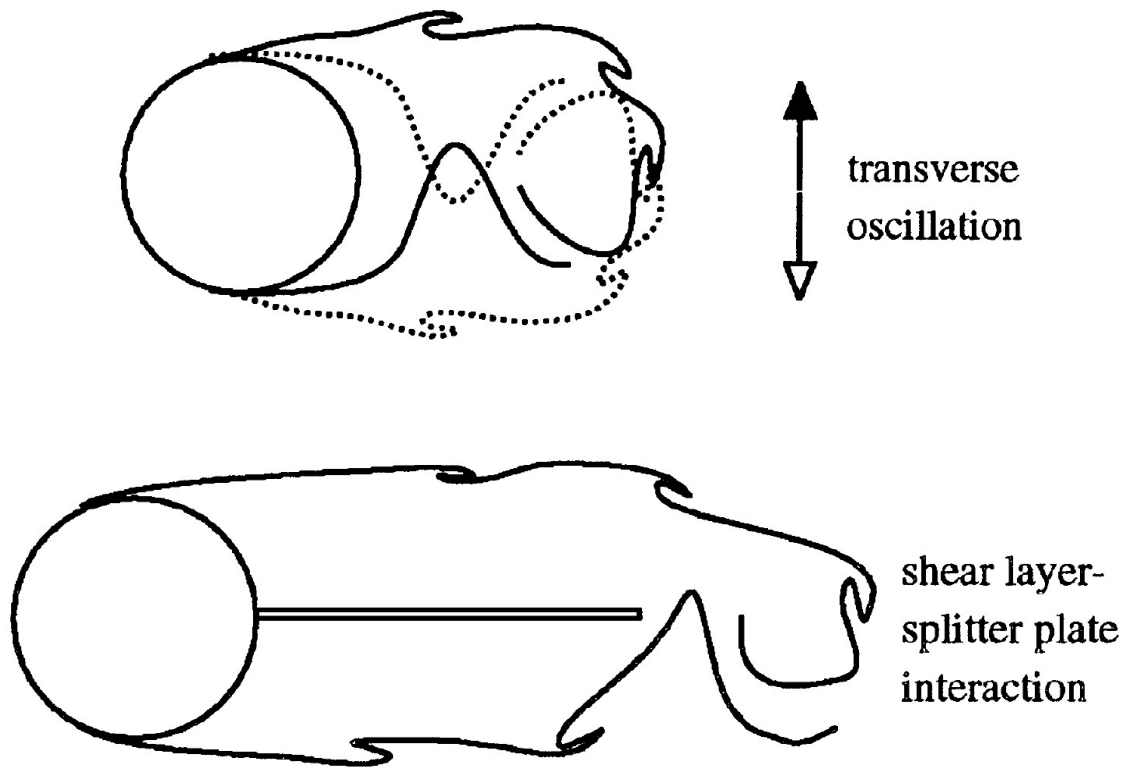


Figure 5.7: Illustration of shear layer interaction in the wake of a circular cylinder without a splitter plate (above) and with a splitter plate of length greater than $1.5D$ (below) (from Anderson and Szewczyk 1997); figure used with permission from Copyright Clearance Center

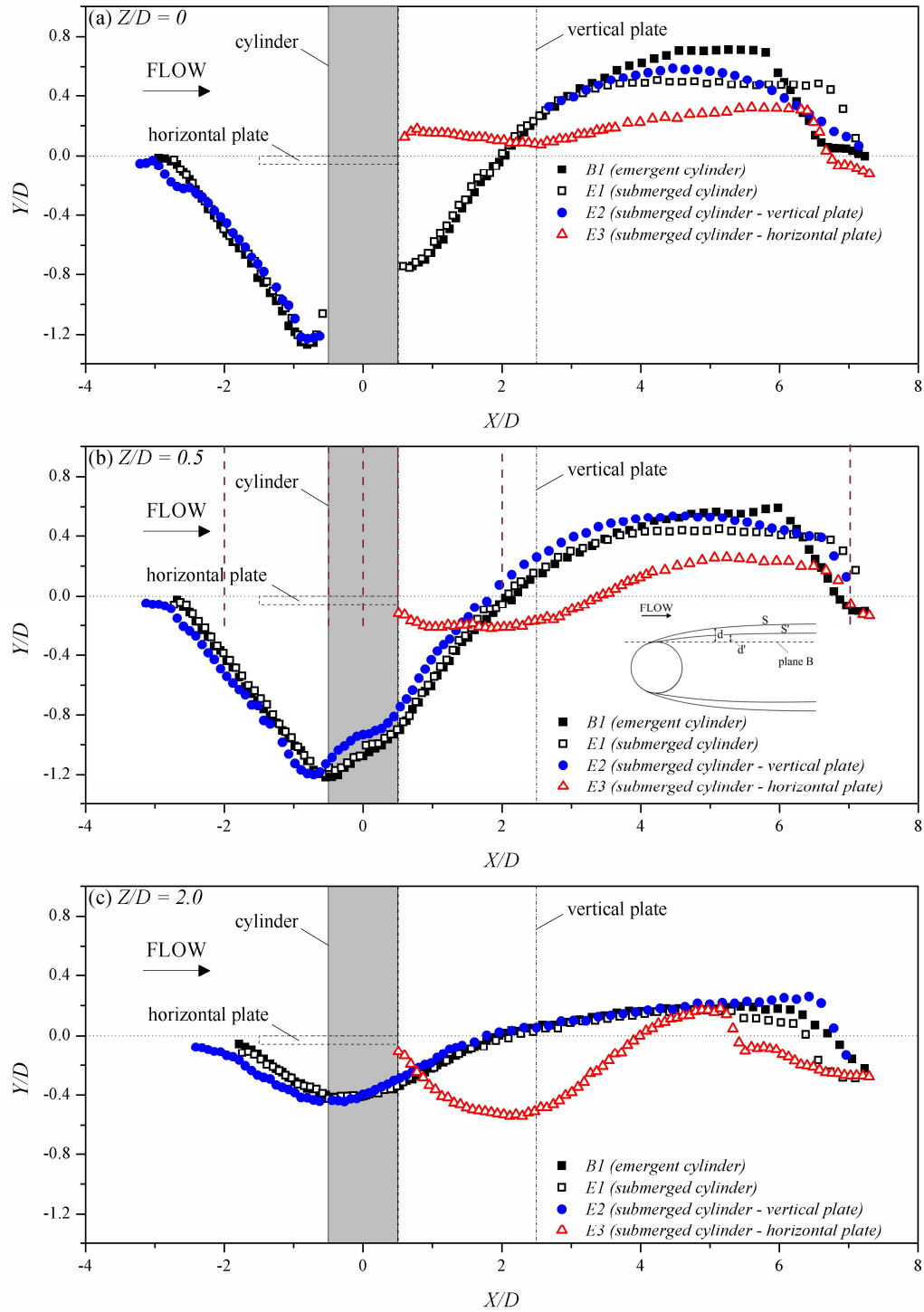


Figure 5.8: Bed profile measurements of equilibrium scour formation for tests B1, E1, E2 and E3 in XY plane along (a) central plane (plane A, $Z/D = 0$), (b) near-cylinder plane (plane B, $Z/D \approx 0.5$) and (c) mid-cylinder-wall plane (plane C, $Z/D = 2.0$)

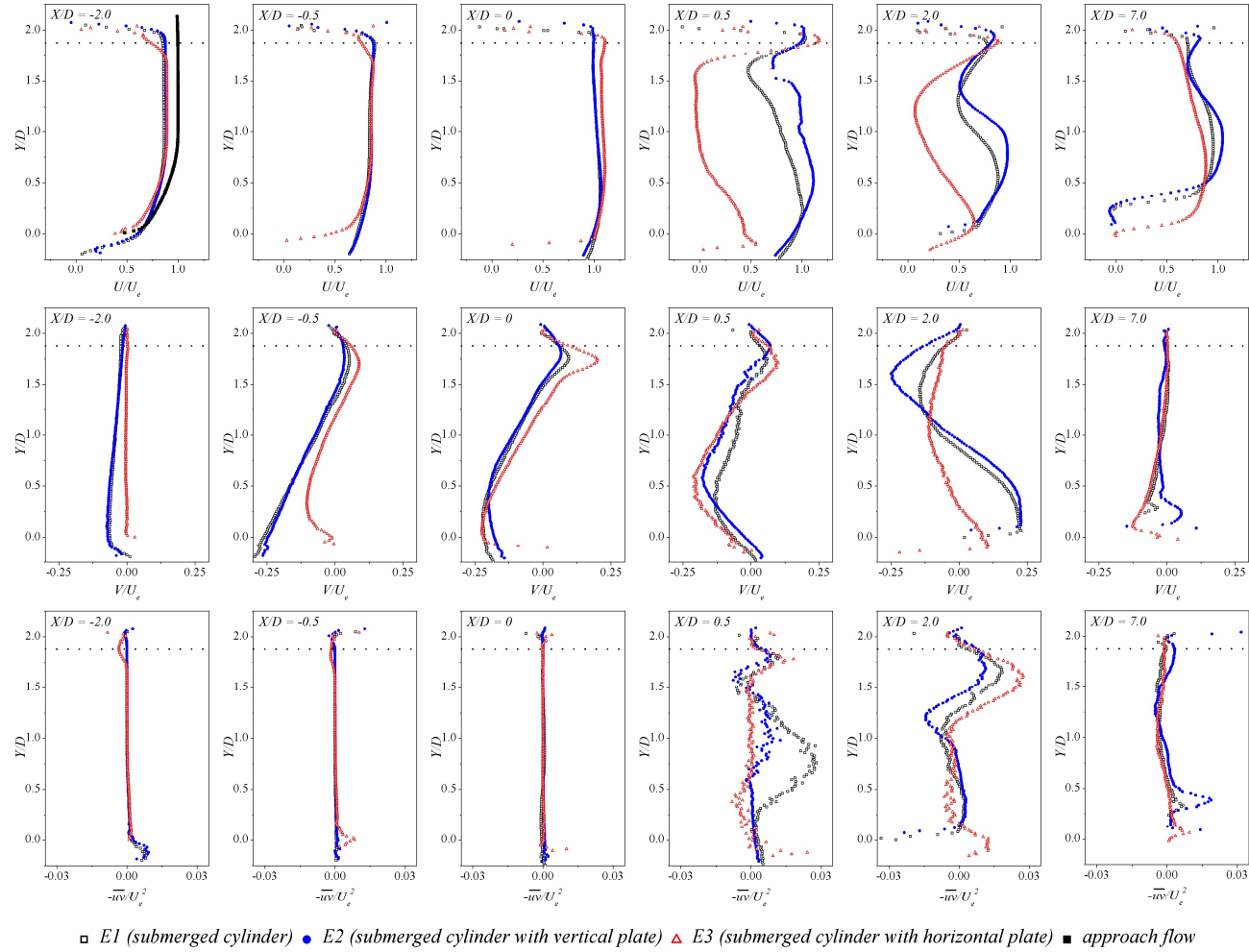


Figure 5.9: Distribution of mean streamwise velocity U/U_e , mean vertical velocity V/U_e and Reynolds shear stress $-\overline{u'v'}/U_e^2$ over the depth of flow in plane B for $X/D = \{-2.0, -0.5, 0, 0.5, 2.0, 7.0\}$

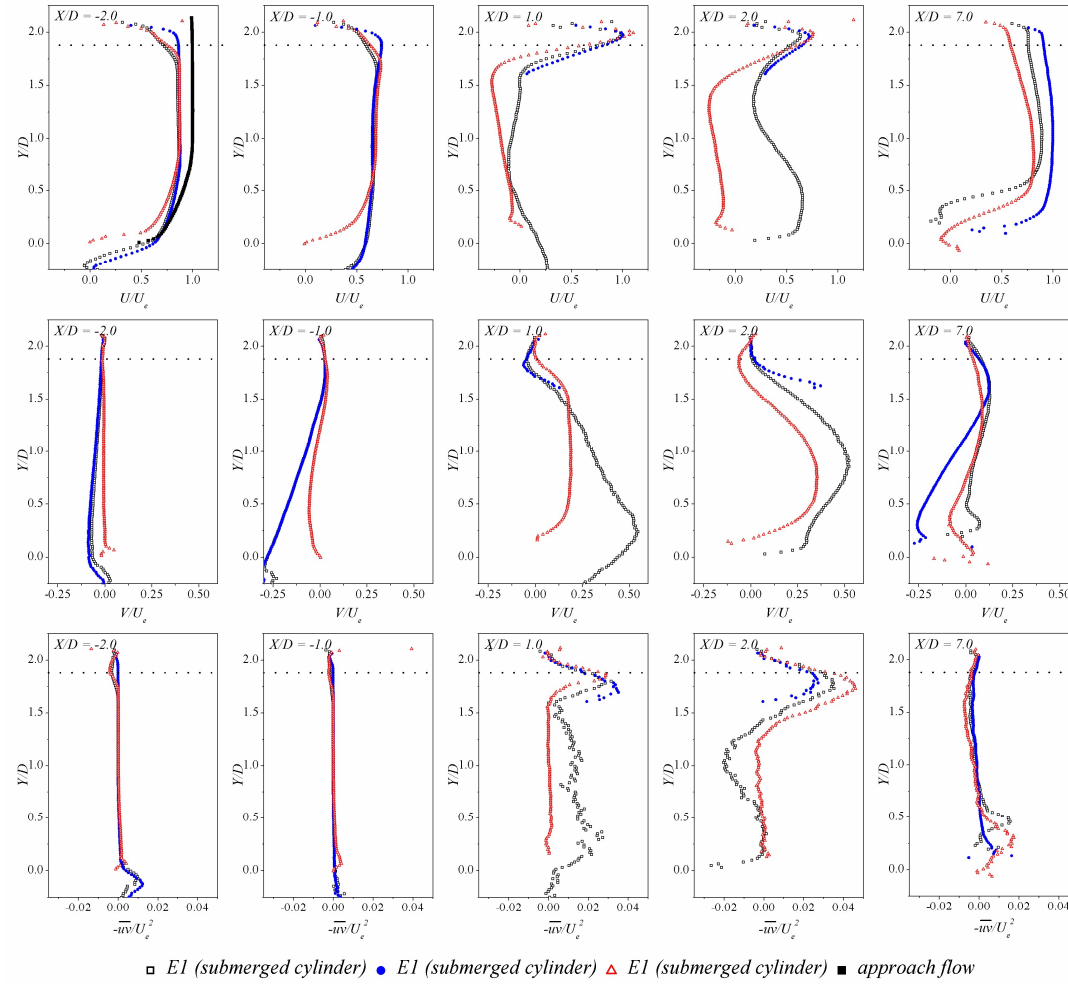


Figure 5.10: Distribution of mean streamwise velocity U/U_e , mean vertical velocity V/U_e and Reynolds shear stress $-\overline{uv}/U_e^2$ over the depth of flow in plane A for $X/D = \{-2.0, -1, 1.0, 2.0, 7.0\}$

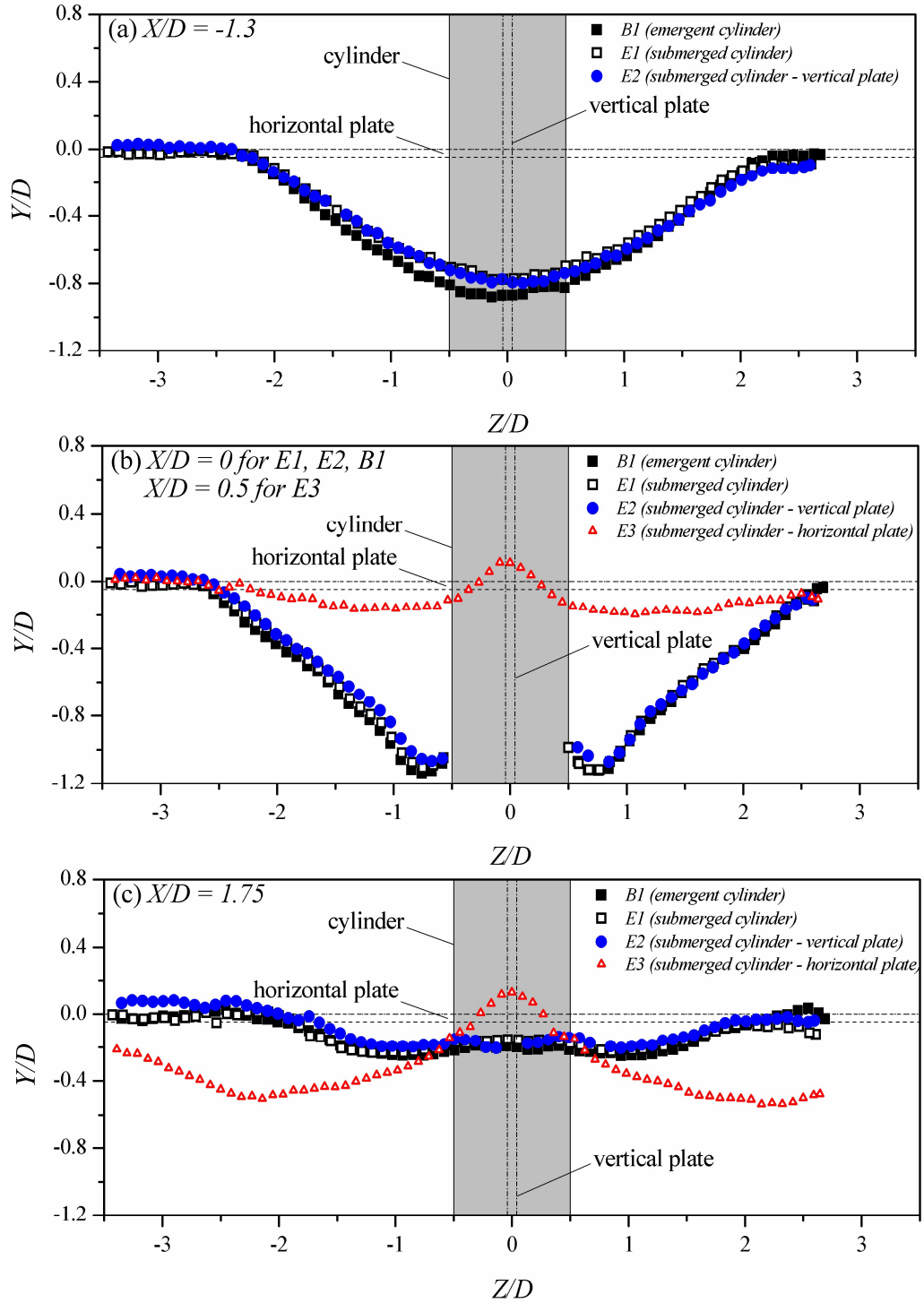


Figure 5.11: Transverse bed profile measurements of equilibrium scour formation for tests B1, E1, E2 and E3 in YZ plane along (a) spanwise upstream plane ($X/D = -1.3$), (b) spanwise central plane ($X/D = 0$ for tests B1, E1 and E2, $X/D = 0.5$ for test E3) and (c) spanwise downstream plane ($X/D = 1.75$)

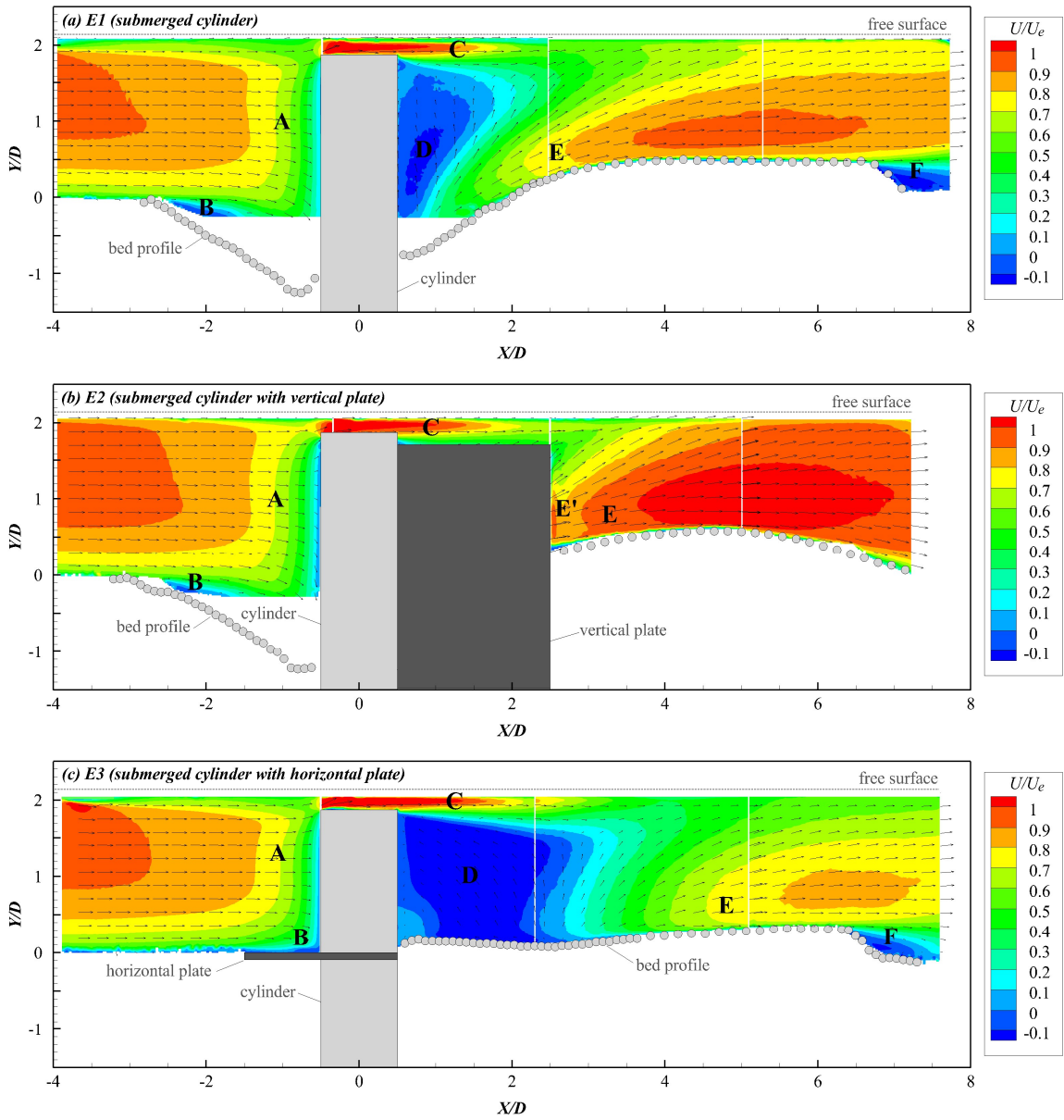


Figure 5.12: Distribution of normalised streamwise velocity U/U_e in the central plane (plane A, $Z/D = 0$) for (a) test E1 (submerged cylinder), (b) test E2 (submerged cylinder with vertical plate) and (c) test E3 (submerged cylinder with horizontal plate)

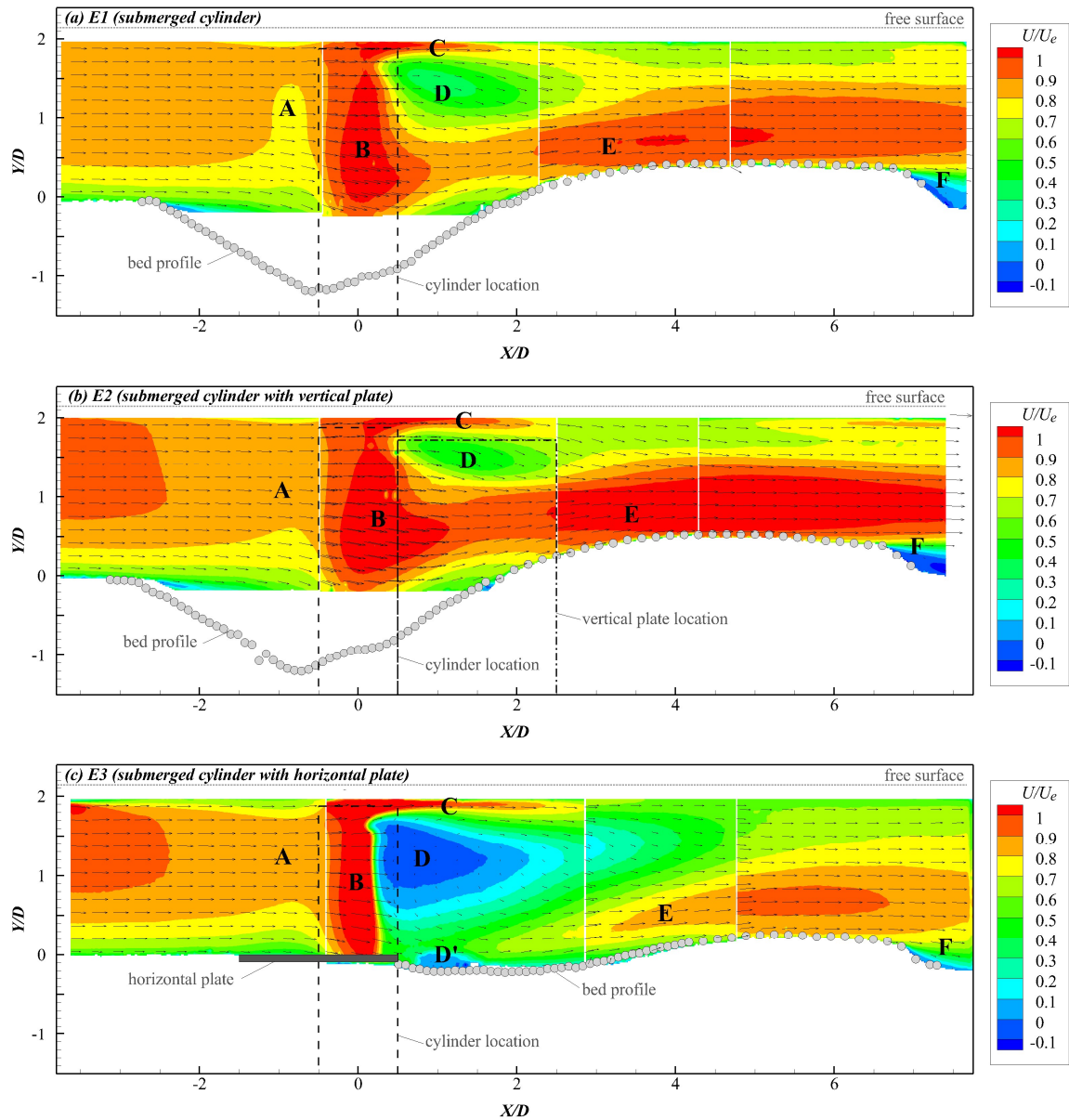


Figure 5.13: Distribution of normalised streamwise velocity U/U_e in the near-cylinder plane (plane B, $Z/D \approx 0.5$) for (a) test E1 (submerged cylinder), (b) test E2 (submerged cylinder with vertical plate) and (c) test E3 (submerged cylinder with horizontal plate)

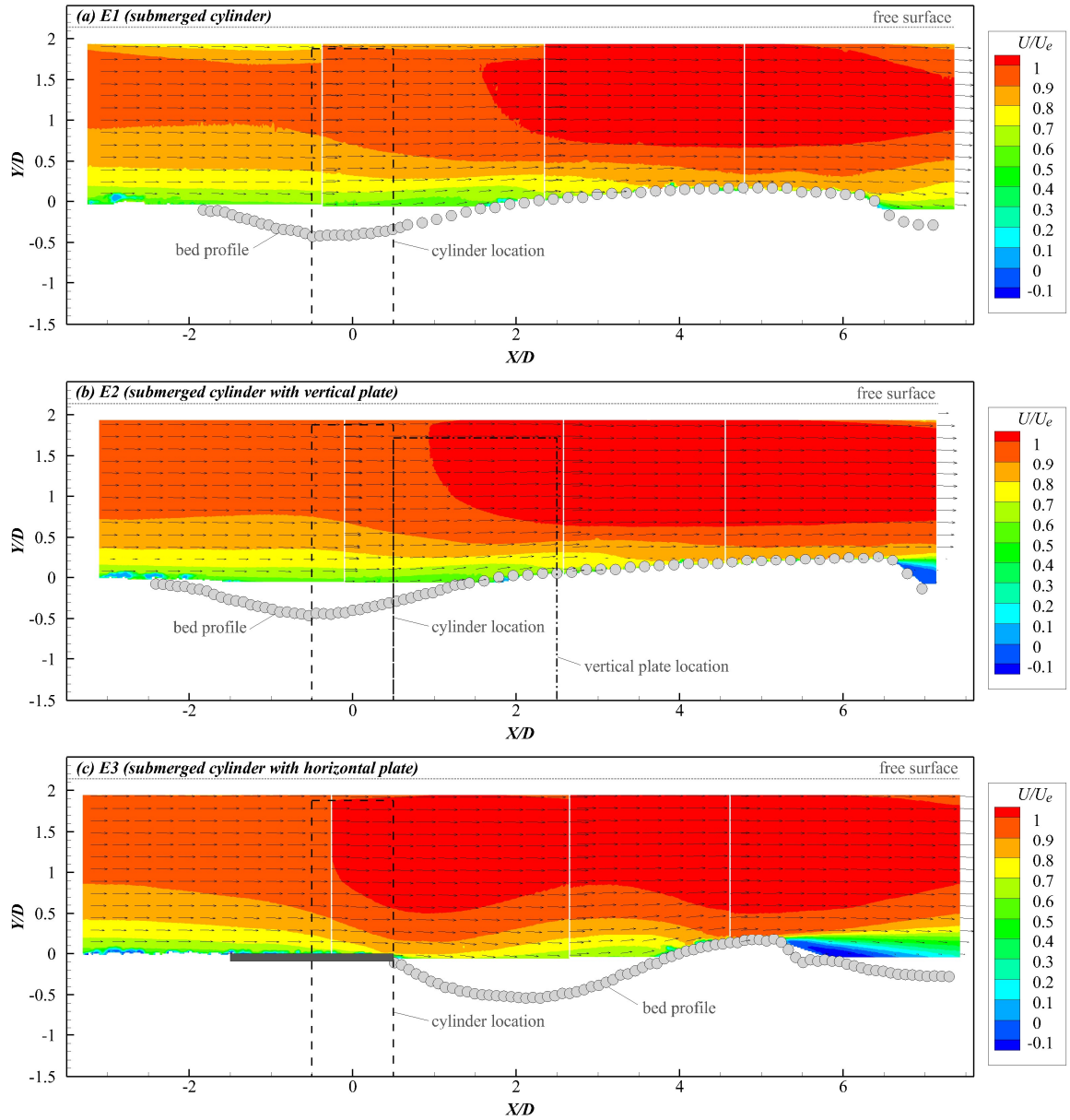


Figure 5.14: Distribution of normalised streamwise velocity U/U_e in the mid-cylinder-wall plane (plane C, $Z/D = 2.0$) for (a) test E1 (submerged cylinder), (b) test E2 (submerged cylinder with vertical plate) and (c) test E3 (submerged cylinder with horizontal plate)

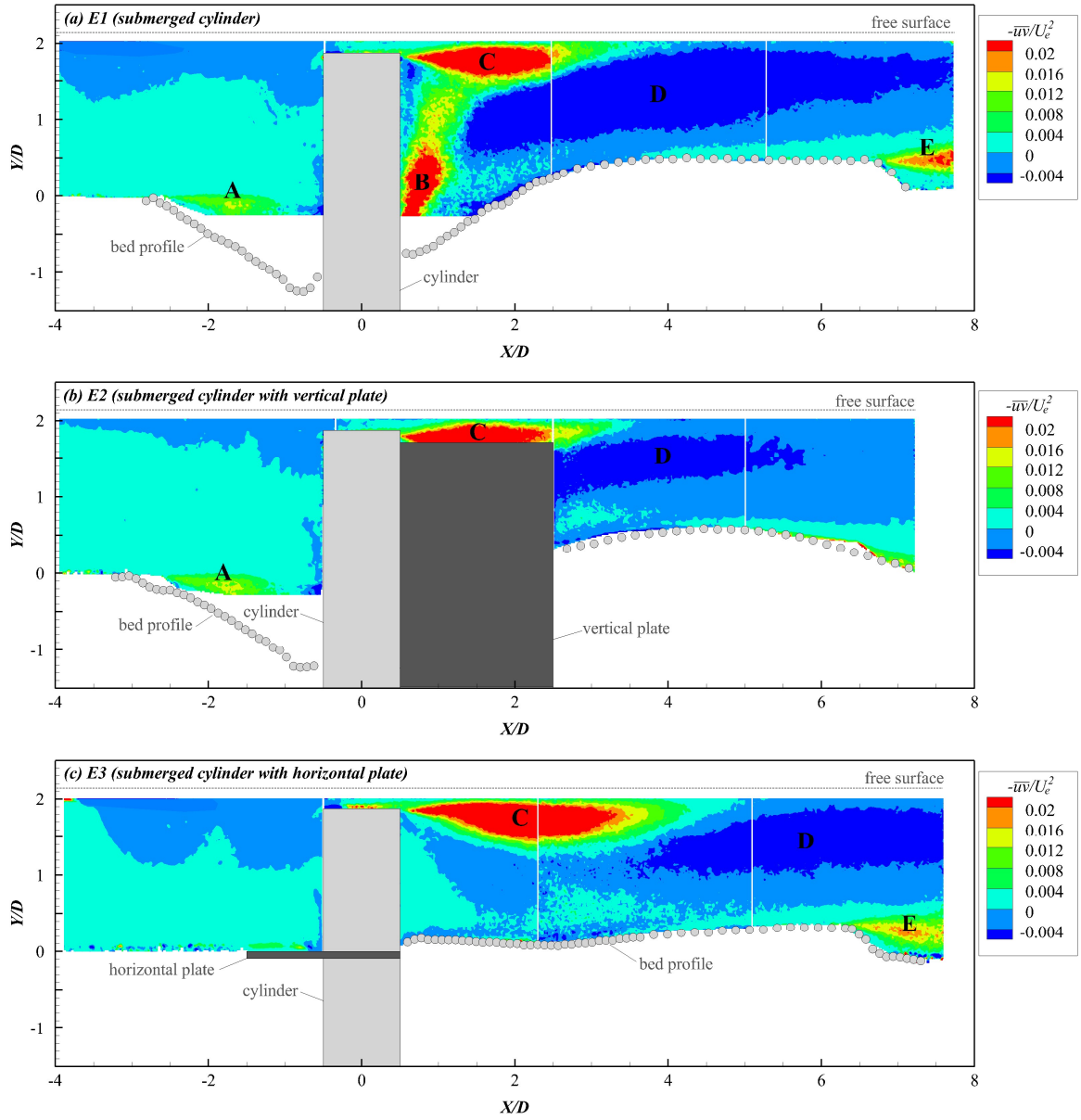


Figure 5.15: Distribution of Reynolds shear stress $-\overline{uv}/U_e^2$ in the central plane (plane A, $Z/D = 0$) for (a) test E1 (submerged cylinder), (b) test E2 (submerged cylinder with vertical plate) and (c) test E3 (submerged cylinder with horizontal plate)

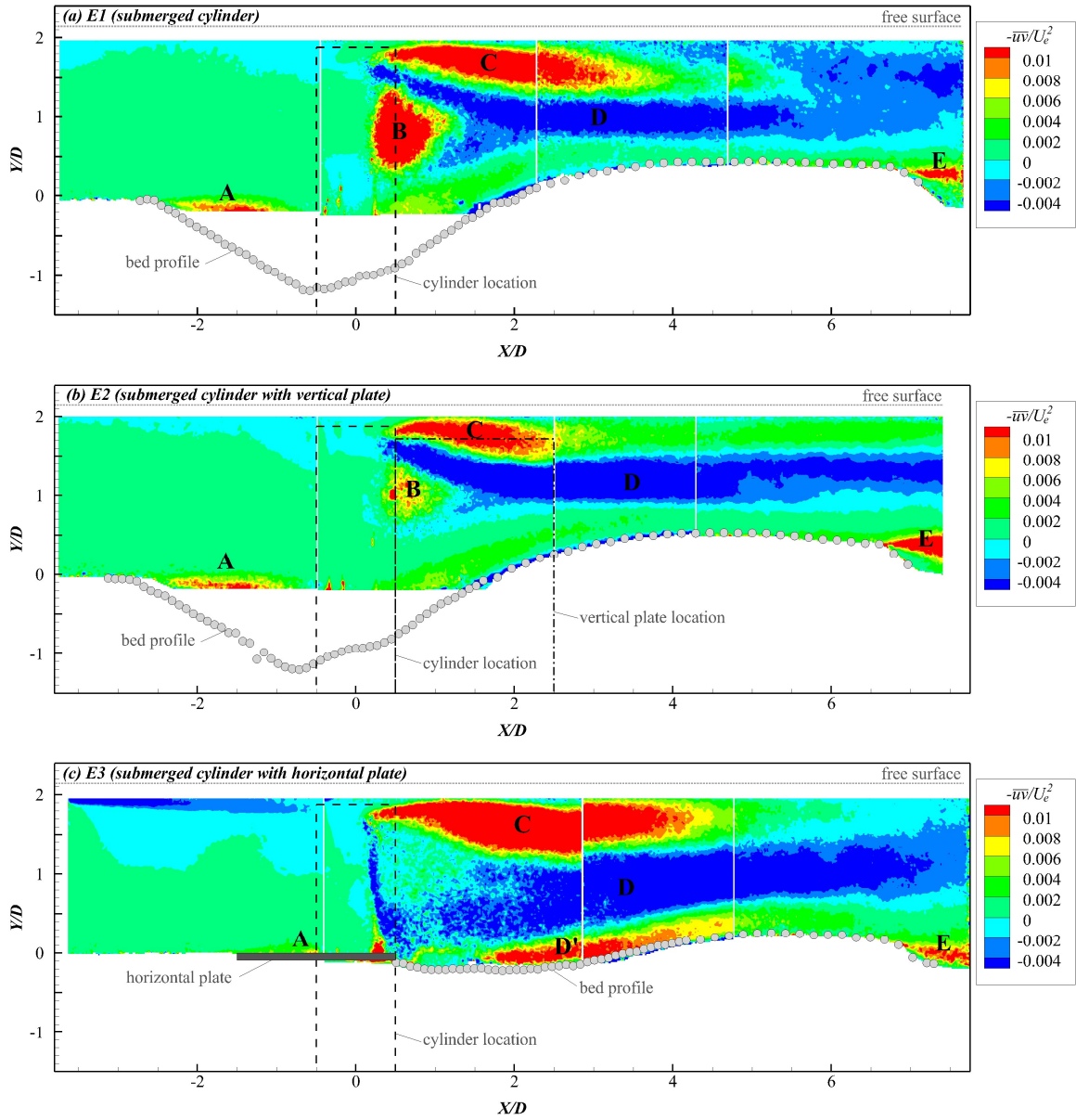


Figure 5.16: Distribution of Reynolds shear stress $-\overline{u'v'}/U_e^2$ in the near-cylinder plane (plane B, $Z/D \approx 0.5$) for (a) test E1 (submerged cylinder), (b) test E2 (submerged cylinder with vertical plate) and (c) test E3 (submerged cylinder with horizontal plate)

5.5 References

1. Anderson, E. A., & Szewczyk, A. A. (1997). Effects of a splitter plate on the near wake of a circular cylinder in 2 and 3-dimensional flow configurations. *Experiments in Fluids*, 23(2), 161–174. <https://doi.org/10.1007/s003480050098>
2. Chiew, Y. (1992). Scour protection at bridge piers. *Journal of Hydraulic Engineering*, 118(9), 1260–1269. [https://doi.org/10.1061/\(ASCE\)0733-9429\(1992\)118:9\(1260\)](https://doi.org/10.1061/(ASCE)0733-9429(1992)118:9(1260))
3. D'Alessandro, C. (2013). *Effect of blockage on cylindrical bridge pier local scour*. M.A.Sc. thesis. University of Windsor, Windsor, Canada.
4. Dey, S., Raikar, R. V., & Roy, A. (2008). Scour at submerged cylindrical obstacles under steady flow. *Journal of Hydraulic Engineering*, 134(1), 105–109. [https://doi.org/10.1061/\(ASCE\)0733-9429\(2008\)134:1\(105\)](https://doi.org/10.1061/(ASCE)0733-9429(2008)134:1(105))
5. Dey, S., Sumer, B. M., & Fredsøe, J. (2006). Control of scour at vertical circular piles under waves and current. *Journal of Hydraulic Engineering*, 132(3), 270–279. [https://doi.org/10.1061/\(ASCE\)0733-9429\(2006\)132:3\(270\)](https://doi.org/10.1061/(ASCE)0733-9429(2006)132:3(270))
6. Ettema, R., Melville, B.W., & Constantinescu, G. (2011). *Evaluation of bridge scour research: Pier scour processes and predictions*. Washington, DC: Transportation Research Board of the National Academies.
7. Gaudio, R., Tafarojnoruz, A., & Calomino, F. (2012). Combined flow-altering countermeasures against bridge pier scour. *Journal of Hydraulic Research*, 50(1), 35–43. <https://doi.org/10.1080/00221686.2011.649548>

8. Gerrard, J. H. (1966). The mechanics of the formation region of vortices behind bluff bodies. *Journal of Fluid Mechanics*, 25(2), 401–413. <https://doi.org/10.1017/S0022112066001721>
9. Graf, W. H., & Istiarto, I. (2002). Flow pattern in the scour hole around a cylinder. *Journal of Hydraulic Research*, 40(1), 13–20. <https://doi.org/10.1080/00221680209499869>
10. Hodi, B. (2009). *Effect of blockage and densimetric Froude number on circular bridge pier local scour*. M.A.Sc. thesis. University of Windsor, Windsor, Canada.
11. Jahangirzadeh, A., Basser, H., Akib, S., Karami, H., Najji, S., & Shamshirband, S. (2014). Experimental and numerical investigation of the effect of different shapes of collars on the reduction of scour around a single bridge pier. *PLOS ONE*, 9(6), e98592. <https://doi.org/10.1371/journal.pone.0098592>
12. Khwairakpam, P., & Mazumdar, A. (2009). Local scour around hydraulic structures. *International Journal of Recent Trends in Engineering*, 1(6), 59–61.
13. Kirkil, G., Constantinescu, G., & Ettema, R. (2008). Coherent structures in the flow field around a circular cylinder with scour hole. *Journal of Hydraulic Engineering*, 134(5), 572–587. [https://doi.org/10.1061/\(ASCE\)0733-9429\(2008\)134:5\(572\)](https://doi.org/10.1061/(ASCE)0733-9429(2008)134:5(572))
14. Kirkil, G., Constantinescu, G., & Ettema, R. (2009). Detached Eddy Simulation investigation of turbulence at a circular pier with scour hole. *Journal of Hydraulic Engineering*, 135(11), 888–901. [https://doi.org/10.1061/\(ASCE\)HY.1943-7900.0000101](https://doi.org/10.1061/(ASCE)HY.1943-7900.0000101)

15. Kumar, V., Raju, K. G. R., & Vittal, N. (1999). Reduction of local scour around bridge piers using slots and collars. *Journal of Hydraulic Engineering*, 125(12), 1302–1305. [https://doi.org/10.1061/\(ASCE\)0733-9429\(1999\)125:12\(1302\)](https://doi.org/10.1061/(ASCE)0733-9429(1999)125:12(1302))
16. Lachaussée, F., Bertho, Y., Morize, C., Sauret, A., & Gondret, P. (2018). Competitive dynamics of two erosion patterns around a cylinder. *Physical Review Fluids*, 3(1), 012302. <https://doi.org/10.1103/PhysRevFluids.3.012302>
17. Lee, S. O., & Sturm, T. W. (2009). Effect of sediment size scaling on physical modeling of bridge pier scour. *Journal of Hydraulic Engineering*, 135(10), 793–802. [https://doi.org/10.1061/\(ASCE\)HY.1943-7900.0000091](https://doi.org/10.1061/(ASCE)HY.1943-7900.0000091)
18. Moncada-M, A. T., Aguirre-Pe, J., Bolívar, J. C., & Flores, E. J. (2009). Scour protection of circular bridge piers with collars and slots. *Journal of Hydraulic Research*, 47(1), 119–126. <https://doi.org/10.3826/jhr.2009.3244>
19. Lagasse, P. F., Clopper, P. E., Zevenbergen, L. W., & Girard, L. G. (2007). Countermeasures to Protect Bridge Piers from Scour. *National Cooperative Highway Research Program (NCHRP) Rep. No. 593*. Washington, DC: Transportation Research Board
20. Nezu, I., & Nakagawa, H. (1993). *Turbulence in Open-Channel Flows*, IAHR monograph series. AA Balkema, Rotterdam, 1–281.
21. Parker, G., Toro-Escobar, C., & Voigt, R. L. J. (1998). *Countermeasures to Protect Bridge Piers from Scour* [Report]. Retrieved from St. Anthony Falls Laboratory
22. Roshko, A. (1954). *On the drag and shedding frequency of two-dimensional bluff bodies*.

23. Tafarojnoruz, A., Gaudio, R., & Dey, S. (2010). Flow-altering countermeasures against scour at bridge piers: a review. *Journal of Hydraulic Research*, 48(4), 441–452. <https://doi.org/10.1080/00221686.2010.491645>
24. Tafarojnoruz, A., Gaudio, R., & Calomino, F. (2012). Evaluation of flow-altering countermeasures against bridge pier scour. *Journal of Hydraulic Engineering*, 138(3), 297–305. [https://doi.org/10.1061/\(ASCE\)HY.1943-7900.0000512](https://doi.org/10.1061/(ASCE)HY.1943-7900.0000512)
25. Tejada, S. (2014). *Effects of blockage and relative coarseness on clear water bridge pier scour*. M.A.Sc. thesis. University of Windsor, Windsor, Canada.
26. Williams, P., Bolisetti, T., & Balachandar, R. (2018). Blockage correction for pier scour experiments. *Canadian Journal of Civil Engineering*, 45(5), 413–417. <https://doi.org/10.1139/cjce-2017-0563>
27. Williams, P. (2014). *Scale effects on design estimation of scour depths at piers*. M.A.Sc. thesis. University of Windsor, Windsor, Canada.
28. Wu, P., Balachandar, R., & Ramamurthy, A. (2018). Effects of splitter plate on reducing local scour around bridge pier. *River Research and Applications*, 34(10), 1338–1346. <https://doi.org/10.1002/rra.3363>
29. Zarrati, A. R., Nazariha, M., & Mashahir, M. B. (2006). Reduction of local scour in the vicinity of bridge pier groups using collars and riprap. *Journal of Hydraulic Engineering*, 132(2), 154–162. [https://doi.org/10.1061/\(ASCE\)0733-9429\(2006\)132:2\(154\)](https://doi.org/10.1061/(ASCE)0733-9429(2006)132:2(154))
30. Zhao, M., Cheng, L., & Zang, Z. (2010). Experimental and numerical investigation of local scour around a submerged vertical circular cylinder in steady currents.

Coastal Engineering, 57(8), 709–721.

<https://doi.org/10.1016/j.coastaleng.2010.03.002>

6 CONCLUSIONS AND RECOMMENDATIONS

The present investigation has employed the use of planar Particle Image Velocimetry (PIV) measurements for characterization of flow in hydraulic modelling. It has been established that detailed flow field measurements of this type are required in order to gain an understanding of specific influences in open-channel flow and flow around a circular cylinder in an erodible bed. Deficiencies in local scour modelling have been established by analysis of scour data in literature; however, the role of some parameters remains unclear without a description of changes to flow field mechanisms. In particular, the effect of channel blockage ratio (D/b) on local scour has been neglected. In order to isolate the influence of D/b in flume experiments, channel width b is typically altered through the use of movable sidewalls. However, in altering channel width b , the channel aspect ratio AR (b/h , where h is the flow depth) was also affected. Therefore, the effect of AR on the approach flow conditions was explored in **Chapter 3** prior to local scour experimentation. In **Chapter 4**, the effect of D/b on local scour around an emergent circular cylinder has been presented. In **Chapter 5**, the efficacy of a vertical splitter plate and horizontal base plate on local scour around a submerged circular cylinder under controlled approach flow conditions has been investigated. Detailed conclusions of **Chapter 3**, **Chapter 4** and **Chapter 5** are located therein. The findings of each chapter are summarized below, along with recommendations for future work.

In **Chapter 3**, the role of aspect ratio ($AR = b/h$) on flow characteristics over a transitionally rough porous bed was characterized. PIV measurements were acquired in the centre of the channel for AR values in the range of 1.90 to 10.2. The distribution of flow properties including mean streamwise velocity, streamwise and vertical turbulence

intensities, third-order turbulent moments and quadrant analysis was analyzed. The following conclusions were drawn from this work:

1. The distribution of the streamwise and vertical turbulence intensities cannot be described by the value of AR alone; rather, analysis of the distribution of u_{rms}/u_τ and v_{rms}/u_τ has indicated that changes in vertical confinement (changing h) and horizontal confinement (changing b) have distinct influences. While the velocity deficit profiles were shown to be similar for all AR, the magnitude of u_{rms}/u_τ and v_{rms}/u_τ decreased with increasing vertical confinement (in addition, the percent difference due to increasing vertical confinement decreased with decreasing horizontal confinement and the percentage of the boundary layer over which the difference was seen increased with decreasing horizontal confinement).
2. The third-order turbulent moments $\overline{u^3}$, $\overline{v^3}$, $\overline{u^2v}$ and $\overline{uv^2}$ decreased in the boundary layer (in addition, the percent of the boundary layer over which difference occurred increased with decreasing horizontal confinement).
3. The magnitude of the contributions from Q1 and Q3 to the Reynolds shear stress increased with increasing vertical confinement and Q2 and Q4 decreased with increasing vertical confinement (in addition, the percent difference due to increasing vertical confinement increased with decreasing horizontal confinement).
4. In general, the drag increment due to roughness decreased with increasing horizontal confinement.

The findings of **Chapter 3** have indicated that careful consideration of approach flow conditions is required for hydraulic modelling. Changes in b and h have been shown to have an appreciable effect on the distribution of flow properties, and controllability of

conditions is required for future work. Flow measurements in the cross-stream direction would be useful in relating the conclusions of the present investigation to the structure of secondary flow cells across the channel.

In **Chapter 4**, PIV results were analyzed for the flow field around an emergent cylinder with channel blockage ratio D/b of 0.05, 0.07 and 0.14. Distribution of the mean streamwise velocity, the Reynolds shear stress and spanwise vorticity were presented for three streamwise-vertical planes (in the centre of the channel, close to the side of the cylinder and between the cylinder and the wall). The effect of sidewall proximity on local scour geometry and the flow field surrounding the cylinder at an equilibrium condition were explored and the findings are as follows:

1. Sidewall proximity was found to influence the equilibrium scour formation, including the size of the scour hole and shape of the dune downstream of the cylinder. Comparison of bed profiles indicated that the primary deposit became increasingly narrow as D/b increased due to confinement of the wake.
2. The size and the shape of the dune were influenced by confinement of the wake, and since the flow was both subcritical and shallow, changes in the bed formation resulted in changes in the flow upstream of the cylinder; in effect, the streamwise velocity increased with decreasing D/b , corresponding to an increase in scour depth upstream of the cylinder for decreasing D/b .
3. The magnitude of the Reynolds shear stress was found to increase with increasing D/b . This was in agreement with the analysis of approach flow conditions in **Chapter 3**, in which it was determined that $-\overline{uv}/U_e^2$ increased in the boundary layer as

channel width b increased. Examination of the distribution of spanwise vorticity Ω indicated that increasing D/b also enhanced vorticity.

The conclusions of **Chapter 4** are indicative of the complicated effect of D/b on local scour mechanisms. The analysis has indicated that use of a correction factor for scour data acquired under high values of blockage ratio is unlikely to be sufficient. Further experimentation should be carried out under highly controlled conditions in which channel blockage is as minimal as possible. The influence of changes in the approach flow conditions should also be carefully considered. Experimental methods under which local scour data is conducted require significant improvement for development of useful scour prediction methods and design of scour countermeasures through modelling.

In **Chapter 5**, changes in the flow field surrounding a submerged cylinder under local scour conditions due to installation of two countermeasures were reported. A vertical splitter plate and a horizontal base plate (i.e. a rectangular collar) were the two flow-altering devices considered in this investigation. The efficacy of both methods on scour depth reduction was analyzed, and the mechanisms by which each countermeasure altered the flow surrounding the cylinder was explored by comparison with a control case (i.e. scour around a submerged cylinder with no flow-altering attachment). PIV measurements were carried out in three vertical planes and the distribution of the streamwise velocity and Reynolds shear stress were presented.

1. The splitter plate was found to decrease the frequency of vortex shedding by disruption of the interaction between the shear layers emanating from either side of the cylinder in the wake region. The width of the wake was also reduced by the

splitter plate, and both influences resulted in a slight increase in the size of the scour hole upstream of the cylinder.

2. The streamwise velocity downstream of the plate showed an increase due to acceleration along the sides of the plate. The Reynolds shear stress was reduced in the plane close to the cylinder. However, the scour formation at an equilibrium condition did not show significant changes due to the splitter plate, which was in agreement with literature.
3. The horizontal base plate (rectangular collar) eliminated scour entirely upstream of the cylinder, which was in agreement with literature. The bed shear stress at the surface of the horizontal plate near the sides of the cylinder was shown to exceed the critical bed shear stress of the erodible sediment by a factor between 2.5 and 3, demonstrating the importance of bed protection at this location.
4. The flow field in the wake of the cylinder was significantly altered from the control case. The mean streamwise velocity and Reynolds shear stress were greatly reduced by the presence of the horizontal plate, and the depth of scour was also minimized in the wake region (particularly in the central plane).

The findings of **Chapter 5** have provided background for development of effective scour countermeasures. Reduction of the bed shear stress at the sides of the cylinder (or scour protection at this location) appears to be imperative for optimization of scour depth reduction in the vicinity of the cylinder. Minimization of the streamwise velocity and Reynolds shear stress in the wake of the cylinder also appear to be desirable characteristics of efficient scour mitigation. Finally, the flow field in the plane midway between the cylinder and the wall was largely unchanged by either countermeasure. This implies that

the width of the horizontal plate could likely be reduced without affecting its performance as a countermeasure. Further experimentation on plate width should be carried out in order to determine an optimal rectangular collar design for use in practice.

APPENDICES

Appendix A: Figure permissions

Re: Figure use permissions for J.H.Eng. publication

PERMISSIONS <permissions@asce.org>

Thu, Aug 1, 2019 at 10:47 AM

To: Priscilla Williams <[REDACTED]>

Dear Priscilla,

Thank you for your inquiry. You have permission to reuse figure 7, from Large scale clear-water local pier scour experiments. *Journal of Hydraulic Engineering* (2004) in your thesis provided this figure in total does not account for more than **25% of the new work**.

A full credit line must be added to the material being reprinted. For reuse in non-ASCE publications, add the words "With permission from ASCE" to your source citation. For Intranet posting, add the following additional notice: "This material may be downloaded for personal use only. Any other use requires prior permission of the American Society of Civil Engineers. This material may be found at [https://doi.org/10.1061/(ASCE)0733-9429(2004)130:10(957)]."

Each license is unique, covering only the terms and conditions specified in it. Even if you have obtained a license for certain ASCE copyrighted content, you will need to obtain another license if you plan to reuse that content outside the terms of the existing license. For example: If you already have a license to reuse a figure in a journal, you still need a new license to use the same figure in a magazine. You need a separate license for each edition.

Sincerely,

Leslie Connelly

Senior Marketing Coordinator

American Society of Civil Engineers

1801 Alexander Bell Drive

Reston, VA 20191

PERMISSIONS@asce.org

703-295-6169

Internet: www.asce.org/pubs | www.ascelibrary.org | <http://ascelibrary.org/page/rightsrequests>

Re: Figure use permissions for Wiley Journal publication

Wiley Global Permissions <permissions@wiley.com>
To: Priscilla Williams <[REDACTED]>

Mon, Aug 19, 2019 at 7:19 AM

Dear Priscilla,

Thank you for your email.

Permission is granted for you to use the material requested for your thesis/dissertation subject to the usual acknowledgements (author, title of material, title of book/journal, ourselves as publisher) and on the understanding that you will reapply for permission if you wish to distribute or publish your thesis/dissertation commercially.

You should also duplicate the copyright notice that appears in the Wiley publication in your use of the Material. Permission is granted solely for use in conjunction with the thesis, and the material may not be posted online separately.

Any third-party material is expressly excluded from this permission. If any material appears within the article with credit to another source, authorisation from that source must be obtained.

Should you require any further information, please do not hesitate to contact me.

Kind regards,

Paisley Chesters
Permissions Co-Ordinator

Wiley

The Atrium

Southern Gate

Chichester

West Sussex

PO19 8SQ
www.wiley.com

WILEY

John Wiley & Sons Limited is a private limited company registered in England with registered number 641132. Registered office address: The Atrium, Southern Gate, Chichester, West Sussex, United Kingdom. PO19 8SQ

From: Priscilla Williams <[REDACTED]>
Sent: 17 August 2019 14:00
To: Wiley Global Permissions <permissions@wiley.com>
Subject: Re: Figure use permissions for Wiley Journal publication

Hello,

My name is Priscilla Williams and I am a PhD candidate at the University of Windsor in Ontario, Canada. I am writing to look into acquiring permission to include a figure from a Wiley Journal paper in my dissertation. The publication reference is:

Wu, P., Balachandar, R., & Ramamurthy, A. (2018). Effects of splitter plate on reducing local scour around bridge pier. *River research and applications*, 34(10), 1338-1346.

I would like to include Figure 1 (which will be, of course, properly referenced) from this paper in my dissertation.

Please let me know if there is any additional information required.

I look forward to hearing from you at your convenience.

Regards,

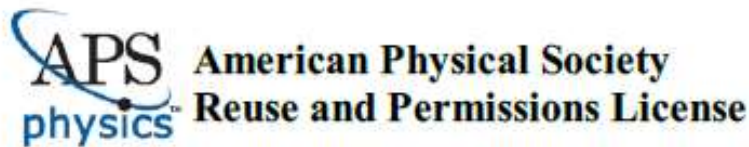
—

Priscilla Williams, Ph.D candidate, E.I.T.

CEI 1113/3184

Department of Civil and Environmental Engineering

University of Windsor



31-Aug-2019

This license agreement between the American Physical Society ("APS") and Priscilla Williams ("You") consists of your license details and the terms and conditions provided by the American Physical Society and SciPris.

Licensed Content Information

License Number: RNP/19/AUG/018293
License date: 31-Aug-2019
DOI: 10.1103/PhysRevFluids.3.012302
Title: Competitive dynamics of two erosion patterns around a cylinder
Author: F. Lachaussée et al.
Publication: Physical Review Fluids
Publisher: American Physical Society
Cost: USD \$ 0.00

Request Details

Does your reuse require significant modifications: No
Specify intended distribution locations: Worldwide
Reuse Category: Reuse in a thesis/dissertation
Requestor Type: Student
Items for Reuse: Figures/Tables
Number of Figure/Tables: 1
Figure/Tables Details: Figure 2
Format for Reuse: Electronic and Print
Total number of print copies: Up to 1000

Information about New Publication:

University/Publisher: University of Windsor
Title of dissertation/thesis: Characterizing the role of approach flow and blockage on local scour around circular cylinders with and without countermeasures
Author(s): Priscilla D. Williams
Expected completion date: Oct. 2019

License Requestor Information

Name: Priscilla Williams
Affiliation: Individual
Email Id: [REDACTED]
Country: Canada

TERMS AND CONDITIONS

The American Physical Society (APS) is pleased to grant the Requestor of this license a non-exclusive, non-transferable permission, limited to Electronic and Print format, provided all criteria outlined below are followed.

1. You must also obtain permission from at least one of the lead authors for each separate work, if you haven't done so already. The author's name and affiliation can be found on the first page of the published Article.
2. For electronic format permissions, Requestor agrees to provide a hyperlink from the reprinted APS material using the source material's DOI on the web page where the work appears. The hyperlink should use the standard DOI resolution URL, [http://dx.doi.org/\(DOI\)](http://dx.doi.org/(DOI)). The hyperlink may be embedded in the copyright credit line.
3. For print format permissions, Requestor agrees to print the required copyright credit line on the first page where the material appears: "Reprinted (abstract/excerpt/figure) with permission from [(FULL REFERENCE CITATION) as follows: Author's Names, APS Journal Title, Volume Number, Page Number and Year of Publication.] Copyright (YEAR) by the American Physical Society."
4. Permission granted in this license is for a one-time use and does not include permission for any future editions, updates, databases, formats or other matters. Permission must be sought for any additional use.
5. Use of the material does not and must not imply any endorsement by APS.
6. APS does not imply, purport or intend to grant permission to reuse materials to which it does not hold copyright. It is the requestor's sole responsibility to ensure the licensed material is original to APS and does not contain the copyright of another entity, and that the copyright notice of the figure, photograph, cover or table does not indicate it was reprinted by APS with permission from another source.
7. The permission granted herein is personal to the Requestor for the use specified and is not transferable or assignable without express written permission of APS. This license may not be amended except in writing by APS.
8. You may not alter, edit or modify the material in any manner.
9. You may translate the materials only when translation rights have been granted.
10. APS is not responsible for any errors or omissions due to translation.
11. You may not use the material for promotional, sales, advertising or marketing purposes.
12. The foregoing license shall not take effect unless and until APS or its agent, Aptara, receives payment in full in accordance with Aptara Billing and Payment Terms and Conditions, which are incorporated herein by reference.
13. Should the terms of this license be violated at any time, APS or Aptara may revoke the license with no refund to you and seek relief to the fullest extent of the laws of the USA. Official written notice will be made using the contact information provided with the permission request. Failure to receive such notice will not nullify revocation of the permission.
14. APS reserves all rights not specifically granted herein.
15. This document, including the Aptara Billing and Payment Terms and Conditions, shall be the entire agreement between the parties relating to the subject matter hereof.

Re: Figure use permissions for Lachaussee et al. (2018)

Philippe Gondret <[REDACTED]>

Thu, Sep 5, 2019 at 2:51 AM

To: Priscilla Williams <[REDACTED]>

Cc: Florent Lachaussee <[REDACTED]>, Yann Bertho <[REDACTED]>, Cyprien Morize <[REDACTED]>, Alban Sauret <[REDACTED]>

Yes you can Priscilla!
And we would be interested to read next your ongoing manuscript and publications
Kind regards
Philippe

Le 3 sept. 2019 à 20:42, Priscilla Williams <williamq@uwindsor.ca> a écrit :

Hi Dr. Gondret,

I hope this e-mail finds you well. My name is Priscilla Williams and I am a Ph.D candidate at the University of Windsor in Windsor, Canada. I am working in the area of local scour and would like to obtain permission to include a figure from one of your publications in my dissertation (properly referenced, of course). I have acquired the proper license for figure reuse from APS, and the agreement requires that permission also be obtained from one of the publication's leading authors. I would like to use Figure 2 from the following publication:

Lachaussee, F., Bertho, Y., Morize, C., Sauret, A. and Gondret, P. (2018). Competitive dynamics of two erosion patterns around a cylinder. *Physical Review Fluids*, 3(1), p.012302.

I look forward to hearing from you at your convenience.

Regards,

--

Priscilla Williams, Ph.D candidate, E.I.T.
CEI 1113/3184
Department of Civil and Environmental Engineering
University of Windsor



Confirmation Number: 11843314
 Order Date: 08/20/2019

Customer Information

Customer: Priscilla Williams
 Account Number: 3001504154
 Organization: University of Windsor
 Email: [REDACTED]
 Phone: [REDACTED]
 Payment Method: Invoice

This is not an invoice

Order Details

Experiments in fluids

Billing Status: N/A

Order detail ID: 71985611
 ISSN: 0723-4864
 Publication Type: Journal
 Volume:
 Issue:
 Start page:
 Publisher: SPRINGER-VERLAG
 Author/Editor: MERZKIRCH, W

Permission Status: **Granted**
 Permission type: Republish or display content
 Type of use: Thesis/Dissertation
 Order License Id: 4653110282269

Requestor type	Academic institution
Format	Print, Electronic
Portion	chart/graph/table/figure
Number of charts/graphs/tables/figures	1
The requesting person/organization	Priscilla Williams
Title or numeric reference of the portion(s)	Figure 11
Title of the article or chapter the portion is from	Effects of a splitter plate on the near wake of a circular cylinder in 2 and 3-dimensional flow configurations
Editor of portion(s)	N/A
Author of portion(s)	Anderson, E.A., Szewczyk, A.A.
Volume of serial or monograph	23
Issue, if republishing an article from a serial	2
Page range of portion	161-174
Publication date of portion	1997-06-01
Rights for	Main product
Duration of use	Current edition and up to 5 years
Creation of copies for the disabled	no

With minor editing privileges	no
For distribution to	Worldwide
In the following language(s)	Original language of publication
With incidental promotional use	no
Lifetime unit quantity of new product	Up to 499
Title	Characterizing the role of approach flow and blockage on local scour around circular cylinders with and without countermeasures
Institution name	University of Windsor
Expected presentation date	Oct 2019

Note: This item was invoiced separately through our [RightsLink service](#). [More info](#)

\$ 0.00

Total order items: 1	Order Total: \$0.00
-----------------------------	----------------------------

[About Us](#) | [Privacy Policy](#) | [Terms & Conditions](#) | [Pay an Invoice](#)

Copyright 2019 Copyright Clearance Center

Appendix B: Bed profile measurements

Chapter	ID	Plane(s) of interest	<i>b</i> (m)	<i>h</i> (m)	<i>U</i> (m/s)	Cylinder type	Feature
4 (effect of blockage ratio)	B1	A, B, C	0.4	0.12	0.262	emergent	-
	B2	A, B, C	0.8	0.12	0.261	emergent	-
	B3	A, B, C	1.22	0.12	0.254	emergent	-
	S1	A	0.4	0.12	0.262	submerged	
	S2	A	0.8	0.12	0.261	submerged	
	S3	A	1.22	0.12	0.254	submerged	
5 (scour counter-measures)	E1	A, B, C	0.4	0.12	0.262	submerged	-
	E2	A, B, C	0.4	0.12	0.262	submerged	vertical plate
	E3	A, B, C	0.4	0.12	0.262	submerged	horizontal plate

Test ID: B1 ($b = 0.4$ m, $h = 0.12$ m, $U = 0.262$ m/s, $D = 0.056$ m, $d_{50} = 0.74$ mm, emergent cylinder)													
Z/D = 0		Z/D = 0.5		Z/D = 2.0		Y/D = 0		X/D = 0		X/D = -1.3		X/D = 1.75	
X/D	Y/D	X/D	Y/D	X/D	Y/D	X/D	Z/D	Z/D	Y/D	Z/D	Y/D	Z/D	Y/D
-2.94643	-0.01607	-2.67857	-0.02500	-1.78571	-0.05536	6.80357	3.30357	2.68750	-0.03571	-3.34821	0.00000	2.68750	-0.02857
-2.85714	-0.01964	-2.58929	-0.07679	-1.69643	-0.07500	6.73214	3.16071	2.63393	-0.04286	-3.25893	0.00893	2.63393	0.00714
-2.76786	-0.03750	-2.50000	-0.11250	-1.60714	-0.09464	6.66071	3.00000	2.54464	-0.07857	-3.16964	0.00357	2.54464	0.03393
-2.67857	-0.05893	-2.41071	-0.17500	-1.51786	-0.12321	6.60714	2.89286	2.45536	-0.12143	-3.08036	0.00357	2.45536	0.02143
-2.58929	-0.11071	-2.32143	-0.23214	-1.42857	-0.15893	6.30357	2.89286	2.36607	-0.19821	-2.99107	0.00179	2.36607	-0.00357
-2.50000	-0.16429	-2.23214	-0.27500	-1.33929	-0.19286	6.03571	2.92857	2.27679	-0.25536	-2.90179	-0.00179	2.27679	-0.01250
-2.41071	-0.23214	-2.14286	-0.34107	-1.25000	-0.22679	5.83929	2.96429	2.18750	-0.29821	-2.81250	0.00357	2.18750	-0.03571
-2.32143	-0.29107	-2.05357	-0.36964	-1.16071	-0.24821	5.48214	2.94643	2.09821	-0.34821	-2.72321	-0.01607	2.09821	-0.04107
-2.23214	-0.35893	-1.96429	-0.44107	-1.07143	-0.28393	5.12500	2.92857	2.00893	-0.40000	-2.63393	-0.00536	2.00893	-0.06429
-2.14286	-0.40357	-1.87500	-0.48393	-0.98214	-0.31250	4.66071	2.91071	1.91964	-0.41250	-2.54464	-0.00893	1.91964	-0.08036
-2.05357	-0.46607	-1.78571	-0.54821	-0.89286	-0.32500	4.26786	2.89286	1.83036	-0.45893	-2.45536	-0.03036	1.83036	-0.08571
-1.96429	-0.52321	-1.69643	-0.61250	-0.80357	-0.35714	3.92857	2.87500	1.74107	-0.50536	-2.36607	-0.02321	1.74107	-0.10000
-1.87500	-0.58036	-1.60714	-0.65893	-0.71429	-0.36250	3.62500	2.83929	1.65179	-0.54286	-2.27679	-0.03929	1.65179	-0.13750
-1.78571	-0.62143	-1.51786	-0.70357	-0.62500	-0.39286	3.25000	2.78571	1.56250	-0.59821	-2.18750	-0.06607	1.56250	-0.16607
-1.69643	-0.66964	-1.42857	-0.76250	-0.53571	-0.40000	2.91071	2.75000	1.47321	-0.66607	-2.09821	-0.10893	1.47321	-0.19286
-1.60714	-0.72857	-1.33929	-0.80714	-0.44643	-0.41429	2.55357	2.66071	1.38393	-0.71964	-2.00893	-0.15000	1.38393	-0.21429
-1.51786	-0.82500	-1.25000	-0.85357	-0.35714	-0.41429	2.23214	2.60714	1.29464	-0.76786	-1.91964	-0.18929	1.29464	-0.22143
-1.42857	-0.85714	-1.16071	-0.90536	-0.26786	-0.42857	1.96429	2.58929	1.20536	-0.81786	-1.83036	-0.23929	1.20536	-0.23929
-1.33929	-0.92500	-1.07143	-0.95714	-0.17857	-0.40714	1.66071	2.58929	1.11607	-0.88393	-1.74107	-0.29464	1.11607	-0.24643
-1.25000	-0.97857	-0.98214	-1.00893	-0.08929	-0.41071	1.33929	2.60714	1.02679	-0.94821	-1.65179	-0.33929	1.02679	-0.24643
-1.16071	-1.04643	-0.89286	-1.03929	0.00000	-0.40893	0.89286	2.62500	0.93750	-1.03750	-1.56250	-0.39286	0.93750	-0.25000
-1.07143	-1.14464	-0.80357	-1.11071	0.08929	-0.39464	0.44643	2.62500	0.84821	-1.11071	-1.47321	-0.42857	0.84821	-0.23214
-0.98214	-1.18393	-0.71429	-1.17143	0.17857	-0.38571	0.00000	2.64286	0.75893	-1.12143	-1.38393	-0.48393	0.75893	-0.23571
-0.89286	-1.25893	-0.62500	-1.19643	0.26786	-0.36429	-0.46429	2.60714	0.66964	-1.11964	-1.29464	-0.51607	0.66964	-0.22679
-0.80357	-1.27500	-0.53571	-1.21964	0.35714	-0.36250	-0.75000	2.53571	0.58036	-1.06964	-1.20536	-0.57143	0.58036	-0.22143
-0.71429	-1.26250	-0.44643	-1.21786	0.44643	-0.36071	-1.05357	2.46429	-0.58036	-1.08036	-1.11607	-0.60179	0.49107	-0.21429
0.71429	-0.74643	-0.35714	-1.20357	0.53571	-0.33929	-1.39286	2.30357	-0.66964	-1.12500	-1.02679	-0.63036	0.40179	-0.19107
0.80357	-0.72143	-0.26786	-1.15536	0.62500	-0.30714	-1.60714	2.12500	-0.75893	-1.13750	-0.93750	-0.66964	0.31250	-0.19464
0.89286	-0.70357	-0.17857	-1.12857	0.71429	-0.29643	-1.91071	1.91071	-0.84821	-1.11786	-0.84821	-0.70714	0.22321	-0.21071

0.98214	-0.65536	-0.08929	-1.08571	0.80357	-0.27143	-2.16071	1.69643	-0.93750	-1.05893	-0.75893	-0.75536	0.13393	-0.21429
1.07143	-0.59821	0.00000	-1.07679	0.89286	-0.24821	-2.33929	1.42857	-1.02679	-0.96250	-0.66964	-0.75893	0.04464	-0.19643
1.16071	-0.56429	0.08929	-1.05000	0.98214	-0.22321	-2.48214	1.17857	-1.11607	-0.88750	-0.58036	-0.79107	-0.04464	-0.19286
1.25000	-0.49286	0.17857	-1.02500	1.07143	-0.20179	-2.58929	0.89286	-1.20536	-0.82500	-0.49107	-0.80893	-0.13393	-0.20179
1.33929	-0.42143	0.26786	-1.00536	1.16071	-0.18214	-2.67857	0.60714	-1.29464	-0.77857	-0.40179	-0.85000	-0.22321	-0.19464
1.42857	-0.35536	0.35714	-0.96429	1.25000	-0.16250	-2.73214	0.26786	-1.38393	-0.72857	-0.31250	-0.86250	-0.31250	-0.18750
1.51786	-0.29821	0.44643	-0.93036	1.33929	-0.13750	-2.76786	-0.01786	-1.47321	-0.67321	-0.22321	-0.86250	-0.40179	-0.20357
1.60714	-0.25000	0.53571	-0.90179	1.42857	-0.11250	-2.75000	-0.32143	-1.56250	-0.59821	-0.13393	-0.88036	-0.49107	-0.21786
1.69643	-0.18036	0.62500	-0.84107	1.51786	-0.09643	-2.69643	-0.60714	-1.65179	-0.53214	-0.04464	-0.87143	-0.58036	-0.22679
1.78571	-0.14286	0.71429	-0.76429	1.60714	-0.07857	-2.64286	-0.91071	-1.74107	-0.50357	0.04464	-0.86964	-0.66964	-0.24107
1.87500	-0.07143	0.80357	-0.71786	1.69643	-0.06250	-2.53571	-1.14286	-1.83036	-0.44643	0.13393	-0.86429	-0.75893	-0.24821
1.96429	-0.04286	0.89286	-0.64286	1.78571	-0.03214	-2.41071	-1.41071	-1.91964	-0.41964	0.22321	-0.82500	-0.84821	-0.24464
2.05357	0.00179	0.98214	-0.60893	1.87500	-0.01250	-2.23214	-1.60714	-2.00893	-0.37143	0.31250	-0.81964	-0.93750	-0.24821
2.14286	0.06786	1.07143	-0.53750	1.96429	0.00179	-2.03571	-1.83929	-2.09821	-0.33036	0.40179	-0.81607	-1.02679	-0.24464
2.23214	0.10714	1.16071	-0.48393	2.05357	0.01786	-1.78571	-2.01786	-2.18750	-0.28750	0.49107	-0.82500	-1.11607	-0.23750
2.32143	0.15536	1.25000	-0.44107	2.14286	0.03393	-1.57143	-2.19643	-2.27679	-0.24286	0.58036	-0.77679	-1.20536	-0.23036
2.41071	0.20000	1.33929	-0.37143	2.23214	0.03036	-1.33929	-2.32143	-2.36607	-0.17679	0.66964	-0.75357	-1.29464	-0.21786
2.58929	0.26786	1.42857	-0.31250	2.41071	0.05000	-1.08929	-2.46429	-2.45536	-0.12500	0.75893	-0.70893	-1.38393	-0.19821
2.76786	0.32679	1.51786	-0.28393	2.58929	0.07143	-0.78571	-2.58929	-2.54464	-0.07143	0.84821	-0.68571	-1.47321	-0.18929
2.94643	0.39464	1.60714	-0.23214	2.76786	0.06964	-0.51786	-2.64286	-2.63393	-0.02500	0.93750	-0.65714	-1.56250	-0.15714
3.12500	0.44643	1.69643	-0.20000	2.94643	0.08929	-0.23214	-2.71429	-2.72321	-0.00714	1.02679	-0.63571	-1.65179	-0.11964
3.30357	0.48750	1.78571	-0.15893	3.12500	0.10536	0.16071	-2.73214	-2.81250	0.00536	1.11607	-0.58750	-1.74107	-0.10000
3.48214	0.52321	1.87500	-0.11786	3.30357	0.12321	0.62500	-2.73214	-2.90179	0.01071	1.20536	-0.55536	-1.83036	-0.08036
3.66071	0.57321	1.96429	-0.05714	3.48214	0.13214	1.21429	-2.69643	-2.99107	0.01429	1.29464	-0.51786	-1.91964	-0.05357
3.83929	0.60536	2.05357	-0.01429	3.66071	0.15000	1.62500	-2.62500	-3.08036	0.01607	1.38393	-0.46250	-2.00893	-0.04643
4.01786	0.62321	2.14286	-0.02679	3.83929	0.16429	2.05357	-2.51786	-3.16964	0.00536	1.47321	-0.42500	-2.09821	-0.03036
4.19643	0.65179	2.23214	0.02679	4.01786	0.16071	2.57143	-2.55357	-3.25893	0.00893	1.56250	-0.37500	-2.18750	-0.02857
4.37500	0.67321	2.32143	0.07857	4.19643	0.15893	2.91071	-2.62500	-3.34821	0.01429	1.65179	-0.31607	-2.27679	-0.00714
4.55357	0.70536	2.41071	0.10893	4.37500	0.17857	3.28571	-2.67857			1.74107	-0.26071	-2.36607	0.00357
4.73214	0.70536	2.58929	0.15179	4.55357	0.18036	3.66071	-2.69643			1.83036	-0.21786	-2.45536	0.02679
4.91071	0.70357	2.76786	0.21250	4.73214	0.17321	4.05357	-2.71429			1.91964	-0.17679	-2.54464	0.01607
5.08929	0.70714	2.94643	0.25714	4.91071	0.17321	4.30357	-2.73214			2.00893	-0.13929	-2.63393	0.02500

5.26786	0.71250	3.12500	0.29107	5.08929	0.17679	4.83929	-2.73214			2.09821	-0.08393	-2.72321	0.02321
5.44643	0.71071	3.30357	0.33393	5.26786	0.18750	4.94643	-2.71429			2.18750	-0.06964	-2.81250	-0.01071
5.62500	0.70714	3.48214	0.37857	5.44643	0.19286	5.12500	-2.71429			2.27679	-0.04107	-2.90179	-0.01786
5.80357	0.69286	3.66071	0.41964	5.62500	0.18929	5.51786	-2.73214			2.36607	-0.04107	-2.99107	-0.01250
5.98214	0.55714	3.83929	0.43750	5.80357	0.17321	2.05357	-2.46429			2.45536	-0.03571	-3.08036	-0.02679
6.07143	0.49464	4.01786	0.46250	5.98214	0.17857	2.12500	-2.23214			2.54464	-0.04107	-3.16964	-0.03929
6.16071	0.43750	4.19643	0.50179	6.16071	0.17143	2.23214	-2.03571			2.63393	-0.02679	-3.25893	-0.02679
6.25000	0.36071	4.37500	0.51250	6.33929	0.13750	2.41071	-1.78571			2.68750	-0.03214	-3.34821	-0.02500
6.33929	0.28571	4.55357	0.52321	6.51786	0.06964	2.44643	-1.55357						
6.42857	0.23214	4.73214	0.54821	6.69643	0.01607	2.50000	-1.41071						
6.51786	0.13571	4.91071	0.55714	6.87500	-0.06071	2.44643	-1.17857						
6.60714	0.08750	5.08929	0.56429	7.05357	-0.16071	2.32143	-0.91071						
6.69643	0.05714	5.26786	0.55179	7.23214	-0.22321	2.19643	-0.67857						
6.78571	0.05000	5.44643	0.55000			2.08929	-0.41071						
6.87500	0.04821	5.62500	0.56250			2.01786	-0.19643						
6.96429	0.04643	5.80357	0.58393			2.01786	0.12500						
7.05357	0.03214	5.98214	0.59107			2.05357	0.35714						
7.14286	0.01250	6.16071	0.50357			1.94643	0.64286						
7.23214	-0.00357	6.25000	0.44464			2.26786	0.92857						
		6.33929	0.39107			2.37500	1.16071						
		6.42857	0.30893			2.42857	1.35714						
		6.51786	0.24643			2.41071	1.55357						
		6.60714	0.18929			2.28571	1.78571						
		6.69643	0.11786			2.07143	2.05357						
		6.78571	0.03036			1.92857	2.30357						
		6.87500	-0.02321			1.75000	2.44643						
		6.96429	-0.06607										
		7.05357	-0.10000										
		7.14286	-0.10357										
		7.23214	-0.10000										

Test ID: B2 ($b = 0.8$ m, $h = 0.12$ m, $U = 0.261$ m/s, $D = 0.056$ m, $d_{50} = 0.74$ mm, emergent cylinder)													
Z/D = 0		Z/D = 0.5		Z/D = 3.8		Y/D = 0		X/D = 0		X/D = -1.3		X/D = 1.75	
X/D	Y/D	X/D	Y/D	X/D	Y/D	X/D	Z/D	Z/D	Y/D	Z/D	Y/D	Z/D	Y/D
-3.08036	-0.02560	-2.90179	-0.03274	6.65179	-0.06667	9.15179	-4.62500	2.94643	-0.05952	2.58929	-0.03631	-3.03571	0.00655
-2.99107	-0.02917	-2.81250	-0.04524	6.74107	-0.05952	8.79464	-4.62500	2.85714	-0.06310	2.50000	-0.05774	-2.94643	0.02619
-2.90179	-0.06131	-2.72321	-0.08631	6.83036	-0.07202	8.43750	-4.64286	2.76786	-0.11667	2.41071	-0.08095	-2.85714	0.02083
-2.81250	-0.09524	-2.63393	-0.12381	6.91964	-0.07381	8.16964	-4.60714	2.67857	-0.15417	2.32143	-0.11131	-2.76786	0.01369
-2.72321	-0.14702	-2.54464	-0.18095	7.00893	-0.07917	7.84821	-4.42857	2.58929	-0.21310	2.23214	-0.16488	-2.67857	-0.00595
-2.63393	-0.19524	-2.45536	-0.24702	7.09821	-0.10417	7.54464	-4.37500	2.50000	-0.27560	2.14286	-0.21310	-2.58929	-0.04524
-2.54464	-0.26131	-2.36607	-0.29167	7.18750	-0.14702	7.33036	-4.25000	2.41071	-0.31667	2.05357	-0.25060	-2.50000	-0.05595
-2.45536	-0.29881	-2.27679	-0.36131	7.27679	-0.18452	7.16964	-4.14286	2.32143	-0.35774	1.96429	-0.29345	-2.41071	-0.08452
-2.36607	-0.36845	-2.18750	-0.40595	7.36607	-0.22024	7.02679	-4.00000	2.23214	-0.40774	1.87500	-0.33095	-2.32143	-0.10060
-2.27679	-0.40060	-2.09821	-0.47024	7.45536	-0.23452	6.91964	-3.82143	2.14286	-0.43274	1.78571	-0.38988	-2.23214	-0.11488
-2.18750	-0.47381	-2.00893	-0.52024	7.54464	-0.24167	6.83036	-3.66071	2.05357	-0.47560	1.69643	-0.43810	-2.14286	-0.13452
-2.09821	-0.53452	-1.91964	-0.57560	7.63393	-0.25060	6.65179	-3.46429	1.96429	-0.50060	1.60714	-0.47560	-2.05357	-0.15952
-2.00893	-0.58631	-1.83036	-0.63452	7.72321	-0.28452	6.47321	-3.42857	1.87500	-0.55238	1.51786	-0.52560	-1.96429	-0.18095
-1.91964	-0.62560	-1.74107	-0.66488	7.81250	-0.28274	5.99107	-3.42857	1.78571	-0.60238	1.42857	-0.56845	-1.87500	-0.20238
-1.83036	-0.71310	-1.65179	-0.71845	7.90179	-0.29524	5.49107	-3.42857	1.69643	-0.65595	1.33929	-0.60952	-1.78571	-0.21310
-1.74107	-0.71488	-1.56250	-0.73631	7.99107	-0.28810	5.04464	-3.42857	1.60714	-0.71667	1.25000	-0.66488	-1.69643	-0.25774
-1.65179	-0.77381	-1.47321	-0.80774	8.08036	-0.26667	4.59821	-3.44643	1.51786	-0.79702	1.16071	-0.68988	-1.60714	-0.28988
-1.56250	-0.84167	-1.38393	-0.87381	8.16964	-0.25952	4.15179	-3.44643	1.42857	-0.84524	1.07143	-0.73631	-1.51786	-0.30952
-1.47321	-0.92917	-1.29464	-0.94167	8.25893	-0.24524	3.79464	-3.41071	1.33929	-0.91845	0.98214	-0.73274	-1.42857	-0.35060
-1.38393	-0.99702	-1.20536	-0.95238	8.34821	-0.23274	3.34821	-3.32143	1.25000	-0.94345	0.89286	-0.78631	-1.33929	-0.36131
-1.29464	-1.04702	-1.11607	-1.03095	8.43750	-0.20595	2.88393	-3.17857	1.16071	-1.01131	0.80357	-0.82738	-1.25000	-0.38274
-1.20536	-1.11310	-1.02679	-1.08631	8.52679	-0.19702	2.54464	-3.03571	1.07143	-1.07560	0.71429	-0.86310	-1.16071	-0.38810
-1.11607	-1.18452	-0.93750	-1.14524	8.61607	-0.17917	2.27679	-2.92857	0.98214	-1.15417	0.62500	-0.89524	-1.07143	-0.39524
-1.02679	-1.26667	-0.84821	-1.19524	8.70536	-0.12917	2.09821	-2.83929	0.89286	-1.22560	0.53571	-0.90238	-0.98214	-0.39524
-0.93750	-1.34167	-0.75893	-1.27024	8.79464	-0.09702	1.79464	-2.83929	0.80357	-1.24345	0.44643	-0.94167	-0.89286	-0.39881
-0.84821	-1.36845	-0.66964	-1.31310	8.88393	-0.05595	1.47321	-2.85714	0.71429	-1.23452	0.35714	-0.94524	-0.80357	-0.38631
-0.75893	-1.38631	-0.58036	-1.32024	8.97321	-0.03452	0.95536	-2.89286	0.62500	-1.19345	0.26786	-0.96131	-0.71429	-0.39524
-0.66964	-1.35238	-0.49107	-1.31845	9.06250	-0.02202	0.61607	-2.89286	-0.62500	-1.25774	0.17857	-0.96667	-0.62500	-0.37917
0.66964	-0.86131	-0.40179	-1.32381	9.15179	-0.00060	0.22321	-2.92857	-2.67857	-0.11310	0.08929	-0.98095	-0.53571	-0.36845

0.75893	-0.84345	-0.31250	-1.30595	9.24107	0.01726	-0.04464	-2.92857	-2.58929	-0.15060	0.00000	-0.98988	-0.44643	-0.36131
0.84821	-0.81845	-0.22321	-1.26488	9.33036	0.04048	-0.43750	-2.89286	-2.50000	-0.20060	-0.08929	-0.97738	-0.35714	-0.34702
0.93750	-0.79167	-0.13393	-1.24167	9.41964	0.06369	-0.83036	-2.80357	-2.41071	-0.25060	-0.17857	-0.95238	-0.26786	-0.34167
1.02679	-0.72738	-0.04464	-1.19702	9.50893	0.05833	-1.11607	-2.67857	-2.32143	-0.31310	-0.26786	-0.94881	-0.17857	-0.34345
1.11607	-0.69881	0.04464	-1.17738	9.59821	0.05298	-1.29464	-2.57143	-2.23214	-0.35238	-0.35714	-0.91845	-0.08929	-0.34881
1.20536	-0.64702	0.13393	-1.15060			-1.56250	-2.41071	-2.14286	-0.37917	-0.44643	-0.91488	0.00000	-0.35060
1.29464	-0.60060	0.22321	-1.13631			-1.83036	-2.23214	-2.05357	-0.43810	-0.53571	-0.89345	0.08929	-0.35060
1.38393	-0.51310	0.31250	-1.10595			-2.11607	-2.00000	-1.96429	-0.46310	-0.62500	-0.86310	0.17857	-0.35238
1.47321	-0.45595	0.40179	-1.08095			-2.27679	-1.82143	-1.87500	-0.51310	-0.71429	-0.83988	0.26786	-0.36310
1.56250	-0.41131	0.49107	-1.04702			-2.40179	-1.62500	-1.78571	-0.56488	-0.80357	-0.77738	0.35714	-0.37560
1.65179	-0.36310	0.58036	-1.00952			-2.54464	-1.35714	-1.69643	-0.61310	-0.89286	-0.74524	0.44643	-0.38274
1.74107	-0.31131	0.66964	-0.94881			-2.72321	-1.16071	-1.60714	-0.65952	-0.98214	-0.73274	0.53571	-0.39345
1.83036	-0.27381	0.75893	-0.91131			-2.81250	-0.92857	-1.51786	-0.72560	-1.07143	-0.70060	0.62500	-0.39881
1.91964	-0.22917	0.84821	-0.84167			-2.86607	-0.71429	-1.42857	-0.77560	-1.16071	-0.65595	0.71429	-0.38988
2.00893	-0.19167	0.93750	-0.78274			-2.97321	-0.44643	-1.33929	-0.84345	-1.25000	-0.62024	0.80357	-0.39881
2.09821	-0.13810	1.02679	-0.75417			-2.95536	-0.08929	-1.25000	-0.90238	-1.33929	-0.57381	0.89286	-0.38810
2.18750	-0.09345	1.11607	-0.69524			-2.99107	0.39286	-1.16071	-0.95774	-1.42857	-0.54167	0.98214	-0.39881
2.27679	-0.03988	1.20536	-0.62917			-2.91964	0.67857	-1.07143	-1.01667	-1.51786	-0.50595	1.07143	-0.40417
2.36607	-0.00595	1.29464	-0.59345			-2.86607	0.92857	-0.98214	-1.10060	-1.60714	-0.46310	1.16071	-0.40417
2.45536	0.04583	1.38393	-0.51667			-2.77679	1.14286	-0.89286	-1.17381	-1.69643	-0.41845	1.25000	-0.39345
2.54464	0.07083	1.47321	-0.47917			-2.65179	1.37500	-0.80357	-1.22202	-1.78571	-0.37202	1.33929	-0.38988
2.63393	0.11012	1.56250	-0.43631			-2.54464	1.57143	-0.71429	-1.24702	-1.87500	-0.32381	1.42857	-0.37560
2.81250	0.17440	1.65179	-0.39524			-2.33036	1.78571			-1.96429	-0.28631	1.51786	-0.34524
2.99107	0.23869	1.74107	-0.35952			-2.13393	1.85714			-2.05357	-0.22381	1.60714	-0.32024
3.16964	0.26726	1.83036	-0.30417			-1.97321	2.23214			-2.14286	-0.18988	1.69643	-0.29702
3.34821	0.32083	1.91964	-0.27024			-1.84821	2.32143			-2.23214	-0.12917	1.78571	-0.25952
3.52679	0.34048	2.00893	-0.23274			-1.70536	2.39286			-2.32143	-0.09881	1.87500	-0.22381
3.70536	0.37798	2.09821	-0.18810			-1.56250	2.50000			-2.41071	-0.04345	1.96429	-0.20060
3.88393	0.41548	2.18750	-0.16310			-1.43750	2.55357			-2.50000	-0.01310	2.05357	-0.17202
4.06250	0.42619	2.27679	-0.12202			-1.29464	2.64286			-2.58929	0.01726	2.14286	-0.13631
4.24107	0.46369	2.36607	-0.10238			-1.06250	2.71429			-2.67857	0.03690	2.23214	-0.13274
4.41964	0.47798	2.45536	-0.06131			-0.84821	2.76786					2.32143	-0.12560

4.59821	0.50119	2.63393	-0.00952			-0.59821	2.85714					2.41071	-0.10774
4.77679	0.51190	2.81250	0.04940			-0.34821	2.89286					2.50000	-0.09702
4.95536	0.52619	2.99107	0.11905			-0.08036	2.92857					2.58929	-0.08452
5.13393	0.54048	3.16964	0.15119			0.20536	2.92857					2.67857	-0.05774
5.31250	0.55119	3.34821	0.19048			0.66964	2.92857					2.76786	-0.02202
5.49107	0.55298	3.52679	0.22083			1.29464	2.92857					2.85714	-0.01310
5.66964	0.57440	3.70536	0.25119			1.70536	2.92857					2.94643	-0.00774
5.84821	0.57619	3.88393	0.29405			2.00893	2.89286					3.03571	-0.02560
6.02679	0.59405	4.06250	0.31726			2.31250	2.87500						
6.20536	0.58690	4.24107	0.35119			2.61607	2.96429						
6.38393	0.60119	4.41964	0.36369			2.99107	3.12500						
6.56250	0.60655	4.59821	0.38333			3.34821	3.23214						
6.74107	0.61726	4.77679	0.39405			3.70536	3.23214						
6.91964	0.62262	4.95536	0.42440			4.24107	3.21429						
7.09821	0.61548	5.13393	0.43512			4.59821	3.14286						
7.27679	0.61012	5.31250	0.42798			4.90179	3.07143						
7.45536	0.43512	5.49107	0.44940			5.13393	3.12500						
7.63393	0.28690	5.66964	0.44762			5.47321	3.21429						
7.81250	0.15298	5.84821	0.45476			5.75893	3.33929						
7.99107	0.05298	6.02679	0.46726			5.97321	3.46429						
8.16964	0.06548	6.20536	0.46548			6.09821	3.64286						
8.34821	0.03512	6.38393	0.47798			6.29464	3.89286						
8.52679	-0.00060	6.56250	0.48869			6.47321	4.05357						
8.70536	-0.03095	6.74107	0.48690			6.61607	4.19643						
8.88393	-0.06310	6.91964	0.47976			6.81250	4.28571						
9.06250	-0.05952	7.09821	0.49583			7.27679	4.32143						
9.24107	-0.06667	7.27679	0.49226			7.77679	4.23214						
9.41964	-0.08452	7.45536	0.48333			8.20536	4.21429						
		7.63393	0.49226			8.45536	4.19643						
		7.81250	0.36012			8.74107	4.23214						
		7.99107	0.23512			9.13393	4.28571						
		8.16964	0.15298			9.59821	4.25000						

		8.34821	-0.01131			1.86607	2.85714						
		8.52679	-0.11131			2.04464	2.57143						
		8.70536	-0.21845			2.27679	2.23214						
		8.88393	-0.22917			2.47321	1.87500						
		9.06250	-0.28452			2.68750	1.60714						
		9.24107	-0.40060			2.77679	1.33929						
		9.41964	-0.43631			2.68750	1.01786						
						2.47321	0.87500						
						2.34821	0.41071						
						2.22321	0.01786						
						2.31250	-0.35714						
						2.41964	-0.67857						
						2.65179	-1.00000						
						2.77679	-1.21429						
						2.77679	-1.53571						
						2.63393	-1.80357						
						2.41964	-2.08929						
						2.09821	-2.21429						
						1.86607	-2.62500						

Test ID: B3 ($b = 1.22$ m, $h = 0.12$ m, $U = 0.254$ m/s, $D = 0.056$ m, $d_{50} = 0.74$ mm, emergent cylinder)													
$Z/D = 0$		$Z/D = 0.5$		$Z/D = 5.7$		$Y/D = 0$		$X/D = 0$		$X/D = -1.3$		$X/D = 1.75$	
X/D	Y/D	X/D	Y/D	X/D	Y/D	X/D	Z/D	Z/D	Y/D	Z/D	Y/D	Z/D	Y/D
-3.25893	-0.04405	-3.16964	-0.04583	-	-	10.22321	4.53571	3.25893	0.00595	-2.72321	-0.02798	3.16964	-0.00119
-3.16964	-0.06726	-3.08036	-0.06012	-	-	10.04464	4.48214	3.16964	-0.00119	-2.63393	-0.03155	3.08036	0.02381
-3.08036	-0.07976	-2.99107	-0.07976	-	-	9.66964	4.50000	3.08036	-0.00298	-2.54464	-0.07440	2.99107	0.00952
-2.99107	-0.13155	-2.90179	-0.11190	-	-	9.15179	4.57143	2.99107	-0.02619	-2.45536	-0.10655	2.90179	0.01131
-2.90179	-0.15476	-2.81250	-0.14405	-	-	8.79464	4.50000	2.90179	-0.07262	-2.36607	-0.13333	2.81250	-0.00298
-2.81250	-0.22440	-2.72321	-0.17619	-	-	8.40179	4.41071	2.81250	-0.12440	-2.27679	-0.17262	2.72321	-0.03333
-2.72321	-0.24762	-2.63393	-0.24940	-	-	8.18750	4.48214	2.72321	-0.16905	-2.18750	-0.23155	2.63393	-0.04940
-2.63393	-0.30476	-2.54464	-0.27976	-	-	7.81250	4.46429	2.63393	-0.22083	-2.09821	-0.27440	2.54464	-0.07262
-2.54464	-0.35833	-2.45536	-0.33333	-	-	7.27679	4.46429	2.54464	-0.27262	-2.00893	-0.32083	2.45536	-0.08512
-2.45536	-0.38690	-2.36607	-0.37083	-	-	7.06250	4.50000	2.45536	-0.32083	-1.91964	-0.36369	2.36607	-0.11190
-2.36607	-0.45298	-2.27679	-0.42083	-	-	6.74107	4.50000	2.36607	-0.36190	-1.83036	-0.39940	2.27679	-0.12619
-2.27679	-0.49940	-2.18750	-0.46726	-	-	6.38393	4.28571	2.27679	-0.41012	-1.74107	-0.46905	2.18750	-0.14583
-2.18750	-0.55298	-2.09821	-0.51369	-	-	5.93750	3.83929	2.18750	-0.46548	-1.65179	-0.50476	2.09821	-0.16905
-2.09821	-0.60119	-2.00893	-0.57262	-	-	5.72321	3.48214	2.09821	-0.50119	-1.56250	-0.54762	2.00893	-0.20476
-2.00893	-0.66905	-1.91964	-0.60476	-	-	5.54464	3.39286	2.00893	-0.55833	-1.47321	-0.58333	1.91964	-0.25655
-1.91964	-0.70655	-1.83036	-0.68333	-	-	5.06250	3.23214	1.91964	-0.59940	-1.38393	-0.62798	1.83036	-0.30119
-1.83036	-0.74940	-1.74107	-0.72262	-	-	4.65179	3.35714	1.83036	-0.66369	-1.29464	-0.66905	1.74107	-0.32798
-1.74107	-0.80655	-1.65179	-0.76369	-	-	4.29464	3.35714	1.74107	-0.71726	-1.20536	-0.73333	1.65179	-0.36905
-1.65179	-0.86012	-1.56250	-0.81369	-	-	4.11607	3.28571	1.65179	-0.78512	-1.11607	-0.76012	1.56250	-0.39048
-1.56250	-0.89762	-1.47321	-0.83512	-	-	3.74107	3.23214	1.56250	-0.82440	-1.02679	-0.80298	1.47321	-0.40833
-1.47321	-0.99583	-1.38393	-0.90655	-	-	3.34821	3.21429	1.47321	-0.90298	-0.93750	-0.84226	1.38393	-0.41548
-1.38393	-1.03333	-1.29464	-0.97262	-	-	3.04464	3.14286	1.38393	-0.96369	-0.84821	-0.86012	1.29464	-0.42619
-1.29464	-1.10655	-1.20536	-1.00476	-	-	2.58036	3.03571	1.29464	-0.99405	-0.75893	-0.88869	1.20536	-0.43869
-1.20536	-1.16012	-1.11607	-1.06012	-	-	2.08036	2.98214	1.20536	-1.07440	-0.66964	-0.88869	1.11607	-0.45476
-1.11607	-1.22262	-1.02679	-1.09048	-	-	1.72321	2.92857	1.11607	-1.15833	-0.58036	-0.96012	1.02679	-0.45655
-1.02679	-1.29226	-0.93750	-1.14405	-	-	1.38393	2.85714	1.02679	-1.20833	-0.49107	-0.95476	0.93750	-0.43690
-0.93750	-1.40476	-0.84821	-1.20655	-	-	1.00893	2.91071	0.93750	-1.28690	-0.40179	-1.01369	0.84821	-0.41190
-0.84821	-1.44940	-0.75893	-1.26190	-	-	0.58036	2.92857	0.84821	-1.31190	-0.31250	-1.03155	0.75893	-0.41548
-0.75893	-1.47976	-0.66964	-1.34583	-	-	0.08036	2.89286	0.75893	-1.30298	-0.22321	-1.05298	0.66964	-0.37798

-0.66964	-1.44048	-0.58036	-1.37619	-	-	-0.45536	2.87500	0.66964	-1.27976	-0.13393	-1.05655	0.58036	-0.37798
-0.58036	-1.38690	-0.49107	-1.40298	-	-	-0.88393	2.78571	0.58036	-1.18155	-0.04464	-1.07262	0.49107	-0.36905
0.58036	-0.92083	-0.40179	-1.38869	-	-	-1.20536	2.67857	-0.58036	-1.28512	0.04464	-1.05476	0.40179	-0.35119
0.66964	-0.90833	-0.31250	-1.37440	-	-	-1.63393	2.53571	-0.66964	-1.30655	0.13393	-1.03512	0.31250	-0.33155
0.75893	-0.90476	-0.22321	-1.35833	-	-	-2.09821	2.25000	-0.75893	-1.28333	0.22321	-1.04226	0.22321	-0.33512
0.84821	-0.88333	-0.13393	-1.33512	-	-	-2.29464	1.98214	-0.84821	-1.23869	0.31250	-1.01726	0.13393	-0.36012
0.93750	-0.83512	-0.04464	-1.28512	-	-	-2.52679	1.64286	-0.93750	-1.18333	0.40179	-1.01726	0.04464	-0.33690
1.02679	-0.77262	0.04464	-1.27083	-	-	-2.72321	1.28571	-1.02679	-1.07976	0.49107	-1.00119	-0.04464	-0.34048
1.11607	-0.70298	0.13393	-1.25655	-	-	-2.90179	1.01786	-1.11607	-0.99226	0.58036	-0.97976	-0.13393	-0.37440
1.20536	-0.64048	0.22321	-1.22798	-	-	-3.08036	0.69643	-1.20536	-0.95298	0.66964	-0.97262	-0.22321	-0.37262
1.29464	-0.59226	0.31250	-1.20298	-	-	-3.20536	0.37500	-1.29464	-0.89583	0.75893	-0.88155	-0.31250	-0.37976
1.38393	-0.52619	0.40179	-1.16548	-	-	-3.22321	0.10714	-1.38393	-0.84048	0.84821	-0.88512	-0.40179	-0.38690
1.47321	-0.46548	0.49107	-1.10833	-	-	-3.20536	-0.19643	-1.47321	-0.78155	0.93750	-0.81190	-0.49107	-0.37083
1.56250	-0.41012	0.58036	-1.08512	-	-	-3.24107	-0.58929	-1.56250	-0.73333	1.02679	-0.78512	-0.58036	-0.38512
1.65179	-0.38155	0.66964	-1.01905	-	-	-3.16964	-0.87500	-1.65179	-0.66905	1.11607	-0.77440	-0.66964	-0.41548
1.74107	-0.29762	0.75893	-0.96012	-	-	-3.06250	-1.12500	-1.74107	-0.62619	1.20536	-0.74583	-0.75893	-0.37798
1.83036	-0.24405	0.84821	-0.87976	-	-	-2.90179	-1.44643	-1.83036	-0.57976	1.29464	-0.68512	-0.84821	-0.35119
1.91964	-0.19762	0.93750	-0.82619	-	-	-2.68750	-1.82143	-1.91964	-0.52976	1.38393	-0.64762	-0.93750	-0.36905
2.00893	-0.16190	1.02679	-0.76905	-	-	-2.45536	-2.16071	-2.00893	-0.49940	1.47321	-0.58512	-1.02679	-0.38869
2.09821	-0.11012	1.11607	-0.69940	-	-	-2.18750	-2.50000	-2.09821	-0.45655	1.56250	-0.55833	-1.11607	-0.38690
2.18750	-0.04762	1.20536	-0.64762	-	-	-1.88393	-2.62500	-2.18750	-0.41369	1.65179	-0.53155	-1.20536	-0.37619
2.27679	-0.00119	1.29464	-0.60833	-	-	-1.65179	-2.80357	-2.27679	-0.36726	1.74107	-0.49048	-1.29464	-0.37262
2.36607	0.01845	1.38393	-0.54405	-	-	-1.41964	-2.92857	-2.36607	-0.31726	1.83036	-0.43869	-1.38393	-0.34940
2.45536	0.02738	1.47321	-0.51190	-	-	-1.09821	-3.03571	-2.45536	-0.26905	1.91964	-0.38869	-1.47321	-0.32083
2.54464	0.08988	1.56250	-0.45833	-	-	-0.70536	-3.05357	-2.54464	-0.21012	2.00893	-0.33512	-1.56250	-0.30298
2.63393	0.13631	1.65179	-0.40833	-	-	-0.49107	-3.12500	-2.63393	-0.12976	2.09821	-0.29583	-1.65179	-0.28155
2.72321	0.15060	1.74107	-0.37619	-	-	0.02679	-3.19643	-2.72321	-0.10655	2.18750	-0.26548	-1.74107	-0.24048
2.81250	0.19167	1.83036	-0.31548	-	-	0.41964	-3.25000	-2.81250	-0.05298	2.27679	-0.20655	-1.83036	-0.22798
2.90179	0.22738	1.91964	-0.27798	-	-	1.11607	-3.26786	-2.90179	-0.03512	2.36607	-0.18690	-1.91964	-0.18690
2.99107	0.27024	2.00893	-0.22440	-	-	1.91964	-3.21429	-2.99107	-0.01726	2.45536	-0.12262	-2.00893	-0.17262
3.08036	0.28988	2.09821	-0.20298	-	-	2.54464	-3.21429	-3.08036	-0.00833	2.54464	-0.09940	-2.09821	-0.13690
3.16964	0.32024	2.18750	-0.14940	-	-	3.20536	-3.32143	-3.16964	0.00060	2.63393	-0.05476	-2.18750	-0.12440

3.25893	0.34881	2.27679	-0.11012	-	-	3.79464	-3.39286			2.72321	-0.03512	-2.27679	-0.09583
3.34821	0.37560	2.36607	-0.07440	-	-	4.49107	-3.50000			2.81250	0.00238	-2.36607	-0.08512
3.43750	0.40952	2.45536	-0.02619	-	-	5.02679	-3.55357			2.90179	0.00774	-2.45536	-0.07619
3.61607	0.43810	2.54464	0.02560	-	-	5.38393	-3.62500			2.99107	0.01310	-2.54464	-0.04583
3.79464	0.47381	2.63393	0.02024	-	-	5.83036	-3.71429			3.08036	0.01845	-2.63393	-0.02262
3.97321	0.50952	2.72321	0.02381	-	-	6.04464	-3.71429			3.16964	0.03810	-2.72321	-0.01012
4.15179	0.54345	2.81250	0.04167	-	-	6.11607	-3.98214			3.25893	0.03274	-2.81250	0.00774
4.33036	0.57738	2.90179	0.08988	-	-	6.27679	-4.28571			3.34821	0.02917	-2.90179	-0.00119
4.50893	0.59345	2.99107	0.12917	-	-	6.58036	-4.51786			3.43750	0.03810	-2.99107	-0.01369
4.68750	0.61488	3.08036	0.15952	-	-	7.20536	-4.87500					-3.08036	-0.02262
4.86607	0.62560	3.16964	0.16667	-	-	7.24107	-5.03571					-3.16964	-0.01369
5.04464	0.63452	3.25893	0.19167	-	-	7.49107	-5.08929					-3.25893	-0.01726
5.22321	0.65238	3.34821	0.22024	-	-	8.06250	-5.17857						
5.40179	0.66310	3.43750	0.23810	-	-	8.16964	-5.07143						
5.58036	0.65417	3.61607	0.28452	-	-	8.77679	-5.00000						
5.75893	0.68095	3.79464	0.30417	-	-	8.97321	-4.92857						
5.93750	0.68274	3.97321	0.34881	-	-	9.36607	-5.28571						
6.11607	0.69167	4.15179	0.37202	-	-	9.68750	-5.42857						
6.29464	0.69167	4.33036	0.38810	-	-	10.09821	-5.48214						
6.47321	0.68452	4.50893	0.41845	-	-	10.40179	-5.53571						
6.65179	0.56488	4.68750	0.41845	-	-	2.00893	-2.85714						
6.83036	0.39702	4.86607	0.42560	-	-	2.45536	-2.67857						
7.00893	0.28274	5.04464	0.43452	-	-	2.77679	-2.51786						
7.18750	0.13988	5.22321	0.45417	-	-	3.04464	-2.28571						
7.36607	0.05595	5.40179	0.46845	-	-	3.18750	-1.87500						
7.54464	0.04167	5.58036	0.47738	-	-	3.11607	-1.51786						
7.72321	-0.00833	5.75893	0.49167	-	-	2.93750	-1.08929						
7.90179	-0.05476	5.93750	0.49524	-	-	2.68750	-0.78571						
8.08036	-0.07440	6.11607	0.50952	-	-	2.49107	-0.37500						
8.25893	-0.09762	6.29464	0.52202	-	-	2.49107	-0.03571						
8.43750	-0.10833	6.47321	0.52917	-	-	2.54464	0.25000						
8.61607	-0.12976	6.65179	0.54345	-	-	2.77679	0.60714						

8.79464	-0.11905	6.83036	0.54524	-	-	2.91964	1.00000						
8.97321	-0.12440	7.00893	0.54702	-	-	2.95536	1.35714						
9.15179	-0.12262	7.18750	0.46488	-	-	2.90179	1.73214						
9.33036	-0.09940	7.36607	0.35774	-	-	2.63393	2.08929						
9.50893	-0.09940	7.54464	0.21488	-	-	2.20536	2.33929						
9.68750	-0.09583	7.72321	0.09345	-	-								
9.86607	-0.08869	7.90179	-0.09940	-	-								
10.04464	-0.07619	8.08036	-0.13869	-	-								
10.22321	-0.06369	8.25893	-0.21905	-	-								
		8.43750	-0.27798	-	-								
		8.61607	-0.36905	-	-								
		8.79464	-0.42798	-	-								
		8.97321	-0.47619	-	-								
		9.15179	-0.48869	-	-								
		9.33036	-0.49583	-	-								
		9.50893	-0.49940	-	-								
		9.68750	-0.48333	-	-								
		9.86607	-0.49048	-	-								
		10.04464	-0.49940	-	-								
		10.22321	-0.47262	-	-								

Test ID: S1 ($b = 0.4$ m, $h = 0.12$ m, $U = 0.262$ m/s, $D = 0.056$ m, $d_{50} = 0.74$ mm, submerged cylinder)													
$Z/D = 0$		$Z/D = 0.5$		$Z/D = 1.5$		$Y/D = 0$		$X/D = 0$		$X/D = -1.3$		$X/D = 1.75$	
X/D	Y/D	X/D	Y/D	X/D	Y/D	X/D	Z/D	Z/D	Y/D	Z/D	Y/D	Z/D	Y/D
-2.81250	-0.06429					5.83036	3.42857						
-2.72321	-0.02679					5.74107	3.28571						
-2.63393	-0.09286					5.74107	3.16071						
-2.54464	-0.13214					5.56250	3.10714						
-2.45536	-0.18929					5.24107	3.08929						
-2.36607	-0.26429					4.88393	3.08929						
-2.27679	-0.30893					4.59821	3.07143						
-2.18750	-0.36250					4.29464	3.05357						
-2.09821	-0.41964					3.99107	3.01786						
-2.00893	-0.49286					3.74107	2.94643						
-1.91964	-0.53929					3.45536	2.87500						
-1.83036	-0.57321					3.29464	2.83929						
-1.74107	-0.61964					2.97321	2.78571						
-1.65179	-0.65893					2.70536	2.71429						
-1.56250	-0.71250					2.40179	2.66071						
-1.47321	-0.79464					2.20536	2.58929						
-1.38393	-0.85000					1.99107	2.55357						
-1.29464	-0.91071					1.66964	2.51786						
-1.20536	-0.96250					1.49107	2.55357						
-1.11607	-1.02679					1.24107	2.58929						
-1.02679	-1.09286					0.99107	2.58929						
-0.93750	-1.20357					0.77679	2.58929						
-0.84821	-1.24286					0.49107	2.58929						
-0.75893	-1.25000					-0.00893	2.58929						
-0.66964	-1.20357					-0.29464	2.58929						
-0.58036	-1.06250					-0.63393	2.58929						
0.58036	-0.74643					-0.91964	2.53571						
0.66964	-0.75714					-1.06250	2.42857						
0.75893	-0.72143					-1.54464	2.28571						

0.84821	-0.69286					-1.79464	2.07143						
0.93750	-0.65357					-1.90179	1.92857						
1.02679	-0.57679					-1.90179	1.75000						
1.11607	-0.52143					-1.97321	1.60714						
1.20536	-0.47143					-2.16964	1.37500						
1.29464	-0.40357					-2.20536	1.21429						
1.38393	-0.33393					-2.27679	1.10714						
1.47321	-0.30000					-2.36607	0.92857						
1.56250	-0.21071					-2.38393	0.71429						
1.65179	-0.15357					-2.45536	0.42857						
1.74107	-0.11786					-2.50893	0.32143						
1.83036	-0.11964					-2.50893	0.17857						
1.91964	-0.07143					-2.54464	-0.05357						
2.00893	0.01607					-2.47321	-0.30357						
2.09821	0.07143					-2.45536	-0.46429						
2.18750	0.12857					-2.40179	-0.64286						
2.27679	0.18036					-2.29464	-0.83929						
2.36607	0.20000					-2.24107	-1.05357						
2.45536	0.23036					-2.11607	-1.23214						
2.54464	0.26607					-1.97321	-1.37500						
2.63393	0.30179					-1.88393	-1.53571						
2.81250	0.36607					-1.70536	-1.69643						
2.99107	0.39464					-1.56250	-1.78571						
3.16964	0.41786					-1.47321	-1.89286						
3.34821	0.44821					-1.25893	-1.96429						
3.52679	0.46786					-1.22321	-2.01786						
3.70536	0.48393					-1.16964	-2.07143						
3.88393	0.48750					-1.02679	-2.16071						
4.06250	0.48750					-0.75893	-2.25000						
4.24107	0.50536					-0.56250	-2.30357						
4.41964	0.49464					-0.25893	-2.37500						
4.59821	0.49464					-0.15179	-2.41071						

4.77679	0.49821					0.08036	-2.42857						
4.95536	0.48393					0.58036	-2.42857						
5.13393	0.49464					0.88393	-2.42857						
5.31250	0.47679					1.31250	-2.42857						
5.49107	0.47857					1.54464	-2.42857						
5.66964	0.47143					1.91964	-2.42857						
5.84821	0.47679					2.13393	-2.42857						
6.02679	0.47321					2.31250	-2.50000						
6.20536	0.47500					2.43750	-2.53571						
6.38393	0.46607					2.49107	-2.57143						
6.56250	0.48393					2.58036	-2.60714						
6.74107	0.44107					1.56250	-2.32143						
6.91964	0.31250					1.68750	-2.08929						
7.09821	0.11607					1.91964	-1.92857						
						2.06250	-1.75000						
						2.13393	-1.60714						
						2.25893	-1.42857						
						2.24107	-1.21429						
						2.24107	-0.89286						
						2.09821	-0.67857						
						1.95536	-0.23214						
						1.88393	0.00000						
						1.88393	0.17857						
						2.08036	0.41071						
						2.06250	0.66071						
						2.04464	0.87500						
						2.09821	1.01786						
						2.08036	1.25000						
						1.95536	1.39286						
						1.77679	1.57143						
						1.56250	1.66071						
						1.36607	1.94643						

						1.25893	2.17857						
						1.15179	2.37500						
						1.02679	2.46429						

Test ID: S2 ($b = 0.8$ m, $h = 0.12$ m, $U = 0.261$ m/s, $D = 0.056$ m, $d_{50} = 0.74$ mm, submerged cylinder)													
$Z/D = 0$		$Z/D = 0.5$		$Z/D = 1.5$		$Y/D = 0$		$X/D = 0$		$X/D = -1.3$		$X/D = 1.75$	
X/D	Y/D	X/D	Y/D	X/D	Y/D	X/D	Z/D	Z/D	Y/D	Z/D	Y/D	Z/D	Y/D
-2.81250	-0.04464					9.24107	3.00000						
-2.72321	-0.06429					8.81250	3.00000						
-2.63393	-0.07500					8.43750	2.94643						
-2.54464	-0.12143					8.16964	2.91071						
-2.45536	-0.16250					7.95536	2.76786						
-2.36607	-0.20714					7.81250	2.62500						
-2.27679	-0.25893					7.74107	2.42857						
-2.18750	-0.31071					7.77679	2.32143						
-2.09821	-0.36429					7.70536	2.25000						
-2.00893	-0.42857					7.45536	2.23214						
-1.91964	-0.48036					7.27679	2.23214						
-1.83036	-0.51250					7.09821	2.21429						
-1.74107	-0.56964					6.93750	2.19643						
-1.65179	-0.63036					6.74107	2.30357						
-1.56250	-0.68214					6.47321	2.41071						
-1.47321	-0.72321					6.24107	2.41071						
-1.38393	-0.80179					5.93750	2.44643						
-1.29464	-0.86071					5.66964	2.55357						
-1.20536	-0.89107					5.36607	2.71429						
-1.11607	-0.98214					5.13393	2.82143						
-1.02679	-1.02679					4.77679	2.92857						
-0.93750	-1.10179					4.54464	3.00000						
-0.84821	-1.21250					4.20536	3.00000						
-0.75893	-1.24107					3.91964	2.98214						
-0.66964	-1.21964					3.66964	2.96429						
-0.58036	-1.17143					3.29464	2.92857						
0.58036	-0.66250					2.86607	2.85714						
0.66964	-0.71071					2.54464	2.80357						
0.75893	-0.70000					2.06250	2.64286						

0.84821	-0.68393					1.91964	2.57143						
0.93750	-0.65357					1.65179	2.48214						
1.02679	-0.61786					1.33036	2.39286						
1.11607	-0.56607					1.06250	2.48214						
1.20536	-0.50536					0.79464	2.58929						
1.29464	-0.42321					0.52679	2.66071						
1.38393	-0.37321					0.24107	2.66071						
1.47321	-0.30179					-0.08036	2.67857						
1.56250	-0.24107					-0.40179	2.62500						
1.65179	-0.15714					-0.77679	2.57143						
1.74107	-0.08036					-1.08036	2.50000						
1.83036	-0.05893					-1.31250	2.41071						
1.91964	-0.07500					-1.54464	2.26786						
2.00893	-0.02500					-1.79464	2.07143						
2.09821	0.03036					-1.95536	1.92857						
2.18750	0.10714					-2.09821	1.78571						
2.27679	0.15357					-2.31250	1.51786						
2.36607	0.18929					-2.45536	1.28571						
2.45536	0.21786					-2.50893	1.07143						
2.54464	0.24821					-2.59821	0.80357						
2.63393	0.27500					-2.66964	0.55357						
2.72321	0.29821					-2.66964	0.30357						
2.81250	0.32143					-2.66964	-0.03571						
2.90179	0.33750					-2.66964	-0.26786						
2.99107	0.35179					-2.65179	-0.60714						
3.08036	0.36071					-2.52679	-0.89286						
3.16964	0.38036					-2.40179	-1.12500						
3.25893	0.38929					-2.25893	-1.35714						
3.34821	0.39107					-2.09821	-1.48214						
3.43750	0.40893					-1.86607	-1.80357						
3.52679	0.41071					-1.74107	-1.92857						
3.61607	0.42321					-1.59821	-2.05357						

3.70536	0.43036					-1.47321	-2.14286						
3.88393	0.42500					-1.24107	-2.25000						
4.06250	0.43393					-1.04464	-2.39286						
4.24107	0.43393					-0.75893	-2.48214						
4.41964	0.44107					-0.41964	-2.55357						
4.59821	0.43214					-0.15179	-2.58929						
4.77679	0.43750					0.15179	-2.64286						
4.95536	0.44821					0.63393	-2.64286						
5.13393	0.44821					1.13393	-2.58929						
5.31250	0.46964					1.43750	-2.55357						
5.49107	0.46964					1.81250	-2.58929						
5.66964	0.48214					2.25893	-2.57143						
5.84821	0.48571					2.58036	-2.55357						
6.02679	0.49464					2.99107	-2.60714						
6.20536	0.50000					3.27679	-2.67857						
6.38393	0.50357					3.70536	-2.78571						
6.56250	0.51607					4.41964	-2.82143						
6.74107	0.51786					4.70536	-2.78571						
6.91964	0.51607					5.09821	-2.60714						
7.09821	0.52321					5.34821	-2.50000						
7.27679	0.53393					5.66964	-2.35714						
7.45536	0.51964					5.97321	-2.21429						
7.63393	0.43571					6.20536	-2.21429						
7.81250	0.29464					6.79464	-2.25000						
7.99107	0.14821					7.09821	-2.25000						
8.16964	0.13750					7.38393	-2.25000						
8.34821	0.13571					7.61607	-2.14286						
8.52679	0.14821					7.81250	-2.17857						
8.70536	0.13929					8.08036	-2.41071						
8.88393	0.15893					8.33036	-2.51786						
9.06250	0.18036					8.70536	-2.55357						
9.24107	0.19821					9.00893	-2.53571						

9.41964	0.21786					9.24107	-2.57143						
						9.41964	-2.57143						
						1.27679	-2.57143						
						1.43750	-2.30357						
						1.68750	-2.10714						
						2.00893	-1.78571						
						2.18750	-1.53571						
						2.16964	-1.30357						
						2.13393	-1.07143						
						2.09821	-0.82143						
						1.97321	-0.57143						
						1.95536	-0.35714						
						1.91964	-0.10714						
						1.95536	0.23214						
						2.00893	0.44643						
						2.13393	0.69643						
						2.24107	0.92857						
						2.33036	1.12500						
						2.31250	1.35714						
						2.24107	1.58929						
						1.99107	1.82143						
						1.81250	2.03571						
						1.52679	2.21429						
						1.36607	2.33929						

Test ID: S3 ($b = 1.22$ m, $h = 0.12$ m, $U = 0.254$ m/s, $D = 0.056$ m, $d_{50} = 0.74$ mm, submerged cylinder)													
$Z/D = 0$		$Z/D = 0.5$		$Z/D = 1.5$		$Y/D = 0$		$X/D = 0$		$X/D = -1.3$		$X/D = 1.75$	
X/D	Y/D	X/D	Y/D	X/D	Y/D	X/D	Z/D	Z/D	Y/D	Z/D	Y/D	Z/D	Y/D
-2.90179	-0.02321					10.22321	3.26786						
-2.81250	-0.05714					9.97321	3.30357						
-2.72321	-0.10536					9.50893	3.33929						
-2.63393	-0.12857					8.97321	3.33929						
-2.54464	-0.16786					8.43750	3.41071						
-2.45536	-0.20357					7.90179	3.26786						
-2.36607	-0.26071					7.50893	3.44643						
-2.27679	-0.33036					7.09821	3.51786						
-2.18750	-0.38571					6.59821	3.55357						
-2.09821	-0.41429					6.15179	3.50000						
-2.00893	-0.45536					5.81250	3.35714						
-1.91964	-0.52321					5.54464	3.08929						
-1.83036	-0.56607					5.40179	2.98214						
-1.74107	-0.63571					5.29464	2.89286						
-1.65179	-0.67857					4.95536	2.98214						
-1.56250	-0.68036					4.63393	3.01786						
-1.47321	-0.74286					4.33036	3.07143						
-1.38393	-0.81250					3.79464	3.12500						
-1.29464	-0.88929					3.50893	2.91071						
-1.20536	-0.93036					3.15179	3.03571						
-1.11607	-1.00893					2.88393	3.00000						
-1.02679	-1.07321					2.61607	2.91071						
-0.93750	-1.18750					2.29464	2.78571						
-0.84821	-1.26429					2.00893	2.67857						
-0.75893	-1.26429					1.65179	2.64286						
-0.66964	-1.24643					1.09821	2.62500						
-0.58036	-1.20714					0.72321	2.64286						
0.58036	-0.70714					0.29464	2.66071						
0.66964	-0.71071					-0.24107	2.69643						

0.75893	-0.70714					-0.77679	2.71429						
0.84821	-0.68393					-1.18750	2.58929						
0.93750	-0.62321					-1.54464	2.42857						
1.02679	-0.57679					-1.75893	2.28571						
1.11607	-0.52679					-1.99107	2.00000						
1.20536	-0.47321					-2.27679	1.73214						
1.29464	-0.39286					-2.45536	1.44643						
1.38393	-0.33750					-2.63393	1.19643						
1.47321	-0.27321					-2.72321	0.91071						
1.56250	-0.20893					-2.79464	0.66071						
1.65179	-0.16964					-2.84821	0.37500						
1.74107	-0.10000					-2.90179	0.14286						
1.83036	-0.04286					-2.88393	-0.23214						
1.91964	-0.00357					-2.81250	-0.48214						
2.00893	0.02500					-2.72321	-0.83929						
2.09821	0.06964					-2.59821	-1.12500						
2.18750	0.11250					-2.49107	-1.39286						
2.36607	0.17679					-2.31250	-1.67857						
2.54464	0.26071					-2.13393	-1.87500						
2.72321	0.30000					-1.91964	-2.05357						
2.90179	0.34286					-1.70536	-2.17857						
3.08036	0.37321					-1.43750	-2.30357						
3.25893	0.40714					-1.08036	-2.44643						
3.43750	0.41964					-0.74107	-2.53571						
3.61607	0.43393					-0.49107	-2.62500						
3.79464	0.42857					-0.11607	-2.69643						
3.97321	0.44821					0.25893	-2.75000						
4.15179	0.44464					0.59821	-2.71429						
4.33036	0.44107					0.90179	-2.67857						
4.50893	0.43393					1.15179	-2.69643						
4.68750	0.44107					1.61607	-2.80357						
4.86607	0.44643					1.97321	-2.85714						

5.04464	0.45179					2.45536	-2.98214						
5.22321	0.45000					2.90179	-3.10714						
5.40179	0.45000					3.40179	-3.19643						
5.58036	0.46250					3.88393	-3.25000						
5.75893	0.46964					4.50893	-3.19643						
5.93750	0.47321					5.02679	-3.08929						
6.11607	0.48214					5.27679	-2.98214						
6.29464	0.48214					5.40179	-2.92857						
6.47321	0.46964					5.54464	-3.14286						
6.65179	0.33571					5.66964	-3.39286						
6.83036	0.15714					5.99107	-3.66071						
7.00893	0.10893					6.29464	-3.78571						
7.18750	0.08214					6.58036	-3.83929						
7.36607	0.06786					6.93750	-3.87500						
7.54464	0.06250					7.29464	-3.85714						
7.72321	0.05893					7.75893	-3.76786						
7.90179	0.05714					8.24107	-3.66071						
8.08036	0.06964					8.58036	-3.60714						
8.25893	0.08036					8.97321	-3.48214						
8.43750	0.08571					9.31250	-3.42857						
8.61607	0.11071					9.54464	-3.37500						
8.79464	0.13750					9.75893	-3.32143						
8.97321	0.15000					10.13393	-3.26786						
9.15179	0.19286					10.47321	-3.23214						
9.33036	0.22321					1.63393	-2.50000						
9.50893	0.22500					1.99107	-2.30357						
9.68750	0.23929					2.29464	-2.01786						
9.86607	0.26250					2.40179	-1.69643						
10.04464	0.26250					2.40179	-1.37500						
10.22321	0.25357					2.36607	-1.01786						
						2.22321	-0.69643						
						2.09821	-0.37500						

						2.00893	-0.08929							
						1.97321	0.10714							
						2.06250	0.39286							
						2.16964	0.69643							
						2.33036	1.00000							
						2.40179	1.28571							
						2.34821	1.55357							
						2.18750	1.83929							
						1.99107	2.08929							
						1.63393	2.33929							

Test ID: E1 ($b = 0.4$ m, $h = 0.12$ m, $U = 0.262$ m/s, $D = 0.056$ m, $d_{50} = 0.74$ mm, submerged cylinder)													
Z/D = 0		Z/D = 0.5		Z/D = 1.5		Y/D = 0		X/D = 0		X/D = -1.3		X/D = 1.75	
X/D	Y/D	X/D	Y/D	X/D	Y/D	X/D	Z/D	Z/D	Y/D	Z/D	Y/D	Z/D	Y/D
-2.81250	-0.06429	-2.72321	-0.06071	-1.83036	-0.10179	5.83036	3.42857	2.60714	-0.11429	-3.42857	-0.01607	2.60714	-0.12143
-2.72321	-0.02679	-2.63393	-0.04286	-1.74107	-0.11786	5.74107	3.28571	2.55357	-0.10536	-3.33929	-0.01429	2.55357	-0.11250
-2.63393	-0.09286	-2.54464	-0.05893	-1.65179	-0.11071	5.74107	3.16071	2.46429	-0.12679	-3.25000	-0.03214	2.46429	-0.07500
-2.54464	-0.13214	-2.45536	-0.12321	-1.56250	-0.13036	5.56250	3.10714	2.37500	-0.15000	-3.16071	-0.02857	2.37500	-0.08393
-2.45536	-0.18929	-2.36607	-0.17321	-1.47321	-0.16250	5.24107	3.08929	2.28571	-0.20714	-3.07143	-0.02857	2.28571	-0.06429
-2.36607	-0.26429	-2.27679	-0.21786	-1.38393	-0.19643	4.88393	3.08929	2.19643	-0.26786	-2.98214	-0.03393	2.19643	-0.07679
-2.27679	-0.30893	-2.18750	-0.27857	-1.29464	-0.21250	4.59821	3.07143	2.10714	-0.31964	-2.89286	-0.02500	2.10714	-0.07143
-2.18750	-0.36250	-2.09821	-0.33750	-1.20536	-0.23750	4.29464	3.05357	2.01786	-0.37857	-2.80357	-0.01607	2.01786	-0.05893
-2.09821	-0.41964	-2.00893	-0.38750	-1.11607	-0.26964	3.99107	3.01786	1.92857	-0.41250	-2.71429	-0.00893	1.92857	-0.06607
-2.00893	-0.49286	-1.91964	-0.43571	-1.02679	-0.28750	3.74107	2.94643	1.83929	-0.45357	-2.62500	-0.01071	1.83929	-0.08393
-1.91964	-0.53929	-1.83036	-0.48571	-0.93750	-0.32857	3.45536	2.87500	1.75000	-0.48750	-2.53571	-0.01786	1.75000	-0.10357
-1.83036	-0.57321	-1.74107	-0.53929	-0.84821	-0.33929	3.29464	2.83929	1.66071	-0.52143	-2.44643	-0.01429	1.66071	-0.12143
-1.74107	-0.61964	-1.65179	-0.60357	-0.75893	-0.34643	2.97321	2.78571	1.57143	-0.59286	-2.35714	-0.02679	1.57143	-0.13214
-1.65179	-0.65893	-1.56250	-0.63929	-0.66964	-0.36071	2.70536	2.71429	1.48214	-0.61964	-2.26786	-0.03036	1.48214	-0.16250
-1.56250	-0.71250	-1.47321	-0.69286	-0.58036	-0.38929	2.40179	2.66071	1.39286	-0.67857	-2.17857	-0.03929	1.39286	-0.16607
-1.47321	-0.79464	-1.38393	-0.73214	-0.49107	-0.42500	2.20536	2.58929	1.30357	-0.74464	-2.08929	-0.07679	1.30357	-0.19464
-1.38393	-0.85000	-1.29464	-0.79821	-0.40179	-0.41786	1.99107	2.55357	1.21429	-0.78750	-2.00000	-0.11429	1.21429	-0.18750
-1.29464	-0.91071	-1.20536	-0.86250	-0.31250	-0.40893	1.66964	2.51786	1.12500	-0.83571	-1.91071	-0.15179	1.12500	-0.21250
-1.20536	-0.96250	-1.11607	-0.91429	-0.22321	-0.40893	1.49107	2.55357	1.03571	-0.91964	-1.82143	-0.20536	1.03571	-0.21607
-1.11607	-1.02679	-1.02679	-0.95357	-0.13393	-0.40357	1.24107	2.58929	0.94643	-1.01071	-1.73214	-0.24107	0.94643	-0.21429
-1.02679	-1.09286	-0.93750	-1.01607	-0.04464	-0.41250	0.99107	2.58929	0.85714	-1.07143	-1.64286	-0.27857	0.85714	-0.22500
-0.93750	-1.20357	-0.84821	-1.07321	0.04464	-0.40179	0.77679	2.58929	0.76786	-1.11964	-1.55357	-0.31250	0.76786	-0.21786
-0.84821	-1.24286	-0.75893	-1.11071	0.13393	-0.38571	0.49107	2.58929	0.67857	-1.11786	-1.46429	-0.36786	0.67857	-0.19286
-0.75893	-1.25000	-0.66964	-1.18393	0.22321	-0.38929	-0.00893	2.58929	0.58929	-1.08214	-1.37500	-0.40357	0.58929	-0.18750
-0.66964	-1.20357	-0.58036	-1.19464	0.31250	-0.36607	-0.29464	2.58929	0.50000	-0.98929	-1.28571	-0.44464	0.50000	-0.17679
-0.58036	-1.06250	-0.49107	-1.15536	0.40179	-0.35893	-0.63393	2.58929	-0.57143	-1.04821	-1.19643	-0.49107	0.41071	-0.16250
0.58036	-0.74643	-0.40179	-1.17321	0.49107	-0.34107	-0.91964	2.53571	-0.66071	-1.09107	-1.10714	-0.52857	0.32143	-0.16429
0.66964	-0.75714	-0.31250	-1.15536	0.58036	-0.31429	-1.06250	2.42857	-0.75000	-1.10893	-1.01786	-0.56250	0.23214	-0.15714
0.75893	-0.72143	-0.22321	-1.12143	0.66964	-0.28393	-1.54464	2.28571	-0.83929	-1.07679	-0.92857	-0.59464	0.14286	-0.16250

0.84821	-0.69286	-0.13393	-1.08571	0.84821	-0.25893	-1.79464	2.07143	-0.92857	-1.01964	-0.83929	-0.62500	0.05357	-0.15714
0.93750	-0.65357	-0.04464	-1.07679	1.02679	-0.21786	-1.90179	1.92857	-1.01786	-0.92857	-0.75000	-0.64821	-0.03571	-0.15357
1.02679	-0.57679	0.04464	-1.00536	1.20536	-0.17143	-1.90179	1.75000	-1.10714	-0.84464	-0.66071	-0.64643	-0.12500	-0.15893
1.11607	-0.52143	0.13393	-0.99643	1.38393	-0.12500	-1.97321	1.60714	-1.19643	-0.79286	-0.57143	-0.69821	-0.21429	-0.16250
1.20536	-0.47143	0.22321	-0.99286	1.56250	-0.08750	-2.16964	1.37500	-1.28571	-0.75179	-0.48214	-0.70536	-0.30357	-0.16250
1.29464	-0.40357	0.31250	-0.95714	1.74107	-0.07500	-2.20536	1.21429	-1.37500	-0.69821	-0.39286	-0.71429	-0.39286	-0.17500
1.38393	-0.33393	0.40179	-0.93214	1.91964	-0.03214	-2.27679	1.10714	-1.46429	-0.62857	-0.30357	-0.72500	-0.48214	-0.16964
1.47321	-0.30000	0.49107	-0.90000	2.09821	-0.01786	-2.36607	0.92857	-1.55357	-0.58571	-0.21429	-0.75714	-0.57143	-0.18929
1.56250	-0.21071	0.58036	-0.84821	2.27679	0.01429	-2.38393	0.71429	-1.64286	-0.51964	-0.12500	-0.77857	-0.66071	-0.20536
1.65179	-0.15357	0.66964	-0.80714	2.45536	0.02679	-2.45536	0.42857	-1.73214	-0.47321	-0.03571	-0.77679	-0.75000	-0.21429
1.74107	-0.11786	0.75893	-0.71429	2.63393	0.04821	-2.50893	0.32143	-1.82143	-0.41607	0.05357	-0.77143	-0.83929	-0.22500
1.83036	-0.11964	0.84821	-0.65357	2.81250	0.04821	-2.50893	0.17857	-1.91071	-0.37321	0.14286	-0.77143	-0.92857	-0.23214
1.91964	-0.07143	0.93750	-0.60179	2.99107	0.08571	-2.54464	-0.05357	-2.00000	-0.33571	0.23214	-0.74821	-1.01786	-0.22857
2.00893	0.01607	1.02679	-0.54464	3.16964	0.09643	-2.47321	-0.30357	-2.08929	-0.28036	0.32143	-0.75179	-1.10714	-0.23036
2.09821	0.07143	1.11607	-0.47857	3.34821	0.10179	-2.45536	-0.46429	-2.17857	-0.24821	0.41071	-0.74107	-1.19643	-0.23214
2.18750	0.12857	1.20536	-0.43214	3.52679	0.11250	-2.40179	-0.64286	-2.26786	-0.19464	0.50000	-0.69643	-1.28571	-0.22679
2.27679	0.18036	1.29464	-0.36786	3.70536	0.12679	-2.29464	-0.83929	-2.35714	-0.14821	0.58929	-0.69107	-1.37500	-0.21786
2.36607	0.20000	1.38393	-0.30179	3.88393	0.13393	-2.24107	-1.05357	-2.44643	-0.09464	0.67857	-0.64286	-1.46429	-0.20536
2.45536	0.23036	1.47321	-0.27143	4.06250	0.14643	-2.11607	-1.23214	-2.53571	-0.05893	0.76786	-0.65357	-1.55357	-0.16429
2.54464	0.26607	1.56250	-0.21786	4.24107	0.15714	-1.97321	-1.37500	-2.62500	-0.02321	0.85714	-0.61429	-1.64286	-0.13929
2.63393	0.30179	1.65179	-0.15893	4.41964	0.15714	-1.88393	-1.53571	-2.71429	-0.01964	0.94643	-0.60179	-1.73214	-0.13214
2.81250	0.36607	1.74107	-0.09286	4.59821	0.16429	-1.70536	-1.69643	-2.80357	-0.01250	1.03571	-0.56071	-1.82143	-0.06964
2.99107	0.39464	1.83036	-0.08750	4.77679	0.16964	-1.56250	-1.78571	-2.89286	-0.01786	1.12500	-0.51786	-1.91071	-0.03036
3.16964	0.41786	1.91964	-0.08393	4.95536	0.16786	-1.47321	-1.89286	-2.98214	-0.02321	1.21429	-0.48929	-2.00000	-0.01071
3.34821	0.44821	2.00893	-0.05714	5.13393	0.16250	-1.25893	-1.96429	-3.07143	-0.02500	1.30357	-0.45179	-2.08929	0.01071
3.52679	0.46786	2.09821	0.01607	5.31250	0.16429	-1.22321	-2.01786	-3.16071	-0.03036	1.39286	-0.40714	-2.17857	0.01071
3.70536	0.48393	2.18750	0.06786	5.49107	0.11607	-1.16964	-2.07143	-3.25000	-0.00357	1.48214	-0.36786	-2.26786	0.01071
3.88393	0.48750	2.27679	0.09464	5.66964	0.11429	-1.02679	-2.16071	-3.33929	-0.01786	1.57143	-0.31607	-2.35714	-0.00714
4.06250	0.48750	2.45536	0.15179	5.84821	0.10179	-0.75893	-2.25000	-3.42857	-0.01071	1.66071	-0.28571	-2.44643	0.00000
4.24107	0.50536	2.63393	0.19286	6.02679	0.08750	-0.56250	-2.30357			1.75000	-0.23393	-2.53571	-0.05357
4.41964	0.49464	2.81250	0.25714	6.20536	0.08036	-0.25893	-2.37500			1.83929	-0.18750	-2.62500	0.00893
4.59821	0.49464	2.99107	0.29821	6.38393	0.00893	-0.15179	-2.41071			1.92857	-0.15893	-2.71429	-0.01429

4.77679	0.49821	3.16964	0.31786	6.56250	-0.16786	0.08036	-2.42857			2.01786	-0.12857	-2.80357	-0.02321
4.95536	0.48393	3.34821	0.35000	6.74107	-0.24643	0.58036	-2.42857			2.10714	-0.10893	-2.89286	-0.03750
5.13393	0.49464	3.52679	0.37321	6.91964	-0.28393	0.88393	-2.42857			2.19643	-0.10179	-2.98214	-0.02321
5.31250	0.47679	3.70536	0.40357	7.09821	-0.28750	1.31250	-2.42857			2.28571	-0.08571	-3.07143	-0.02321
5.49107	0.47857	3.88393	0.41607			1.54464	-2.42857			2.37500	-0.09286	-3.16071	-0.03036
5.66964	0.47143	4.06250	0.42857			1.91964	-2.42857			2.46429	-0.08929	-3.25000	-0.03036
5.84821	0.47679	4.24107	0.43214			2.13393	-2.42857			2.55357	-0.09107	-3.33929	-0.00714
6.02679	0.47321	4.41964	0.42857			2.31250	-2.50000			2.60714	-0.08929	-3.42857	-0.00536
6.20536	0.47500	4.59821	0.43750			2.43750	-2.53571						
6.38393	0.46607	4.77679	0.43214			2.49107	-2.57143						
6.56250	0.48393	4.95536	0.43393			2.58036	-2.60714						
6.74107	0.44107	5.13393	0.44643			1.56250	-2.32143						
6.91964	0.31250	5.31250	0.43214			1.68750	-2.08929						
7.09821	0.11607	5.49107	0.42500			1.91964	-1.92857						
		5.66964	0.42500			2.06250	-1.75000						
		5.84821	0.42321			2.13393	-1.60714						
		6.02679	0.40536			2.25893	-1.42857						
		6.20536	0.40893			2.24107	-1.21429						
		6.38393	0.39464			2.24107	-0.89286						
		6.56250	0.39464			2.09821	-0.67857						
		6.74107	0.37321			1.95536	-0.23214						
		6.91964	0.30000			1.88393	0.00000						
		7.09821	0.17143			1.88393	0.17857						
						2.08036	0.41071						
						2.06250	0.66071						
						2.04464	0.87500						
						2.09821	1.01786						
						2.08036	1.25000						
						1.95536	1.39286						
						1.77679	1.57143						
						1.56250	1.66071						
						1.36607	1.94643						

						1.25893	2.17857						
						1.15179	2.37500						
						1.02679	2.46429						

Test ID: E2 ($b = 0.4$ m, $h = 0.12$ m, $U = 0.262$ m/s, $D = 0.056$ m, $d_{50} = 0.74$ mm, submerged cylinder with vertical plate)													
Z/D = 0		Z/D = 0.5		Z/D = 1.5		Y/D = 0		X/D = 0		X/D = -1.3		X/D = 1.75	
X/D	Y/D	X/D	Y/D	X/D	Y/D	X/D	Z/D	Z/D	Y/D	Z/D	Y/D	Z/D	Y/D
-3.21429	-0.05298	-3.12500	-0.04940	-2.41071	-0.07798	1.73214	-0.03571	2.59821	-0.10476	-3.34821	0.02381	2.59821	-0.03869
-3.12500	-0.04940	-3.03571	-0.05655	-2.32143	-0.08155	1.73214	-0.33929	2.54464	-0.09583	-3.25893	0.02381	2.54464	-0.04762
-3.03571	-0.03333	-2.94643	-0.05655	-2.23214	-0.09405	1.73214	-0.50000	2.45536	-0.13869	-3.16964	0.03095	2.45536	-0.04048
-2.94643	-0.06905	-2.85714	-0.06726	-2.14286	-0.10655	1.80357	-0.66071	2.36607	-0.16548	-3.08036	0.02560	2.36607	-0.01905
-2.85714	-0.12798	-2.76786	-0.08690	-2.05357	-0.10833	1.89286	-0.80357	2.27679	-0.22262	-2.99107	0.02560	2.27679	-0.02798
-2.76786	-0.17976	-2.67857	-0.15298	-1.96429	-0.13512	1.94643	-1.05357	2.18750	-0.26548	-2.90179	0.00774	2.18750	-0.03333
-2.67857	-0.21012	-2.58929	-0.20655	-1.87500	-0.14405	1.91071	-1.26786	2.09821	-0.31369	-2.81250	0.01667	2.09821	-0.03333
-2.58929	-0.22440	-2.50000	-0.23869	-1.78571	-0.16548	1.91071	-1.46429	2.00893	-0.37083	-2.72321	0.00952	2.00893	-0.04405
-2.50000	-0.21726	-2.41071	-0.27083	-1.69643	-0.20476	1.85714	-1.66071	1.91964	-0.42440	-2.63393	0.00595	1.91964	-0.03690
-2.41071	-0.25298	-2.32143	-0.32976	-1.60714	-0.23690	1.75000	-1.85714	1.83036	-0.46190	-2.54464	0.01310	1.83036	-0.05476
-2.32143	-0.27976	-2.23214	-0.38512	-1.51786	-0.26726	1.60714	-2.01786	1.74107	-0.51190	-2.45536	0.00417	1.74107	-0.07798
-2.23214	-0.31905	-2.14286	-0.42976	-1.42857	-0.28333	1.42857	-2.16071	1.65179	-0.54940	-2.36607	0.00060	1.65179	-0.09762
-2.14286	-0.37083	-2.05357	-0.49226	-1.33929	-0.29405	1.14286	-2.28571	1.56250	-0.61012	-2.27679	-0.03869	1.56250	-0.12798
-2.05357	-0.41190	-1.96429	-0.54226	-1.25000	-0.33333	0.94643	-2.37500	1.47321	-0.64940	-2.18750	-0.05119	1.47321	-0.14048
-1.96429	-0.45476	-1.87500	-0.58690	-1.16071	-0.34940	0.76786	-2.44643	1.38393	-0.69226	-2.09821	-0.08869	1.38393	-0.15298
-1.87500	-0.51905	-1.78571	-0.63155	-1.07143	-0.36369	0.41071	-2.50000	1.29464	-0.73690	-2.00893	-0.13512	1.29464	-0.15833
-1.78571	-0.56190	-1.69643	-0.66548	-0.98214	-0.38512	0.07143	-2.53571	1.20536	-0.77619	-1.91964	-0.16905	1.20536	-0.18690
-1.69643	-0.61369	-1.60714	-0.73333	-0.89286	-0.41726	-0.28571	-2.53571	1.11607	-0.85119	-1.83036	-0.19762	1.11607	-0.18512
-1.60714	-0.68155	-1.51786	-0.73690	-0.80357	-0.41905	-0.64286	-2.51786	1.02679	-0.94226	-1.74107	-0.24940	1.02679	-0.19405
-1.51786	-0.73155	-1.42857	-0.83869	-0.71429	-0.43333	-1.01786	-2.48214	0.93750	-1.01905	-1.65179	-0.28512	0.93750	-0.20476
-1.42857	-0.78333	-1.33929	-0.86190	-0.62500	-0.44226	-1.33929	-2.35714	0.84821	-1.07262	-1.56250	-0.31012	0.84821	-0.19405
-1.33929	-0.85119	-1.25000	-1.07262	-0.53571	-0.46190	-1.66071	-2.25000	0.75893	-1.07262	-1.47321	-0.36190	0.75893	-0.18690
-1.25000	-0.88690	-1.16071	-0.98333	-0.44643	-0.43512	-1.82143	-2.07143	0.66964	-1.03690	-1.38393	-0.39226	0.66964	-0.17262
-1.16071	-0.97083	-1.07143	-1.06369	-0.35714	-0.43690	-2.26786	-1.76786	0.58036	-0.98690	-1.29464	-0.42976	0.58036	-0.14405
-1.07143	-1.00655	-0.98214	-1.12619	-0.26786	-0.44405	-2.44643	-1.53571	-0.58036	-1.05298	-1.20536	-0.48690	0.49107	-0.14226
-0.98214	-1.09583	-0.89286	-1.16905	-0.17857	-0.42619	-2.57143	-1.33929	-0.66964	-1.06726	-1.11607	-0.50298	0.40179	-0.13690
-0.89286	-1.21726	-0.80357	-1.19405	-0.08929	-0.42440	-2.62500	-1.12500	-0.75893	-1.05476	-1.02679	-0.56012	0.31250	-0.15476
-0.80357	-1.22976	-0.71429	-1.20119	0.00000	-0.39583	-2.69643	-0.94643	-0.84821	-1.01012	-0.93750	-0.58869	0.22321	-0.17083
-0.71429	-1.22262	-0.62500	-1.18333	0.08929	-0.38690	-2.76786	-0.71429	-0.93750	-0.93512	-0.84821	-0.61190	0.13393	-0.17619

-0.62500	-1.21190	-0.53571	-1.12976	0.17857	-0.36548	-2.85714	-0.50000	-1.02679	-0.83869	-0.75893	-0.63869	0.04464	16.95774
2.67857	0.32560	-0.44643	-1.08512	0.26786	-0.34583	-2.89286	-0.21429	-1.11607	-0.77083	-0.66964	-0.67976	-0.04464	16.95774
2.85714	0.36667	-0.35714	-1.03690	0.35714	-0.32798	-2.91071	0.05357	-1.20536	-0.71905	-0.58036	-0.68869	-0.13393	-0.20476
3.03571	0.39167	-0.26786	-1.00833	0.44643	-0.30476	-2.91071	0.41071	-1.29464	-0.67440	-0.49107	-0.72262	-0.22321	-0.19940
3.21429	0.43810	-0.17857	-0.97440	0.53571	-0.28690	-2.85714	0.71429	-1.38393	-0.62619	-0.40179	-0.73869	-0.31250	-0.16190
3.39286	0.47381	-0.08929	-0.94405	0.62500	-0.26726	-2.78571	0.92857	-1.47321	-0.56905	-0.31250	-0.76548	-0.40179	-0.15476
3.57143	0.50774	0.00000	-0.93333	0.71429	-0.24405	-2.69643	1.14286	-1.56250	-0.53155	-0.22321	-0.77083	-0.49107	-0.15298
3.75000	0.52381	0.08929	-0.92798	0.80357	-0.21726	-2.62500	1.37500	-1.65179	-0.47976	-0.13393	-0.79405	-0.58036	-0.17976
3.92857	0.54167	0.17857	-0.90655	0.89286	-0.19583	-2.48214	1.58929	-1.74107	-0.42798	-0.04464	-0.77440	-0.66964	-0.18512
4.10714	0.55952	0.26786	-0.89226	0.98214	-0.18512	-2.19643	1.82143	-1.83036	-0.40298	0.04464	-0.79405	-0.75893	-0.18512
4.28571	0.57202	0.35714	-0.85476	1.07143	-0.14940	-1.96429	2.00000	-1.91964	-0.35119	0.13393	-0.79762	-0.84821	-0.19583
4.46429	0.58810	0.44643	-0.81190	1.16071	-0.12083	-1.82143	2.07143	-2.00893	-0.31548	0.22321	-0.78869	-0.93750	-0.19405
4.64286	0.57917	0.53571	-0.74583	1.25000	-0.09048	-1.75000	2.16071	-2.09821	-0.25655	0.31250	-0.78690	-1.02679	-0.19226
4.82143	0.57917	0.62500	-0.69405	1.33929	-0.07976	-1.58929	2.19643	-2.18750	-0.20476	0.40179	-0.75833	-1.11607	-0.19405
5.00000	0.57024	0.71429	-0.63512	1.42857	-0.06548	-1.42857	2.28571	-2.27679	-0.14762	0.49107	-0.73869	-1.20536	-0.17976
5.17857	0.55774	0.80357	-0.55476	1.60714	-0.04226	-1.21429	2.39286	-2.36607	-0.09940	0.58036	-0.72798	-1.29464	-0.16726
5.35714	0.53988	0.89286	-0.49405	1.78571	0.00238	-0.98214	2.44643	-2.45536	-0.06548	0.66964	-0.70476	-1.38393	-0.14940
5.53571	0.50952	0.98214	-0.43155	1.96429	0.02381	-0.53571	2.50000	-2.54464	-0.01905	0.75893	-0.68155	-1.47321	-0.11726
5.71429	0.47917	1.07143	-0.37262	2.14286	0.03274	-0.17857	2.51786	-2.63393	0.00774	0.84821	-0.63690	-1.56250	-0.08869
5.89286	0.43631	1.16071	-0.32976	2.32143	0.05417	0.21429	2.51786	-2.72321	0.01131	0.93750	-0.63512	-1.65179	-0.05119
6.07143	0.38452	1.25000	-0.29226	2.50000	0.05417	0.53571	2.46429	-2.81250	0.02738	1.02679	-0.59405	-1.74107	-0.01369
6.25000	0.33452	1.33929	-0.23333	2.67857	0.06667	0.80357	2.32143	-2.90179	0.03274	1.11607	-0.56190	-1.83036	-0.03690
6.42857	0.27917	1.42857	-0.17976	2.85714	0.09702	1.10714	2.14286	-2.99107	0.02738	1.20536	-0.53155	-1.91964	-0.02440
6.60714	0.22917	1.51786	-0.14226	3.03571	0.10060	1.37500	2.01786	-3.08036	0.03631	1.29464	-0.48690	-2.00893	0.00238
6.78571	0.16131	1.60714	-0.07798	3.21429	0.09881	1.71429	1.75000	-3.16964	0.03452	1.38393	-0.46012	-2.09821	0.01845
6.96429	0.12738	1.78571	-0.03690	3.39286	0.12560	1.87500	1.55357	-3.25893	0.02738	1.47321	-0.42083	-2.18750	0.03452
7.14286	0.06667	1.96429	0.07381	3.57143	0.13452	1.92857	1.35714	-3.34821	0.04167	1.56250	-0.37083	-2.27679	0.05060
		2.14286	0.14167	3.75000	0.14524	1.94643	1.08929			1.65179	-0.33155	-2.36607	0.07560
		2.32143	0.21131	3.92857	0.15595	1.91071	0.82143			1.74107	-0.30833	-2.45536	0.07917
		2.50000	0.25952	4.10714	0.17024	1.85714	0.58929			1.83036	-0.25655	-2.54464	0.05417
		2.67857	0.30060	4.28571	0.18095	1.82143	0.35714			1.91964	-0.22083	-2.63393	0.03631
		2.85714	0.35595	4.46429	0.17381	1.78571	0.14286			2.00893	-0.18690	-2.72321	0.05238

		3.03571	0.39524	4.64286	0.19167	0.78571	2.48214			2.09821	-0.16012	-2.81250	0.06667
		3.21429	0.42024	4.82143	0.21488	1.05357	2.50000			2.18750	-0.13155	-2.90179	0.08095
		3.39286	0.46131	5.00000	0.20774	1.42857	2.50000			2.27679	-0.11369	-2.99107	0.07560
		3.57143	0.48452	5.17857	0.21845	1.78571	2.50000			2.36607	-0.11369	-3.08036	0.07202
		3.75000	0.49702	5.35714	0.21488	2.14286	2.51786			2.45536	-0.11726	-3.16964	0.07738
		3.92857	0.51667	5.53571	0.22738	2.57143	2.55357			2.54464	-0.10476	-3.25893	0.08095
		4.10714	0.52560	5.71429	0.22202	2.94643	2.60714			2.59821	-0.09405	-3.34821	0.06488
		4.28571	0.52560	5.89286	0.23631	3.25000	2.64286						
		4.46429	0.53452	6.07143	0.25060	3.73214	2.69643						
		4.64286	0.53452	6.25000	0.24167	4.14286	2.76786						
		4.82143	0.52738	6.42857	0.25952	4.53571	2.82143						
		5.00000	0.52738	6.60714	0.21667	5.00000	2.91071						
		5.17857	0.52381	6.78571	0.05060	5.39286	2.96429						
		5.35714	0.50417	6.96429	-0.13333	5.82143	3.00000						
		5.53571	0.49167			6.25000	3.00000						
		5.71429	0.47202			6.67857	3.00000						
		5.89286	0.45060			6.85714	3.08929						
		6.07143	0.43810			7.10714	3.25000						
		6.25000	0.41845			7.17857	3.35714						
		6.42857	0.39881			3.07143	-2.60714						
		6.60714	0.38988			2.66071	-2.60714						
		6.78571	0.26667			2.30357	-2.41071						
		6.96429	0.12738			2.03571	-2.39286						
						1.75000	-2.39286						
						1.46429	-2.39286						
						1.08929	-2.32143						

Test ID: E3 ($b = 0.4$ m, $h = 0.12$ m, $U = 0.262$ m/s, $D = 0.056$ m, $d_{50} = 0.74$ mm, submerged cylinder with horizontal plate)													
$Z/D = 0$		$Z/D = 0.5$		$Z/D = 1.5$		$Y/D = 0$		$X/D = 0$		$X/D = -1.3$		$X/D = 1.75$	
X/D	Y/D	X/D	Y/D	X/D	Y/D	X/D	Z/D	Z/D	Y/D	Z/D	Y/D	Z/D	Y/D
0.59821	0.12440	0.50893	-0.11845	0.50893	-0.10952	3.65179	-2.64286	2.64286	-0.10417	-	-	-3.39286	-0.21310
0.68750	0.16012	0.59821	-0.13095	0.59821	-0.13631	3.66964	-2.55357	2.58929	-0.08988	-	-	-3.30357	-0.23631
0.77679	0.17798	0.68750	-0.16845	0.68750	-0.19345	3.66964	-2.33929	2.50000	-0.07024	-	-	-3.21429	-0.23988
0.86607	0.15655	0.77679	-0.17917	0.77679	-0.24702	3.65179	-2.12500	2.41071	-0.08095	-	-	-3.12500	-0.26845
0.95536	0.15298	0.86607	-0.20060	0.86607	-0.28274	3.63393	-1.87500	2.32143	-0.10952	-	-	-3.03571	-0.28810
1.04464	0.15119	0.95536	-0.21131	0.95536	-0.33452	3.61607	-1.62500	2.23214	-0.10952	-	-	-2.94643	-0.32381
1.13393	0.15119	1.04464	-0.21131	1.04464	-0.36488	3.50893	-1.39286	2.14286	-0.11310	-	-	-2.85714	-0.34345
1.22321	0.14940	1.13393	-0.21131	1.13393	-0.40952	3.38393	-1.21429	2.05357	-0.12560	-	-	-2.76786	-0.37024
1.31250	0.14226	1.22321	-0.19702	1.22321	-0.41667	3.24107	-1.03571	1.96429	-0.12024	-	-	-2.67857	-0.39167
1.40179	0.13512	1.31250	-0.20595	1.31250	-0.45238	3.09821	-0.87500	1.87500	-0.13274	-	-	-2.58929	-0.42381
1.49107	0.12619	1.40179	-0.19702	1.40179	-0.46310	2.88393	-0.71429	1.78571	-0.15774	-	-	-2.50000	-0.44881
1.58036	0.12083	1.49107	-0.19702	1.49107	-0.48631	2.59821	-0.53571	1.69643	-0.17738	-	-	-2.41071	-0.47202
1.66964	0.12262	1.58036	-0.18810	1.58036	-0.49702	2.38393	-0.48214	1.60714	-0.18274	-	-	-2.32143	-0.49345
1.75893	0.12083	1.66964	-0.20952	1.66964	-0.50417	2.08036	-0.44643	1.51786	-0.17738	-	-	-2.23214	-0.48810
1.84821	0.10833	1.75893	-0.21488	1.75893	-0.51131	1.86607	-0.42857	1.42857	-0.17381	-	-	-2.14286	-0.50417
1.93750	0.10298	1.84821	-0.22024	1.84821	-0.51667	1.59821	-0.46429	1.33929	-0.16845	-	-	-2.05357	-0.48274
2.02679	0.10298	1.93750	-0.21488	1.93750	-0.52381	1.25893	-0.50000	1.25000	-0.17560	-	-	-1.96429	-0.47917
2.11607	0.08512	2.02679	-0.21131	2.02679	-0.53095	0.91964	-0.50000	1.16071	-0.18274	-	-	-1.87500	-0.45595
2.20536	0.08512	2.11607	-0.21310	2.11607	-0.54167	0.68750	-0.53571	1.07143	-0.19524	-	-	-1.78571	-0.45417
2.29464	0.08869	2.20536	-0.19524	2.20536	-0.53095	0.54464	-0.53571	0.98214	-0.18274	-	-	-1.69643	-0.44345
2.38393	0.08512	2.29464	-0.20595	2.29464	-0.54167	0.54464	-2.62500	0.89286	-0.18095	-	-	-1.60714	-0.43274
2.47321	0.07976	2.38393	-0.17560	2.38393	-0.51845	0.54464	0.41071	0.80357	-0.17202	-	-	-1.51786	-0.43631
2.56250	0.07440	2.47321	-0.17202	2.47321	-0.50952	0.86607	0.39286	0.71429	-0.16845	-	-	-1.42857	-0.42738
2.65179	0.09405	2.56250	-0.16488	2.56250	-0.48274	1.31250	0.41071	0.62500	-0.15417	-	-	-1.33929	-0.40238
2.74107	0.09405	2.65179	-0.14524	2.65179	-0.48452	1.63393	0.41071	0.53571	-0.14702	-	-	-1.25000	-0.38452
2.83036	0.11190	2.74107	-0.16131	2.74107	-0.46310	2.09821	0.42857	0.44643	-0.12202	-	-	-1.16071	-0.36488
2.91964	0.11190	2.83036	-0.14167	2.83036	-0.43810	2.41964	0.46429	0.35714	-0.07917	-	-	-1.07143	-0.35060
3.00893	0.11905	2.91964	-0.11131	2.91964	-0.40238	2.70536	0.50000	0.26786	-0.02202	-	-	-0.98214	-0.33631
3.09821	0.14226	3.00893	-0.08988	3.00893	-0.38274	2.91964	0.62500	0.17857	0.03690	-	-	-0.89286	-0.31310

3.18750	0.14405	3.09821	-0.07917	3.09821	-0.34702	3.09821	0.75000	0.08929	0.07976	-	-	-0.80357	-0.28631
3.27679	0.14762	3.18750	-0.06131	3.18750	-0.31488	3.24107	0.82143	0.00000	0.11012	-	-	-0.71429	-0.25595
3.36607	0.16726	3.27679	-0.02917	3.27679	-0.25595	3.41964	0.94643	-0.08929	0.11190	-	-	-0.62500	-0.21667
3.45536	0.17262	3.36607	-0.00952	3.36607	-0.24345	3.59821	1.01786	-0.17857	0.05655	-	-	-0.53571	-0.14345
3.54464	0.18333	3.45536	0.01012	3.45536	-0.20774	3.72321	1.12500	-0.26786	-0.00595	-	-	-0.44643	-0.10952
3.63393	0.18690	3.54464	0.02083	3.54464	-0.16845	3.81250	1.35714	-0.35714	-0.04881	-	-	-0.35714	-0.07560
3.81250	0.22083	3.63393	0.04762	3.63393	-0.12381	3.88393	1.51786	-0.44643	-0.10060	-	-	-0.26786	0.00655
3.99107	0.22440	3.72321	0.07262	3.72321	-0.11667	3.88393	1.78571	-0.53571	-0.10952	-	-	-0.17857	0.06190
4.16964	0.24583	3.81250	0.09762	3.81250	-0.06310	3.81250	2.01786	-0.62500	-0.14702	-	-	-0.08929	0.11726
4.34821	0.25655	3.90179	0.10655	3.90179	-0.03274	3.75893	2.23214	-0.71429	-0.14702	-	-	0.00000	0.12976
4.52679	0.25119	3.99107	0.12262	3.99107	-0.00060	3.68750	2.55357	-0.80357	-0.15238	-	-	0.08929	0.10298
4.70536	0.27619	4.08036	0.14226	4.08036	0.03333	3.58036	2.76786	-0.89286	-0.15417	-	-	0.17857	0.06905
4.88393	0.28155	4.16964	0.16190	4.16964	0.04940	3.36607	3.05357	-0.98214	-0.16131	-	-	0.26786	-0.00060
5.06250	0.28512	4.34821	0.17262	4.25893	0.07976	3.22321	3.19643	-1.07143	-0.15417	-	-	0.35714	-0.11131
5.24107	0.29048	4.52679	0.20119	4.34821	0.09048	2.97321	3.33929	-1.16071	-0.15774	-	-	0.44643	-0.13452
5.41964	0.31369	4.70536	0.21726	4.43750	0.11190	1.20536	3.33929	-1.25000	-0.16131	-	-	0.53571	-0.14881
5.59821	0.32083	4.88393	0.23869	4.52679	0.11905	0.97321	3.07143	-1.33929	-0.16310	-	-	0.62500	-0.22024
5.77679	0.31726	5.06250	0.25476	4.61607	0.13333	0.90179	2.85714	-1.42857	-0.13988	-	-	0.71429	-0.27381
5.95536	0.31726	5.24107	0.25655	4.70536	0.13512	0.65179	2.57143	-1.51786	-0.14702	-	-	0.80357	-0.30238
6.13393	0.31369	5.41964	0.25119	4.79464	0.16190	0.50893	2.30357	-1.60714	-0.13631	-	-	0.89286	-0.33452
6.31250	0.30655	5.59821	0.24405	4.88393	0.17083			-1.69643	-0.10238	-	-	0.98214	-0.35595
6.40179	0.29940	5.77679	0.22976	4.97321	0.17083			-1.78571	-0.09702	-	-	1.07143	-0.37560
6.49107	0.22440	5.95536	0.23155	5.06250	0.15655			-1.87500	-0.10238	-	-	1.16071	-0.39167
6.58036	0.15833	6.13393	0.23155	5.15179	0.18155			-1.96429	-0.09167	-	-	1.25000	-0.40060
6.66964	0.03333	6.31250	0.19940	5.24107	0.14048			-2.05357	-0.07738	-	-	1.33929	-0.41667
6.75893	-0.02738	6.49107	0.19940	5.33036	0.04762			-2.14286	-0.06845	-	-	1.42857	-0.43631
6.84821	-0.06845	6.66964	0.17083	5.41964	-0.04524			-2.23214	-0.04524	-	-	1.51786	-0.46667
6.93750	-0.06488	6.84821	0.10476	5.50893	-0.10595			-2.32143	-0.01131	-	-	1.60714	-0.48452
7.02679	-0.07202	7.02679	-0.05595	5.59821	-0.07560			-2.41071	-0.03452	-	-	1.69643	-0.48810
7.11607	-0.08988	7.20536	-0.12560	5.68750	-0.08810			-2.50000	-0.05417	-	-	1.78571	-0.49881
7.20536	-0.10595	7.29464	-0.13452	5.77679	-0.07560			-2.58929	-0.02381	-	-	1.87500	-0.49881
7.29464	-0.12381			5.86607	-0.08988			-2.67857	0.00298	-	-	1.96429	-0.50417

				5.95536	-0.09524			-2.76786	-0.00417	-	-	2.05357	-0.50774
				6.04464	-0.12738			-2.85714	0.00119	-	-	2.14286	-0.53631
				6.13393	-0.14524			-2.94643	0.00298	-	-	2.23214	-0.52917
				6.22321	-0.17024			-3.03571	0.02083	-	-	2.32143	-0.53452
				6.31250	-0.19702			-3.12500	0.00655	-	-	2.41071	-0.52381
				6.40179	-0.20417			-3.21429	0.02083	-	-	2.50000	-0.49881
				6.49107	-0.21131			-3.30357	0.01726	-	-	2.58929	-0.48274
				6.58036	-0.23274			-3.39286	0.01012	-	-	2.64286	-0.47560
				6.66964	-0.24881					-	-		
				6.75893	-0.25417					-	-		
				6.84821	-0.25595					-	-		
				6.93750	-0.26667					-	-		
				7.02679	-0.27202					-	-		
				7.11607	-0.27024					-	-		
				7.20536	-0.27202					-	-		
				7.29464	-0.27738					-	-		

Appendix C: Summary of PIV measurement details

Summary of PIV measurement details: data acquisition												
Chapter	Test ID	Description	b (m)	h (m)	FOV no.	Z/D	No. frames	Δt (ms)				
3	R1	sand bed	0.4	0.12	1	0	2000	2000				
	R2	sand bed	0.4	0.21	1	0	2000	2200				
	R3	sand bed	0.8	0.12	1	0	2000	1900				
	R4	sand bed	0.8	0.24	1	0	2000	2800				
	R5	sand bed	1.22	0.12	1	0	2000	2000				
	R5-C	sand bed	1.22	0.12	1	5.7	2000	2300				
	R6	sand bed	1.22	0.185	1	0	2000	2900				
4	B1	emergent cylinder $D = 0.056$ m	0.4	0.12	1	0	2000	2700				
					2	0	3000	3000				
					3	0	3000	3000				
					4	0	3000	3000				
					1	0.5	2000	2300				
					2	0.5	3000	2900				
					3	0.5	3043	3000				
					4	0.5	3000	2900				
					1	2	2000	2000				
					2	2	2000	1800				
					3	2	2000	1800				
					4	2	2000	1800				
					B2	emergent cylinder $D = 0.056$ m	0.8	0.12	1	0	1994	2200
									2	0	3000	2400
	3	0	3000	2300								
	4	0	2000	2000								
	1	0.5	2000	2000								
	2	0.5	3000	2300								
	3	0.5	3000	2650								
	4	0.5	2000	2650								
	1	3.8	2000	2000								
	2	3.8	2000	2000								
	3	3.8	2000	1900								
	4	3.8	2000	1800								
	B3	emergent cylinder $D = 0.056$ m	1.22	0.12	1	0	2000	2300				
					2	0	3000	2600				
					3	0	3000	2600				
					4	0	2000	2400				
1					0.5	2000	2000					
2					0.5	3000	2200					

					3	0.5	3000	2200
					4	0.5	2000	2500
					1	5.7	2000	2500
					2	5.7	2000	2500
					3	5.7	2000	2500
					4	5.7	2000	2400
5	E1	submerged cylinder $D = 0.056$ m	0.4	0.12	1	0	2000	2500
					2	0	2916	2800
					3	0	2876	2500
					4	0	2000	2500
					1	0.5	2000	2200
					2	0.5	3000	2600
					3	0.5	3000	2300
					4	0.5	2000	2600
					1	2	2000	2000
					2	2	2000	1800
					3	2	1998	1800
					4	2	2000	1700
	E2	submerged cylinder with vertical plate $D = 0.056$ m	0.4	0.12	1	0	2000	2500
					2	0	2000	2800
					3	0	3000	2800
					4	0	2000	2500
					1	0.5	2000	2500
					2	0.5	3000	2800
					3	0.5	3000	2700
					4	0.5	2000	2400
					1	2	2000	2000
					2	2	2000	1800
					3	2	2000	1600
					4	2	2000	1900
E3	submerged cylinder with horizontal plate $D = 0.056$ m	0.4	0.12	1	0	2000	2650	
				2	0	2500	2400	
				3	0	2500	2600	
				4	0	2500	2800	
				1	0.5	2000	2300	
				2	0.5	3000	2900	
				3	0.5	3000	2800	
				4	0.5	2500	2600	
				1	2	2000	1800	
				2	2	2000	1700	
				3	2	2000	1700	
				4	2	2000	1700	

Summary of PIV measurement details: resolution of images								
Chapter	Test ID	Description	b (m)	h (m)	FOV no.	Z/D	Δx^+	Δy^+
3	R1	sand bed	0.4	0.12	1	0	13.5	13.5
	R2	sand bed	0.4	0.21	1	0	12.9	12.9
	R3	sand bed	0.8	0.12	1	0	13.1	13.1
	R4	sand bed	0.8	0.24	1	0	19.8	19.8
	R5	sand bed	1.22	0.12	1	0	16.3	16.3
	R5-C	sand bed	1.22	0.12	1	5.7	18.9	18.9
	R6	sand bed	1.22	0.185	1	0	16.5	16.5

Appendix D: Uncertainty analysis of PIV measurements

Particle Image Velocimetry (PIV) measurements are subject to many sources of error in practice. In this section, the random errors associated with various components of calibration, data acquisition and post-processing will be calculated for a sample test. The quantification of uncertainty follows the method described by Park et al. (2008), adapted from the Visualization Society of Japan's guidelines (2002). The sample calculation below was conducted for test R1 (see Appendix C for details).

Test R1 ($b = 0.4$ m, $h = 0.12$ m, sand bed): test details		
target flow of measurement		
target flow		two-dimensional water flow
measurement facility		horizontal recirculating laboratory flume
measurement area		3312 × 2488 px
uniform flow speed		0.262 m/s
calibration		
distance of reference points	l_T	10 mm
distance of reference image	L_T	167 px
magnification factor	α	0.05988024 mm/px
flow visualisation		
tracer particle		spherical glass particle
average diameter	d_p	0.011 mm
standard deviation of diameter	s_p	0.002 mm
average specific gravity		1.07
light source		double pulse Nd:YAG laser
laser power		135 mJ
time interval	Δt	2 ms
image detection		
camera		8 MP CCD array camera
spatial resolution		3312 × 2488 px
sampling frequency		2.07 Hz
optical system		
distance from the target	l_t	500 mm
length of focus		50 mm
perspective angle	θ	0.087 rad
data processing		
pixel unit analysis		cross correlation method
correlation area size		32 × 32 px
search area size		16 × 16 px
sub-pixel analysis		3-point Gaussian fitting

Error sources and propagation of error						
calibration, α		sensitivity factor		error/uncertainty		combined uncertainty
calibration board		c_i		$u(x_i)$		$c_i u(x_i)$
						u_c
<i>image distance of reference points</i>	$-l_T/L_T^2$	-0.0004	mm/px ²	0.7	px	0.0003
<i>physical distance of reference points</i>	l/L_T	0.0060	1/px	0.02	mm	0.0001
optical system						
<i>image distortion by lens</i>	$-l_T/L_T^2$	-0.0004	mm/px ²	0.835	px	0.0003
<i>distortion and other errors of CCD</i>	$-l_T/L_T^2$	-0.0004	mm/px ²	0.0056	px	2.0E-06
experimental condition						
<i>reference board position</i>	$l_T/(L_T l_T)$	0.0060	1/px	0.5	mm	0.003
<i>parallel reference board</i>	$-l_T \theta / L_T$	-0.0021	mm/px	0.035	rad	7.3E-05
displacement of particle image, Δx						0.003 mm/px
visualization						
<i>laser power fluctuation</i>	l/α	16.7	px/mm	0.0071	mm	0.119
image detection						
<i>CCD distortion</i>		1		0.0056	px	0.0056
<i>normal view angle</i>	$-l_T \theta / L_T$	-0.0021	mm/px	0.035	rad	7.3E-05
data processing						
<i>mis-matching error</i>		1		0.2		0.2
<i>sub-pixel analysis</i>		1		0.03		0.03
time interval, Δt						0.234 px
<i>delay generator</i>		1		1.0E-09	s	1.0E-09
<i>pulse timing accuracy</i>		1		5.0E-09	s	5.0E-09
experiment, δu						5.1E-09 s
<i>particle trajectory</i>		1		0.0262	mm/s	0.0262
<i>3D effects on perspective of velocity</i>		1		0.263	mm/s	0.263
						0.264 mm/s
velocity, u						
<i>calibration, α</i>		4375	px/s	0.003	mm/px	13.2
<i>displacement of particle image, Δx</i>		29.9	mm/px/s	0.234	px	7.02
<i>time interval, Δt</i>		0.52	mm/s ²	5.10E-09	s	2.7E-09

<i>experiment, δu</i>	1	0.264 mm/s	0.264	15.0 mm/s
displacement, x				
<i>centre position of correlation area, X_s, X_e</i>	0.0599 mm/px	0.5 px	0.030	
<i>non-uniformity of tracer particle distribution</i>	0.0599 mm/px	8 px	0.479	
<i>origin correlation</i>	0.0599 mm/px	2 px	0.120	0.495 mm
measurement time, t				
<i>delay generator</i>	1	1.00E-09 s	1.0E-09	
<i>pulse timing accuracy</i>	1	5.00E-09 s	5.0E-09	5.1E-09 s

VITA AUCTORIS

NAME: Priscilla D. Williams

PLACE OF BIRTH: Kingston, ON

YEAR OF BIRTH: 1989

EDUCATION: Vincent Massey Secondary School, Windsor,
ON, 2007

University of Windsor, B.A.Sc. – Civil
Engineering, Windsor, ON, 2011

University of Windsor, M.A.Sc. – Civil
Engineering, Windsor, ON, 2014